2015

Numerical Simulation of Cold Front-Related Hydrodynamics of Wax Lake Delta

Qian Zhang
Louisiana State University and Agricultural and Mechanical College

NUMERICAL SIMULATION OF COLD FRONT-RELATED HYDRODYNAMICS OF WAX LAKE DELTA

A Dissertation

Submitted to the Graduate Faculty of the
Louisiana State University and
Agricultural and Mechanical College
in partial fulfillment of the
requirements for the degree of
Doctor of Philosophy

in

The Department of Oceanography and Coastal Sciences

by
Qian Zhang
B.S., Harbin Engineering University, 2006
M.S., Harbin Institute of Technology, 2008
M.S., Louisiana State University, 2011
August 2015

ACKNOWLEDGEMENTS

This dissertation would have been incomplete without the dedicated help from numerous people as listed below:

First of all, I would like to express my deep gratitude to my supervisor Dr. Chunyan Li, who made this research possible and indoctrinates me in the research methods. His support, encouragement, guidance, patience and faith through every bump in the road were invaluable. Thanks also to my committee members Dr. Sibel Bargu Ates, Dr. Kemin Zhou and Dr. Rebecca Saunders for their sincere help, comments and scientific suggestions on the dissertation. I want to acknowledge LSU WAVCIS lab and CSI (Coastal Studies Institute) for the valuable field measurement data.

I would also like to thank Dr. Jun Lin (College of Marine Sciences, Shanghai Ocean University, China), Dr. Jianrong Zhu (State Key Laboratory of Estuarine and Coastal Research, Institute of Estuarine and Coastal Research) and Dr. Hui Wu (East China Normal University) for sharing the code for the numerical model used in this study; thank Dr. Yangdong Li, Dr. Baozhu Liu, and Dr. Mohammadnabi Allahdadi, who have shared their experience in numerical modeling and thesis writing. I want furthermore to acknowledge the assistance I received from my fellow students Chenguang Zhang, Wei Huang, Nazanin Chaichi, Shima Massiha, Fan Zhang and Christopher Kunz for their encouragement and valuable suggestions.

Finally, I would like to give my special thanks to my parents and friends for their unconditional love and support. Thanks for being there for me through all of the ups and downs.

TABLE OF CONTENTS

ABSTRACT

This study applies a three-dimensional numerical model ECOM-si to simulate the circulation in the Wax Lake delta under winter cold front conditions. This model uses real topography and bathymetry of the area to reproduce tides and the circulation between December 2012 and January 2013, which captures a total of seven cold front passages.

The model results demonstrate that the circulation in the Wax Lake delta area is significantly affected by the winter cold fronts. The major findings are: (1) Water fluxes in the delta distributary network are not solely propagated within the channels but also between the channels, indicating inundation process by water intrusion onto the saltmarshes, which accounts for ~25% of water flux. (2). The current flows follow the wind direction change. Along-channel current dominates while cross-channel water transport occurs at the southwester lobe during post-frontal passage. The long-term impact on sediment transport will be the lobe shift to southeastward and thus lead to a significant change in geomorphology in the delta. Water intrusion and a temporary reverse flow are observed from model results in the delta channel tip during prefrontal passage. (3) The cold-front-induced flushing event lasts 41-185 hours that flushed out 32% to 76% of total waters by seven cold front events. (4). Subtidal energy accounts for over 45% of total energy while tidal energy contributes to less than 25%. (5) Cold front-induced wind is the most important factor and dominates the hydrodynamic circulations of the Wax Lake delta in winter.

CHAPTER 1 INTRODUCTION

1.1 BACKGROUND

1.1.1 Deltas

1.1.1.1 Definition and Formation

River delta, a "triangular" area at a river mouth, similar to the shape of the Greek letter delta (Δ), is defined as a geographic landform of coastal sediment deposition where the river flows into a standing body water (Celoria, 1966; Coleman et al., 1986; Roberts et al., 2012). A river delta is formed due to sediment accumulation delivered by the river where the deposition is faster than the re-suspension and redistribution of sediments by waves, tides, and currents. These depositional features have both subaerial and subaqueous expressions (Coleman et al., 1986; Roberts et al., 2012). Deltas can form in seas, oceans, estuaries or lakes. Deltas can have dynamic deposition that undergoes significant changes in short time (~ days - months) and experience alteration in both horizontal and vertical directions over very short distances (~ m - km). The rapid change of deltaic landscape through very short time is due to large volumes of sediment transport. In terms of the size of sediment, coarse sediment including sand and gravel, is found in high energy environment near the river mouth; in contrast, fine sediment, consisting of silt and clay, is found in low energy environment near the open ocean. One typical deltaic environment has three components: flat subaerial delta plain, shallow water steep delta front, as well as deeper water pro-delta which is far from the river mouth. Delta is usually characteristic as a distributary network system, crossed by either active or abandoned channels that are separated by vegetated or shallow water areas. One way these distributary networks may form is the result of deposition of mouth bars (a sand and/or gravel bar created in the middle of a river channel). When this mid-channel bar is deposited at the mouth, the original flow is routed around

it, leading to additional deposition at the upstream of the mouth bar and therefore splits the river into two distributary channels. One good example of this process is the Wax Lake Delta in Louisiana (NCED, 2007; Edmonds, 2009; Coasts & Habitats, 2010) .

Most of the world's major deltas occur at mid- to low-latitudes, so that they usually form extensive wetlands of high biological productivity and fertility, making them very important conservation areas. These are the regions where sediment and vegetation accumulate rapidly.

1.1.1.2 Processes and Classification

Deltas are typically classified according to the dominating control of sediment transport in front of the delta, either by a river, waves, or tidal currents. Those controls have different impacts on the way the sediment is redistributed, thus having a large effect on the shape of the resulting delta. The shape of a delta, accordingly, represents the balance between sediment accumulation and removal by the ocean. In order for a delta to maintain its size, the river has to carry enough sediment to keep marine processes under control (Coleman et al., 1986).

In river-dominated deltas where the speed of river water is relatively high compared to the tidal currents, outflow is turbulent that promotes mixing. River-dominated deltas are supplied by a strong flow of fresh water and continental sediments, and are usually formed in marginal seas. The well-known examples are the Yellow River Delta in China; and the Mississippi River delta (including the Wax Lake delta) formed where the Mississippi river discharges into the Gulf of Mexico (Frazier, 1967). River-dominated delta usually extends seaward, terminates in well-developed distributaries (i.e., the split end of the river), and thus leads to a bird-foot shape or

bifurcating distributary channel network. The wave-dominated delta is formed where wave energy overweighs the influence of river and tides. In this case, wave erosion controls the shape of the delta, causing the sediment from river mouth deviated along the coastline. Wave refraction takes place and thus wave crests tend to become parallel to the shoreline. Deltas of this form, such as Nile Delta, tend to have a characteristic triangular shape, fewer channels (usually one main exit channel), and a smooth beach front/shoreline. Wave-dominated deltas are generally smaller than river- and tide-dominated deltas. Tide-dominated deltas are obviously formed where tidal currents are stronger than freshwater discharge and wave action, such that they prevent density stratification and thus the distributary mouth becomes well mixed. Sediment is moved when sediment ridges are formed within the distributary mouth, parallel to the direction of river flow and perpendicular to the coast, producing a ragged outline to the delta. Tidal deltas behave very differently from river- or wave-dominated deltas, since tide-dominated deltas may tend to have more than one main distributary channels. For river- and wave-dominated deltas, however, as soon as a distributary silts up, it will be abandoned; and at the meanwhile a new channel will form elsewhere. In a tidal delta, in contrast, new distributaries are formed during high-water volume times, such as floods or storm surges. And those distributary channels will silt up slowly at a nearly constant rate until they fail. In addition, tide-dominated deltas are generally funnel-shaped, having many braided channels, when sediment transports perpendicular to the shoreline.

However, few deltas fall into one of the above three types. Instead, in most occasions, the delta shape is determined by more than one process so that a large number of deltas are classified as having more than one characteristics of river-dominated, wave-dominated and tide-dominated deltas.

1.1.2 Overview of the Mississippi River Delta

1.1.2.1 Introduction

The Mississippi River Delta (different from Mississippi Delta, which is an alluvial plain located about 300 miles northward in western Mississippi along the Mississippi River.) is the modern deposited alluvium built-up from the Mississippi River when it slows down and enters into the Gulf of Mexico (GOM). The Mississippi River is the largest river on the North American continent, draining approximately $6559{,}500\ km^2$ (Roberts and Sneider, 2003). While this deltaic region, over 5,000 years, is a 3-million-acre ($12{,}000\ km^2$) area, stretching from Vermilion Bay east to the Chandeleur Islands on the southern Louisiana coast, including the city of New Orleans (Couvillion, et al., 2011). The Mississippi River Delta Complex contains numerous fluvial landforms, including major river channels and levees, bayous, swamps and marshes, lakes, tidal flats, barrier islands, and other shallow environments. The water salinity changes from fresh to brackish to marine. Although the climate is subtropical, hurricanes and winter storms, as the major climatic events, usually strike the region, causing flooding derived from upstream runoff. It is not only part of the Louisiana coastal plain, but one of the largest areas of coastal wetlands in the United States. The Mississippi River Delta is the 7th largest delta on Earth (USGS) and is an important coastal region for the United States, containing more than 2.7 million acres ($4{,}000\ mi^2\ or\ 11{,}000\ km^2$) of coastal wetlands and about 40% of the salt marsh in the U.S. The coastal area is the nation's largest drainage basin and drains about 41% of the United States into the Gulf of Mexico at an average rate of 470,000 ft^3/s (or 1330.8918 m^3/s). The delta studies in the Holocene Mississippi delta system have mainly focused on the Atchafalaya-Wax Lake deltas since the early 1970s, when the deltas emerged as subaerial features after the unusually high flood of 1973 with the peak discharge of about 20,000 m^3/s.

1.1.2.2 Wetland Loss

The Mississippi River Delta together with Chenier plains in LA, are the two most severe sites in the U.S. that are experiencing wetland loss and barrier island erosion (Penland, et al., 1990). The rapid sea level rise (the highest rate record of 1.19 cm/yr at Eugene Island, LA) due to delta-plain subsidence and the deficiency of terrigenous wetland sediment are two main factors that lead to rapid deterioration of the Louisiana costal zones (Penland, et al., 1990). The wetlands are rapidly eroded or turned into open-water habitats, with the land loss rate exceeding 100 km^2/yr between 1939 and 1974 (Gagliano et al., 1981; Penland, et al., 1990). And recently (from 1985 to 2010) the rate has decreased to around 43 km^2/yr (16.57 mi^2/yr), equivalent to Louisiana losing an area the size of one football field per hour (Couvillion et al., 2011). Even so, coastal Louisiana remains the largest (37%) wetland region in the nation, accounting for about 90% of the nation's total annual costal wetland loss (USGS-NWRC, 2003; Couvillion et al., 2011). If this loss were to continue at a constant rate, without restoration, an estimate of 2150 km^2 of wetland will be lost in next 50 years, directly increasing flooding threats to urban areas like New Orleans and severely impacting the state's economy, too (Stone et al. 1997). Besides the reasons mentioned above, a combination of natural and human interactions also contribute to the wetland loss. Catastrophic tropical storms and hurricanes (such as Katrina in 2005), less energetic but more frequent winter storms (such as cold fronts) significantly affect wetlands of the Mississippi Deltaic Plain, where hurricane-induced storm surge convert wetland into open water (Lovelace, 1992; Day et al., 2007). Wind-induced salt water intrusion causes previously protected freshwater vegetation to die, exacerbating extensive erosion. In addition, man-made constructions such as channel alteration may also lead to wetland loss in this area. It is quantitatively estimated that, from 1932 to 2010, the coastal Louisiana has experienced a net loss

of land area of approximately 1883 square miles (Couvillion et al., 2011), which is equal to the size of Delaware. Currently the State of Louisiana and the federal government are spending over $40 million per year to mitigate wetland loss and associated problems.

1.1.3 Wax Lake Delta

1.1.3.1 The Wax Lake Outlet

The Atchafalaya River serves as a distributary of the Mississippi (Fisk, 1952), which is 300 km shorter than the Mississippi (Roberts and Sneider, 2003). Both the Mississippi and Atchafalaya rivers contributed immense freshwater and sediment to coastal Louisiana. Because of extensive progradation during the last 800 years, the course of modern Mississippi River in coastal Louisiana has undergone a reduction in gradient and thus produced a flow efficiency in the Atchafalaya River channel. There are two outlets for water and sediment from the Atchafalaya River into the Atchafalaya Bay (Figure 1.1): the first one is the natural Lower Atchafalaya River outlet that passes Morgan City; the other is the artificial Wax Lake Outlet to the west, which was dredged from Grand Lake - Six Mile Lake to the bay in 1941. **S**ince the 1940s, sediments have been accumulating at the mouth of the two outlets to form two bayhead deltas that represent the embryonic stage of a new major Mississippi River delta lobe (delta growth > 6 m/yr since 1950s; Roberts et al., 1980; Roberts, et al., 2003a). The Wax Lake is a lake located in St. Mary Parish, Louisiana, converted into an outlet channel (the Wax Lake Outlet) to divert water and sediment from the Atchafalaya River through Wax Lake outlet channel to the Gulf of Mexico. The Wax Lake outlet, about 20 km upstream from Morgan City in Louisiana, is a man-made 30-mile long channel created by the U.S. Army Corps of Engineers (USACE) in 1941 to divert about 30% of the water and sediment from Mississippi River by the Atchafalaya River to the Gulf of Mexico.

It serves not only as an efficient and shorter path (The of the Wax Lake channel dredging in 1942 shortened the distance between the lower basin lakes and Atchafalaya Bay by 21 km; Schlemon, 1975) for Atchafalaya discharge to flow into the Gulf of Mexico (Latimer and Schweizer, 1951; FitzGerald, 1998), but also helps reduce the flooding threats at Morgan City, LA, with the design flood flow capacity of the outlet $12{,}000\ \mathrm{m}^3/s$ (USGS, 2008). The significant gradient advantage due to shorter path resulted in the flow increase down the man-made Wax Lake Channel, from initial design of 20% to approximately 30% of total Atchafalaya flow.

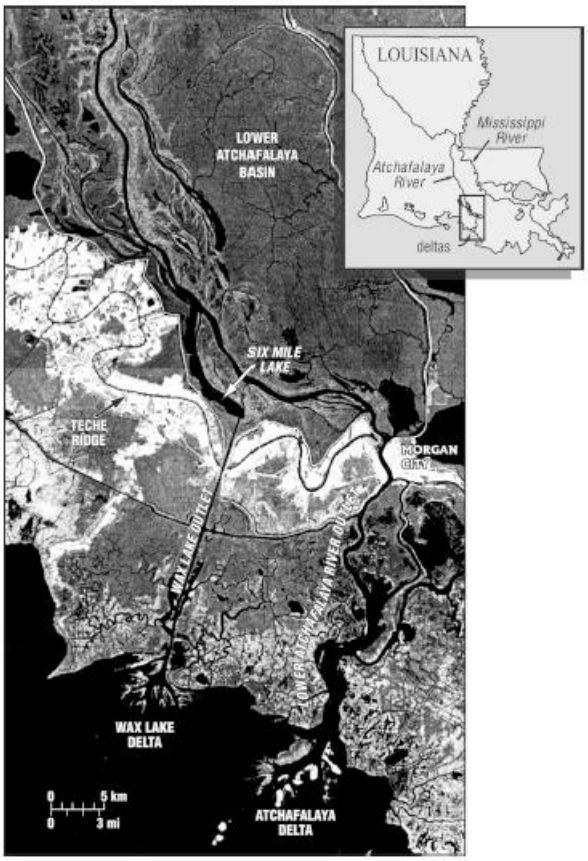

Figure 1.1 Location map of the Atchafalaya River, Atchafalaya Basin, and both the Atchafalaya and Wax Lake Deltas (Roberts et al., 2003).

1.1.3.2 The Wax Lake Delta

The Wax Lake Delta started building seaward since about 1980s (Kim et al., 2009; Roberts et al., 2003). The average annual discharge between 1981 and 2000 has been calculated at $6{,}523\ \mathrm{m}^3/s$

and average sediment discharge down the Atchafalaya is approximately $75{,}200 \times 10^3\ ton/yr$ (Roberts et al., 2003). The Wax Lake delta, as part of the Atchafalaya-Wax Lake bayhead delta complex, is a river-dominated delta (Wellner et al., 2005; Falcini and Jerolmack, 2010; Edmonds et al., 2011) formed by rapid sediment deposition following the creation of a canal through Wax Lake off of the Atchafalaya River in 1941. It is located downstream end of the Wax Lake Outlet, roughly 20 miles southwest of Morgan City adjacent to the Atchafalaya delta. It receives 34 million tons of sediment per year. In the 64 years between 1941 and 2005, the Wax Lake was completely filled with sediment and the delta prograded with a rate of approximately $400\ \mathrm{m/yr}$ (Roberts, 1997). Associated with this growth has been the development of a network of channels (Wellner et al., 2005; Edmonds and Slingerland, 2007), separated by vegetated islands/bars that continues to evolve as the delta advances seaward around 1980 (Roberts et al., 2003). The Atchafalaya River receives about 30% of the Mississippi River flow discharge at the Old River Diversion (Roberts, 1998; Allison et al., 2000; Walker and Hammack, 2000) and 40%-50% of sediment load (Mossa, 1990). The Lower Atchafalaya River (LAR) transports ~70% of the upper Atchafalaya River freshwater discharge, meaning a significant source of both freshwater and sediment. LAR max freshwater discharge occurs from Jan through July, with transport rate as high as 7200 m^3/s (USGS, 2001). In contrast, the Wax Lake Outlet (WLO) transports most of the remaining 30% water and sediment of the upper Atchafalaya freshwater discharge to Wax Lake Delta (Allison et al., 2000), with freshwater outflow as high as 5800 m^3/s from Jan through July (USGS, 2001). The Atchafalaya-Wax Lake Delta system represents an embryonic stage of a new major delta lobe in the Mississippi River delta system (Roberts, et al., 2003a). Even though the Atchafalaya River captures nearly 60% of the Mississippi's suspended load, the Coastal Studies Institutes (CSI) studies at Louisiana State University (LSU) show that the

Atchafalaya and the Wax Lake Delta are both sand-rich (nearly 70% sand). Wave action, water level setup and setdown, and abrupt wind shifts associated with winter cold front passages resuspend fine-grained by bay sediments and transport them to the adjacent continental shelf. Roberts et al., (2003) stated that the deltas currently fill most of Atchafalaya Bay and will soon prograde onto the continental shelf announcing the final stage of this evolution from lake deltas (Atchafalaya Basin) to bayhead deltas (Atchafalaya Bay) to a shelf delta on the inner continental shelf. At the point of becoming a shelf delta, a new major delta lobe in the Mississippi River delta system will be developing.

The Wax Lake Delta has not been altered by human activities (such as navigation channel dredging in the adjacent Atchafalaya delta) and represents an outstanding natural setting example for studying deltaic formation in early stages and sedimentary processes. The delta has built up into Atchafalaya Bay since 1973 and is still growing rapidly at present. Since Hurricane Katrina, the delta drew much more attention as a model for delta regrowth in the Mississippi River Delta to restore habitat and protect against storm surge.

1.1.3.3 Why Wax Lake is So Important/Special?

1) A growing delta;

The current state of modern Mississippi Delta lobe, which has been built in the past 600-800 years, has illustrated many key issues of how human have affected a natural self-organized system and dramatically reduced its resilience. Although the motivations for manipulating, stabilizing and developing the Mississippi channels into the coastal economic zone are good and understandable, their consequences on the delta as a self-maintaining structure have been proved

to be catastrophic. If we trace back to the history, the Mississippi River Delta has existed since Cretaceous period (146-66 Ma), and has maintained itself through Pleistocene epoch (2.58 Ma-11,000 yrs) with sea level changes over 100 meters. This deltaic process thus created most of the modern Louisiana coast over the past 5000 years, which however has now lost nearly 1/3 of its total area. One interesting disruption pattern took place by comparing the shape and channel network of the current bird-foot Mississippi Delta (Figure 1.2 right) with that of a healthy, prograding, and natural Wax Lake delta (Figure 1.2 left) created in the Gulf of Mexico from an adjoining distributary but not impacted by human activity.

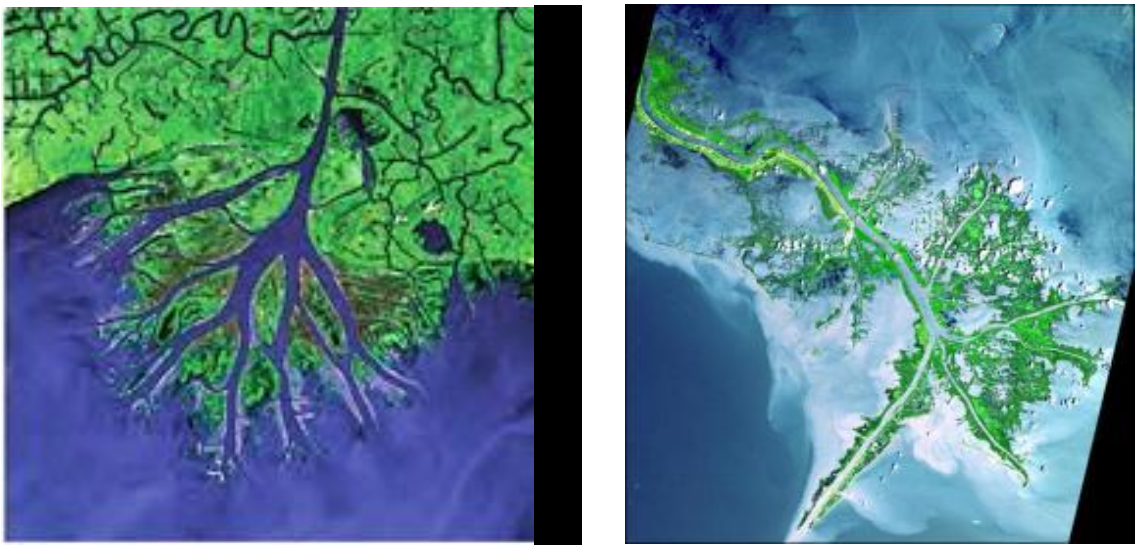

Figure 1.2 The Active, Prograding Wax Lake Delta (left) in Contrast to the Main Bird-foot Mississippi Dela (right). Sources: (A) LANDSAT 7 WorldWind Geocover 2000. (B) Courtesy of United States Geological Society National Center for EROS and NASA Landsat Project Science Office.

Figure 1.3 shows the USGS prediction on 100+ years of land change for southeast coastal Louisiana since 2003. “Coastal Louisiana has lost an average of 34 square miles of land, primary marsh, per year for the last 50 year. From 1932 to 2000, coastal Louisiana has lost 1900 square miles of land, roughly an area the size of the state of Delaware. If nothing is done to stop this land loss, Louisiana could potentially lose approximately 700 square miles of land, or about

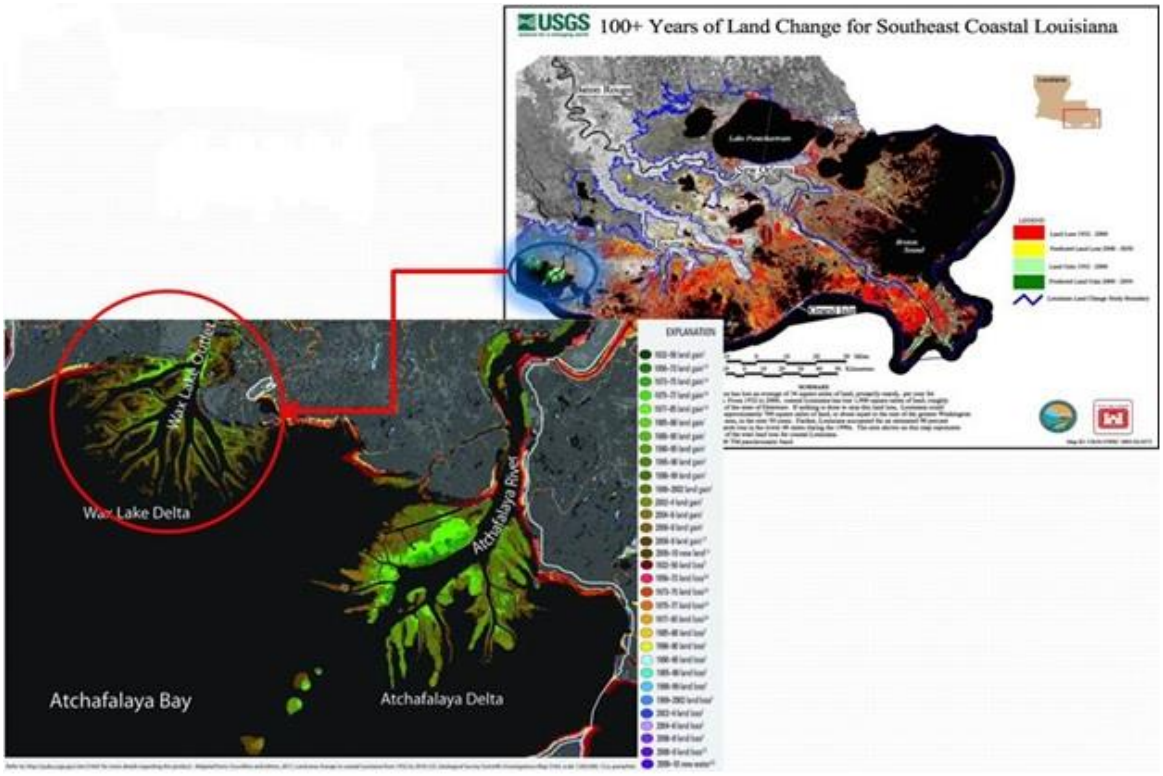

Figure 1.3 USGS 100+ Years of Land Change for Southeast Coastal Louisiana

equal to the size of the greater Washington D.C.-Baltimore area, in the next 50 years. Further, Louisiana accounted for an estimated 90% of the coastal marsh loss in the lower 48 states during the 1990s" (USGS-NWRC, 2003). The area shown on this map represents over 75% of the total land loss for coastal Louisiana. However if we take a closer look at those 'red' areas in the map, we may see a bit of green, where the Atchafalaya Basin is still growing: One lobe is the main Atchafalaya delta; the other is Wax Lake delta. According to van Heerden and Roberts (1988), in the 1970s, subaerial growth of the bayhead Atchafalaya delta resulted from sediment infilling of the Atchafalaya River Basin and flood events that delivered an increased sediment load from the basin to the river mouth in the Atchafalaya Bay. Since then, flood events and human alterations have contributed to or reduced delta growth (Flocks et al., 2002). Van Heerden and Roberts (1988) described the delta stratigraphy as "old bay" fill and prodelta deposits that coarsen

upward into distributary and levee deposits. Roberts et al., (1997) described a similar geologic framework from the Wax Lake Delta. Figure 1.4 shows the full progression of images on the Wax Lake delta building, which are from aerial photography and satellite images. The Wax Lake Delta represents one of Louisiana's most dynamic coastal environments. The growing Wax Lake delta does not counters the statement of insufficient sediment for land building against subsidence but also proves the feasibility of land building to the lower Mississippi River (Kim et al., 2009).

2) A self-maintaining, healthy, and stable delta;

The Wax Lake Outlet dated back to the 1940's, when the U.S. Army Corps of Engineers dredged a 30-mile long diversion to funnel off some of the Atchafalaya's flow and spare a catastrophic flood in Morgan City. The Wax Lake delta, where the Atchafalaya River flows into the Gulf of Mexico, was then formed by sediment following this construction of a canal through Wax Lake in 1941. And then not much happened, until the abnormal spring flood in 1973, which is considered to be with the largest discharge in the century, sent a giant plug of mud and dirt down the Atchafalaya River and into the Wax Lake. Ever since then, the new delta maintained itself, by sewing together a maze of tiny bayous, islands and mud flats. There's been a staggering amount of land building. By air, even in high tide, the new delta pops through the surface, a mix of muddy water, greens and pastels. In fact, the Wax Lake Outlet carries far more sediment than meets the untrained eyes, as sand and dirt fall to the water bottom. The very existence of southeast Louisiana proves that such diversions build land. The wax Lake Delta is also a clear example of how a thriving marsh can recover from a storm. Since after Hurricane Katrina and Hurricane Rita struck the area in 2005, damage to these wetlands was observed in the aftermath

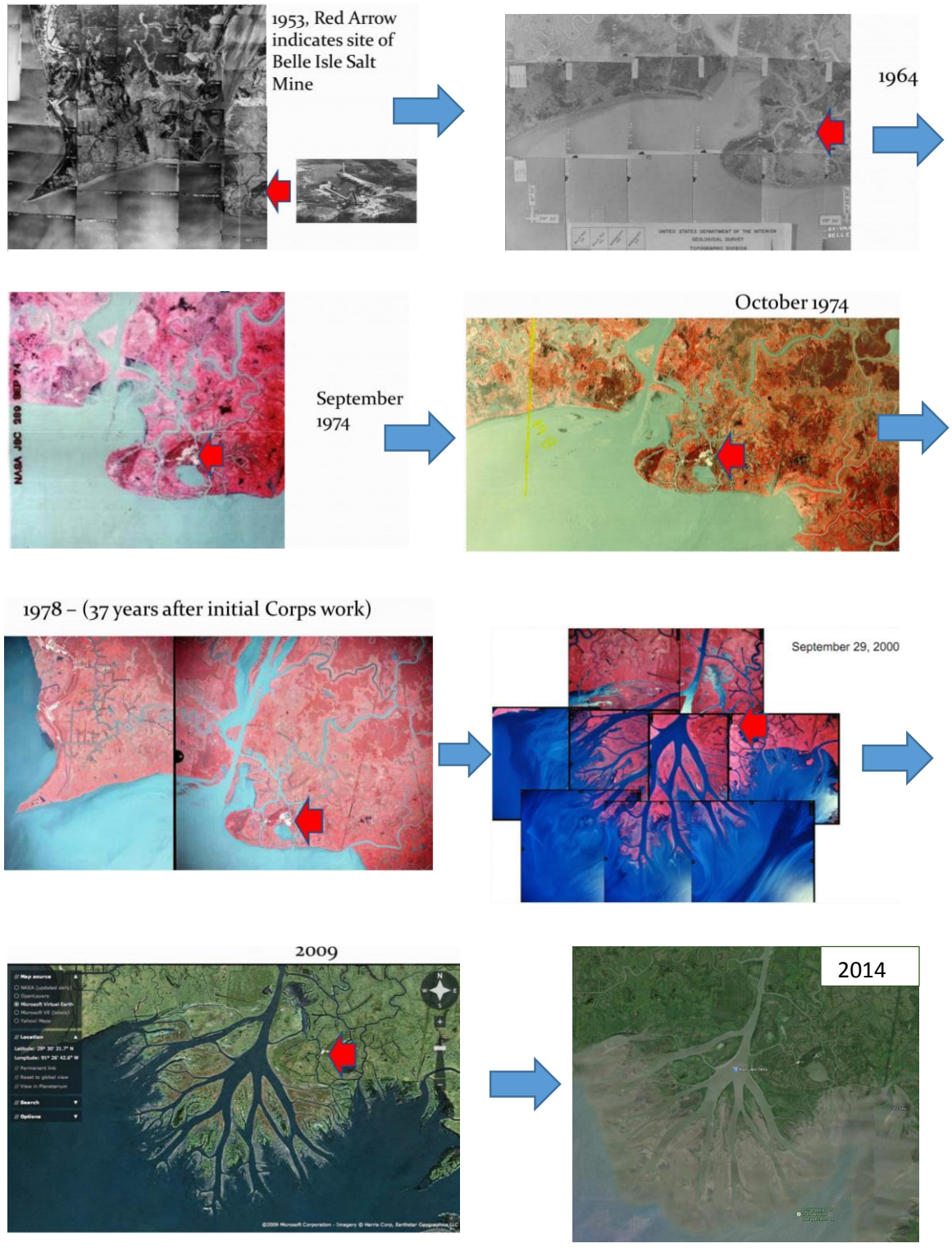

Figure 1.4 The full progression of images on the Wax Lake Delta Building (http://noladishu.blogspot.com/2011_11_01_archive.html, http://www.fieldandstream.com/files/editor_files/images/WaxLakePhotos.pdf, google earth)

of the storm, but there was not a significant lasting impact. Instead, the delta has served as a model for restoring wildlife habitat and protection against storm surge in the Mississippi River delta region. The Wax Lake Delta has been a rare success story in coastal restoration because it is fed with sediment from the Atchafalaya River. The steady supply of mineral-rich sediments from the river helps make these wetlands more resilient and allows them to recover quickly when damaged. This passage has been a monumental victory for the cost and that funding in the near future should help move along big coastal restoration projects. The Conservationist Blog at Field & Stream even commented the Wax Lake Delta as an accidental Eden in the Atchafalaya since it is "the biggest success story (so far) in restoring the marshes of southern Louisiana".

3) A good example for study of deltaic formation.

Although the Wax Lake delta was initially constructed entirely artificial by USACE, it has been allowed to build naturally by sediments deposited through the diversion with little anthropogenic pressure ever since. The nascent and rapid evolution of this growing delta is apparently consequently often used in studies of deltaic formation. The discussion on whether it is feasible to build new land in the Mississippi River delta has become a heat topic. Among them, Kim et al., (2009) advanced earlier models (Parker et al., 1998; Kostic and Parker, 2003; Parker et al., 2006, 2008) to bring up a quantitative sediment transport and delta-building model in order to explore the feasibility of building new land in the Mississippi delta. Furthermore, the Wax Lake delta was successfully hindcasted and verified by this land-building model.

As an actively prograding sub-delta of the greater Mississippi River Delta, the Wax Lake delta is viewed by geoscientists, engineers, and ecologists as the primary analogue for land-building processes that can be harnessed elsewhere in the region. The delta is currently exposed to several patterns of flooding, due to tropical or winter storms, which can produce very high storm surges that significantly influence the delta morphology. So the study of hydrodynamics of the Wax Lake Delta is especially important for Louisiana residents as well. That is also one of the motivations of this dissertation. This study is not only helpful to understand environmental, social and economic sustainability in Wax Lake delta, but also sets a good example for coastal landscapes of the Mississippi River and deltaic coasts around the world.

4) Economy, ecosystem and residence

The environments in the coastal Louisiana are muddy, shallow, and rich in nutrients, which contributes substantially to the seafood and economy of the state. The state economy and the well-being of the citizens of Louisiana are intricately linked to how we act to preserve our coast and the environment. Louisiana boasts 40% of the country's wetlands (Stone et al., 1997; Penland et al., 1990; Coleman et al., 1998), but accounting for 80% of the nation's wetland loss resulting from the combined effects from natural processes as well as human activities (Penland et al., 1990). This disparity impacts not just our state, but our entire country. And this dissertation focusing on coastal deltas will help provide solutions to these important problems. On the other hand, a better understanding of hydrodynamic circulation and sediment transport within those coastal areas is essential to environmental, economic, ecosystem (larval transport and fish population by strong advection) and residential aspects.

In addition, coastal Louisiana is rich in oil and gas and has a heavy industry presence. As we have seen from the ongoing biggest oil spill in history following the explosion and sinking of the Deepwater Horizon oil platform on April 20, 2010, Louisiana coast is facing a serious problem of contamination by the massive oil and dispersant applied at the spill site. As the oil gets to the shore and coastal wetland, windinduced transport plays an important role in the extent of the affected area.

1.1.4 Cold Fronts

1.1.4.1 Definition

From meteorological and climatological points of view, the cold front weather system is defined as the leading edge or the boundary/transition zone (25-250km) interface between heterogeneous air masses where colder, drier and denser mass of southward polar air is advancing towards, finally replacing, warmer, moister and lighter northward air, which lies within a fairly sharp surface trough of low pressure (Hsu, 1988; Mossa and Roberts, 1990; Grenci and Nese, 2006). Figure 1.5 represents an idealized model, a schematic plan view of the surface wind fields associated with a cold front as it advances from NW to SE summarizing the wind system of a passing cold front. In the literature, weather systems related to strong cold fronts are also called winter storms, extratropical storms, or extratropical cyclones (Walker and Hammack, 2000; Pepper and Stone, 2002; Keen, 2002).

When the cooler and denser air wedges under the less-dense warmer air, the cooler air lifts. This upward lifting motion causes lowered pressure along the cold front and can cause the formation of a narrow line of showers and thunderstorms when enough moisture is present. On weather

maps, the surface position of the cold front is marked with the symbol of a blue line of triangles/spikes pointing in the direction of travel (Figure 1.5). A cold front's location is at the leading edge of the temperature drop off, which in an isotherm analysis would show up as the leading edge of the isotherm gradient, and it normally lies within a sharp surface trough. Cold fronts move faster than warm fronts and can produce sharper changes in weather. Since cold air is denser than warm air, it rapidly replaces the warm air preceding the boundary (Carlson, 1991; Browning and Gurney, 1999; Grenci and Nese, 2001, 2006; Holton, 2004; Ahrens, 2007; Markowski and Richardson, 2011)

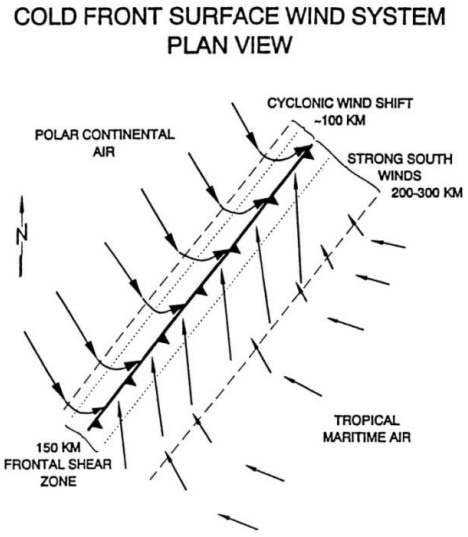

Figure 1.5 winds of the cold front system (from Roberts et al., 1987)

1.1.4.2 Meteorological Characteristics of Cold Front Passages

Cold front processes take effects a large spatial scales. Temperature changes across the boundary can exceed $30\ ^{o}C\ (54\ ^{o}F)$ (e.g., The largest 24-hour temperature change in Lamberton, Minnesota was 71 degrees on April 3, 1982, where the high was 78 degrees and a vigorous cold front dropped the temperature to 7).When enough moisture is present, rain can occur along the boundary. If the instability along the boundary is significant, a narrow line of thunderstorms can

form along the frontal zone. If the instability is less, a broad shield of rain can move in behind the front, which increases the temperature differences across the boundary. Cold fronts are strong in the fall and spring transition seasons and weakest during the summer.

In the northern hemisphere, a cold front usually causes a shift of wind from southwest to northwest clockwise, also known as veering, and in the southern hemisphere a shift from northwest to southwest, in an anticlockwise manner. During a typical frontal passage (Crout 1983), winds from the southeast and south intensify as the front approaches from the northwest. Generally, cold fronts can be summarized by these characteristics in Table 1.1.

Table 1.1 Summary of Characteristics of Cold fronts (Li and Chen, 2014)

Weather Phenomenon	Prior to the Passing of the Front	While the Front is Passing	After the Passing of the Front
Temperature	Deceasing steadily	Cooling suddenly	Steadily cooling
Winds	• SW to SE (northern hemisphere) • NW to NE (southern hemisphere)	Gusty; shifting	• N to W, usually NW (northern hemisphere) • S to W, usually SW (southern hemisphere)
Air Pressure	Deceasing steadily	Lowest, then sudden increase	Starts to increase steadily
Precipitation	Light rain is possibly produced in the warm sector.	Prolonged rain or thunderstorms	Showers, then clearing

1.1.4.3 Cold Fronts vs. Tropical Storms

Tropical storm, by definition, is an organized system of thunderstorms around a circular low-pressure center that derives its energy from warm ocean waters and has winds between 63 and 119 km/hr (Kusky, 2003). Tropical storm is generally stronger than a tropical depression, but weaker than a hurricane. If the winds continue to increase in speed, a tropical storm may become a hurricane. On the other hand, if the subtropical storm remains over warm water for several

days, it may eventually become fully tropical, and be called a tropical storm. This happens when thunderstorm activity starts building close to the center of circulation, and the strongest winds and rain are no longer in a band far from the center. The core of the storm becomes warm, and the cyclone derives all of its energy from the "latent heat" released when water vapor that has evaporated from warm ocean waters condenses into liquid water.

Because cold fronts are of higher frequency of occurrence, have larger area of coverage, and shift wind as a persistent sequence from repeated directions of approach, they are thought to be affecting more on a cumulative basis than the occasional tropical storms. One does not find warm fronts or cold fronts associated with a tropical cyclone (Roberts et al., 1987; Moeller et al., 1993; Li et al., 2009).

Although the destructive effects of tropical storms and cold fronts (also winter storms) can be similar, the two types of storms differ in their source of energy and structure. Tropical storms derive energy from warm ocean water and the latent heat that is released as rising air condenses to form clouds. While cold fronts obtain their energy from the horizontal temperature contrast between air masses on either side of a front. Structurally, tropical storms have their strongest winds near the earth's surface (a consequence of being "warm-core" in the troposphere), while winter storms have their strongest winds near the tropopause (a consequence of being "warm-core" in the stratosphere and "cold-core" in the troposphere). "Warm-core" refers to being relatively warmer than the environment at the same pressure surface. "Pressure surfaces" are simply another way to measure height or altitude.

1.1.4.4 Characteristics of Cold fronts along LA Coast

Cold fronts are the prevailing regional weather pattern along the U.S. GOM, with a 3- to 7-day interval (i.e., recurrent period; Fernandez-Partagas and Mooers, 1975; Angelovic, 1976; DiMego et al., 1976). There are totally about 30-40 cold fronts passage across the Louisiana coast each year between mid-October and late March-early April (Chuang and Wiseman, 1983; Hsu, 1988; Roberts et al., 2003a; Moeller et al., 1993). Along the subtropical Gulf coast, the southernmost, trailing edges of the cold fronts predominate, with cyclonic activity passing normally farther north. Cold fronts generally move from west to east, transiting temperate and subtropical regions, and are characterized by a sequence of orderly spatial and temporal changes in wind speed, wind direction, barometric pressure, air temperature, and humidity in the coast environment (Figure 1.6; Roberts et al., 1987; Mossa and Roberts, 1990). The natural variability of cold fronts through the season includes orientation, direction of propagation (west to east, or north to south), angle of approach (the angle to that of the coastline orientation,), propagation speed (controlling the duration of wind forcing), cold front wind strength/forcing or energy (characterized by pressure gradient force, propagation speed, air temperature, and humidity characteristics). All of these factors will determine in large part the kind and amount of impact that a cold front passage will have on a coastal region/environment, and are ultimately the main factors to sedimentation processes such as sediment transport, erosion, and accretion (Robert et al., 1987; Mossa and Roberts, 1990). These factors also affect coastal wave and current generation in addition to sea level setup and setdown. While the ordered pattern of change in a cold front passage is similar from case to case, there is much individual variability, which we can see from the literature review section and the result analysis in this study.

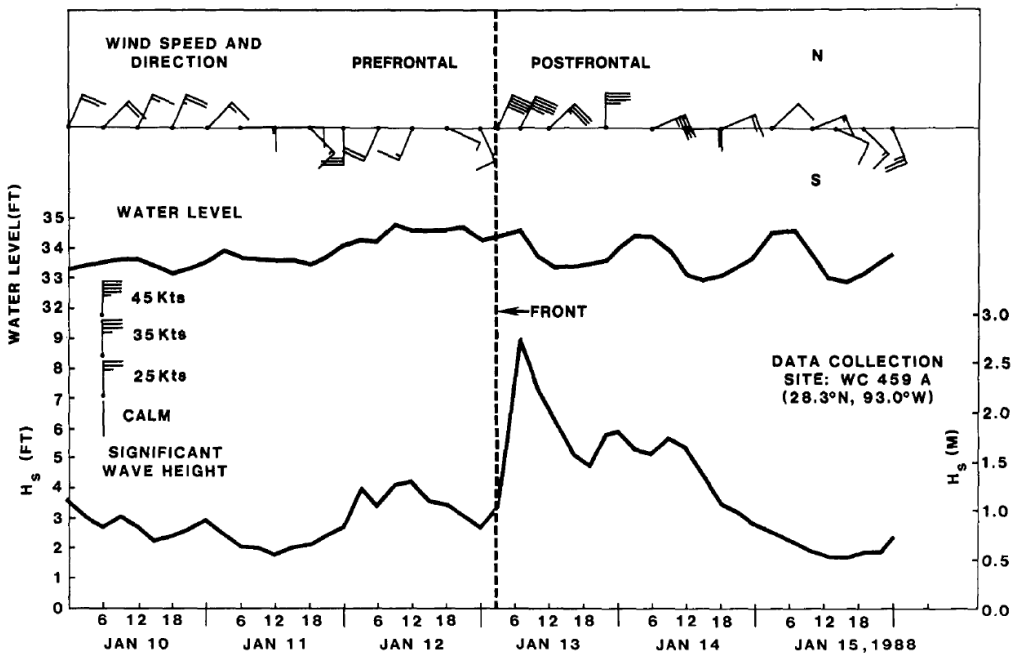

Figure 1.6 The response of wind speed/direction, water level, and significant wave height changes during the passage of a winter cold front (from Mossa and Roberts, 1990)

Along the Louisiana coast, pre-frontal southerly winds drive saline water into coastal bays and marshes. Onshore wave action created by southerly winds erodes sediment starved sandy portions of the coastline (such as Chandeleur Islands) while depositing sediment along muddy regions of the coastline (such as portions of Chenier Plain). After the cold front passes, winds shift to a northerly direction, driving down water levels in coastal areas and reducing onshore wave action. At the meanwhile, the dry air behind the front rapidly dries newly formed deposits on the shoreface, thus expediting sediment consolidation of the coastal progradation processes (Huh et al., 1991). Water levels continue to drop, promoting marsh drainage and discharge of bay waters onto continental shelf of GOM, cooling most rapidly in shallow regions.

Linking atmospheric forcing to dynamic responses in coastal environment is important for understanding the processes of coastal change. The responses of coastal environments to cold

front passages will be discussed in Literature Review section and meanwhile is the main objective of this study as well.

1.1.4.5 A Cold Front Event Consists of 3 Basic Phases

Changes associated with cold front passages can be summarized in three basic stages: pre-frontal, frontal passage, and post-frontal phase (Figure 1.6; Huh, et al., 1978; Roberts, et al., 1987; Mossa and Roberts, 1990). Roberts et al., (1987) defined those 3 phases of cold front passage, and pointed out that cold fronts have a both spatially and temporally ordered system of changes in surface wind speed, wind direction, barometric pressure, air temperature, and humidity. Below is the anatomy analysis of three phases in a cold front passage.

1) Pre-frontal phase:

This phase occurs ahead of frontal passage, in which the strong moist southerly component of Gulf winds dominate and flow towards the advancing front. At the meanwhile, warm, humid atmospheric conditions exist with generally falling barometric pressure accompanied by very small diurnal air temperature fluctuations. The frontal orientation determines surface wind direction. If the fronts approaches the coast obliquely (with an angle to that of the coastline orientation), surface winds are characterized as blowing from southeast; if the front orientation is parallel to the coast, it will promote both winds and sea surface currents from the southwest. Moreover, southerly winds blowing towards the advancing front, regardless of orientation, will always cause water setup and in the meanwhile drive a strong surface wave erosion to the barrier islands and sandy deltaic lobes (Penland, et al., 1988), resulting in sediment resuspension in shallow waters.

2) Frontal passage phase:

The cold polar continental air mass overruns warm tropical maritime air mass, causing a synoptic-scale convergence of two air masses, characterized by a squall line at its leading edge, abruptly reverses the conditions induced by the prefrontal phase with winds rapidly clockwise rotating to northerly. During this phase, winds have a stronger vertical (cross-shore) component than the horizontal (alongshore) component, accompanied by decreasing barometric pressure and rain squalling. Strong and variable winds exist with a characteristic sharp shift of wind direction from a southerly to a westerly component (Roberts et al., 1987; Mossa and Roberts, 1990).

3) Post-frontal or cold air outbreak phase:

The strongest winds associated with cold front passage are during the cold air outbreak/high-pressure phase, and these winds are directed offshore. This phase happens after the frontal passage, in which wind quickly becomes northerly and strong while air temperature and humidity significantly drop with a dramatic rise in barometric pressure. The cumulative effect of is to quickly set down the elevated prefrontal water levels and produce offshore flow. Therefore it is the pre-frontal, long-fetched southerly winds that power the turbid resupension sedimentary processes, with post-frontal winds mostly setting them down and most strongly affecting sea level (Roberts et al., 1987; Mossa and Roberts, 1990).

1.1.4.6 Two End Member Types of Cold Fronts

Based on a preliminary study of 5-year historical climatological data, two kinds of cold front were discerned by Roberts et al., (1987), and both types impact the Gulf coast region: the rarer but powerful southward arctic surge (AS) and the eastward migrating cyclone (MC)

accompanied by strong low pressure. The essential differences lie in (1) the orientation of the fronts with respect to the coastline, and (2) the resulting behavior of wind-driven surface waters. The arctic surge usually produced the most extreme changes, with highest wind speed and wave heights, and a reversal of winds, which includes the longest period of SW winds. However SW winds occur rarely in migrating cyclones, replaced with SE and NNE winds instead. It is not difficult to note that the SE winds are those driving the most effective surface wave attack on Atchafalaya delta and Wax Lake delta. Besides, the strongest winds associated with cold front passage are during the post-frontal/high-pressure phase (Roberts et al, 1987; Moller et al., 1993; Lee et al., 1990; Denes & Caffrey, 1988), and these winds are directed offshore. Therefore it is the pre-frontal, long-fetched southerly winds that power sedimentary processes, with post-frontal winds mostly setting them down and most strongly affecting sea level.

1.2 MOTIVATION

The evolution of the Wax Lake Delta is dependent on: 1). Geological settings of the upstream; 2). Sediment load; 3). River discharge; 4). Tidal variations; 5). Weather induced water level fluctuations (fronts, hurricanes); and 6). Other longer term factors such as sea level change, subduction and compaction (Li et al., 2014). Aside from the sediment load and geological factors, the rest of these factors are related to hydrodynamic processes. Therefore, understanding of the hydrodynamic processes is a prerequisite of the understanding of how the Wax Lake Delta system works in its evolution. The tidal range in the Wax Lake delta is usually microtidal (less than 0.5 m), while wind-induced subtidal oscillations may cause significant water exchange, especially during strong cold front events. Therefore the research topic on the water level variation and associated bay-shelf water exchange during the cold front passage is essential for a

fully understanding of land-sea interaction as well as ecosystem dynamics for better coastal management. The Atchafalaya and Wax Lake deltas are sand-rich (nearly 70% sand). Wave action, water level setup and setdown, and abrupt wind shifts associated with winter cold front passages resuspend fine-grained bay sediments and transport them to the adjacent continental shelf. It has been estimated that the average cold front exports ~400,000 metric tons of sediment from the bay.

Winter cold fronts have a significant impact on the resuspension and transport of sediments in this region, and a better understanding of the circulation during these events is absolutely necessary for determining the sediment transport patterns of the Wax Lake Delta and even the Atchafalaya-Wax Lake delta system, as well as the adjacent shelf area. Understanding the circulation of this region is also crucial for environmental studies as well. On the other hand, understanding the mechanisms of coastal change and their response to cold fronts is necessary in order to develop effective coastal management programs.

The importance of physical processes driven primarily by the winter cold front passages has been realized by Kemp et al., (1980) as a modifier of deltaic deposition both in the bay and on the inner continental shelf. Walker and Hammack (1999, 2000), Walker (2001), and Roberts et al. (2003b) have demonstrated from both satellite and in situ collected data sets that vast quantities of suspended sediments are resuspended from the delta front and exported to the adjacent continental shelf during the passage of each cold front. However no one has yet actually modeled the dynamics process of cold front passages in the region. Especially, the study of the complicated Wax Lake will eventually need the use of high-resolution numerical models. That is

why, in this study, we describe and implement a realistic numerical hydrodynamic simulation of the Wax Lake delta region.

However, this area is in the meanwhile subject to sea level rise and coastal erosion, with an average short-term (less than 30 years) rate of shoreline retreat as high as 30.9ft/yr (Penland et al., 2005). Luckily, the extensive wetlands also serve as a natural barrier to protect the cities such as New Orleans and Morgan City from hurricane-induced storm surges and flooding, respectively. At the very end, the long-term survival of those vulnerable areas will depend on both hydrodynamic circulation and sediment transport. Therefore, a better understanding of the two above processes within those coastal environments is essential to environmental, economic, and residential aspects.

Furthermore, this study of the Atchafalaya-Wax Lake system is motivated by the fact that there is a lack of understanding of hydrodynamics in this area that is constantly changing, partially because of a lack of data and partially because of a lack of a high-resolution numerical model that can resolve wet and dry or inundation in this complex area of extensive wetland. The challenge lies in that a detailed topography and bathymetry will be needed for such a model. This work can be very important because these deltas represent the next major lobe of the Mississippi River Delta Complex (Roberts and Sneider, 2003). In addition, initiation of delta building in Atchafalaya Bay provides an opportunity to study and investigate major delta lobe progradation from infancy and an understanding of the hydrodynamics is crucial for that.

As an actively prograding sub-delta of the greater Mississippi River Delta, the Wax Lake delta is viewed by geoscientists, engineers, and ecologists as the primary analogue for land-building processes that can be harnessed elsewhere in the region. The delta is currently exposed to several patterns of flooding, due to tropical or winter storms, which can produce very high storm surges that significantly influence the delta morphology. So the study of hydrodynamics of the Wax Lake delta is especially important for the safety of Louisiana residents, who live near deltas. That is also one of the motivations of this dissertation.

The Mississippi Delta has been a benchmark for understanding deltas worldwide; it is a "barometer" for coastal response to rising sea level. Using our coast as a laboratory, we will write a new chapter of deltaic research to help understand and solve coastal problems on a global scale. The ultimate goals are to: develop scientific knowledge, engineering principles, and planning tools to facilitate a resilient human presence on deltaic coasts, and to enhance the research in coastal and shelf-sea research around the world.

1.3 OBJECTIVES

The objective of this work is to determine the circulation and wind driven flows in the Wax Lake delta area during cold fronts, with numerical model experiments. The numerical model used in this dissertation is the ECOM-si (Blumberg, 1994). We are interested in the wind induced transports in the bays. The model study is for the period of December, 2012 to January, 2013. The influence of tidal and atmospheric forcing factors on nearshore hydrodynamics and exchange processes with the continental shelf will also be discussed.

The work will include:

a. Compiling data for hydrodynamics, topography and bathymetry of the study area. The data include measurements of waves, vertical profiles of horizontal velocity, river discharge and LIDAR topography data.
b. Conducting the numerical experiments.
c. Quantifying the effect of tides.
d. Quantifying cold front-induced water exchange between the Wax Lake delta and surrounding area.
e. Determining the transport over the Wax Lake delta (WLD) under winter storms.
f. Quantifying the importance of wind to transport.
g. Determining the hydrodynamics responses to wind particularly from cold front.

1.4 ORGANIZATION OF DISSERTATION

Chapter 1 provides an introduction, which includes the background information, motivation, and objectives of the study. Chapter 2 reviews related research on the Wax Lake delta and cold front. Chapter 3 describes the data and methodologies for pre- and post-processing of the data and model results. Chapter 4 introduces the numerical model ECOM-si for the numerical experiments in the Wax Lake delta region. Chapter 5, applies the ECOM-si to cold front events. Chapter 6 analyzes the model output for water elevation, currents, and transportTime series and spectral analyses are carried out with a discussion in different frequency bands. Chapter 7 summarizes all the significant findings and some suggestions for potential future work are discussed.

CHAPTER 2 LITERATURE REVIEW

2.1 THE WAX LAKE DELTA

2.1.1 The Evolution of Wax Lake Delta

The Wax Lake and the Atchafalaya deltas, are undergoing changes in the Atchafalaya Bay. Approximately 70% of flow at the Atchafalaya River passes through the lower Atchafalaya River to eastern Atchafalaya Bay, and the remainder passes through the 21 km shortcut to the western part of the bay created by Wax Lake Outlet (Roberts et al., 1980; Allison et al., 2000).

Sediments reaching the Atchafalaya Bay changed from a dominance of silt and clay to fine sand between mid-1950s and mid-1970s, during which time the lower part of the Atchafalaya River Basin was filled with assemblage of channels, sand-rich lacustrine deltas, and fine-grained overbank deposits (Coleman, 1966; Tye and Coleman, 1989). That led to a rapid sedimentation in the Atchafalaya Bay. Until late 1940s and early 1950s, when the basin was filled close to its capacity, the excessive sediment carried by the river passed the coast in huge quantities to initiate the delta building processes (Schlemon, 1975; Roberts et al., 1980). In 1963, the U.S. Army Corps of Engineers established a control structure at the confluence where the Atchafalaya and Mississippi rivers flow together, since then the Atchafalaya River has been regulated about 30% of combined discharge input from the Mississippi River and from the Red River flow regime (Roberts et al., 1980). However this initial delta building event was not noticed until a few lobes from the emerging delta became marginally subaerial in 1972 (Shlemon 1975) and fully exposed in 1973. It is also in 1973 when the abnormally high-water flood event accelerated this process, accompanied by unusually large volume and size of sediment (fine sands) diverted from the lower Atchafalaya River course and re-deposited into the Atchafalaya Bay, representing the

continuation of a systematic subaerial growth from these early stages (Roberts et al., 1980). The increased sand transport in suspended load during the spring flood of 1973 was also associated with the source and re-suspension during rapid accretion of distributary-mouth bar sand bodies (Roberts and Sneider, 2003). It is not until the early 1980s when the navigation dredging activities in the Wax Lake delta ceased, that the delta started expanding significantly. However, a weir was installed in the delta in 1988 designed to deflect discharge from the Wax Lake Outlet to the Lower Atchafalaya River Outlet. That resulted in a reduction in the growth rate of the Wax Lake delta but a coincident increase in Atchafalaya delta growth until 1994, when the weir was removed. Although the delta is in the channel elongation and bifurcation phase, it will finally fill the Atchafalaya Bay and soon prograde onto the continental shelf, finalizing the evolution from lake delta (Atchafalaya Basin) to bay-head delta (Atchafalaya Bay) to a shelf delta on the inner continental shelf. At soon as becoming a shelf delta, a new major delta lobe in the Mississippi River Delta system will be developing in a new delta cycle (Roberts et al., 2003a).

2.1.2 The Wax Lake Delta vs. the Atchafalaya Delta

Both the Atchafalaya and Wax Lake deltas have experienced similar morphological evolution and facies development (Roberts and van Heerden, 1992). Sedimentologically, both deltas are characterized as relatively coarse sediment (medium to fine sand and coarse silt) but a very thin (< 1 m) prodelta facies above the highly burrowed, and shell-rich bay bottom sediments, which remains in the Atchafalaya Bay as part of the deltas, especially in the western Wax Lake delta (Roberts et al., 1997). The growth patterns of both deltas also followed a similar trend, with the Wax Lake delta being younger due to its delayed subaerial growth.

These two deltas have prograded as silt/sand-rich wedges consisting of numerous bifurcating channels separating sandy lobes. However, their subaerial growth pattern histories do have differences, as shown in Figure 2.1 (Roberts et al., 1997; Roberts and Sneider, 2003), which was with the subaerial growth curve comparison between the Wax Lake delta and the Atchafalaya delta: Because the smaller sedimentary basins along the Wax Lake Outlet had to be filled before significant sedimentation could occur in the Atchafalaya Bay, the Wax Lake delta displayed an initial delay in the early stages of growth development. In contrast, the Atchafalaya delta was featured by numerous channels and small subaerial lobes in the 1970s. But starting from 1980, the Wax Lake delta demonstrated a dramatically increasing rate of rapid growth, indicating the Wax Lake and the surrounding open water bodies attained a sediment-filled state such that the sediment could pass straight down the Wax Lake Outlet to the Atchafalaya Bay for more subaerial exposure (Roberts et al., 1997; Roberts and Sneider, 2003). Therefore the Wax Lake delta during this period had a complex channel network and many subaerial lobes. In addition, the navigation dredging activities in the Wax Lake delta ceased in the early 1980s, signifying the delta has grown "naturally" ever since. That is why the Wax Lake delta is still being in the channel elongation-bifurcation and bar formation phase, where progradation and lobe fusion occur concurrently (Roberts et al., 1997; Roberts and Sneider, 2003); while the Atchafalaya delta is experiencing channel abandonment, lobe fusion, and bypassing of sediment to the continental shelf (via the dredged navigation channel), with channel bifurcation and progradation ceased. The significant difference between the two deltas growth patterns reflects that the east Atchafalaya delta is slowly being bypassed because of continuing of navigation dredging activities, whereas the Wax Lake delta is in a more natural state due to ceased dredging since the early 1980s. Ultimately over decades the fine-grained sediments bypassing the bay would be

transported to the inner continental shelf and downdrift coasts and produce significant deposition.

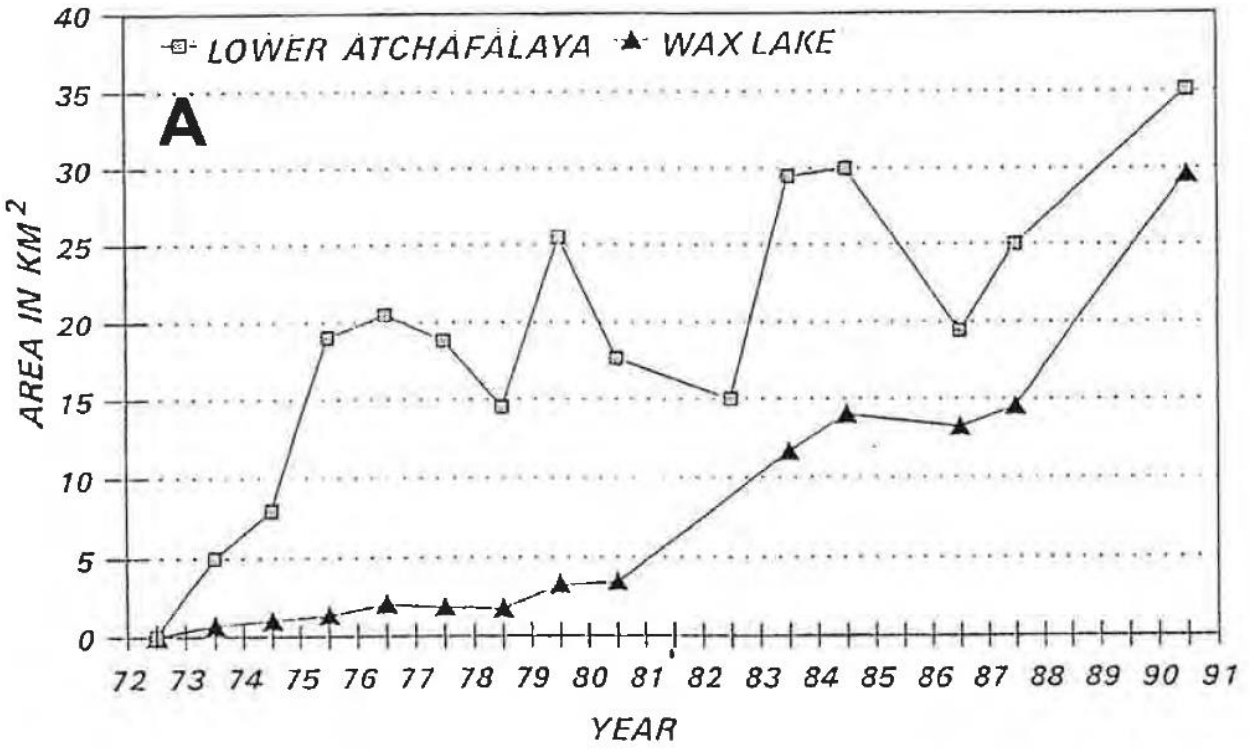

Figure 2.1 Growth history of Atchafalaya and Wax Lake deltas, calculated from areas measured from air photos and satellite images (from Roberts and Sneider, 2003)

2.1.3 Early Research

The Wax Lake delta is characterized by an incipient delta, accretional coastline and aggradational mid-upper shoreface (Li et al., 2010). This area drew a lot of attention in the last few decades because it represents one of the rapidly evolved and formed new deltas around the mouths of the Atchafalaya River and Wax Lake. This emerging delta area makes it a unique natural laboratory for multidisciplinary studies (Roberts et al., 1980, 1989, 1997; Allison et al., 2000; Neill & Allison, 2005). The initial investigations and research on the Atchafalaya-Wax Lake delta complex have started since the early 1950s, most of which were supported by many

funding agencies such as the Office of Naval Research (Geography Branch), the U.S. Army Corps of Engineers (USACE), the Center for Wetlands Resources at LSU, NASA, U.S. Geological Survey (USGS), Louisiana Sea Grant, and ExxonMobil, etc.

2.1.3.1 Sedimentary Architecture and Delta Growth:

Sedimentation study in the Atchafalaya River was initiated since Morgan et al. (1953), followed by Morgan and Larimore (1957), focusing on the interaction between suspended sediment and shoreline change at the Atchafalaya River as well as downdrift coasts. Thompson (1951, 1955) documented a guideline on monitoring delta growth in the Atchafalaya Bay. Cratsley (1975) investigated the deltatic sedimentation process in the Atchafalaya Bay, with input coming from the Lower Atchafalaya River Outlet and the Wax Lake Outlet, respectively. After noticing that the early subaerial phase of delta development was initiated during the abnormal high flood of 1973 (Shlemon, 1975), many researchers (Rouse et al., 1978; Roberts et al., 1980; van Heerden, 1980, 1983) worked on producing an up-to-date view of the nascent stages of this important developing lobe of the Mississippi River Delta Complex by starting from this very early development stage. Van Heerden (1983) provided the first detailed analysis of the important response features. According to van Heerden and Roberts (1988), in the 1970s, subaerial growth of the two bay-head deltas resulted from sediment infilling of the Atchafalaya River Basin and flood events that delivered an increased sediment load from the basin to the river mouth in the Atchafalaya Bay. Since then, flood events and human alterations have contributed to or reduced delta growth (Flocks et al., 2002). At almost the same time, the significance cold front impacts on modifying deltaic deposition patterns both in the bay (Kemp et al., 1980) and on the inner continental shelf (Adams et al., 1982) was also realized. The deltas in Atchafalaya Bay will

rapidly expand over the entire bay bottom. Soon the sand-rich subaerial deltas will emerge from the bay onto the inner continental shelf. At this point, delta evolution will have progressed from early stage lacustrine deltas of the Atchafalaya Basin to the present bay-head deltas filling Atchafalaya Bay to a shelf delta on the inner continental shelf opposite the bay.

As the Wax Lake delta became more pronounced, plus its naturally growing feature, some attention was paid to this depositional landform. Some important studies have been conducted on the sedimentation processes in the Wax Lake delta. The distributary evolution, geological framework, stratigraphy, and morphology features and descriptions of the new bay-head Wax Lake Delta as well as associated land-building processes can be found in Roberts et al. (1980), van Heerden and Roberts (1980), Van Heerden and Roberts (1988), Roberts (1997), Roberts et al., (1997), and Roberts (1998), Flocks and others (2002), Roberts et al., (2003a), Kim et al., (2009), Allison and Meselhe (2010), Paola et al., (2011), and Falcini et al., (2012). Specifically, the kinematics-induced channel-network morphology evolution of the delta growing process (John and David, 2013) was fully investigated and understood. Van Heerden and Roberts (1988) described the delta stratigraphy as "old bay" fill and prodelta deposits that coarsen upward into distributary and levee deposits. Majersky et al. (1997), Roberts et al., (1997), Majersky-FitzGerald (1998), and more recently Roberts et al., (2003a) investigated the sedimentary architecture and surface morphology of 2 bay-head deltas, describing a similar geologic framework (nearly 70% sand) and its bias toward sand-rich facies, which are associated with distributary mouth bar deposits, sand lobe fusion, as well as upstream filling of nearby delta channels. The sandy Wax Lake delta, as one the two Atchafalaya-Wax Lake bay-head deltas, represents the products of the latest delta switching event, which is being in the constructional

phase of the delta cycle (Coleman et al., 1998). In 2003, a field trip was conducted to the bay-head Wax Lake delta in the Atchafalaya Bay, based on which the Wax Lake delta growth evolution was fully investigated and summarized from both the hydrological perspective and the sedimentary deposition patterns. In the following year (2004), Dr. Harry Roberts in the Coastal Studies Institutes (CSI) at Louisiana State University (LSU) led another geological field trip (Lafayette geological society field trip) to the Wax Lake delta, which verified the Red River provenance as well as the sedimentology and sedimentary architecture (sandy) of the delta. Since 2012, the National Center for Earth-surface Dynamics 2 (NCED) set the Wax Lake delta as one of the delta land-building field sites, for the purpose of harnessing the key processes to restore the Mississippi River Delta today (http://www.nced.umn.edu/content/wax-lake-delta).

2.1.3.2 Hydrodynamics Study in the Wax Lake Delta

The Wax Lake delta is vulnerable to various meteorological, oceanic, and hydrological conditions. The bathymetry changes on the Wax Lake Delta front occurs not only during floods (high river flow) when most of the sediment arrives at the delta (Kim et al., 2009; Edmonds and Slingerland, 2007; Geleynse et al., 2010), but also during low flow (Esposito et al., 2013). Bathymetric change over both conditions were measured and the distinct patterns of bathymetric evolution were observed (John and David, 2013). Therefore, the net-deposition process is driving the channel extension.

Nowlin et al. (1998) and Chu et al., (2004) identified fall-winter recurrence of current reversal from westward to eastward on the Texas-Louisiana continental shelf, with a return period of nearly 12 days. Alongshore wind forcing is more responsible for the alongshore current reversal

events than other physical processes such as offshore eddies shed from the Loop Current and the Mississippi-Atchafalaya River discharge. Li et al., (2014) studied the energy regimes in the Wax Lake Delta, concluding that the subtidal energy (accounting for ~70%) associated winter cold front passages overweighs the tidal (~30%) contribution.

2.1.3.3 Cold Fronts Impacts on the Atchafalaya-Wax Lake Delta Complex

The sediment transport processes in the Atchafalaya-Wax Lake delta systems are determined by different mechanisms, including tides, rivers, shelf circulation, and atmospheric forcing. Sediment re-suspension, transport, and deposition are strongly impacted by wind speed and direction, particularly during strong wind events. Investigations of meteorological and oceanographic processes (Daddio et al., 1978; Crout and Hamite, 1981) suggested that significant sedimentological and geomorphic changes in coastal and nearshore shelf environments of the Mississippi River Delta are caused by winds, waves, and currents generated by succession of winter cold front passages. Wave action, water level setup and setdown, and abrupt wind shifts associated with winter cold front passages cause re-suspension of fine-grained bay sediments and transport them to the adjacent continental shelf (Roberts et al., 2003a).

The cold front impacts on modifying deltaic deposition patterns both in the bay (Kemp et al., 1980) and on the inner continental shelf (Adams et al., 1982) was first realized as soon as the subaerial growth of the Wax Lake delta was identified. Mossa and Roberts (1990) revealed an important association between riverine sediment input and the cyclic winter cold front passages that results in a periodic supply of suspended sediments to adjacent wetland or marshes. High

water level associated with floods or water level setup caused by winter frontal passages transport turbid water to adjacent marshes (Mossa and Roberts, 1990).

Roberts et al. (1997) demonstrated that the northerly wind forcing accompanying cold front passages has a tremendous impact on sediment redistribution within the Atchafalaya system (Cunningham, 1978). The storm's northwesterly winds had two main effects: First, the strong winds rapidly re-suspended sediments within the shallow bays and along the shallow shelf seaward of the bays. Second, the offshore northwesterly winds transported water and sediment away from the coast (due to Ekman dynamics) and out of the bays onto the shelf. Details on circulation and sediment dynamics in the Atchafalaya Bay and adjacent continental shelf responding to frequent cold front passages and occasional tropical storms or hurricane impacts can be found in Walker and Hammack (2000), Walker (2001a), Roberts et al., (2003b), Kineke et al, (2006), Cobb et al., (2008a, 2008b), and Li et al. (2009). Those work have demonstrated that cold front could influence the direction of LAR and WLO outflow plumes on adjacent continental shelf, altering transport and sediment deposition pattern in the region, by re-suspension of vast quantities of suspended sediments from the delta front and exported to the adjacent continental shelf. About 12% of the total sediments delivered to the coast by the Atchafalaya River are transported from the bays to the continental shelf by winter storms. However, satellite observations and in situ collected data sets indicate that the sediment plumes result from both strong postfrontal winds and bay flushing process. It is reported that some of these sediment plume can extend as far as 75 km offshore during a single cold front event (Roberts et al., 2003b). Through these processes, the prodelta facies is largely decoupled from the bay-head deltas themselves. Although the cold front process is largely responsible for the sand-rich nature of bay-head delta development of the Wax Lake Delta (Roberts et al., 2003a;

Roberts et al., 2005), Neill and Allison (2005) suggested that winter storms would cause sediment to bypass further offshore and erosion (i.e. shoreline retreat), which would prevent future land building in this area and finally constrain subaerial extension to the modern Wax Lake and Atchafalaya deltas.

Li et al. (2011) investigated the saltwater intrusion in the Wax Lake delta during cold front passages, where the associated salinity increase occurs after a high water slack (setdown) and is usually very short in duration (0.5-2 hours). They also examined the factors contributing to the total surge, among which the wind stress-induced surge constitutes approximately half of the total, while low atmospheric pressure and wave-induced setups contribute 25% each, with Coriolis effect negligible. In addition, the process of sediment accumulation in the Wax Lake delta was modeled in Xu et al. (2011).

2.2 COLD FRONT STUDIES

In the northern Gulf, local weather during the winter is dominated by cold front passages. The cold front as a weather phenomenon has been extensively studied (Carlson, 1991; Browning and Gurney, 1999; Grenci and Nese, 2001, 2006; Holton, 2004; Ahrens, 2007; Markowski and Richardson, 2011; Unified Surface Analysis Manual, 2013). The role of cold fronts and their importance affecting coastal environments is however not well established. Previous studies have shown that wind (direction and speed) is a major controlling factor for coastal water levels, sediment transport and circulation (Murray, 1975; Kemp et al., 1980; Chuang and Wiseman, 1983; Cochrane and Kelly, 1986; Moeller et al., 1993). Numerous oceanic phenomena are associated with cold front passages, such as water level variation, coastal circulation, water

exchange, sediment re-suspension and transport, , shoreline changes, as well as geomorphic evolution (Murray, 1975; Kemp et al., 1980; Kahn and Roberts, 1982; Chuang and Wiseman, 1983; Cochrane and Kelly, 1986; Mossa and Roberts, 1990; Moeller et al., 1993; Walker and Hammack, 2000; Pepper and Stone, 2004; Walker et al., 2005a; Kineke et al., 2006; Li et al., 2009). Apparently, none of those physical processes stands alone but is driven by a combination of tides, winds, river discharge, and suspended sediment load.

2.2.1 Cold Fronts and Nearshore Hydrodynamics

Influenced by the Mississippi and Atchafalaya River flows (with large freshwater discharge and sediment load), the responses of Louisiana complex deltaic coasts and estuaries to cold front systems have some specific characteristics. In general, those estuaries are bar-built, shallow (usually less than 5 m), extending only short distances (tens of kilometers), fringed by coastal marshes and barrier islands with multiple inlets. The unique and complex landscape features thus largely complicate the hydrodynamics of this region. Besides cold fronts, tidal forcing plays a minor role in the Louisiana coasts, where it is dominated by diurnal tides.

Responses of coastal ocean to passing cold fronts, include variations in water level (setup or set down) and associated water volume transport, increased waves, and circulations. Consequently, the hydrodynamics can significantly influence the sediment transport (Cundy et al., 2007) and wetland stability (Valdemoro et al., 2007). The characteristics of winter storms have been discussed and summarized in the last chapter: In the Louisiana coast the winds from these cold fronts typically have a unique pattern of changes, represented by a quick switch of wind direction from onshore or southerly wind causing water setup to a cold and strong northerly (or

northwesterly) or westerly winds that drive a subsequent set down (Hsu, 1988). This is due to the fact that the orientation of the Louisiana coastline is roughly east-west, which is different from the east coast which is basically north-south oriented.

2.2.1.1 Cold Front Impacts on Water Level and Associated Water Transport

Cold fronts can generate significant subtidal (low frequency) oscillations of water levels as well as water transport that are particularly important for the flushing processes in bays and estuaries (Chuang & Wiseman, 1983; Denes & Caffrey, 1988; Lee et al., 1990; Snedden et al., 2007).

Tides, winds, and freshwater input are three factors affecting water level variation as well as associated water exchange and circulation, with each acting on different time scales (Wang, 1979; Denes and Caffrey, 1988; Snedden et al., 2007; Feng and Li, 2010). On one hand, river discharge has a seasonal cycle, prevailing in spring. On the other hand, astronomical tides cause water level to rise and fall on a regular and predicable (diurnal and semidiurnal) basis. Thirdly but most importantly, cold fronts feature the local weather patterns during winter in the northern Gulf of Mexico, with periods of days, during which the associated surface wind field is well organized and predominant in cross-shore direction rather than alongshore direction. Over long-term, especially in winter, wind effects are the main cause of net transport in coastal bays, considering north winds associated with frontal passages which reduce water elevations and increase transport of water out of the bay (Denes and Caffrey, 1988). Kemp et al. (1980) once reported that during a given frontal event the sea level may rise and fall 120 cm in the Atchafalaya Bay. Comparing to the maximum tidal range along the northern Gulf of Mexico, it seldom exceeds 45 cm (Zetler and Hansen, 1972). The water level responses are maximized

when the wind effects are in phase with astronomical tidal effects, particularly during spring tides. Li et al. (2010) estimated the three components that contribute to the water level setup event during pre-frontal stage, and concluded that the most important factor is the wind stress (roughly contributing to 50% of the subtidal water level variations) while the effects of atmospheric pressure and wave setup equally contributed the rest of the variabilities. The Coriolis effect appeared to be negligible in the Wax Lake area where the channels are constricted. During these periods of high water elevations, high sedimentation may occur, when the marshes are flooded by Atchafalaya River or water from the Gulf of Mexico, bringing sediments and nutrients to marshes. Although Cochrane and Kelly (1986) has shown that coastal water levels along the Louisiana/Texas coastline respond most strongly to variations of the east-west wind (alongshore) components, Chuang and Wiseman (1983) found that the regional sea level responses to cold front wind forcing show a spatially non-uniform pattern. This considerable variability is mainly due to the different water depth over the inner shelf, where the shallower water favors setup from cross-shore wind stress while the deeper area is more likely to respond to alongshore wind. Since the wind rotation with cold front passage is clockwise, coastal water levels will start dropping due to offshore Ekman drift on a continental shelf before the arrival of northwest wind with the frontal passage, where rapidly falling water levels are associated with strong northwest and north wind. This sequence of events thus provide a primary mechanism for the increasing rate of water level exchange between the bays and the inner shelf accompanied by the arrival of northwest wind (Walker and Hammack, 2000). In the 3-10 day time scale, the bay and coastal water response is coupled, represented by a major water transport, whose magnitude was larger than river runoff and much stronger in winter than in summer. Wang (1979), Swenson and Chuang (1983), Lee et al., (1990), and Snedden et al. (2007) found

that the subtidal estuary-shelf exchange was mainly driven by remote alongshore wind forcing through coastal Ekman convergence rather than direct local wind stress forcing effect. Especially in winter, it has been verified that the predominant cold front-induced subtidal barotropic fluctuation of volume exchange, which is associated with north-south wind stress during the frontal passage, occurs primarily as large-scale events up to six times larger than normal tidal prism (Swenson and Chuang, 1983). Phase relations between wind, currents, and water level are discussed by Lee et al., (1990): water level lags the wind stress and currents (along-channel currents are much more energetic than cross-channel currents); and wind stress lags the currents. Moreover, strong north winds during winter storms could flush 30-50% of water volume out of the shallow bays accompanied by water level drop by more than 1 m in the Atchafalaya-Vermilion Bay regions (Swenson and Chuang, 1983; Walker and Hammack, 2000; Feng and Li, 2010). However the large variability in water volume flux rate was due to the differences in water bodies and basin geometry. Although both alongshore and cross-shore wind were shown to play almost equally important roles (the same order of magnitude) in driving subtidal water level changes inside the bay, the northwest (rather than north or northeast) wind-induced largest water level changes (Walker and Hammack, 2000) caused the most influential flushing events in the Atchafalaya Bay area. Particularly, the sediment flushed out of the Atchafalaya Bay becomes the major source for the accretion of the Chenier plain to the west (Kineke et al., 2006).

2.2.1.2 Cold Fronts and Currents

Coastal current is an important dynamical process. A coastal current with low-salinity originating from the Mississippi and Atchafalaya deltas, flows westward along the coast forming the Louisiana Coastal Current (Wiseman and Kelly, 1994), which dominates the Louisiana-

Texas inner shelf. The waters of this current system move downcoast (in the direction of Kelvin wave propagation) and are readily identifiable along the Gulf coast during the late fall, winter, and early spring. These waters respond quickly to both local and far-field wind forcing, the most important synoptic wind pattern being cold front passages (Huh et al., 1984), which occur on a time scales of 3 to 10 days during the winter season (Fernandez-Partagas and Mooers, 1975; DiMego et al., 1976). The cold front-induced water level change can be on the order of 1 m and the associated relatively swift wind-driven flow velocity can reach more than 0.5 m/s (Rouse, et al., 2004) accompanied by the current direction reversed for a brief period of time and flowing upcoast. Knowledge of the flow within these waters is important for both strategic and tactical planning for extreme weather response. A model of wind-driven currents in conjunction with a forecast of regional winds will help predict the shifts in the sediment transport and river plume.

It is well known that the upper layer ocean current, opposite to the near bottom flows, responds vigorously to wind on a short time scale (<24 hrs). In an analysis of the coherence between winds and sea surface currents on the Texas-Louisiana continental shelf, Cochrane and Kelly (1986), as well as Wang (1996) concluded that the inner-shelf current is strongly coherent with the along-shore wind component. This was argued by Nowlin et al., (1998), who claimed no significant coherence (neither spatial nor temporal) between local wind and currents in the weather band (2-10 days, i.e., cold fronts) and the diurnal band, indicating the complex variation of the Texas-Louisiana inner shelf circulation. They summarized though, in general, in the cross-shore direction, the coherence decreases with the distance from the coast; while in the alongshore direction, the coherence over the eastern region of shelf is lower than over the western region; but seasonally, the coherence is higher in winter than in the summer stratified season. Later the

wind-current coherence proposition was reasserted in Rouse, et al., (2004) by fully exploring the surface circulation in the area of Texas-Louisiana inner shelf (shallower than 20 m). They concluded that during winter downcoast wind and downcoast flow prevail. Both alongshore and cross-shore currents are wind driven. Downcoast wind induces downcoast current, with the response time of the alongshore current to the alongshore wind less than one day. In the meanwhile, downcoast wind always generate and strengthen onshore currents.

2.2.2 Responses of Coastal Environments to Cold Front Passages

2.2.2.1 Roles of Cold Fronts in Circulation Pattern and Sediment Transport

The wind forcing combined with river discharge and water level variation (rise and fall), affects the coastal circulation, sediment distribution, re-suspension and transport, as well as wetland stability (Walker and Hammack, 2000; Cundy et al., 2007; Valdemoro et al., 2007). A better understanding of the river plume during those events is also needed for environmental studies, especially necessary for determining the sediment transport in the coastal waters (Cobb et al., 2008a; 2008b). Walker and Hammack (2000), from satellite observations, has revealed the consistent patterns of circulation, sediment re-suspension and transport (a direct and rapid response), and salinity changes during the winter storm events.

The sediment plume is affected by Ekman transport (Snedden et al., 2007), wind-wave re-suspension of bottom sediment, as well as wind-forced seaward bay flushing. The final destination of re-suspended sediments is highly dependent on the interaction of river plume, tides, and wind (Roberts et al., 1989; Cobb et al., 2008b). Although Louisiana coastal circulation patterns vary in response to wind, water level, and river discharge, sometimes forced or

modulated by cold front winds (Moeller et al., 1993), the attitude of the coast as related to the front is the most important factor (Roberts et al., 1987): Fronts crossing the coast at a high angle promote strong along shore transfer of momentum, while coast-parallel fronts promote strong onshore-offshore effects. East wind, occurring more than 60% of the time, induces a westward flow of sediment-loaded river water along the coast. However west wind reverses the direction of plume movement and increases the size of the turbid plume, indicating that the river plume structure is significantly altered by the surface wind stress, especially the alongshore component of the wind (Rouse, et al., 2004). Strong northerly winds can reduce water level by more than 1 m and flush 30-50% volume of water out of the shallow bays. Adams et al., (1982) have shown that offshore-directed waves and currents associated with post-frontal phase cause sands to be transported to the southeast, even though the dominant fine-grained sediment transport is to the west. That indicated that this primary southeastward water and sediment flux is temporarily disrupting the westward flow of river water along the coast. Under high river discharge condition, the size and surface suspended sediment concentration, sediment re-suspension (could dramatically increase by 5 times; Walker and Hammack, 2000), sediment transport, as well as the seaward sediment-river water flux, in a good agreement of outgoing currents, are maximized by northwest wind. These processes could produce a large turbid coastal sediment plume as far as 180 km alongshore and 75 km offshore of the coastal Louisiana (Cunningham, 1978; Walker and Hammack, 2000; Roberts et al., 2003a; 2003b), Therefore, coastal circulation and plume dispersion during peak forcing conditions revealed even stronger responses to winds of cold fronts.

2.2.2.2 Cold Fronts and Coastal Gomorphology

As a result of the dynamical process driven by cold front passages over the northern Gulf of Mexico, the importance of storm-related sediment re-suspension and transport has been shown by Kemp et al., (1980) as a modifier of long-term deltaic deposition both in the bay and the inner continental shelf due to associated sediment redistribution. Walker and Hammack (1999, 2000), Walker (2001), and Roberts et al. (2003b) presented from both satellite and in situ collected data sets that huge amounts of suspended sediments are re-suspended from the delta front and exported to the adjacent continental shelf during each cold front passage. Different from occasional but more violent tropical cyclones (such as hurricanes Katrina, Rita, Gustav, and Ike, etc.), the less severe but more frequent cold front passages are thought to have a more cumulative long-term and periodic effect on the coastal geomorphology and they are thus widely studied (e.g. Roberts, 1987; Reed, 1989; Moeller, et al., 1993; Perez, et al., 2000; Walker and Hammack, 2000; Georgiou et al., 2005; Kineke et al., 2006). Roberts et al., (1987) studied the impacts of cold front passages on Louisiana coasts, by focusing on deposition and erosion processes at different parts of the coastline. The paper also pointed out that the intensity, speed of advance, and frontal orientation relative to the coast were primary controls on the effectiveness in forcing oceanographic, sedimentary, and geomorphic processes along the deltaic coast of Louisiana: Fronts crossing the coast at a high angle promote strong alonghshore transfer of momentum; while coast-parallel fronts promote strong onshore-offshore effects. However, as mentioned above, the long-term sediment distribution at Gulf coasts was not determined by cold front processes alone, but a more complex interaction among many other factors. The synergism of river discharge and winter storm-related sediment transport processes in Louisiana's coastal wetlands was first discussed by Rouse et al., (1978), and then by Roberts et al., (1980) van

Heerden (1980; 1983), and Adams et al., (1982), and later further discussed in Mossa and Roberts (1990). The river flood events provide sediment supply and promote the rapid subaerial growth of the exposed delta lobes; Secondly, the winter cold front processes, as another even more important mechanism for sediment distribution, may lead to significant geological consequences (erosion or deposition) at different parts of the coastline. When water level setup in the pre-frontal phase coincides with a high tide, the most effective subsequent surface wave erosion occurs, resulting in inundation of the the surrounding marshes and adjacent wetlands through a complex intersecting network of tidal channels, creating the so-called "back water effects" (Roberts et al., 1987; Mossa and Roberts, 1990). The associated drainage by turbid sediment re-suspension in shallow waters will thus cause aggradation (van Heerden, 1980; Kahn and Roberts, 1980; Roberts et al., 1987; Penland, et al., 1988). As the front passes, strong, dry northerly winds will cause rapid setdown of coastal water level and reduction of wave activity, resulting in sediment desiccation (Walker and Hammack, 2000). During this period two significant shoreline changes may take place depending on different dynamic coastal settings. The first type is shoreline retreat and deflation of washover lobes (Boyd and Penland, 1981; Kahn and Roberts, 1982). For this type of coastal environment, cold front-induced wave erosion reduces the deposition process (such as rapid delta development) as well as sediment redistribution along the inner shelf, resulting in an apparent land loss in sediment-poor coasts (such as Barrier Islands). However, cold front processes are not always associated with erosion. The second is characterized by either a sediment deposition on the shelf due to fine-grained sediment transport coming from sediment-rich coasts (such as Atchafalaya Bay) or a transitional coasts fronted by fluid mud (such as the Chenier Plain of southwestern Louisiana). Along those transitional coasts, post-frontal dry northerly winds strand fluid muds on the shoreface of

Chenier coast by energetic re-suspension events so that they rapidly lose water through evaporation to cause an increase in cohesion, forming shoreface progradation promotion (Kemp, 1986; Roberts et al., 1987; Huh et al., 2001; Draut et al., 2005; Kineke et al., 2006). Abundant suspended sediment supplies altered the marshes from deterioration to accretion after 1950s (Roberts, 1997). A separate study (Reed, 1989) concluded that the contrasting forcing and dynamical processes inherently associated with pre- and post-frontal stages were also important in marsh morphodynamic evolution. The coastal response to interactions between cold-front processes and sediments is related to both sediment supply and sediment size. Therefore cold front processes also impact the overall health and functioning of coastal bays and wetlands.

2.2.3 Cold Fronts on Salinity and Water Temperature

Salt can be used as a conservative tracer to quantify the mixing between fresh and salt water. Li et al. (2010) investigated the impact of cold front passages on saltwater intrusion in the Wax Lake delta, where a rapid and transient increase of salinity (approximately 2 PSU) occurs after a high water slack and lasts for 0.5-2 hours. During the post-frontal offshore north wind period, the salinity generally decreases when river drainage is enhanced by the extremely low water levels. After the winter storm, the salinity rises again during south wind periods (Walker and Hammack, 2000).

The effects of cold fronts on waters in shallow water areas and continental shelf were described, measured, and modeled in Nowlin and Parker (1974), Garwood et al., (1981), Huh and Rouse, (1984), and Walker et al., (1987). The results demonstrated that coastal waters evolve continuously during cold front event, where the records of water temperature shows a direct and

rapid (days) response of these shallow coastal waters to surface winds of the cold front (Moeller et al., 1993). In general, the water temperature demonstrated a daily/tidal variation and an almost steady increasing trend (Li et al., 2010). The pre-frontal southerly warm winds lead to an increase in water temperature at first followed by a rapid temperature drop associated with much colder air in the post-frontal northerly winds. The cold front process would lead to increased mixing, particularly in shallow waters, a sudden temperature decrease but a mild salinity increase through evaporation, sensible heat loss, and radiative heat loss from sea surface to atmosphere (Huh and Rouse, 1984). The more sever the cold front, the higher rate of sensible heat loss. The sea surface temperature (SST) patterns during peak forcing conditions also revealed even stronger responses to winds during post-frontal phase of cold fronts, which induces a rapid shallow water chilling process, transferring the cooler water from shallower into deeper regions, with the lowest temperatures developing in the shallowest regions (Walker et al., 1987; Moeller et al., 1993).

2.2.4 Cold Front Impacts on Ecosystems

In addition to coastal bays and coastlines, the wind-driven oscillation of the shallow bays during a frontal passage has significant implications for Louisiana's ecosystem, impacting coastal, wetland, and marine life.

Many economically important fish and nekton invertebrate species inhabit in the estuaries and bays for foraging, refuge, and reproduction during part of their life cycle, whose distribution, abundance, and diversity can be significantly influenced by cold front passages (Kneib, 1997; Castellanos & Rozas, 2001; Cattrijsse & Hampel, 2006). Spawning grounds, in contrast, are

sometimes offshore, and larvae must be transported across shelf to estuarine nursery grounds in order to achieve successful larval recruitment (Miller et al., 1984, 1985; Shaw et al., 1985, 1988; Boehlert & Mundy, 1988; Miller, 1988; Lyczkowski-Shultz et al., 1990). The successful estuarine larval recruitment is dependent upon both biological conditions and various physical processes (wind forcing, ocean currents, tides, river plumes, etc.), as well as the interactions between them (Garcia, 1983; Norcross and Shaw, 1984; Zimmerman & Minello, 1984; Childers et al., 1990). Particularly in winter, the cold front-induced fluctuation processes include, for example, water level setup and setdown, bay flushing, saltwater intrusion, sediment transport, water temperature and salinity changes. Reduction in water temperature during a cold front may trigger the fall reproductive pulse of a tropical macroalga (Morrison, 1984). The post-larval brown shrimp recruitment was also reported to be affected by cold front events when the wind changes direction, or when the water temperature and salinity change magnitudes following the weather conditions and water level oscillations (Rogers et al., 1993). The annual oyster yields along the Gulf coast are largely determined by the estuarine salinity (Tuner, 2006). For shellfish production and harvesting, the impact occurs due to low gradient in the shallow bathymetry of water bays which makes the shellfish vulnerable to exposure of municipal discharge at low water within a cold front passage with mixing and dispersion of polluted water becoming less efficient caused by water setdown after the frontal passage (Li et al., 2010). Besides netons, the cold front-induced bay oscillation and saltwater intrusion can also have a potential impact on wetland plants. A severe saltwater intrusion can put excessive stress on the marsh community and even cause mortality which will in turn cause the wetland to lose its hundreds of years of carbon storage and release excessive carbon into the atmosphere, adding more greenhouse gases (Delaune et al., 1978, 1983a, b; DeLaune & Smith, 1984; Nyman et al., 1995; J. White, personal

communications). It appears evident that the entire ecosystem can be altered by these winter storms (Gallucci & Netto, 2004).

CHAPTER 3 DATA AND METHODOLOGY

3.1 DATA DESCRIPTION

In order to investigate the influences of cold fronts on the hydrodynamics in Wax Lake delta and surrounding areas, a number of factors should be considered. It is a challenge to include all of these factors. Wind, currents, water level, and river discharges from various stations provide data to study inner-delta circulation (including the entire Atchafalaya bay). The subsequent examination of the data shall extend existing knowledge and provide new findings, such as the understanding of the momentum balance and water flux variability in this area.

3.1.1 Meteorological and Oceanographic Data

The meteorological data for this study includes winds (speed and direction), sea level air pressure, air temperature, sea surface temperature (SST), and humidity. Those data are used to study the characteristics of cold fronts from a meteorological perspective. While the parameters in oceanographic data contain water levels, currents (velocity and direction), and wave measurements. Both the wind and current time series are plotted with vectors and expressed in east-west and north-south components for analysis, or alongshore and cross-shore directions when the coastline is not east-west oriented. The water level data are used for the bay oscillations. The relative importance of different driving forces, such as tides, winds, river discharge, and Coriolis effect, can be determined by spectral analysis method which is described below.

Both the meteorological and oceanographic data along the Louisiana coast can be obtained from the National Oceanographic and Atmospheric Administration's (NOAA) National Data Buoy Center (NDBC).

NOAA's Center for Operational Oceanographic Products and Services (CO-OPS) is the authoritative source for accurate, reliable, and timely water level and current measurements. NOAA's Tides and Currents Map, which is also developed and supported by CO-OPS, provide water levels, meteorological observations, and current observations, as well as short-term (0 hr. – 48 hr.) tide forecast prediction as a product of Operational Nowcast and Forecast Hydrodynamic Model Systems (called OFS). This tidal prediction from OFS is especially used for validation of the numerical model ECOM-si discussed in Chapter 4.

The Wave-Current-Surge Information System (WAVCIS) lab of Coastal Studies Institute (CSI) at Louisiana State University (LSU) maintains offshore instrumentations in the continental shelf region off Louisiana, providing current profiles by bottom mounted acoustic Doppler current profilers (ADCP), and meteorological sensors on a near-real time basis. In this study, three offshore stations (CSI03, CSI06, and CSI09) are chosen, which are located near 5-m isobath 18 km south of Marsh Island, on the inner shelf near the 20-m isobath 20 km south of Timbalier Island, and south of the Grand Isle, respectively. It is worth mentioned that due to the sidelobe effect, the current velocity data near the surface are always contaminated, meaning 10-15% of the total depth on the top layer is usually distorted (Li, et al., 2010, Li, 2013). That is why we use near-surface and near-bottom current profiles for analysis.

Besides the above data, several surveys to the Wax Lake delta have been conducted by researchers of LSU including H. Robert and C. Li, for collecting water level and current data. From them we selected two locations with ADCP data. The first station, named Delta #1, is located in the 4th channel from the east with the water depth of approximately 1.7 m. The second is in the Big Hog Bayou between the Wax Lake delta and the Atchafalaya delta, about 1.4 m deep (Figure 3.1).

In addition, weather maps and image of cold fronts are downloaded from surface analysis map archive at both Unisys and Weather Prediction Center (WPC) and at National Weather Service (NWS), which clearly depicts the frontal squall line, isobars, and high/low pressure positions for identifying the exact location of cold fronts and associated approaching orientation.

3.1.2 Other Data

3.1.2.1 Topography and Bathymetry Data

As discussed in Chapter 1, the challenge of the Wax Lake delta is due to its constantly changing topography and bathymetry, which are can be affected by inundation by local or remote winds, high river discharge, and other physical processes. Compiling topography and bathymetry data of this complex area is the foundation to investigating this area in any aspect.

In this study, five data sources are used to incorporate the bathymetry in the Wax Lake delta. National Geophysical Data Center's (NGDC) 3 arc-second (~90 meters) U.S. Coastal Relief Model (CRM) integrates offshore bathymetry with land topography to provide a comprehensive and seamless representation of the U.S. coastal zone

(http://www.ngdc.noaa.gov/mgg/coastal/crm.html). Among the 10 volumes of coast zones, the Central Gulf of Mexico (Vol. 04), as our interested area, was selected for image and data download. The spatial extents associated with this data set are between longitudes -94^o to -87^o, and latitudes 24^o to 35^o; the time period of data is from 01/01/1999 to 01/01/2001, which is also the time of the first edition of data publication. Bathymetric and topographic data sources in this region consist of NGDC's NOS hydrographic surveys, multibeam bathymetry, track line bathymetry, the U.S. Geological Survey (USGS), and other federal government agencies and academic institutions (NGDC, 2001). And NetCDF data type is available for download. According to CRM supplemental information, the vertical datum for the source bathymetric data was generally mean lower low water (MLLW) while the source topographic data were in NAVD 88. Due to CRM's relatively large cell size (3 arc-seconds or roughly 90 m), the differences between these datums are less than the vertical accuracy of the CRM, so we can assume CRM is referenced to the Mean Sea Level (MSL) if we like.

In addition to being extracted from numerical ocean models, bathymetry data can also be obtained from LIDAR measurements. LIDAR, acronym for Light Detection and Ranging or created as a portmanteau of "light" and "radar", is a remote sensing technique that uses laser pulses to examine both natural and manmade environments for elevation determination from an aerial survey (airlines or helicopters) with high accuracy, precision, and flexibility (Folger, 2011; Carter et al., 2012). LIDAR usually reveals a top-down and profile view over the region, and thus LIDAR data supports activities such as flood modeling, hydrodynamic modeling, coastal changing mapping, emergency response, hydrographic surveying, and coastal vulnerability analysis, etc. (NOAA, 2013). LIDAR has two types: topographic and bathymetric, the first of

which typically uses a near-infrared laser to map the land, while the latter uses water-penetrating green light to measure seafloor and riverbed elevations. In this study, a topographic LIDAR survey (saved LIDAR data file in "waxlake-lidar.img"), led by my advisor Dr. Li, was conducted over the Wax Lake delta, between longitudes -91.5848^{o} to -91.292^{o}, and latitudes 29.3647^{o} to 29.6466^{o}. Different from other elevation data, positive value in the LIDAR data means land elevation, while the zero value implies riverbed without identifying specific water depth, which helps us differentiate between land and water boundaries. Generally the LIDAR data was acquired referenced to the North American Datum 1983 (NAD83).

Finally, we also incorporate Dr. Li's three most recent field trips in the Wax Lake delta for bathymetry survey in winters of 2011, 2012 and 2013, respectively. Those in situ measurements provided more accurate and more complete bathymetric information, and thus very valuable. Figure 3.1 shows the track line of those surveys in the study area.

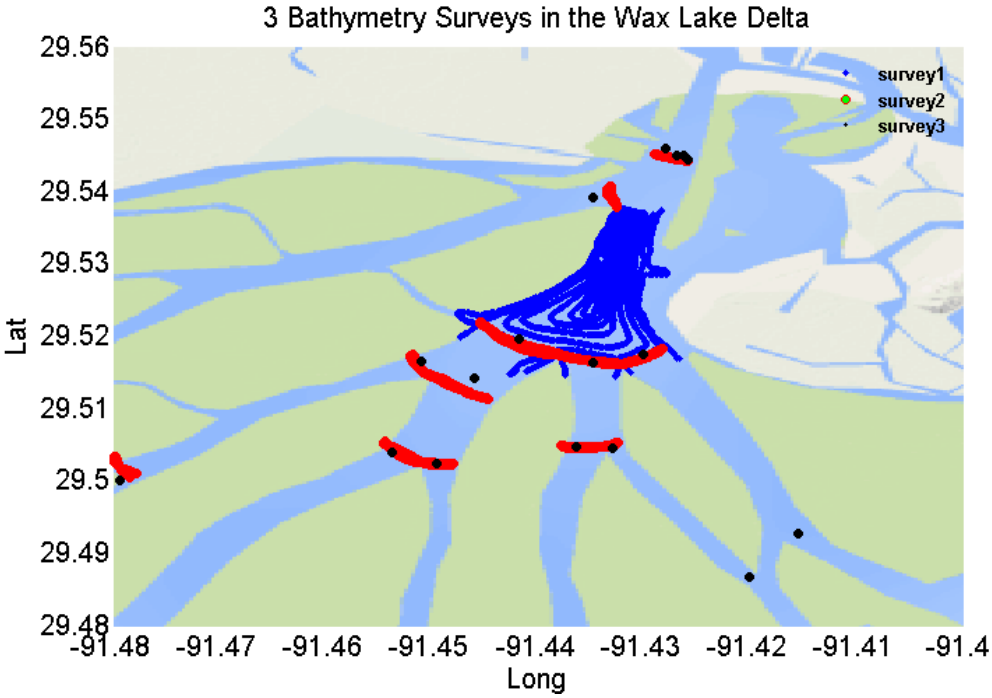

Figure 3.1 Track line of bathymetry surveys in the Wax Lake delta.

The merging processing of topography and bathymetry data sources is going to be detailed discussed in Chapter 5 as pre-processing preparation.

3.1.2.2 River Discharge

The daily mean river discharge into the Wax Lake delta and the Atchafalaya delta were obtained from USGS station 07381590 (the Wax Lake Outlet at Calumet, LA) and USGS station 07381600 (the Lower Atchafalaya River at Morgan City, LA), respectively. The latter is farther downstream and is thus closer to the total discharge at the mouth.

3.1.3 Data Summary

All stations used in this study are shown in Figure 3.2 for all the data used (Table 3.1). Water level data can be obtained from the observational stations across the Gulf coast. Current data are only available from two of the three WAVCIS stations (CSI03 and CSI06) as well as deployed instruments at Wax Lake sites.

Figure 3.2 The Louisiana coast and observational stations in the northern GOM. NOAA, WAVCIS, field ADCPs, and USGS stations are shown with diamonds, circles, stars, and squares, respectively. BHB: Big Hog Bayou; DL1: Delta #1; LAP: LAWMA, Amerada Pass; TESL1: Berwick, LA; FRWL1: Freshwater Canal Locks, LA; GISL1: Grand Isle, LA; PSTL1: Pilot's Station East, SW Pass, LA; PILL1: Pilottown, LA ; PF: Port Fourchon, LA; WLOC: Wax Lake Outlet at Calumet, LA; and LARMC: Lower Atchafalaya River at Morgan City, LA.

Table 3.1 Summary of meteorological and oceanographic data: NDBC, CO-OPS, WAVCIS, and surveys (stars mean available data)

Station	Location		Data				
	Latitude	Longitude	Wind	Barometric Pressure	Air Temperature	Water Level	Current
Delta #1	29.506357^o	-91.472336^o			*	*	*
Big Hogs Bayou	29.518045^o	-91.354841^o			*	*	*
CSI03	29.441^o	-92.061^o	*	*	*	*	*
CSI06	28.867^o	-90.483^o	*	*	*	*	*
CSI09	29.1015^o	-89.9782^o	*	*	*	*	
LAWMA	29.448333^o	-91.336667^o	*	*	*	*	
TESL1	29.666667^o	-91.236667^o	*	*	*	*	
FRWL1	29.555^o	-92.305^o	*	*	*	*	
GISL1	29.263333^o	-89.956667^o	*	*	*	*	
PSTL1	29.178333^o	-89.258333^o	*	*	*	*	
PILL1	28.931667^o	-89.406667^o	*	*	*	*	
PORT FOURCHON	29.113333^o	-90.198333^o				*	
WLOC	29.697778^o	-91.372778^o				*	
LARMC	29.692611^o	-91.211833^o				*	

3.2 METHODOLOGY

3.2.1 Choice of a Coordinate System

Our interests in this study lie in the cold front-induced water level variation, circulation, as well as the associated bay-shelf water exchange, which is largely determined by the wind direction relative to the coastline orientation. We use an empirical approach in defining our coordinate system based on the direction of the coastline, i.e. the *x* axis is parallel to the local coastline or the isobaths; and the y axis is directed offshore, thus the positive x axis is directing down-coast pointing from Louisiana to Texas. This local coordinate system is applied to both the wind and the current data.

3.2.2 Low-pass Filtering

For the time-series data, a 6^{th}-order Butterworth low-pass filter with a cutoff frequency at 0.6 cycles per day (CPD), or equivalently 40-hour period, is used to remove tidal and other high-frequency (>0.6 CPD) oscillations. This filter has a flat frequency response that is very close to the passband and thus is also referred to as the "maximally flat magnitude filter". A 40-hr low-pass filter is used to get rid of energetic oscillations caused by tides, inertial currents, and sea breeze effects at Louisiana coasts (Chen et al. 1996; Di-Marco et al. 2000). On the other hand, cold fronts have a recurrent period of 3 to 7 days (Fernandez-Partagas and Mooers, 1975; Angelovic, 1976; DiMego et al., 1976), which are much longer than 48 hours. So this filter can keep the low-frequency, or subtidal oscillations induced by cold front events. With a proper selection of the order and cutoff frequency, the Butterworth filter has been successfully used by physical oceanographers for data analysis (Emery & Thompson, 2004).

3.2.3 Spectral Analysis Using FFT

Spectral analysis provides an alternative way of representing data: transforming a time series in the time domain into a frequency domain using the Fourier Transform. And the Fast Fourier transform (FFT) is the most efficient algorithm for Fourier Transform (Emery and Thompson, 2004). From the spectral analysis, we can identify the major frequencies at which oscillation occurred, helping for the understanding of the underlying physical mechanisms. In this study, FFT is applied with MATLAB to extract tidal and subtidal wind-driven components in water level, current flow, and water transport.

3.2.4 Water Transport Calculation

In order to calculate the bay-shelf volume exchange rate, the following equation is applied, under the assumptions of a quasi-steady state of water level and no other major source or sink of water.

$$F = v \cdot A \qquad (3-1)$$

where F is the volume flux (m^3/s), which is defined as the rate of water flow across a unit area; A is the cross-transect area (m^2), which can be calculated based on the total water depth consisting of the local undisturbed water depth ($H(x,y)$) and surface elevation (ζ); v is the outflow current velocity (m/s), a time series of which can be obtained from model output. Since the water volume flux can be defined as the amount of water volume that passed through a transect in a unit time, the formula can be also written as:

$$F(x,y,t) = \int_{-H(x,y)}^{\zeta} \int_{0}^{L} v_n(x,y,z,t)\, dldz \qquad (3-2)$$

where $v_n(x,y,z,t)$ is the horizontal velocity component that is normal to the transect, such that the water volume flux is perpendicular to the given transect. And t is time (s) in UTC. Again, the time series of subtial water exchange flux can be achieved by applying the 6th-order Butterworth low-pass filter with a cutoff frequency at 0.6 CPD.

CHAPTER 4 NUMERICAL MODELING: ECOM-si

4.1 INTRODUCTION

The numerical model to be used in this study is a prognostic, three-dimensional (3D), non-orthogonal coordinate transformation, structured-grid, finite-difference, free-surface, primitive equations, and fully nonlinear, time-dependent, mass conservative ocean circulation model. This model is the modified version of the Estuary and Coastal Ocean Model - semi-implicit (ECOM-si; Blumberg, 1994) that was developed based on the POM (Princeton Ocean Model; Blumberg and Mellor, 1987) and further improved by a few researchers (Chen et al., 2001; Wu and Zhu, 2010; Wu et al., 2011). For example, the free-surface model incorporates the Mellor and Yamada's (1982) level 2.5 turbulent closure scheme for parameterization of vertical mixing and Smagorinsky's (1963) closure scheme for horizontal diffusivity. A non-orthogonal coordinate transformation replacing the curvilinear orthogonal transformation was used in the horizontal plane for a proper fitting of the coastline as well as a fast convergence for grid generation (Chen et al., 2001; Zhu et al., 2001; Chen et al., 2004); and a sigma (σ) coordinate transformation was used in the vertical dimension for a smooth representation of finite-amplitude of the irregular bottom topography. Therefore, the combined effect will be the adaptive mesh refinement for different resolution requirements. Wu and Zhu (2010) proposed a robust HSIMT-TVD advection scheme for solving the transport equations, which features a 3rd-order accuracy and can suppress artificial numerical oscillations. By treating both the barotropic pressure gradient in the momentum equations and water transport terms in the continuity equation implicitly, the semi-implicit numerical method used in ECOM-si not only allows a bigger time step but also leads to a linear symmetrical diagonal algebraic system at each time step, which can be solved efficiently by a preconditioned conjugate method without sacrificing computational time (Casulli, 1990;

Casulli and Cheng, 1992). Besides, the wetting/drying scheme (Tao, 2006) and the predictor-corrector scheme (Wang and Ikeda, 1997) are imbedded into ECOM-si to improve the computational precision and the numerical stability.

Previous applications have demonstrated the model's capability to reproduce the processes of circulation, freshwater discharge plume, water exchange and suspended sediment concentration, etc. Blumberg et al. (1993) applied ECOM to the Massachusetts Bay as early as 1993, and then Signell et al., (1996) and HydroQual and Signell (2001) further applied the model. Wang et al. (1994) used this model to investigate the Hudson Bay and then Zheng (2003 a, b) in the Satilla River Estuary, Georgia.

A complete description of the model, including transformations to the governing equations and finite difference formulations, can be found in Blumberg and Mellor (1987), Blumberg (1994) Wang et al. (1994), Chen et al., (2001), and Zhu et al., (2001). A brief description of the governing equations is given next.

4.2 GOVERNING EQUATIONS

The numerical model ECOM-si has coupled with density and velocity fields, river runoff, heating and cooling of the sea surface, so the original version of ECOM-si consists of equations of continuity, momentum, temperature, salinity and density. In a horizontally non-orthogonal, and vertically stretched sigma-coordinate transformation system, the governing equations (Chen et al., 2001) for momentum, continuity, water temperature, and density are given as

$$\frac{\partial DJu_1}{\partial t}+\frac{\partial DJ\hat{U}u_1}{\partial \xi}+\frac{\partial DJ\hat{V}u_1}{\partial \eta}+\frac{\partial J\omega u_1}{\partial \sigma}-Dh_2\hat{V}\left[v_1\frac{\partial}{\partial \xi}\left(\frac{J}{h_1}\right)-u_1\frac{\partial}{\partial \eta}\left(\frac{J}{h_2}\right)+Jf\right]-Dh_2u_1v_1\frac{\partial}{\partial \xi}\left(\frac{h_3}{h_1h_2}\right)$$

$$=-h_2gD\frac{\partial \zeta}{\partial \xi}+\frac{gh_2D}{\rho_o}\frac{\partial D}{\partial \xi}\int_\sigma^0\sigma\frac{\partial \rho}{\partial \sigma}d\sigma-\frac{gh_2D^2}{\rho_o}\frac{\partial}{\partial \xi}\int_\sigma^0\rho d\sigma+\frac{1}{D}\frac{\partial}{\partial \sigma}\left(K_m\frac{\partial Ju_1}{\partial \sigma}\right)+DJF_x \quad (4-1)$$

$$\frac{\partial DJv_1}{\partial t}+\frac{\partial DJ\hat{U}v_1}{\partial \xi}+\frac{\partial DJ\hat{V}v_1}{\partial \eta}+\frac{\partial J\omega v_1}{\partial \sigma}+Dh_1\hat{U}\left[v_1\frac{\partial}{\partial \xi}\left(\frac{J}{h_1}\right)-u_1\frac{\partial}{\partial \eta}\left(\frac{J}{h_2}\right)+Jf\right]-Dh_1u_1v_1\frac{\partial}{\partial \eta}\left(\frac{h_3}{h_1h_2}\right)$$

$$=-h_1gD\frac{\partial \zeta}{\partial \xi}+\frac{gh_1D}{\rho_o}\frac{\partial D}{\partial \eta}\int_\sigma^0\sigma\frac{\partial \rho}{\partial \sigma}d\sigma-\frac{gh_1D^2}{\rho_o}\frac{\partial}{\partial \eta}\int_\sigma^0\rho d\sigma+\frac{1}{D}\frac{\partial}{\partial \sigma}\left(K_m\frac{\partial Jv_1}{\partial \sigma}\right)+DJF_y \quad (4-2)$$

$$\frac{\partial \zeta}{\partial t}+\frac{1}{J}\left[\frac{\partial}{\partial \xi}\left(DJ\hat{U}\right)+\frac{\partial}{\partial \eta}\left(DJ\hat{V}\right)\right]+\frac{\partial \omega}{\partial \sigma}=0 \quad (4-3)$$

$$\frac{\partial JD\theta}{\partial t}+\frac{\partial JD\hat{U}\theta}{\partial \xi}+\frac{\partial JD\hat{V}\theta}{\partial \eta}+\frac{\partial J\omega\theta}{\partial \sigma}=\frac{1}{D}\frac{\partial}{\partial \sigma}\left(K_h\frac{\partial J\theta}{\partial \sigma}\right)+DJF_\theta \quad (4-4)$$

$$\frac{\partial JDs}{\partial t}+\frac{\partial JD\hat{U}s}{\partial \xi}+\frac{\partial JD\hat{V}s}{\partial \eta}+\frac{\partial J\omega s}{\partial \sigma}=\frac{1}{D}\frac{\partial}{\partial \sigma}\left(K_h\frac{\partial Js}{\partial \sigma}\right)+DJF_s \quad (4-5)$$

$$\rho_{total}=\rho_{total}(\theta,P), \quad (4-6)$$

where

$$\omega=w-\sigma\left(\hat{U}\frac{\partial D}{\partial \xi}+\hat{V}\frac{\partial D}{\partial \eta}\right)-\left[(1+\sigma)\frac{\partial \zeta}{\partial t}+\hat{U}\frac{\partial \zeta}{\partial \xi}+\hat{V}\frac{\partial \zeta}{\partial \eta}\right], \quad (4-7)$$

and $\xi, \eta, and\ \sigma$ are defined as

$$\xi=\xi(x,y), \quad \eta=\eta(x,y), \quad \sigma=\frac{z-\zeta}{H+\zeta}. \quad (4-8)$$

Here σ varies from -1 at $z=-H$ to 0 at $z=\zeta$; $x, y,$ and z are the eastward, northward, and upward axes of the orthogonal Cartesian coordinates; ζ is the surface elevation; H is the water depth; D is the total water depth equal to the sum of mean water depth H and the surface elevation ζ; and u_1 and v_1 are the ξ and η components of the velocity that can be converted back to the x and y components (u and v) of the velocity using the relationship of

$$u_1=\frac{h_2}{J}\left(x_\xi u+y_\xi v\right), \quad v_1=\frac{h_1}{J}\left(x_\eta u+y_\eta v\right), \quad (4-9)$$

where J is the Jacobian function with the form of $J = x_\xi y_\eta - x_\eta y_\xi$. The subscripts $\xi \; and \; \eta$ indicate partial derivatives. The metric factors h_1 and h_2 of the coordinate transformation are defined as

$$h_1 = \sqrt{x_\xi^2 + y_\xi^2}, \quad h_2 = \sqrt{x_\eta^2 + y_\eta^2}, \qquad (4-10)$$

and $\widehat{U} \; and \; \widehat{V}$ are given as

$$\begin{aligned} \widehat{U} &= \frac{1}{J}\left(h_2 u_1 - \frac{h_3}{h_1} v_1\right), \\ \widehat{V} &= \frac{1}{J}\left(h_1 v_1 - \frac{h_3}{h_2} u_1\right), \end{aligned} \qquad (4-11)$$

where $h_3 = y_\xi y_\eta + x_\xi x_\eta$; θ is the potential temperature; s is the salinity; f is the Coriolis parameter; g is the gravitational acceleration; K_m is the vertical eddy viscosity coefficient; and K_h is the thermal vertical eddy friction coefficient. Both coefficients of K_m and K_h were calculated using the modified Mellor and Yamada level 2.5 turbulent closure scheme (Mellor and Yamada 1974, 1982; Galperin et al. 1988). F_u, F_v, F_θ and F_s represent the horizontal momentum, thermal and salinity diffusion terms, and they were calculated by Smagorinsky's formula (1963) in which the horizontal diffusion is directly proportional to the product of horizontal grid sizes. ρ and ρ_o are the perturbation and reference densities, which satisfy $\rho_{total} = \rho + \rho_0$;

The prognostic variables are water levels, temperature, salinity, turbulence kinetic energy, turbulence macroscale and the three components of velocity. The momentum equations are nonlinear and incorporate a variable Coriolis parameter. Other computing variables include density, vertical eddy viscosity and vertical eddy diffusivity.

4.3 INITIAL CONDITIONS AND BOUNDARY CONDITIONS

4.3.1 Initial Conditions

Both the current velocity and surface elevation respond very quickly to external forcings, so the initial values are set to be zero:

$$\begin{matrix} u(x,y,\sigma,0)=0 \\ v(x,y,\sigma,0)=0 \\ \omega(x,y,\sigma,0)=0 \\ \zeta(x,y,0)=0 \end{matrix} \qquad (4-12)$$

However, for initial conditions of temperature and salinity, which change relatively slowly, a constant uniform value can be specified based on the literatures or observational measurements.

4.3.2 Boundary Conditions

The surface and bottom boundary conditions for the momentum and heat equations are given by

$$\begin{aligned} &\frac{\rho_0 K_m}{D}\left(\frac{\partial u_1}{\partial \sigma},\frac{\partial v_1}{\partial \sigma}\right)=\left(\tau_{0\xi},\tau_{0\eta}\right);\quad \frac{\partial \theta}{\partial \sigma}=0\quad \frac{\partial s}{\partial \sigma}=0;\quad \omega=0\quad at\ \sigma=0, \\ &\frac{\rho_0 K_m}{D}\left(\frac{\partial u_1}{\partial \theta},\frac{\partial v_1}{\partial \theta}\right)=\left(\tau_{\mathrm{b}\xi},\tau_{b\eta}\right);\quad \frac{\partial \theta}{\partial \sigma}=0;\quad \frac{\partial s}{\partial \sigma}=0\quad \omega=0\quad at\ \sigma=-1, \end{aligned} \qquad (4-13)$$

where $\left(\tau_{0\xi},\tau_{0\eta}\right)=\rho_a C_d^S|U_{10}|U_{10}$ and $\left(\tau_{\mathrm{b}\xi},\tau_{b\eta}\right)=C_d\sqrt{u_1^2+v_1^2}(u_1^2+v_1^2)$ are the ξ and η components of the surface wind and bottom stresses. The surface wind stress was calculated based on the neutral steady-state drag coefficient C_d^S developed by Large and Pond (1981).

$$C_d^S=\begin{cases} 0.0012\ if\ |U_{10}|\le 11\ ms^{-1} \\ 10^{-3}(0.49+0.065|U_{10}|)\ if\ |U_{10}|\ge\ 11\ ms^{-1} \\ 10^{-3}(0.49+0.065\times 25)\ if\ |U_{10}|\ge\ 25\ ms^{-1} \end{cases} \qquad (4-14)$$

where U_{10} is the wind velocity calculated at a height of 10 m above the sea surface and ρ_a is the air density. The drag coefficient C_d^B at the bottom was determined by matching a logarithmic bottom layer to the model at a height z_{ab} above the bottom; that is,

$$C_d^B = \max\left[\frac{\kappa^2}{\ln\left(\frac{z_{ab}}{z_0}\right)^2}, 0.0025\right], \quad (4-15)$$

where $\kappa = 0.4$ is the $von\ Kármán$ constant and z_0 is the bottom roughness parameter, which is essentially 0.001 m in the ocean.

The lateral boundary condition for closed basins and heat flux are specified as $v_n = 0, v_t = 0, \theta_n = 0, and\ s_n = 0$, where v_n and v_t are the normal and tangential velocity component at the boundary, respectively.

4.3.3 Wet/Dry Condition Treatment

One of the most challenging problems in estuarine modeling is to provide an accurate simulation of the water transport while flooding onto and draining out of the inter-tidal zone. The wet and dry of part of the regions modifies the water body area and leads to a significant change in the flux exchange across the main river channel. In ECOM-si, a 3D wet/dry point treatment technique (Tao, 2006) is used. The basic idea of this method is to let the computational domain cover the maximum flooding area, in which the mesh grids consist of wet and dry points with a boundary interface in between. The wet and dry points can be distinguished by the local total water depth $D = H(x, y) + \zeta(x, y, t)$, where H is the reference water depth and ζ is the surface elevation. The wet point is a grid point with $D > 0$, otherwise $D = 0$ at dry points. This treatment technique works only for the case in which a finite-value solution of the governing equations exists as D approaches zero. However, in a σ-coordinate, the wet/dry point treatment is no longer valid as D becomes zero with respect to mass conservation. One alterative way to avoid numerical singularity is to add a viscous boundary (h_c) at the bottom and redefine wet/dry

points using a sum of D and h_c. The grid is treated as a wet point for $D > h_c$, otherwise is a dry point. In a σ-coordinate transformation model, h_c is always related to the thickness of the bottom viscous layer specified at the bottom (also called the critical depth D_{min}). In terms of the nature of the vertical structure of turbulent mixing, a viscous layer always exists below the log boundary layer near a solid wall (Wilcox, 2000). On the other hand, however, in order to avoid adding additional water transport into a dynamic system, the viscous layer should be sufficiently small to satisfy a motionless condition. Good examples of the application of this method can be found in Ip et al. (1998) and Zheng et al. (2003b). So the new wet/dry point treatment method can be summarized using a simple criteria below: redefining the local total water depth $D = H_m + \zeta$, where $H_m = H + D_{min}$ in the water and $H_m = -(h + D_{min})$ on the land. The wet or dry criterion for node points is given as

$$\begin{cases} wet, if\ D = H_m + \zeta > D_{min} \\ dry, if\ D = H_m + \zeta \leq D_{min} \end{cases} \qquad (4-16)$$

where h_B is the bathymetry height related to the edge of the main channel of a river (Figure 4.1).

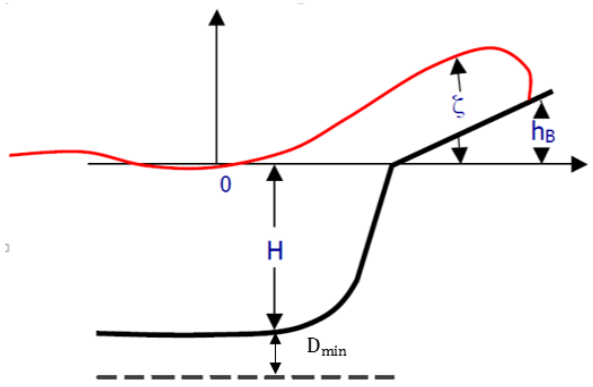

Figure 4.1 Definition of reference depth (H), surface level (ζ), bathymetric height (h_B), and the thickness of the bottom viscous layer (D_{min}).

At each time step, the model will adjust the land-water boundary based on the wet/dry criterion, allowing the model boundary to be movable. Each dry point will be applied to the boundary

conditions. For example, at dry points, the current velocities are automatically specified as zero, but the salinity remains the same as the previous time step. A wet/dry scheme is included in this study using a critical depth of $D_{min} = 0.2\ m$. Because this method is relatively simple, it has been widely used among estuarine models to simulate tidal-induced currents, salinity distribution due to mixing between freshwater and oceanic water in estuaries, as well as water transport over inter-tidal areas. The numerical results have shown that this wet/dry treatment provides an improvement in both computational stability and precision (Leendertse, 1970 & 1987; Flather and Heaps, 1975; Ip et al., 1998, Zheng et al., 2003a).

The estimation of the water transport in the dry-wet transition zone depends on 1) the criterion used to define the wet/dry points, 2) the time step used for numerical integration, 3) the horizontal and vertical resolutions of the model grids, 4) the magnitude of surface elevation, and 5) bathymetry.

With an accurate wet/dry point treatment, failure to resolve the complex geometry of an estuary can result in an incorrect prediction of the water exchange (Chen et al., 2008). Therefore, in this study I will incorporate all these factors for the numerical model experiment in the Wax Lake delta area.

4.4 MODEL CODING DESCRIPTION

4.4.1 The Code Structure of ECOM-si

The original ECOM-si was written in FORTRAN 77 and was subsequently migrated to FORTRAN 90. The currently used version in this study is organized in a modular fashion,

together with other libraries and functions, which makes the coding structure clearer and provides the flexibility for users to add and remove modules according to their own research needs. In addition, all arrays are dynamically allocated at runtime so that a change in problem dimension does not require recompilation. ECOM-si is solved by semi-implicit time integration schemes. The model can be run in either Cartesian or spherical coordinate systems.

The ECOM-si computer programs consist of a main program called "use_ecom.f" and a set of over 85 subroutines. Similar to other coastal ocean models, a schematic of the flow chart consists of preprocessing → start → setup parameters and initialization →main loop: NSTEP = ISTART, IEND → write output files. The baseline refers to the flow chart of the core ECOM-si code with modules of water surface waves, sediments, salinity, temperature, Bio-modules, Lagrange tracking, passive tracer-tracking, etc. The ECOM-si code can be run on Linux or Windows computer architectures. The type of the model run is controlled in the runtime control parameter file (RUN file) "casename.run", which is "wxl.run" in our case. The Delft3D-RGFGRID software is used for the structured-grid generation for ECOM-si. Alternatively, users may use any two-dimensional structured-grid generation program (such as SMS) to create mesh grids used in ECOM-si.

4.4.2 Criterion for Numerical Stability

The time step used in ECOM-si is bounded by the Courant-Friedrich Levy (CFL) stability criterion in the form of

$$\Delta t < \frac{\Delta s}{|u|} \qquad (4-17)$$

where Δt is the time step, Δs is the horizontal resolution and $|u|$ is the magnitude of the current velocity, so equation (4-17) can be written as

$$\Delta t < \frac{\min(\Delta x, \Delta y)}{\sqrt{u^2 + v^2}} \qquad (4-18)$$

ECOM-si incorporates a semi-implicit scheme developed by Vincenzo Casulli (Casulli, 1990) for solving the gravity wave by treating both the barotropic pressure gradient in the momentum equation and water transport terms in the continuity equation implicitly. As a result, the time step of the model is not only set to vary automatically, but also can be one order of magnitude larger than that restricted by the CFL criterion (Wu et al., 2011), which greatly increased the computation efficiency. In our case of model implementation, a variable of time step with a maximum of 5 seconds is used.

4.5 MODEL COMPILATION AND EXECUTION

ECOM-si is a research tool and not commercial software. The source code of ECOM-si in this study was obtained from Dr. Jun Lin. The current ECOM-si is a modified version including many new features and allows multiple choices of different modules. In order to make this model run more efficiently, we take the following four steps to set up and run ECOM-si:

1) Compile the source code,
2) Specify the runtime control parameter file (RUN file),
3) Prepare input files,
4) Run ECOM-si

4.5.1 Compiling ECOM-si

The current version of ECOM-si for our study is compiled and run in Microsoft Visual Studio Intel Fortran under the Windows operating system. In order to compile the model, we first need to create a new empty Intel Fortran Project file (.vfproj) with an icon 'Fo' for Intel Fortran

compiler to recognize. In our case, we created “ecom.vfproj”. The next step is to make sure that all source code files (.f) are added into the “ecom.vfproj” and located under the same directory. And then compile the model by building the solution in the menu bar (Build → Build ecom. If everything goes well, a successful build without any errors will produce an executable program named “ecom.exe”.

Running the ECOM-si executable “*ecom.exe*” needs to read the following three categories of files and/or data: “*casename.txt*”, “*casename.run*”, and input files. At the very beginning, the model must be given a case identification string stored in “*casename.txt*”, which will form the prefix for most input and output files, i.e., the “casename” = “*your casename*”. For example, in our Wax Lake delta model, we have chosen “*wxl*” as our case name. The RUN file is named “*casename.run*” and should be placed in the same directory where the ECOM-si executable (“*ecom.exe*”) resides. All other input and output files should be placed in the directory which is specified in “*casename.run*” with the name called “IN_DIRE” and “OUT_DIRE”, respectively.

4.5.2 Specifying the Runtime Control Parameter File (RUN file)

The RUN file “casename.run” contains all the parameters used to control the execution of ECOM-si. So one needs to specify the parameters to control the ECOM-si run. As a standard, one should first rename this file as your case name “*casename.run*” before editing it. This file is designed to have a flexible format so that the alignment of data values with particular columns is not necessary. This was done to eliminate incorrect reading of values, which can commonly occur with tab formatted input. In the RUN file, a variable is given a value by writing the variable name (all in capital letters) followed by one or more blanks, and then the value for this

variable. Comments may be placed between variables following the assignment of variables if preceded by the exclamation mark (!). There are a total of five parameter types: string, logical, real, integer, and vector. The logical type (for example LOG_FPT) must be assigned the value ".TRUE. (true) or ".FALSE" (false). The real type (for example DTI) must be assigned a numeric value with decimal point included. The integer type (for example IYEAR) must be given an integral numeric value. The vector type (for example DPTHSL) receives one or more floating type values. Finally the string type (for example IN_DIRE) must be assigned a string value (note: quotation marks are not necessary). In most cases, an incorrectly assigned or missing runtime control variable will cause the code to halt and produce some error information. A brief description of the control parameters used in the "*casename.run*" is given below (Table 4.1).

Table 4.1 RUN Controlling Parameter Options to Select before Numerical Simulation
(Table 4.1 continued)

Option	Values	Description
OS PARAMETER		
OSTYPE	Windows	Choose an operating system.
	Linux	
COORDINATE SELCETION		
COORD	BL	Choose coordinates: "BL" for spherical coordinate, "XY" for Cartesian coordinate.
	XY	
INPUT AND OUTPUT DIRECTORIES		
IN_DIRE	string	Choose input directory.
OUT_DIRE	string	Choose output directory.
FOR MODULE SELCETION		
ADVTSCH	HSIMT	Select the advection scheme for transport process.
	HSIMTMPL	
	KIM	
	MPDATA	
	SUPERBEE	
	VANLEER	
	MINIMOD	
	CENTER	
	UPWIND	
TIME SETTINGS		
DTITYPE	variable	Time step selection: "constant" for fixed time step, "variable" for variable time step. If
	constant	

(Table 4.1 continued)

Option	Values	Description
		"variable", time step is determined by CFL criterion automatically.
DTI	real	IF "constant": DTI is time step; if 'variable', DTI is the max time step. Unit: second.
FACTOR	real	FACTOR determines the time step in the mode of variable time step.
IRAMP	integer	Unit: time step, ramp the boundary forces.
T_END	real	Unit: day, numerical computation time
IYEAR	integer	Initial date: year
IMONTH	integer	Initial date: month
IDAY0	integer	Initial date: day
TIDE_LAG	real	Unit: day, tide lag at open boundary.
HOT START PARAMETERS		
RESTAR	cold	"Cold" for cold start, "hot" for hot start.
	hot	
N_RST	integer	Unit: day, output interval of restart file.
RST_SPEC	vector	Unit: day, on which days a specified restart file is output.
TIMESERIES OUTPUT PARAMETERS		
N_OPT	integer	Unit: second, interval for time series output. Establish "tsr" and "sec" file in input directory.
PRT_FPT	integer	time step interval to call prints output.
FIELD DISTRIBUTION OUTPUT PARAMETERS		
LOG_FPT	.TRUE.	Turn on/off the field output.
	.FALSE	
N_FPT	real	Unit: second, interval for field distribution output.
FPTSTAR	real	Unit: day, start time of field output.
FPTEND	real	Unit: day, end time of field output.
LOG_SPT	.TRUE.	Turn on/off salinity field output.
	.FALSE	
LOG_TPT	.TRUE.	Turn on/off temperature field output.
	.FALSE	
LOG_VPT	.TRUE.	Turn on/off current field output.
	.FALSE	
LOG_EPT	.TRUE.	Turn on/off elevation field output.
	.FALSE	
LOG_SEDPT	.TRUE.	Turn on/off sediments field output.
	.FALSE	
LOG_VISPT	.TRUE.	Turn on/off K_m&K_h field output.
	.FALSE	
LOG_MMTPT	.TRUE.	Turn on/off momentum field output.
	.FALSE	
LOG_ENGPT	.TRUE.	Turn on/off energy field output.

(Table 4.1 continued)

Option	Values	Description
	.FALSE	
LOG_TRACPT	.TRUE.	Turn on/off tracer field output.
	.FALSE	
LOG_BIOPT	.TRUE.	Turn on/off biology field output.
	.FALSE	
RESIDUAL CURRENT, FLUX AND FLUX ANALYSIS PARAMETER		
JHM	integer	Residual sigma.
HIST&AVGE	vector	Unit: hour. First number: end time for time averaging. Second: interval
BOTTOM FRICTION PARAMETERS		
Z0BTYP	user_defined	If "user_defined", establish "lba" file in input directory.
	constant	
BFRIC	real	Bottom friction parameter.
Z0B	real	Bottom friction parameter.
HORIZOTAL MIXING AND ADVECTION PARAMETERS		
HORZMIX	closure	Controls the calculation method for the horizontal diffusion.
	constant	
HORCON	real	Horizontal mixing and advection parameter.
HPRNU	real	The horizontal Prandtl number.
ADVECT	non-linear	Horizontal mixing and advection parameter.
VERTICAL MIXXING PARAMETERS		
VERTMIX	closure	Controls the calculation method for the vertical eddy viscosity and thermal diffusivity.
	constant	
CLOSURE	MY25	Vertical mixing parameter.
	KKL	
	KKW	
	KKE	
UMOL	real	If *closure* is selected, UMOL represents a background mixing (m^2/s). If *constant* is selected, UMOL represents a real eddy viscosity value specified by users.
VPRNU	real	Vertical mixing parameter.
KMFACT	real	Vertical eddy viscosity coefficient parameter.
KHFACT	real	Thermal vertical eddy friction coefficient parameter.
SALINITY CALCULATION PARAMETERS		
LOG_SAL	.TRUE.	Turn on/off salinity simulation. If true, establish "its" and "ts_obc" files in input directory.
	.FALSE.	
S_BEG	real	Unit: hour, time when salinity calculation begins.
LOG_BPG	.TRUE.	Turn on/off baroclinic gradient pressure.
	.FALSE.	

(Table 4.1 continued)

Option	Values	Description
BPG_BEG	real	Unit: hour, time when baroclinic gradient pressure calculation begins.
PARAMETERS CONTROLLING SEDIMENT SIMULATION		
LOG_SED	.TRUE.	Turn on/off sediment simulation.
	.FALSE.	
SED_BEG	real	Unit: hour.
F_SD50	real	D_{50}: Particle diameter representing the 50% cumulative percentile value.
F_ALFA	real	Settling coefficient.
F_MCSXS	real	Flushing coefficient.
TAUTYP	user_defined	If "user_defined", establish "TAU" file in input directory.
	constant	
LOG_BED	.TRUE.	Turn on/off sediment bed load.
	.FALSE	
BED_BEG	real	Unit: hour.
PARAMETERS CONTROLLING WAVE INTRODUCED SHEAR STRESS FORCE		
LOG_WAVE	.TRUE.	Turn on/off wave module.
	.FALSE	
WAVE_BEG	real	Unit: hour.
TEMPETURE CALCULATION PARAMETERS		
LOG_TMP	.TRUE.	Turn on/off temperature simulation
	.FALSE	
T_BEG	real	Unit: hour, time when temperature calculation begins.
Passive Tracers Calculation PARAMETERS		
LOG_TRAC	.TRUE.	Turn on/off passive tracers simulation.
	.FALSE	
TC_BEG	real	Unit: hour, time when tracer calculation begins.
ONLINE VIEW PARAMETERS		
LOG_VIEW	.TRUE.	Turn on/off online view.
	.FALSE	
N_VIEW	integer	Interval of online view.
CHC_VIEW	ELEVATION	Select parameter for online view.
	SALINITY	
	DEPTH	
	TEMPERATURE	
	SEDIMENT	
LAYER	integer	Layer: which layer to show.
IVSHOW	integer	Grid interval for displaying the current: i direction.
JVSHOW	integer	Grid interval for displaying the current: j direction.
LOG_SVIEW	.TRUE.	

(Table 4.1 continued)

Option	Values	Description
	.FALSE	Turn on/off save view. If log_view is turned off, then LOG_SVIEW will be set to false automatically.
N_SVIEW	integer	Unit: second, time interval of save view.
LOCTYP	SPECI	'AUTO' or 'SPECI'. If 'auto', the image field will be set up by the grid file automatically; else it should be set up by the user.
	AUTO	
XMIN	real	Specified x coordinate.
XMAX	real	Specified x coordinate.
YMIN	real	Specified y coordinate.
YMAX	real	Specified y coordinate.
LAGRANGE TRACKING PARAMETERS		
LOG_LAG	.TRUE.	Turn on/off Lagrange Tracking. If true, establish "lag" file in input directory.
	.FALSE	
NDT	integer	Interval for Lagrange Tracking, even number.
I_LAG	integer	Output interval for Lagrange Tracking, even number.
RESIDUAL ELEVATION AT OPEN BOUNDARY		
LOG_ELB	.TRUE.	Turn on/off residual water level at open boundary. If true, establish "rel_obc" file in input directory.
	.FALSE	
BIO_MODE		
LOG_BIO	.TRUE.	Turn on/off mod_bio module.
	.FALSE	
LOG_UNI_INI	1	1 for uniform initial bio_all; 2 for uniform initial bio_p,z,d; 3 for pht_remote.
	2	
	3	
DDPT	real	BIO_MODE parameter.
BIO_RST	hot	Call or not call bioinial_hot.
	cold	
BIO_BEG	real	Unit: hour, time when mod_bio calculation begins
NITRI_ON	.TRUE.	TURN ON/OFF nitrification.
	.FALSE	
BION	integer	Ratio of Dti_bio/dti.
BIO_AREA_BIG	.TRUE.	Average value output area.
	.FALSE	
STANDARD LEVEL DEPTHS		
BOTTM	.TRUE.	Bottom data.
	.FALSE	
IKSL	integer	Vertical layers.
DPTHSL	vector	Depth at different vertical layers.
DPTHSL_BIO	vector	Depth at different vertical layers in BIO_MODE.
DRY/WET PARAMENTER		
DMIN	real	Critical depth for wet/dry judgment.

(Table 4.1 continued)

Option	Values	Description
ADD WEIR		
LOG_WEIR	.TRUE. .FALSE	Add/remove weir.
HARMONIC CONTROLLING PARAMETERS		
LOG_HARM	.TRUE. .FALSE	Turn on/off harmonic simulation.
HARM_STARTDAY	real	Unit: day.
HARM_ENDDAY	real	Unit: day.
HARM_INTERVAL	integer	Unit: second.
FLUX OPEN BOUNDARY CONDITIONS (SEA BOUNDARY)		
LOG_FOBC	.TRUE. .FALSE	Turn on/off flux open boundary condition simulation.
LOG_FTID	.TRUE. .FALSE	Turn on/off tide boundary in the form of flux
FTID_BEG	integer	Start time of tide in flux form.
METEOROLOGICAL CONFIGURATION		
LOG_HEAT	.TRUE. .FALSE	Turn on/off heat flux simulation.
HFLX	BULK SPECI	"SPECI" gives the heat flux directly; "BULK" calculate the heat flux via sea/air-temperature, air pressure, relative humidity and wind speed.
HFLXTYP	UNIFORM FIELD	Heat flux data type. When HFLX=SPECI, "UNIFORM" gives the data in *.met, “FIELD” gives it *.hflx.
SWRA	SOLAR SPECI	"SPECI" gives the shortwave radiation directly; "SOLAR" calculate it via astronomic parameters.
SWRTYP	UNIFORM FIELD	Shortwave radiation data type. When SWR=SPECITHE, "UNIFORM" gives the data in *.met, 'FIELD' gives it *.swr.
BULKTYP	AANDBFLX RANDMFLX LANDPFLX	Heat flux type via sea/air-temperature, air pressure, relative humidity and wind speed.
ATTYP	UNIFORM FIELD	Air temperature data type. "UNIFORM" gives the data in *.met; 'FIELD' gives it in *.atp.
RHMTYP	UNIFORM FIELD	Relative humidity data type. "UNIFORM" gives the data in *.met; 'FIELD' gives it in *.rhm.
PRSTYP	UNIFORM FIELD	Air pressure data type. "UNIFORM" gives the data in *.met; 'FIELD' gives it in *.apr.
WDTYP	UNIFORM FIELD	Wind data type. "UNIFORM" gives the data in *.met; 'FIELD' gives it in *.wds.
WDSTYPE	speed stress	“speed” or “stress”.
CLDTYP	UNIFORM	

(Table 4.1 continued)

Option	Values	Description
	FIELD	Cloud data type. "UNIFORM" gives the data in *.met; 'FIELD' gives it in *.cld.
LOG_APR	.TRUE.	In-/exclude air pressure in momentum equations.
	.FALSE	

4.5.3 Preparing Input Files

ECOM-si requires different formats for the input files, which can generally fall into two types of format. The first is the files with ASCII format, which include files named "*casename.grd*", "*casename_dep.dat*", "*casename_fluxbond.dat*", and "*casename_met.dat*", etc. This kind of file is usually formatted and in plain text. The format of these files contain header information that is required at the top of each file. The second is the unformatted binary files, such as "casename.dat", "casename_wds.dat", and "casename_griddepth", etc. When reading or writing very large data sets, it is often more efficient to store the data in the host machine's native binary format (unformatted) rather than in human-readable format. FORTRAN 77 provides unformatted I/O for this purpose. Unformatted files are generally more compact and can be read and written much more quickly, because there is no need for the computer to convert between human-readable text and its native binary format. That is why direct-access I/O of huge data sets is normally carried out on unformatted files, although it can also be used with formatted files, if sufficient caution is used. However, unformatted files cannot be opened with a text editor. They can only be read by a FORTRAN 77 program.

ECOM-si input files must be placed in the directory specified by the variable "IN_DIRE" in the RUN file described in Section 4.5.2. All input files are prefixed by the string "*casename*" referring to the application description string chosen by the user. A description of the input files and their primary data is provided below (Table 4.2). It is also worth noted that not all input files

Table 4.2 ECOM-si Input Files

Input File	Description
casename.grd	Structured mesh information (grid number, latitudes and longitudes, x and y locations of individual node point) and vertical coordinate setup information (sigma layer). Format: ASCII.
casename.cuv	Curvature information of the mesh grids. Format: ASCII.
casename_griddepth	Bathymetry file: water depth and location (Latitude-longitude coordinates). Format: unformatted.
casename_dep.dat	Mesh bathymetry: grid number and water depth. Format: ASCII.
casename_met.dat	Meteorological data file at measurement time, including measurement time, wind, heat flux, shortwave, air temperature, humidity, air pressure, and cloud information. This file includes spatially uniform meteorological information. Format: ASCII.
casename_wds.dat	The real-time field of wind velocity or wind stress. Similarly, this file also can include surface heat flux, shortwave irradiance, air pressure, precipitation/evaporation, and other meteorological forcing data. Format: unformatted
casename_fluxbond.dat	Time series of river discharge at the boundary. This file includes number of transections, grid numbers, discharge volume, discharge temperature, and discharge salinity. Format: ASCII.
casename_dchg.dat	Depth change file. This file allows manually changing water depth at specific point, including grid numbers and modified water depth. Format: ASCII.
casename_its.dat	Initial condition of temperature and salinity on all sigma layers. Format: ASCII.
casename_tsr.dat	Selected stations for the time series output. This file includes locations (Latitude-longitude coordinates) and station names. Format: ASCII.
casename_sec.dat	Section position for calculating the sectional flux. This file includes section names and grid numbers. Format: ASCII.
casename_el_obc.dat	Tidal forcing at open boundary. This file includes grid number at open boundary and tidal constituents (amplitudes and phase). Format: ASCII.
casename_flux_obc.dat	Open boundary flux. Format: ASCII.
casename_flux_tide.dat	Tidal flux at open boundary. Format: ASCII.
casename_ts_fobc.dat	Temperature and salinity flux (on sigma layers) at open boundary.
casename_rel_obc.dat	Residual water level at open boundary. Format: ASCII.
casename_ts_obc.dat	Temperature and salinity (on sigma layers) at open boundary. Format: ASCII.
casename_sed_obc.dat	Sediment information at open boundary. Format: ASCII.
casename_sed_flux.dat	Sediment discharge information. Format: ASCII.
casename_lba.dat	This file is used to adjust bottom friction parameter locally in the study area.
casename_tau.dat	Sediment parameter file. Format: ASCII.

are required for a model run, though, which differs from case to case and totally depends on the modeling purpose. So in this text, we only list input files closely related to hydrodynamics study in here. Other input files, such as waves, passive tracer, or particle tracking, etc., will be omitted.

4.5.4 Running ECOM-si

After successfully building ECOM-si executable "*ecom.exe*", we need to copy "*ecom.exe*" and paste it into the same directory as RUN file ("wxl.run"). Edit the RUN file and choose the desired value for each option (Table 4.1). It is noticed that the ECOM-si executable "ecom.exe" takes no argument. So after configuration of RUN file, execute the model by double clicking "ecom.exe" to run the model.

4.6 ECOM-si OUTPUT FILES

ECOM-si-generated file and/or data are stored in three locations: "*info.txt*" file , "*modgen/*" and "OUT_DIRE/" directories. At soon as the model starts running, the "*info.txt*" file will be automatically generated and stored in the same directory with the ECOM-si executable ("*ecom.exe*"). "*info.txt*" gives a light-weighed summary about model initialization status by copying some basic information from RUN file, which includes time step (type and magnitude), initial and boundary conditions, and external forcing (salinity, baroclinic gradient forcing, residual water level, temperature, and Lagrangian tracking) information. "*modgen/*" as a byproduct of model-generated output, is also a collection of model setup information, including mesh grid, bathymetry, initial and open boundary file and data. At last OUT_DIRE/" directory contains the actual model output, which corresponds to the output parameter setup in the RUN file. For example, "timesseries" directory will contain the station output information that is

specified in “IN_DIRE/casename_tsr.dat”. The “field_distri” directory will include the spatial information of water level, current, salinity, and temperature across the whole computational domain with specified time interval assigned by “N_FPT” in the RUN file. Again, the model output is totally subjective and the users can set the control parameters based on their research purposes. It is worth mentioned that most output files are unformatted due to potentially large data sets computed from massive time integration loops across a high-resolution complicated area. In this sense, the unformatted binary output file demonstrates both time and space efficiency although we need to write codes separately for data extraction and analysis.

CHAPTER 5 NUMERICAL EXPERIMENTS

5.1 OUR QUESTIONS

The previous studies on Wax Lake delta mostly relied on satellite observations and field measurements. Modeling of the dynamics process of cold front passages in the region has not been conducted yet. In situ observations and measurements, when used with a numerical model, can provide useful results for the understanding of the hydrodynamics in a delta environment.

The main objective of the modeling effort is to investigate the basic physical mechanisms responsible for the storm surge in the Wax Lake delta under winter weather. In particular, the following questions will be addressed:

- On the structure (spatial and temporal) of the inner delta circulation: Is the coastal current downcoast (westward, i.e., from Louisiana to Texas, e.g., Cochrane and Kelly, 1986) or of more complicated structure?
- On the mechanisms driving the inner-delta flow: What physical mechanisms are important in driving the water transport near the river mouth and downstream?
- Does the southwestward along-shore coastal current persist during the upcoast wind period during frontal passage? Specifically, how did the cold front of winter 2012 affect the circulation pattern in the Wax Lake delta and the Atchafalaya delta?

To answer these questions, a set of model experiments was conducted to investigate the basic physical mechanisms responsible for circulation and water transport in the Atchafalaya-Wax Lake delta system. Here we describe the model setup and validation followed by the chapter on tidal and storm surge simulations and related discussion on transport.

5.2 MODEL SETUP

Given the main object of this study is the cold front-induced storm surge that is mainly barotropic, the temperature and salinity equations are not included in this study. The model simulations were completed using ECOM-si for the time period of December 15th, 2012 to January 20th, 2013, with the support of measurements from 14 sites. The present model domain contains a 380×250 curvilinear orthogonal grid in the horizontal as shown in Figure 5.1, which extends from longitudes of $-93.68^o\ W$ to $-89.21^o\ W$ and from latitudes of $27.90^o\ N$ to $29.96^o\ N$ with 380 and 250 cells roughly along the easting and northing axes, respectively. The model domain is centered at the Wax Lake delta including the coastal, shelf and shelf break regions covering the entire Wax Lake-Atchafalaya area and parts of northern Gulf of Mexico, with a resolution (square root of grid cell area) varying from 66.5 m to 6.2 km. Procedures to prepare the model configuration are given below.

5.2.1 Mesh Domain

5.2.1.1 Coastline Preparation

To generate the computational grid (structured or unstructured), we need to have first acquired relevant coastline data, which can be downloaded from GSHHG - A Global Self-consistent, Hierarchical, High-resolution Geography Database (http://www.ngdc.noaa.gov/mgg/shorelines/gshhs.html). NOAA has a desktop GEODAS-NG (GEOphysical DAta System - Next Generation) software tool "Coastline Extractor", which allows the selection of region of interest. I also manually sketched all major bifurcating channels in both the Wax Lake and Atchafalaya deltas, based on Google Earth imagery, and saved them

in .kml format. By combining these data sets, a coastline file was generated. ECOM-si is run in Cartesian coordinates while the coastline data are in a geographic format of longitude and latitude. A projection program is needed to convert the longitude and latitude to the Cartesian x-y coordinates relative to a selected reference point.

5.2.1.2 Model Grid

ECOM-si uses structured curvilinear grids. We used the Delft3D-RGFGRID (Delft3D-RGFGRID, 2013) to generate the grids.

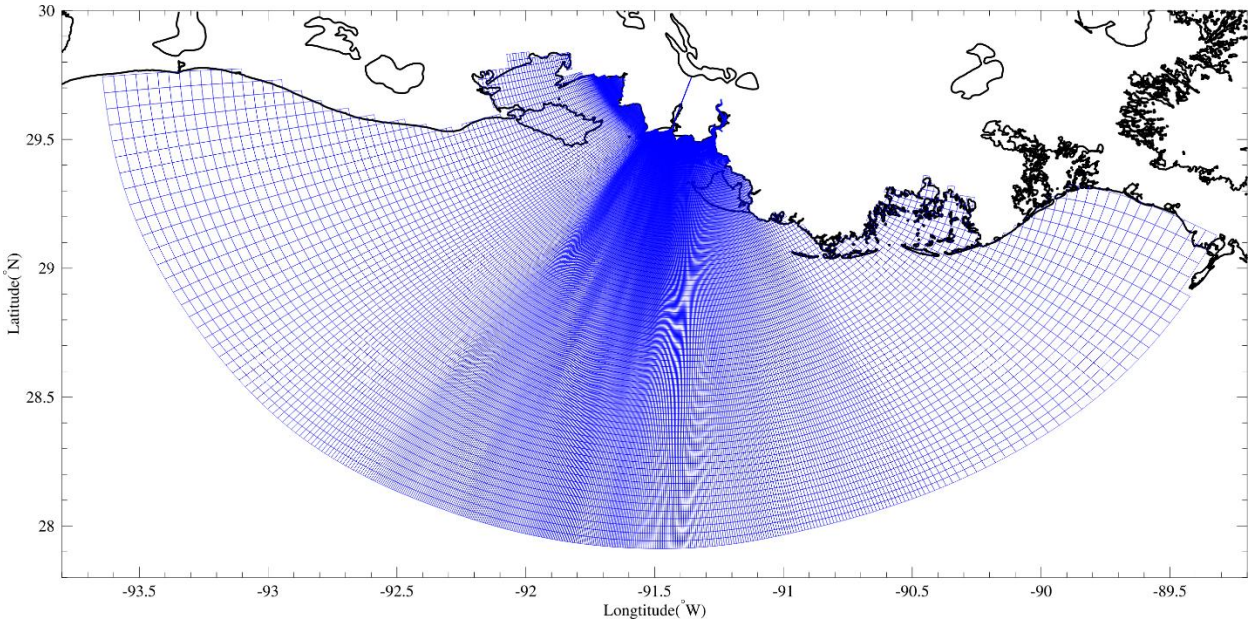

Figure 5.1 The 380 x 250 curvilinear orthogonal model grid of the Atchafalaya-Wax Lake delta system. The mesh resolution varies from 66.5 m to 6.2 km.

The model domain (Figure 5.1) encompasses Louisiana inner shelf from west of Atchafalaya Bay system (consisting of five contiguous bays: Vermillion Bay, West and East Cote Blanche Bays, Atchafalaya Bay, and Fourleague Bay; Cobb et al., 2008a, 2008b) to the Mississippi bight east of the Mississippi bird-foot delta. The southern boundary is extended offshore to the shelf edge in order to accommodate the out shelf phenomena affecting the hydrodynamics on the

inner-shelf. The fan-shaped mesh allows higher-resolution grids to be placed along the inner Wax Lake delta and the zones surrounding the river mouths while reducing the grid resolution offshore and near the open boundary. The mesh has a fine resolution of 63 m to 5.033 km in the cross-shore direction and of about 23 m to 7.752 km in the alongshore direction. The resolution progressively decreases towards offshore, with water depth as the deciding parameter (Figure 5.3).

5.2.2 Boundary Conditions

5.2.2.1 Open Boundary Treatments

For ocean problems, rarely a model has a domain enclosed by lands from all sides. One of the important requirements in applying an ocean model to a coastal region is how to specify a proper conditions on the open boundaries that allow the momentum or mass to be radiated out of or flow into the computational domain. Based on a criterion of a minimum reflection rate at open boundaries, Chapman (1985) made a comprehensive evaluation of numerical methods for the open boundary used in finite-difference models. In our model, the open ocean boundary is roughly an arc around the mouth of the Atchafalaya Bay (Figure 5.1). In the semi-enclosed basin or continental shelf, the sea surface elevation (amplitude and phase of tidal forcing) is specified at the open boundary. Since our model does not involves sediment, waves, salinity or temperature, the model at the open ocean boundary is then forced only by tides using the tidal constituents from the USACE's Eastcoast 2001 (Mukai et al., 2001) computed by ADCIRC-2DDI (the depth-integrated version of the ADCIRC; Westerink, 1993; Westerink et al., 1993; Mukai et al., 2002a, 2002b).. The amplitudes and phases of the tidal constituents are interpolated onto the open boundary nodes using the Eastcoast 2001, which provides elevation and velocity

amplitudes and phases for the three diurnal constituents (O_1, K_1, Q_1) and four semi-diurnal astronomical tidal constituents ($M_2, S_2, N_2, and\ K_2$), as well as the mean, M_4 and M_6 overtides throughout the Eastcoast 2001 domain (encompassing the Western North Atlantic Ocean, Gulf of Mexico, and the Caribbean Sea). The Eastcoast 2001 database can be used to directly evaluate surface-water elevation and current due to tides at locations within the bounds of the WNAT (Western North Atlantic Tidal) database domain. The database can also be used to drive smaller regional hydrodynamic models that incorporate a greater level of geometric, bathymetric, and/or hydrodynamic detail than the Eastcoast 2001 model itself. Therefore applying computed values from the Eastcoast 2001 tidal constituent database as the open ocean forcing for a regional model will typically result in an accurate and physically correct set of forcing functions on the open ocean boundary of the smaller model. The water level at the open ocean boundary is expressed as

$$\zeta = \zeta_{tide} + \zeta_{low-pass} \qquad (5-1)$$

where $\zeta_{tide} = \sum_{i=1}^{N_0} \hat{\zeta}_i \cos(\varphi_i t - \gamma_i)\,.\,\hat{\zeta}_i, \varphi_i, and\ \gamma_i$ are amplitude, frequency, and phase of the i^{th} tidal constituents. N_0 is the total number of tidal constituents, which is eleven in the current version of ECOM-si. This number can be increased if needed. $\zeta_{low-pass}$ is the low-pass filtered residual water level, which is negligible in this study. The periods T_i in hours for each of the 10 constituents included in the database are presented in Table 5.1. At the open boundary, this model was driven by tidal forcing, which consists of water levels and vertically integrated transports for 9 constitutes: K_1, O_1, Q_1, M_2, S_2, N_2, K_2, M_2, and M_4. The magnitudes and phases of the tidal constituents were interpolated onto the open boundary nodes using simulated data from ADCIRC-2DDI tidal database.

Table 5.1 Frequencies and Periods for Eastcoast 2001 Response Constituents (from Mukai et al., 2002b)

Constituent	Frequency (radians/sec)	Period (hr)
Steady	0.000000000000000	∞
K_1	0.00007292115836	23.93446966
O_1	0.00006759774415	25.81934167
M_2	0.00014051890251	12.42060122
S_2	0.00014544410433	12.00000000
N_2	0.00013787969949	12.65834826
K_2	0.00014584231720	11.96723479
Q_1	0.00006495854113	26.86835668
M_4	0.00028103780502	6.210300610
M_6	0.00042155670753	4.140200408

5.2.2.2 Surface Boundary Condition

The surface wind stress is added to ECOM-si using a method widely used in ocean modeling. Users can either run ECOM-si with a constant uniform forcing or with time-dependent, spatially non-uniform forcing fields specified from observational data or from the output of a meteorological model or a combination of both. In our model setup, we used uniform wind, obtained from a nearby station,. After comparison among nine different stations with barometric pressure data, the station FRWL1-8766072 was deemed to be representative of the wind and pressure fields over the study area. In the interior, the model was driven by the wind from site FRWL1-8766072, at Fresh Water Canal Locks, LA (Figure 3.1). FRWL1-8766072 is a buoy station maintained by the National Data Buoy Center (NDBC). The original data were sampled

every 6 minutes, which includes the wind speed and direction was first transformed into the east-west and north-south components and then re-sampled every 30 minutes for model input file ("*caseneme_met.dat*"). The height of the anemometer for this station is 17.37 m. Since wind speed varies with distance above the water and the standard height used in hindcasting is 10 m, for wind records taken at a different height above the water, we will use the following logarithmic velocity profile (Kamphuis, 2000) to correct the wind velocity to the wind speed at 10 m above surface (U_{10}).

$$\frac{U_{10}}{U_z} = \left(\frac{10}{z}\right)^{1/7} \qquad (3.1)$$

where z is the anemometer height in [m], and U_z is the measured wind speed [m/s].
The wind velocity is then converted to wind stress force before used in driving the model.

5.2.2.3 Lateral Boundary Condition

To run the Wax Lake delta regional model, we also need to specify the river discharge to the model. Although there are numerous freshwater outlets into the Atchafalaya Bay system (Goree et al., 2001; Swarzenski, 2003), only those having significant discharge are included. In this study we use two inflow sources (Figure 3.2) for freshwater discharge: the Wax Lake Outlet at Calumet, LA (WLOC, USGS station 07381590) and the Lower Atchafalaya River at Morgan City, LA (LARMC, USGS station 07381590), as riverine input into the Wax Lake delta and the Atchafalaya delta, respectively. Daily mean discharges at the LARMC and WLOC for December 15, 2012 through February 1, 2013 are extracted from the USGS database (Figure 5.2) as a time series. Both stations are located upstream and thus the river discharge is unidirectional. Besides, the river flow represented as a boundary condition for transport should be evenly distributed at

specific grid cells, where we set five for the Wax Lake Outlet and three for the Lower Atchafalaya River, respectively.

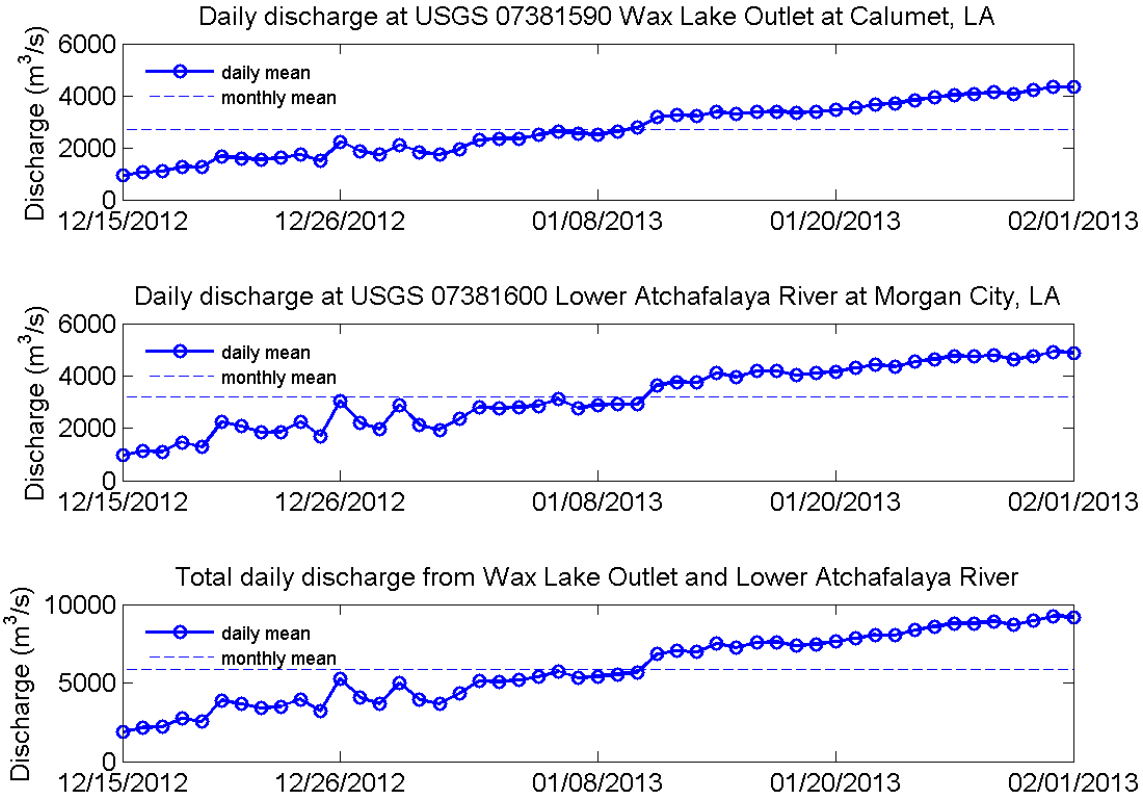

Figure 5.2 Daily mean discharge conditions for the simulation model domain: Wax Lake Outlet (upper panel, measured at Wax Lake Outlet at Calumet, LA or USGS 07381590), Atchafalaya River (middle panel, measured at Lower Atchafalaya River at Morgan City, LA or USGS 07381600), and total discharge (lower panel) from December 15, 2012 to February 1, 2013. The parallel dashed lines are calculated-monthly mean discharge.

5.2.3 Bathymetry

5.2.3.1 Depth Interpolation Techniques

In ECOM-si, because of the grid cell averaged calculation of water level, flow velocities, etc., it is more important to approximate the averaged bathymetric features rather than grid point discrete water depths. Therefore, it is usually recommended in Delft3D-QUICKIN to assign depth values by means of an averaging method that uses all sample data if there is more sample data points than grid points, which happens to be the current status of our case. On the other

hand, we also divide the data sets into smaller areas (for example the Wax Lake-Atchafalaya delta areas) by defining new polygons such that there are less sample points than grid points. In that case, the grid values have to be interpolated through triangulation. For grid points that have no depth value after the grid cell averaging operation or that are not realistically obtained from triangular interpolation, the values can be filled in with the internal diffusion operation. This is a smoothing process to fill in gaps between known depth points. Grid points in an area that is surrounded from all sides by known depth points are assigned a depth that forms a smooth transition with the existing bathymetry.

The model grid bathymetry is shown in Figure 5.3. Depths are given with respect to the reference level (MSL in this study) and negative values are above reference level.

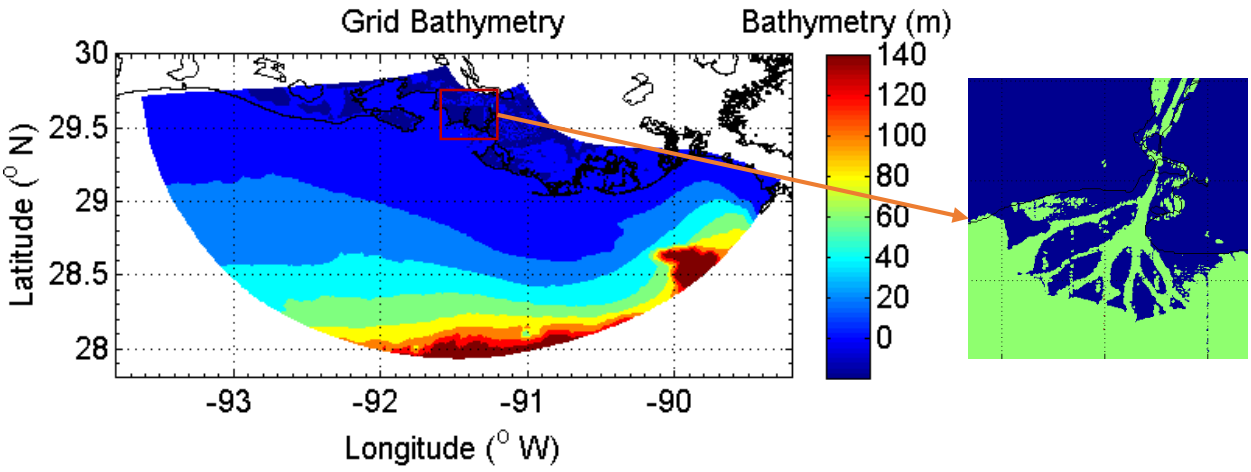

Figure 5.3 Bathymetry used in the model. The contour spacing is approximately 20 m. The bathymetry data consists of six data sources and is manually restricted within 150 m. The coastline and island boundaries was determined using the GEODAS-NG Coastline Extractor from NOAA. The red box indicates the location of the Wax Lake delta on the computational grid. The arrow points to a zoomed-in snapshot of the region.

5.3 NUMERICAL SIMULATION

Numerical simulations were completed using ECOM-si for December 15th, 2012 to January 20th, 2013, which included the measurement and observation of 12 sites and/or stations. Two kinds of simulation have been run on the model domain: (1) tides only, for the purpose of tidal validation as well as model verification; and (2) realistic forcing with surface winds, tides, and river inflow. The initial conditions for both the surface elevation and current velocity in both simulations are set to be zero as initial values. The grid has a vertical discretization of 10 σ layers (11 vertical σ levels) with uniform thickness in the water column. A wet/dry scheme is included in this study using a critical depth of $D_{min} = 0.2\ m$. Because tide was included in the model and the grid resolution was high, the time step was significantly restricted by the maximum flood/ebb currents. To increase the model efficiency, the time step was set to vary automatically based on the CFL criterion and thus allowed the use of a larger time step during low-current periods but a smaller time step when the tidal current was large. That means we can select different time steps for tide-only and realistic forcing simulations. However, in practical implementation, in order to facilitate the efficiency for comparison between different numerical results, time step varied with a maximum of 5 seconds in both simulations.

5.4 COMPARISON OF MODEL RESULTS AND OBSERVATIONS

5.4.1 Tides Only Case

5.4.1.1 Tidal Elevations

As mentioned above, although resolving tide is not the goal of the present study, it is necessary to require that the model can correctly simulate tidal propagation from the offshore open boundary towards the nearshore coastal regions. A tide-only simulation was run first for the

period of December 15, 2012, to January 20, 2013. The 9 tidal constituents at the open boundary are the only driving force in this tidal simulation. The time series of model-predicted tidal elevations are compared with tide predictions extracted from NOAA Tide Prediction database for six stations within the computational domain: LAWMA, FRWL1, GISL1, PSTL1, PILL1, and Port Fourchon (Figure 3.2). NOAA publishes the tidal prediction tables at each station for a short-term tidal forecast (0 – 48 hours), which is the output of Operational Nowcast and Forecast Hydrodynamic Model by considering only astronomical factors and excluding any current meteorological conditions (such as rainfall or drought). In order to eliminate the discrepancy caused by differences in reference elevation and subtidal biases, the means of both the model and NOAA prediction data time series have been removed, where the water level variation is obtained. The results are presented in Figure 5.4. The numerical results were generally consistent with the NOAA tidal predications, especially the phase of the model-predicted and NOAA prediction elevations agrees well at all stations. The disagreement of tidal amplitudes is not very surprising because the regions of the mesh domain were created using multiple sources of bathymetry data collected spanning different years. Since this time there may have been changes in the bathymetry of shallower areas (i.e., inner bay such as the Atchafalaya Bay system).
In addition, all the numerical experiments were initiated from a cold start, and it takes time for the model to spin up. That caused an "overshooting oscillation" at the very beginning of each station.

5.4.2 Realistic Forcing Case Associated with Cold Front

5.4.2.1 Combined water levels

To validate the realistic surface wind forcing-tide-riverine-induced sea surface elevation, we use

water level data measured at 14 sites/stations (7 NOAA stations, 3 WAVCIS stations, 2 USGS

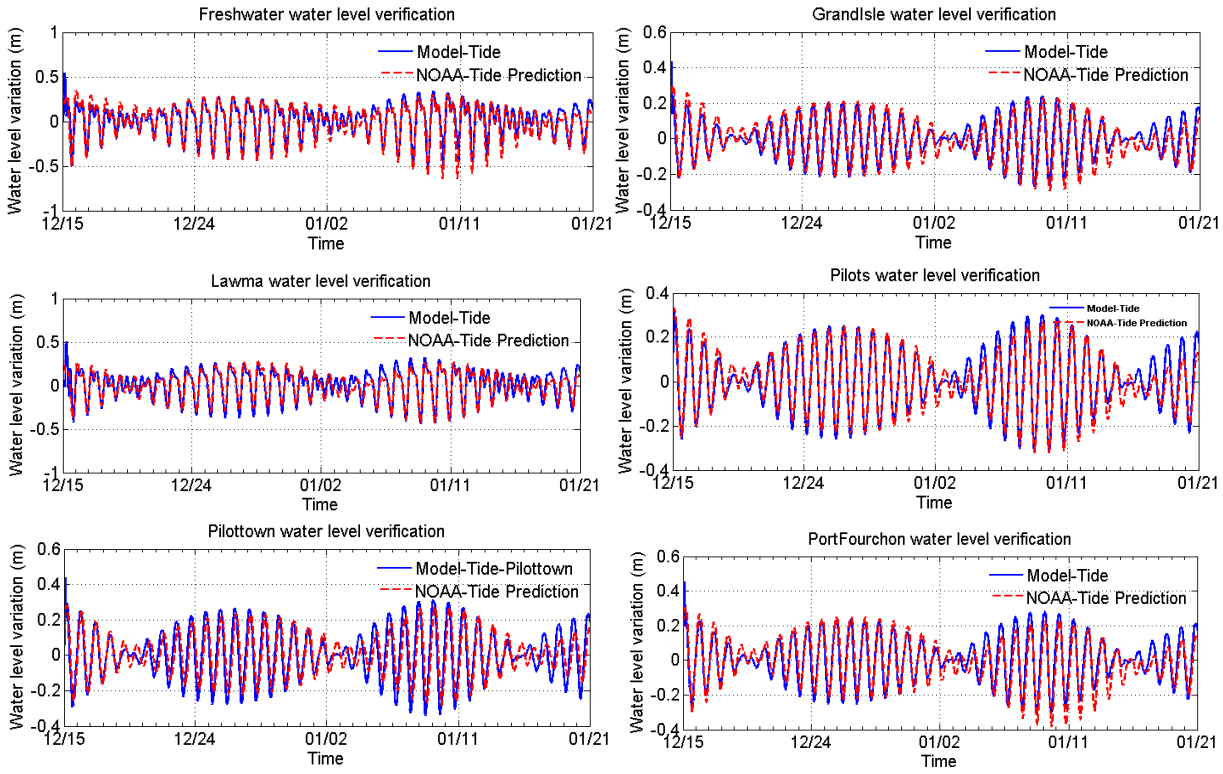

Figure 5.4 Comparison between model simulation and NOAA predicted tidal level, from December 15, 2012, to January 20, 2013, at 6 NOAA stations: Freshwater (upper left), Grand Isle (upper right), Lawma (middle left), Pilots (middle right), Pilottown (lower left), and Port Fourchon (lower right). The means have been removed from both time series.

stations, and 2 local ADCPs) during the same period as the tide only case. The water level predicted by the numerical model at all stations is plotted with the observations in Figure 5.5 and 5.6. The model results reveal the same trend as the observations, but there are several discrepancies. First, the model under predicts the low water levels at offshore and nearshore stations. This could be caused by local bathymetric errors the use of uniform wind. An example of this occurs in the measured water levels at CSI09 on December 27. During this time, strong postfrontal northerly winds created a maximum setdown in the observed water level that was approximately 0.1 m larger (i.e., more negative) than the water level predicted by the model, where the measured local winds were recorded significantly stronger than the model input winds

(from FRWL1). CSI03 has a perfect agreement between numerical model and the measurement in both amplitude and phase. However for FRWL1, since the locally measured winds have been already used as model input, some other mechanism is responsible for the significantly noisy fluctuation during this period, especially the maximum setdown difference of approximately 1 m between the predicted and observed water levels. The model also fails to reproduce the large fluctuations in the elevation during both high and low tides in the upstream of Wax Lake Outlet and Lower Atchafalaya rivers (e.g., 2 USGS stations). This is probably because of differences between the model and the actual bathymetry as previously discussed. Besides, both stations are located at the upper boundary of the computational domain and both narrow river channels are surrounded by large areas of dry lands, which leads to a very delicate wet/dry condition in the iteration loop. Inside the Wax Lake-Atchafalaya delta complex, in spite of the very shallow depth as well as large bathymetry variance among bifurcated channels, the numerical model is still capable of capturing the high water levels with good agreement in both magnitude and phase (Figure 5.5-Delta1 and Berwick). At other locations (e.g., BigHogs1 and Lawma2) inside the delta, the water level varies smoothly with time, following well with field measurements.

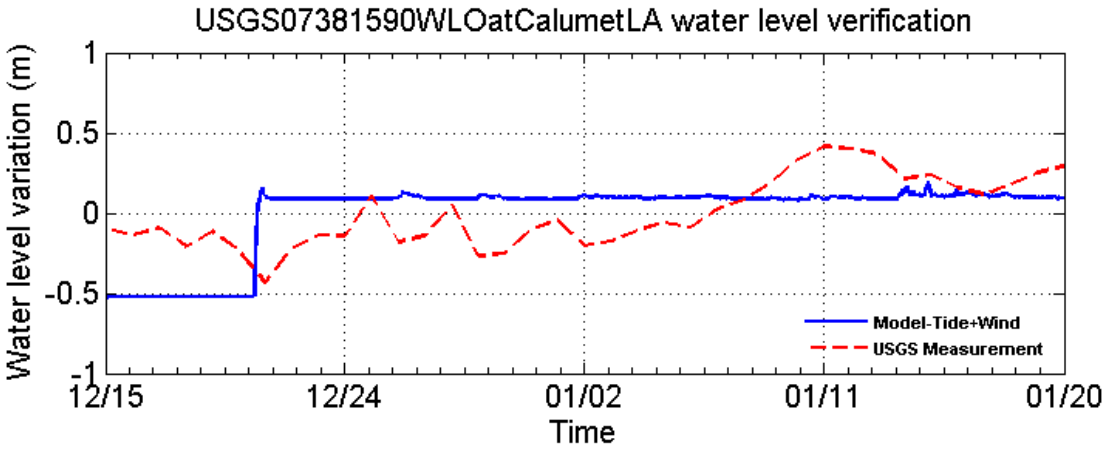

Figure 5.5 Water level (m) at stations/sites in the Wax Lake-Atchafalaya complex (Figure 3.2). The solid line represents the wind-tide-river forced model simulation. The dashed line represents

the water level time series data extracted from public agencies (NOAA) and/or field ADCP measurements. The means have been removed from both time series.

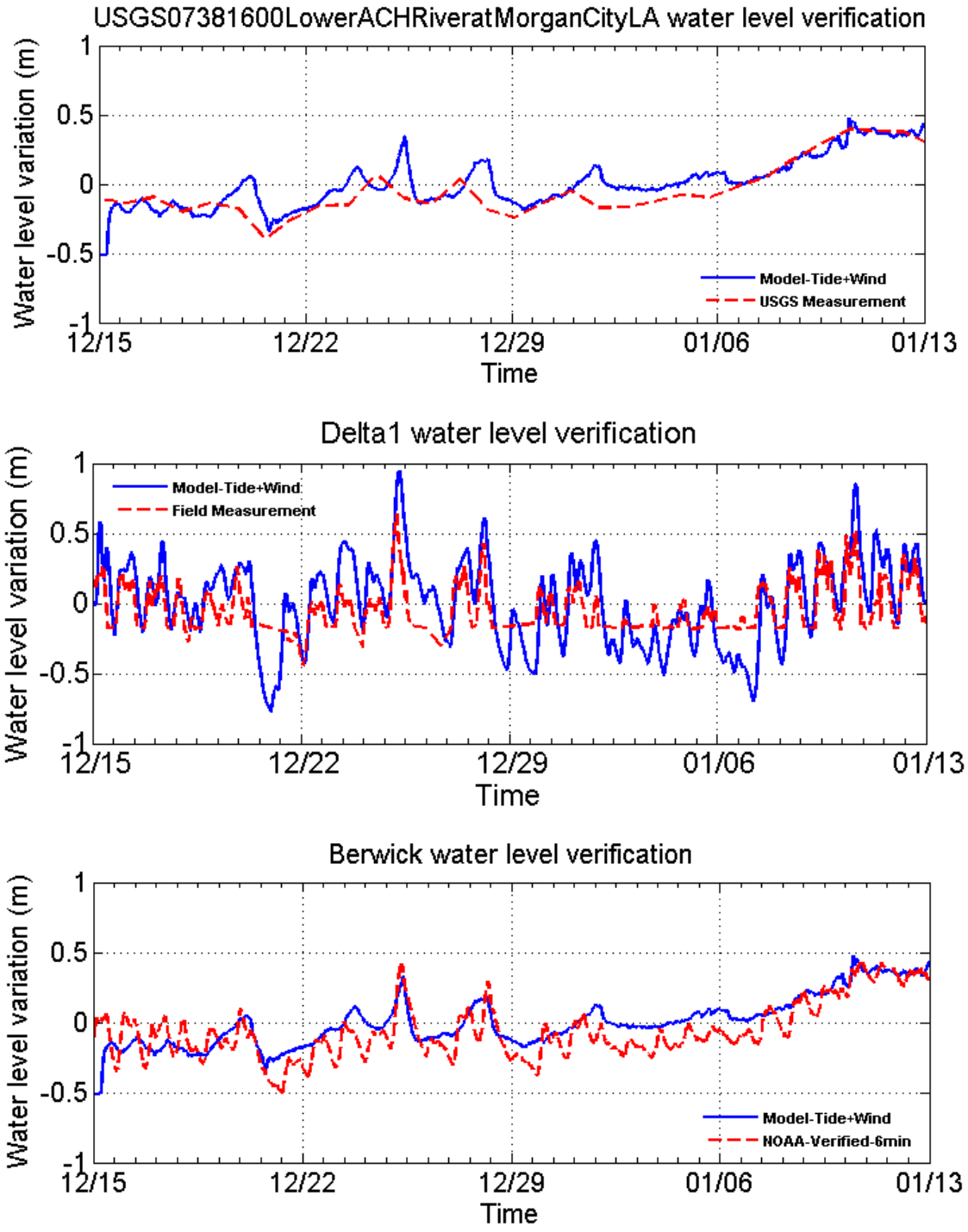

Figure 5.5 continued

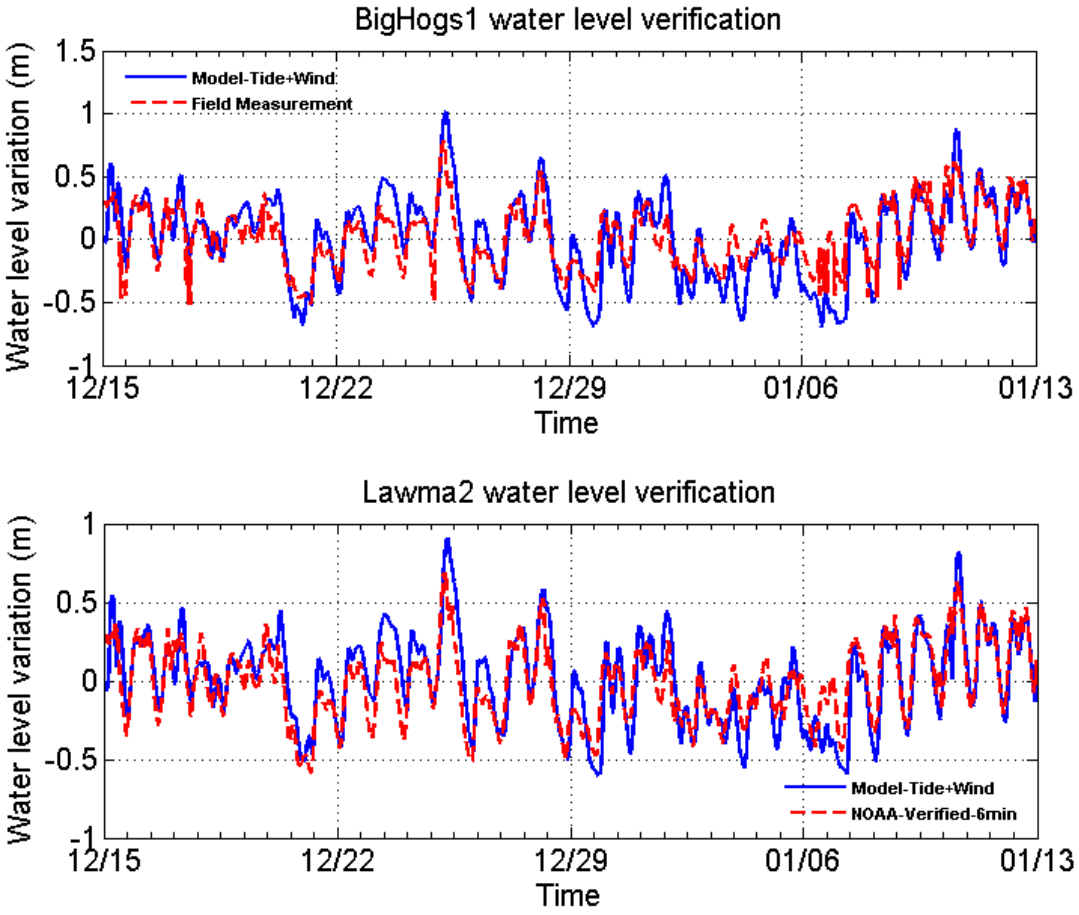

Figure 5.5 continued

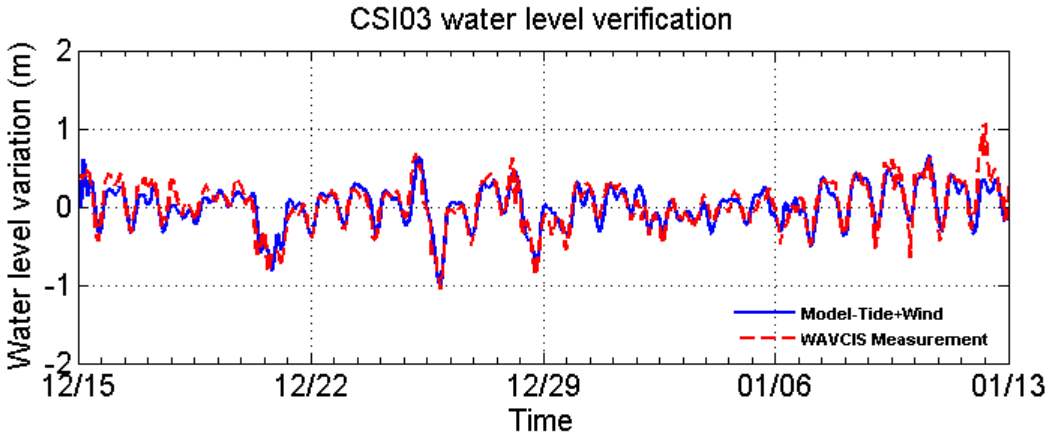

Figure 5.6 Water level (m) at offshore/nearshore stations (Figure 3.2). The solid line represents the wind-tide-river forced model simulation. The dashed line represents the water level time series data extracted from public agencies (NOAA) and/or field measurements (WAVCIS). The means have been removed from both time series.

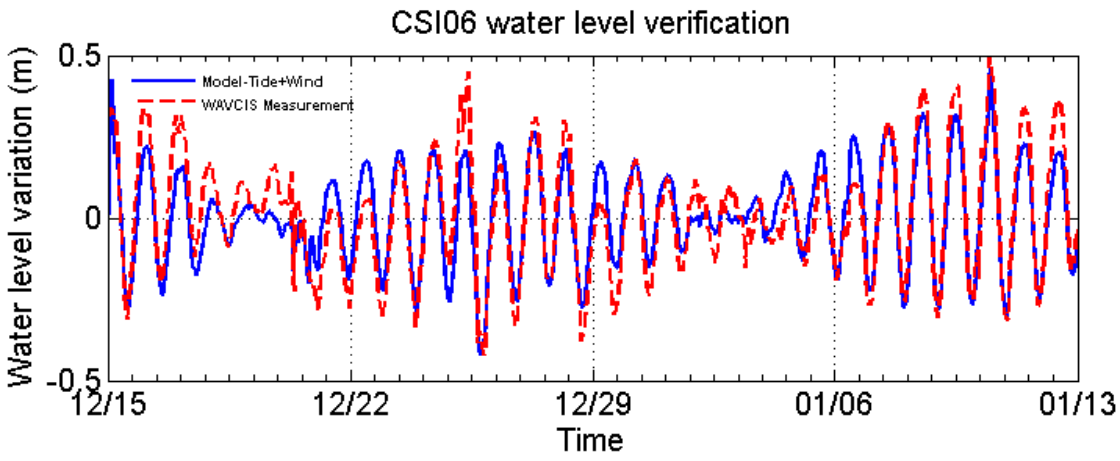

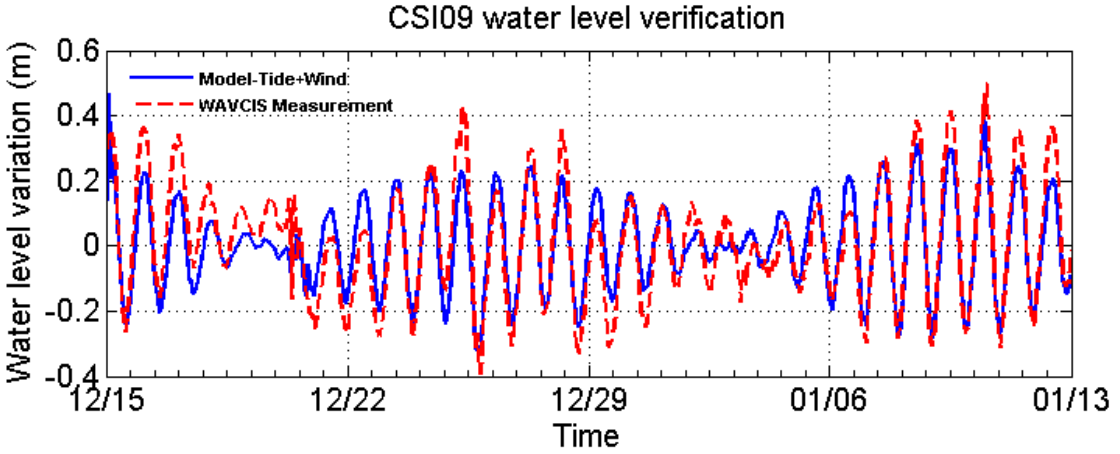

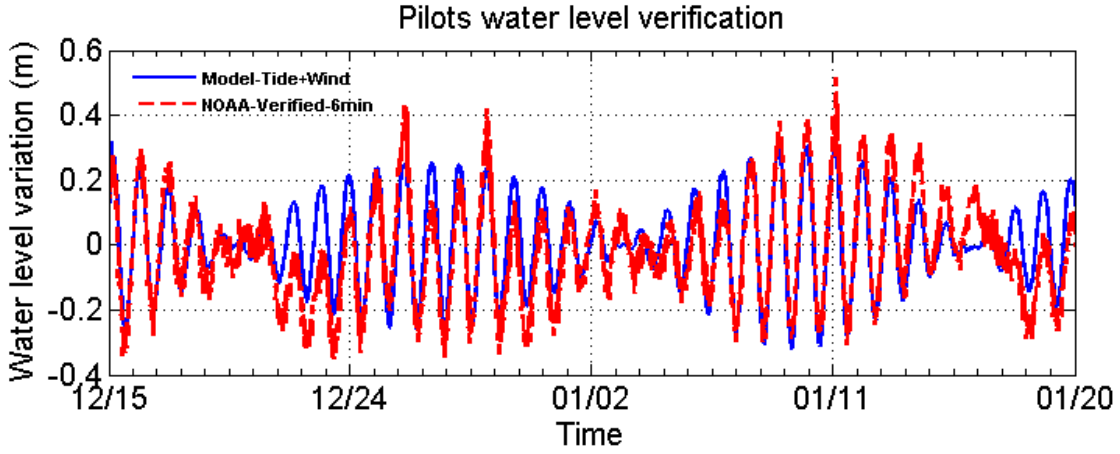

Figure 5.6 continued

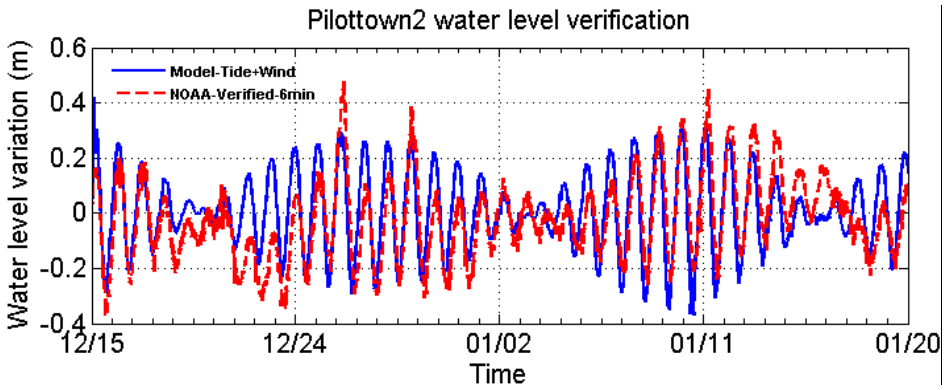

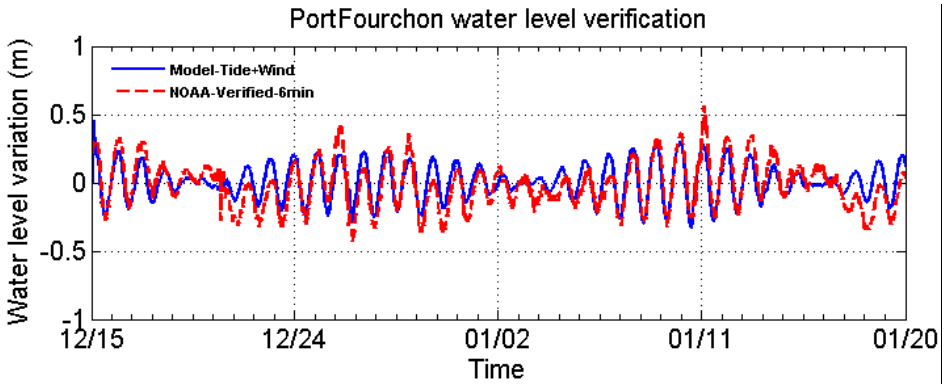

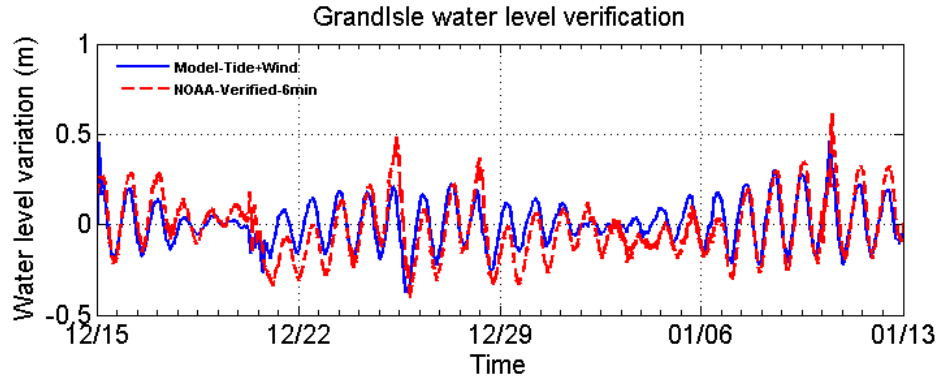

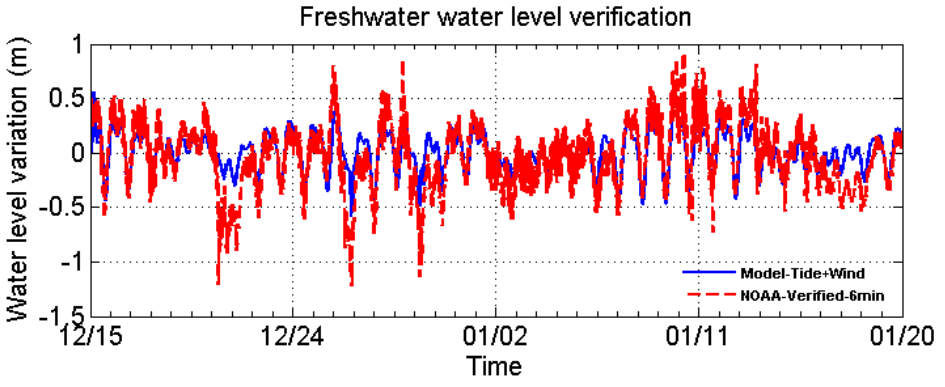

Figure 5.6 continued

5.4.2.2 Current Velocity

The comparison between modeled and measured current velocity time series at WAVCIS stations CSI03 and CSI06 are plotted in Figure 5.7-Figure 12, including the current velocity magnitude and direction at the near-surface, mid- and near-bottom layers, respectively. The measured velocity at the near surface of Delta #1 and Big Hog Bayou are also used for model validation test. The model results at this point demonstrate that the magnitude and phase of the predicted currents are comparable with the in situ observations.

The model-predicted current velocity magnitude and direction at CSI03 (Figure 5.7-5.9) are in good agreement with the observations for most of the study period. This is similar for the water levels (Figure 5.6 upper panel). The phase shift in CSI06 might be the consequence of using the spatially uniform wind data from FRWL1, where the station is approximately 190 km away from CSI06. On January 7 even though a very good agreement in current direction is achieved, the magnitude was under predicted. Again, this is because the model input winds are weaker than the measured winds at CSI06. The fluctuations inside the delta (Delta1 and Big Hog Bayou in Figure 5.13 and 5.14) are underestimated by the model as well, most likely due to bathymetry as discussed earlier. This also could be due to the fact that the channel is very narrow and the cross channel velocity is relatively small. But the current velocity trends in both simulation results were generally consistent with the observations. The over-predictions of the currents on December 19 and December 24 are consistent with the disagreement for the water levels (Figure 5.5), where the predicted water level changes too rapidly because the modeled currents are too strong.

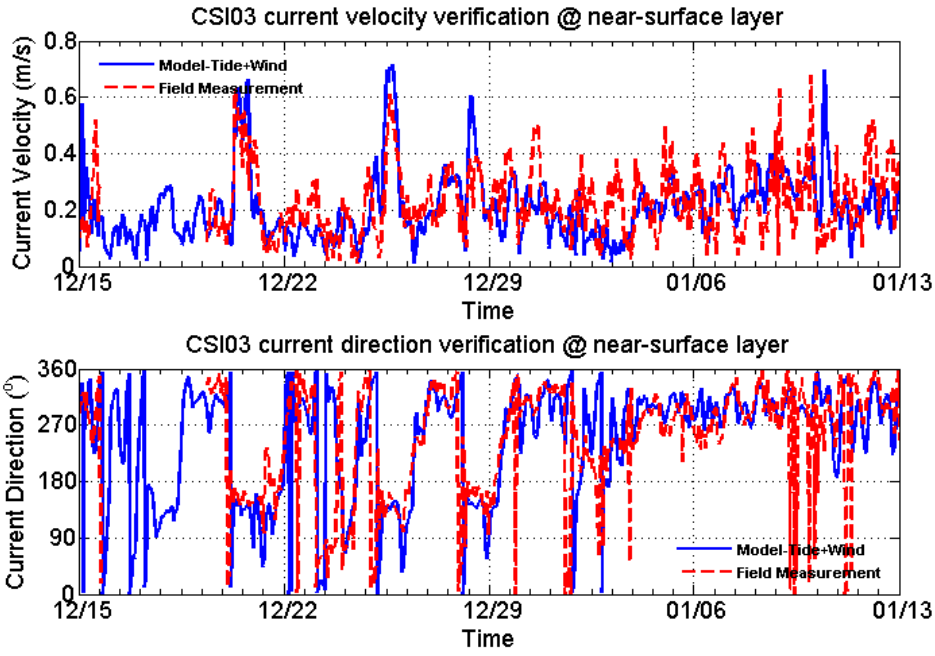

Figure 5.7 Model simulation (solid line) and measured (dashed line) near-surface current magnitude (m/s) and direction (degrees) at WAVCIS-CSI03 between December 15, 2012, and January 13, 2013.

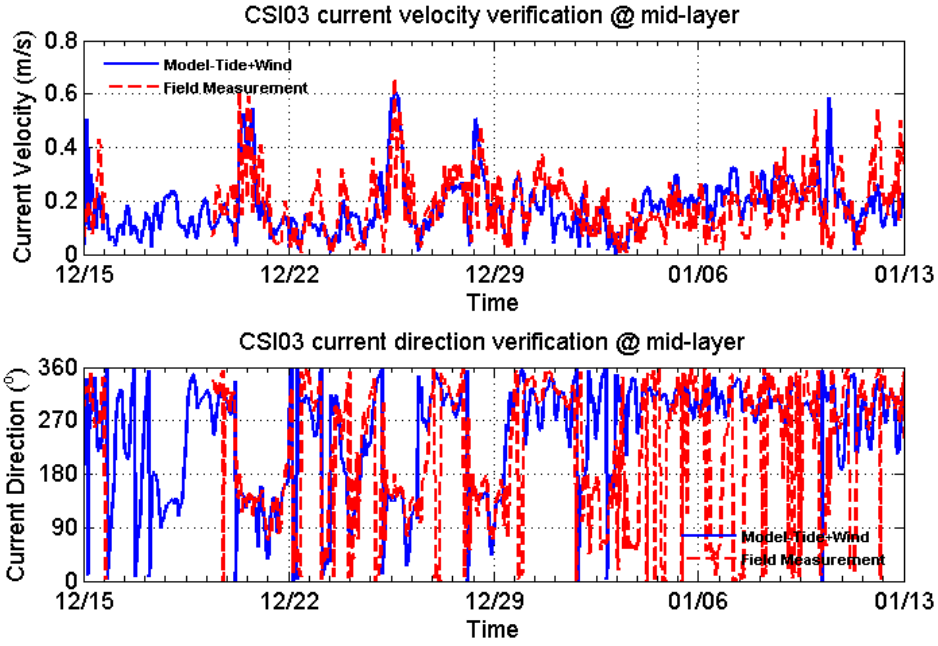

Figure 5.8 Model simulation (solid line) and measured (dashed line) mid-layer current magnitude (m/s) and direction (degrees) at WAVCIS-CSI03 between December 15, 2012, and January 13, 2013.

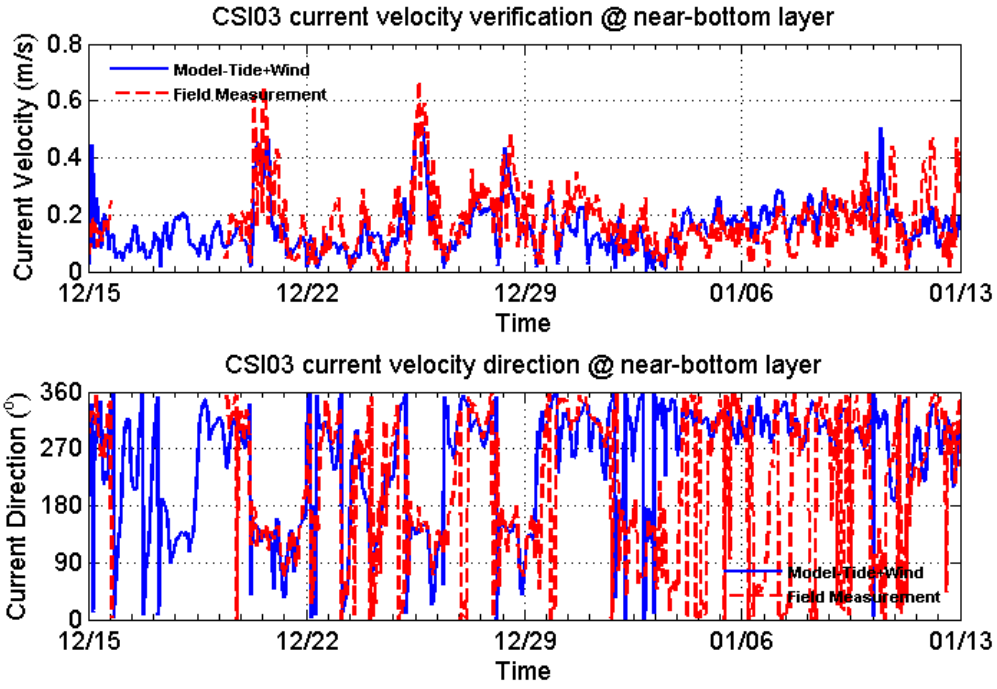

Figure 5.9 Model simulation (solid line) and measured (dashed line) near-bottom current magnitude (m/s) and direction (degrees) at WAVCIS-CSI03 between December 15, 2012, and January 13, 2013.

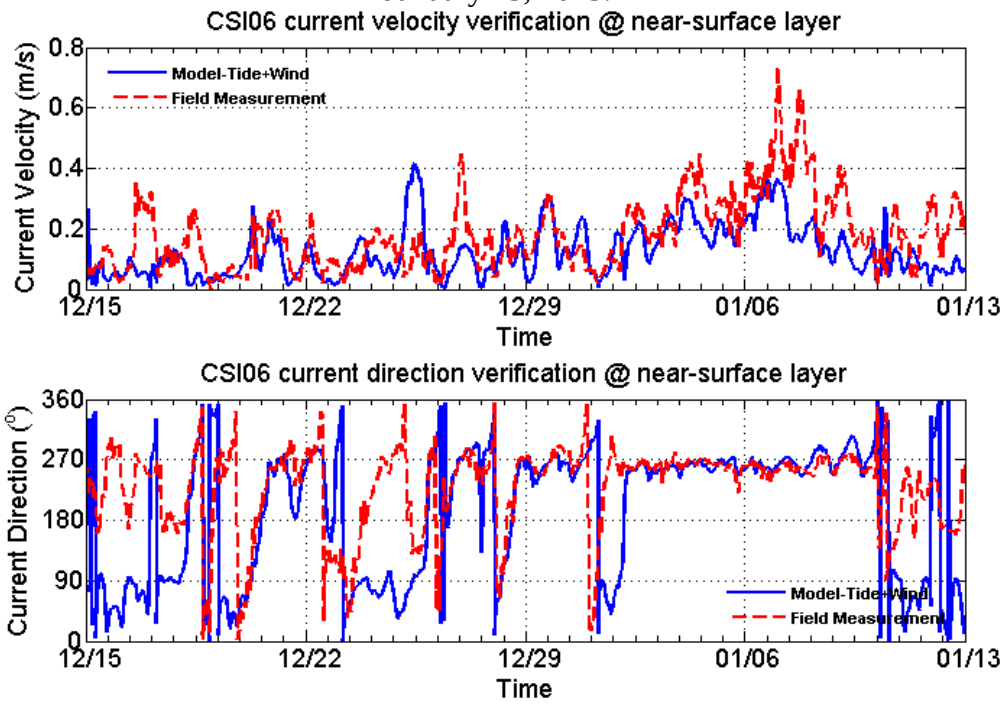

Figure 5.10 Model simulation (solid line) and measured (dashed line) near-surface current magnitude (m/s) and direction (degrees) at WAVCIS-CSI06 between December 15, 2012, and January 13, 2013.

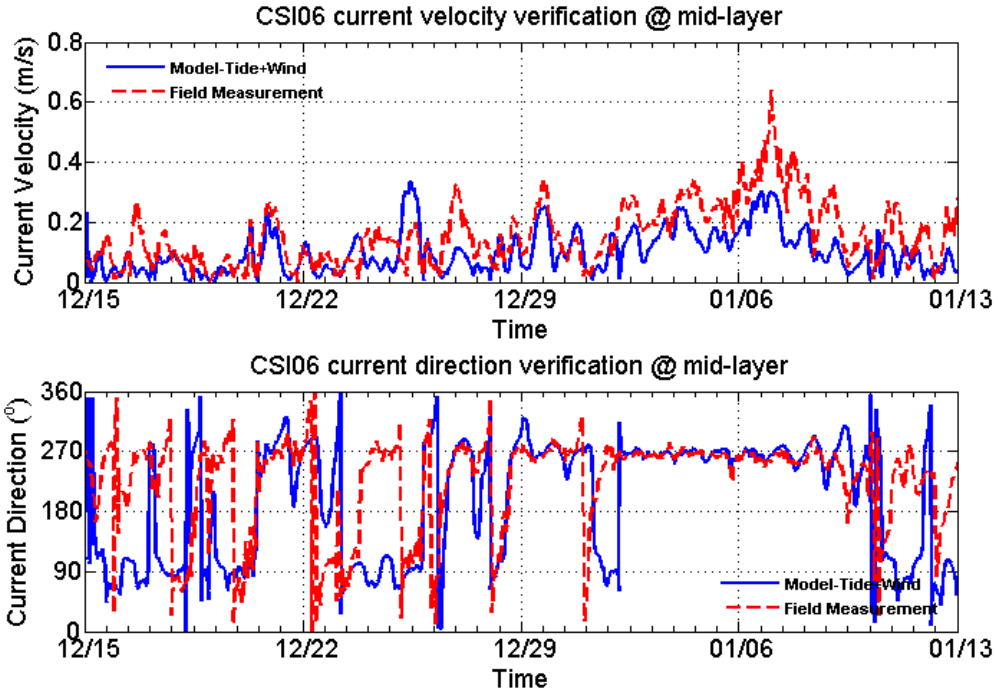

Figure 5.11 Model simulation (solid line) and measured (dashed line) mid-layer current magnitude (m/s) and direction (degrees) at WAVCIS-CSI06 between December 15, 2012, and January 13, 2013.

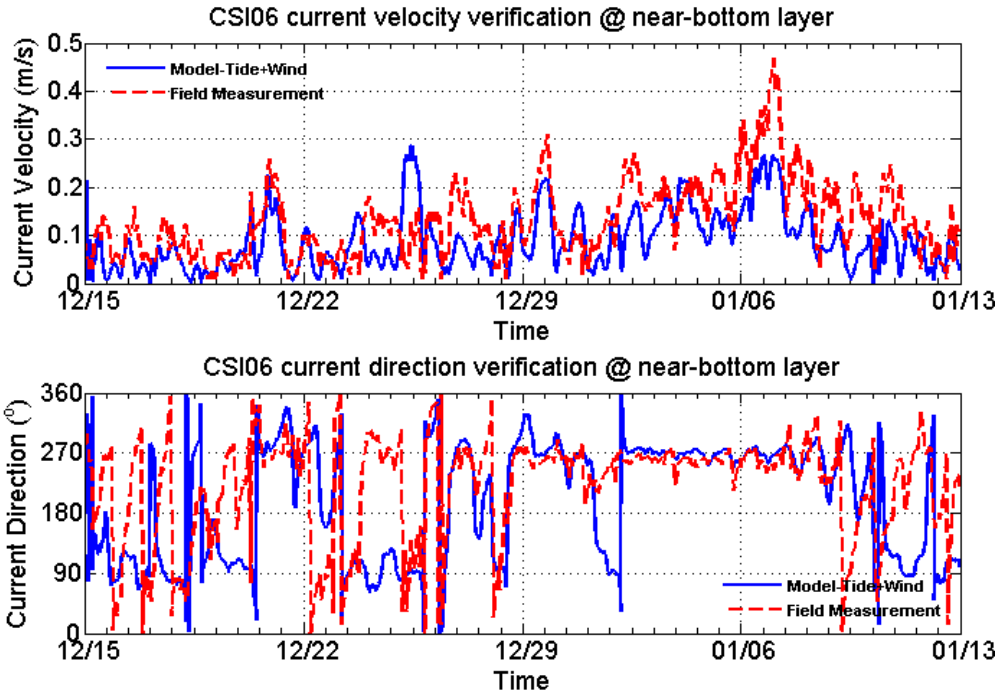

Figure 5.12 Model simulation (solid line) and measured (dashed line) near-bottom current magnitude (m/s) and direction (degrees) at WAVCIS-CSI06 between December 15, 2012, and January 13, 2013.

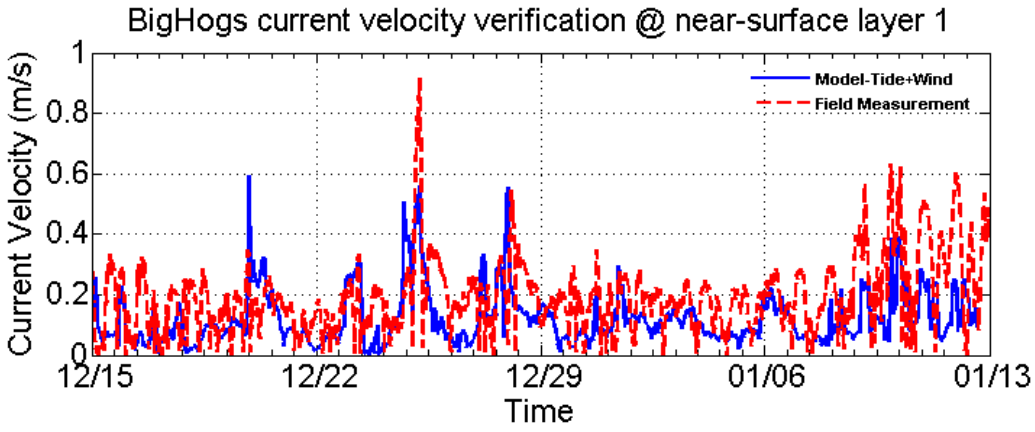

Figure 5.13 Model simulation (solid line) and measured (dashed line) near-surface current magnitude (m/s) at the site in Big Hogs Bayou between December 15, 2012, and January 13, 2013.

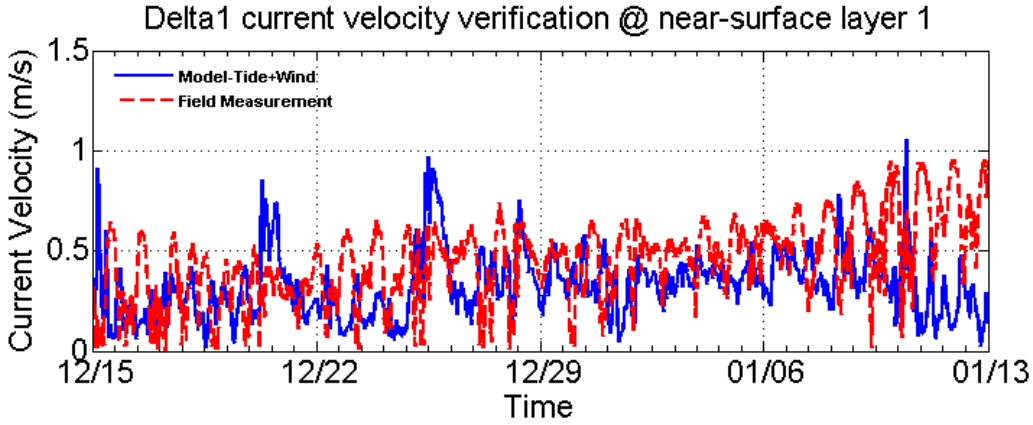

Figure 5.14 Model simulation (solid line) and measured (dashed line) near-surface current magnitude (m/s) at the site Delta #1 inside the Wax Lake delta between December 15, 2012, and January 13, 2013.

In summary the model calculated water level, current speed and direction are fairly well consistent with the observed ones, indicating that the established model can reproduce the dynamic processes, and can be used to study the hydrodynamics process in this delta.

5.4.2.3 Regression Analysis – R-Squared Value

In statistics, the coefficient R-squared value (R^2) is a determination number that quantifies how well a data set fits a statistical model. A general definition of the determination coefficient $R^2$is

$$R^2 \equiv 1 - \frac{SS_{res}}{SS_{tot}} \qquad (5-3)$$

where SS_{res} is the sum of squares of residuals (also called the residual sum of squares); SS_{tot} is the total sum of squares (proportional to the variance of the data), with the expressions

$$SS_{res} = \sum_i (y_i - f_i)^2 \qquad (5-4)$$

$$SS_{tot} = \sum_i (y_i - \bar{y})^2 \qquad (5-5)$$

$$\bar{y} = \frac{1}{n} \sum_{i=1}^{n} y_i \qquad (5-6)$$

And each y_i $(i = 1, \ldots, n)$ is associated with a predicted (or modeled) value f_i (sometimes $\hat{y}_i$). Table 5.2 and 5.3 show the R^2 value of water level and current velocity for all the stations in Figures 5.5-5.14.

Table 5.2 R^2 value of water level for 14 stations in Figures 5.5-5.6

Station Number	R^2 Value
Delta #1	0.5111
Big Hogs Bayou	0.6506
CSI03	0.7878
CSI06	0.7996
CSI09	0.7938
LAWMA	0.5603
TESL1	0.5227
FRWL1	0.5210
GISL1	0.5900

PSTL1	0.7135
PILL1	0.5181
PORT FOURCHON	0.6175
WLOC	0.4549
LARMC	0.6019

Table 5.3 R^2 value of current velocity for 4 stations in Figures 5.7-5.14

Station Number	R^2 Value		
	Near-Surface Layer	Mid-Layer	Near-Bottom Layer
Delta #1	0.6819	*	*
Big Hogs Bayou	-0.6418	*	*
CSI03	-0.4155	0.6076	0.6015
CSI06	0.4032	0.4141	0.6012

CHAPTER 6 RESULTS

6.1 INTRODUCTION

This chapter is about the analysis and discussion of the numerical simulation results. The discussion starts with a discussion of the seven cold front events between December 2012 and January 2013. The second part discusses the model results of ocean response to these cold fronts. We first qualitatively describe the circulation pattern in the big picture, and then study the current profile in interested areas. Next we demonstrate the water level maps to discuss the response to cold fronts. Subtidal analysis is then done before we discuss the water transport during each cold front events.

6.2 COLD FRONT PASSAGES BETWEEN DECEMBER 2012 AND JANUARY 2013

Winter cold fronts of varying intensity pass the Wax Lake-Atchafalaya delta region between October and April. In the present study, by analyzing meteorological data (Figure 6.1) and examining the United States surface weather maps (Figure 6.2), seven cold front events passing over the Wax Lake delta region are identified between December 15, 2012 and January 13, 2013 (Table 6.1): 12/17/2012-12/18/2012; 12/20/2012-12/22/2012; 12/26/2012-12/28/2012; 12/28/2012-12/31/2012; 1/1/2013-1/10/2013; 1/10/2012-1/12/2013; and 1/13/2013-1/18/2013. It is noted that all seven events are associated with migrating cyclones (MC), which usually move southeastward across the Louisiana coast. The Atchafalaya/Vermilion Bays (including FRWL1, offshore CSI03, and the Wax Lake-Atchafalaya delta system) are the first to be impacted after the Calcasieu Lake by the cold fronts, followed by Terrebonne/Timbalier Bays (including offshore CSI06). If we take the distance between Terrebonne Bay and the Atchafalaya Bay as 116 km, and the wind propagation speed at 10 m/s, the time lag of cold front passage between

two locations can be estimated as approximately 3.2 hours. Similarly the Barataria Bay (including GISL1, PF, and offshore CSI09) will be impacted after about another hour later (refer to Figure 3.2).

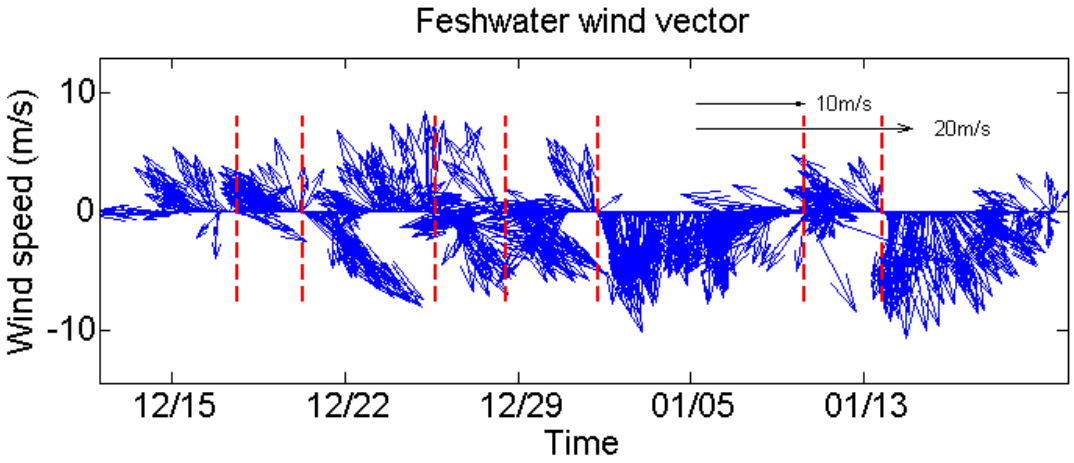

Figure 6.1 Cold front events identification from wind vector at FRWL1 between December 15, 2012 and January 13, 2013 (UTC time). The winds are plotted in vector format. Vertical dashed lines indicate time of cold front passages.

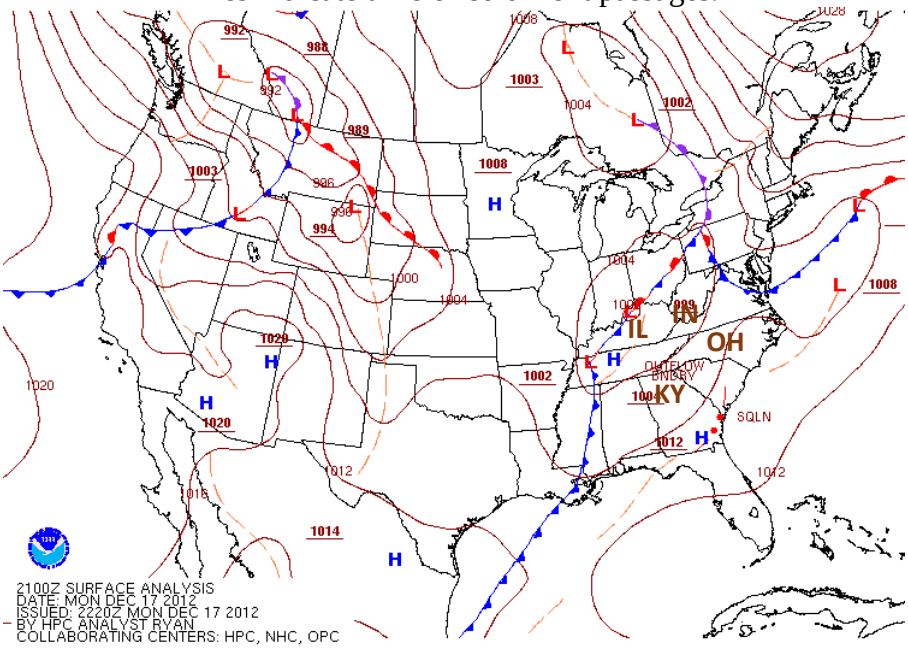

Figure 6.2 Weather maps showing cold front passages between December 15, 2012 and January 13, 2013 (UTC time).

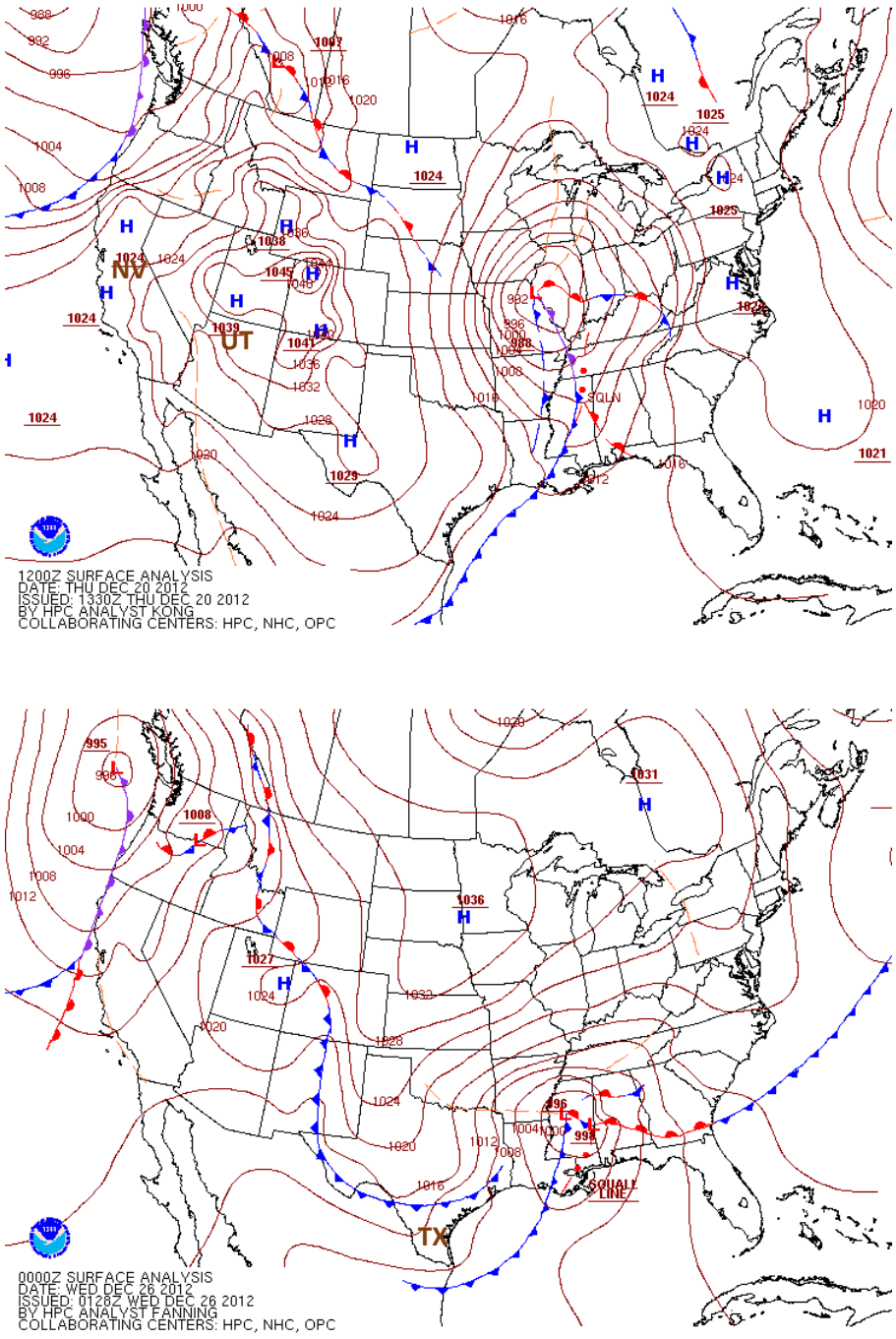

Figure 6.2 continued

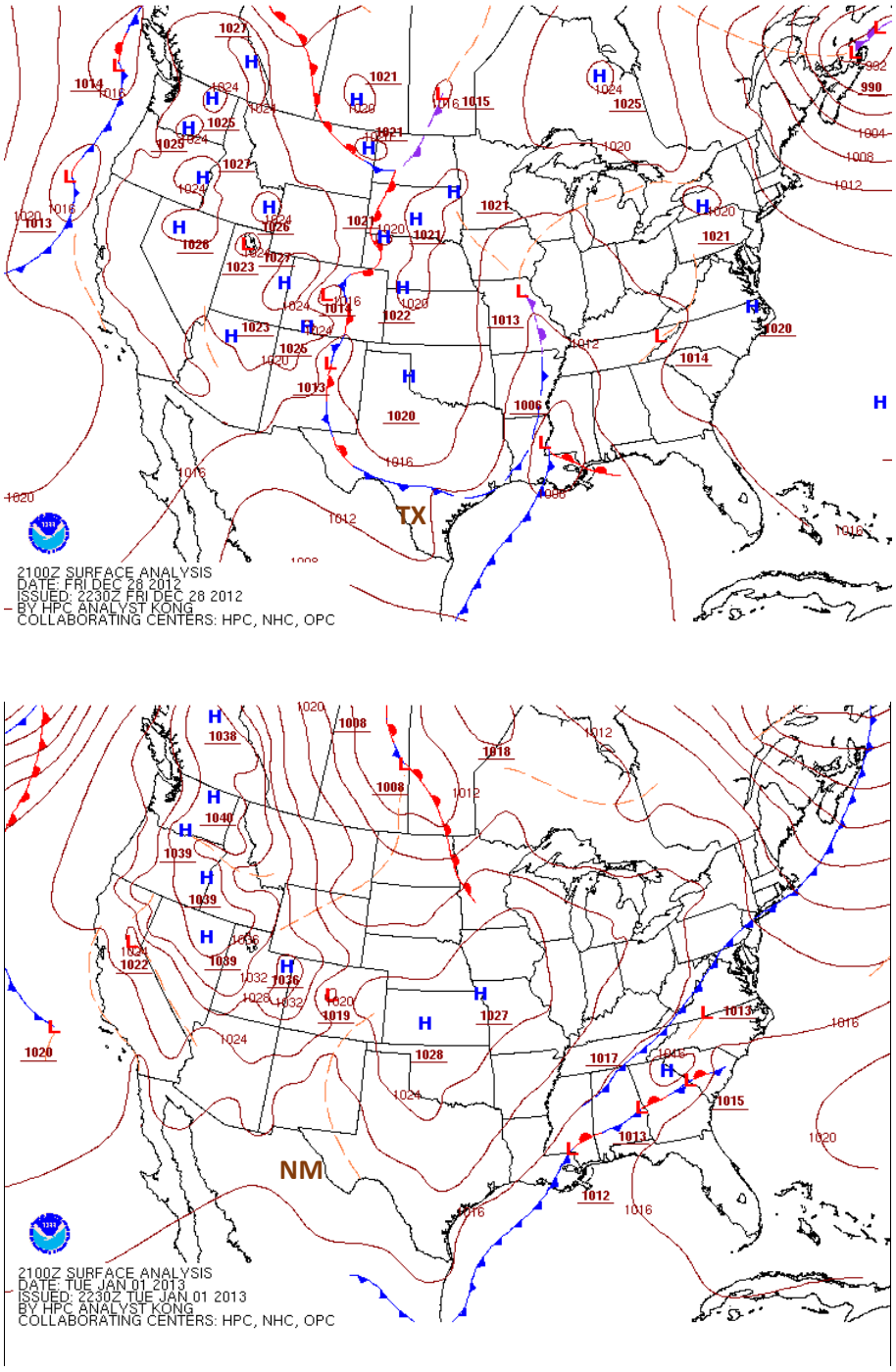

Figure 6.2 continued

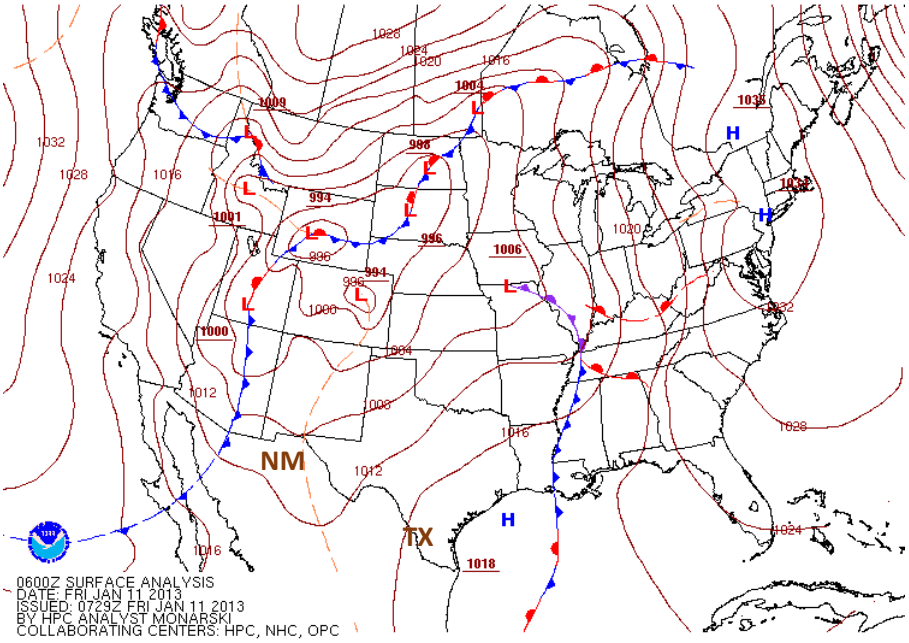

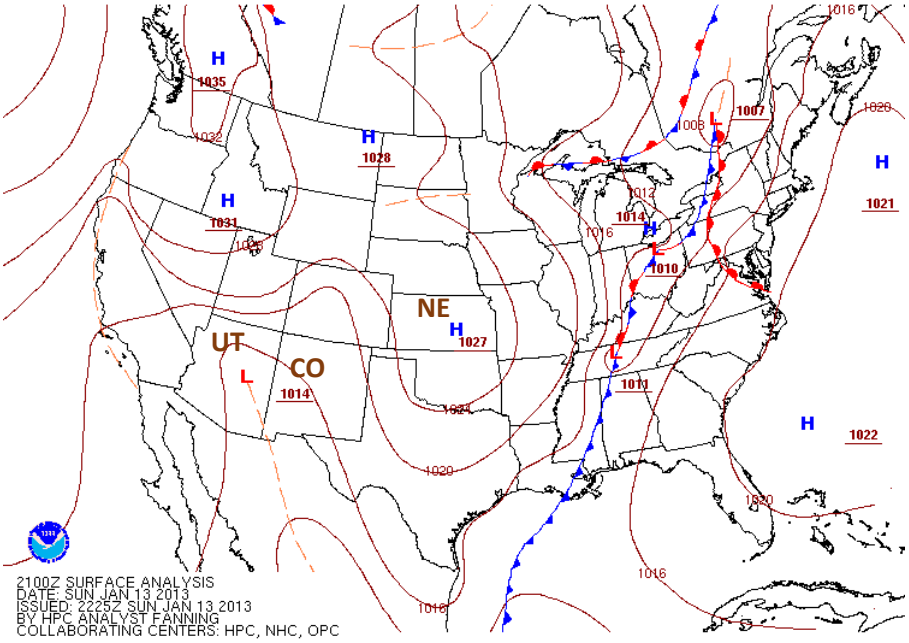

Figure 6.2 continued

Table 6.1 Summary of cold fronts between December 15, 2012 and January 13, 2013 identified from meteorological observations at FRWL1 and weather maps, respectively.

Number	Time of cold front passage (UTC)	
	FRWL1 observation	Weather maps
1	12/17/2012 17:48:00	12/17/2012 21 UTC
2	12/20/2012 11:24:00	12/20/2012 12 UTC
3	12/26/2012 01:30:00	12/26/2012 00 UTC
4	12/28/2012 21:42:00	12/28/2012 21 UTC
5	1/1/2013 18:48:00	1/1/2013 21 UTC
6	1/10/2013 11:18:00	1/11/2013 06 UTC
7	1/13/2013 18:18:00	1/132013 21 UTC

We have used the NDBC wind data at 6 minutes intervals at station FRWL1-8766072- Fresh Water Canal Locks, LA (FRWL1), which is near the mouth of Freshwater Bayou Canal, just west of Vermilion Bay. Wind data from FRWL1 are used for making the wind rose (Figure 6.3), from which we can see that during this time period, the southerly, northerly, and northwesterly winds dominated. In the one-month period, five most frequent wind directions are from the north, northwest, southeast, east and northeast, among which the north winds are the most prevailing, occurring about 65%, 30%. Strong winds of speed more than 10.0 m/s are rare, being observed from only one direction - northwest (~1.2%), which are mostly associated with cold front passages.

During the first two weeks, three cold fronts affected the study area. Before moving into the study area (December 17), two cold fronts were derived from the same low pressure center located on the northern Lake Michigan. Impacted by the adjacent high pressure center in the southwest, one of the fronts weakened and gradually disappeared. The other front, however extended all the way into the Gulf of Mexico, as a frontogenesis passing the region on about 12/17/2012 12:15 PM . The isobar with 1001 hPa in the middle (covering Ohio, Indiana, Illinois, and Kentucky) of the system was completely closed on 12/17/2012 18 UTC, forming a new low pressure center. While it was moving eastward, the cold front passed the study area again around

12/17/2012, 21 UTC. The second cold front was associated with a low pressure center located in Nevada on 12/18/2012 12 UTC. From 12/19/2012 03 UTC, a high pressure extended from Pacific to inland, propelling the low pressure center eastward. Until 12/20/2012 00 UTC, isobar of 1031 hPa closed itself and thus became an independent high pressure center in Utah. The low pressure center continued to strengthen, dominating a larger area while moving eastward. During the frontal passage, U.S. continent was mainly controlled by one high pressure system in the west and one low pressure system in the east, the latter of which developed deeper and deeper with denser isobars, leading to the maximum postfrontal northerly winds of 14.3 m/s following southeasterly winds. The wind returned to southerly prior to the third cold front on December 26. On 12/25/2012 15 UTC, one stable high pressure system dominated part of the northern U.S. while in the south a well-developed cyclone stayed in Texas later that day. Two cold fronts were derived from this meso-scale cyclone: the northern one quickly separated; while the southerly secondary cold front remained and finally became a cold front on 12/25/2012, 18 UTC, accompanied by the lowest pressure of 996 hPa. The fourth event originated from a stationary front associated with the low pressure zone in the Gulf of Mexico off Texas coast, which developed into a low pressure center on 12/28/2012 09 UTC. It was extending northeast while a series of high pressure systems in the northwest pushing the cold front through Louisiana coast. In the beginning of 2013 (January 1, 00 UTC), two large high pressure systems dominated the east coast and the northern part of the U.S. respectively. At the same time, there was a low pressure center in Mexico, on the northeast of which an inverted trough (characterized by decreasing pressure from north to south) formed between those two high pressure systems (one in the east coast and the other in the northern U.S.). The cold front in this event existed right on the inverted trough. Until the cold front passed the study area, the high pressure system in the

north had been moving southward. Furthermore, this anticyclone merged with several high pressure centers in the northwest and expanded into the whole U.S. continent, resulting in a persistent northerly wind in the computational domain dominating the first week of January. The sixth cold front on January 10, 09 UTC evolved from an occluded front associated with a low pressure center in Texas. At the same time, a high pressure center started developing from Mexico. In the next three hours, the pressure gradient intensified and pushed the front eastward. In addition, the high pressure system was continuously developing in the northeast while a series of low pressure centers dominated the northwest. Plus occluded front was located right at the interface zone between those two opposite systems, which is why the wind shear was significant. An elongated cold front was originated from a low pressure center located in Lake Michigan on 1/12/13, 12 UTC. Pushed by the high pressure system on its southwest (Colorado and Nebraska), the low pressure zone at the front tail was isolated, forming a new closed isobar associated with the cold front in Texas. The development of the high pressure system in the northwest (Utah and Colorado) then drove the front southeast entering the Gulf of Mexico. That is how the seventh cold front was derived.

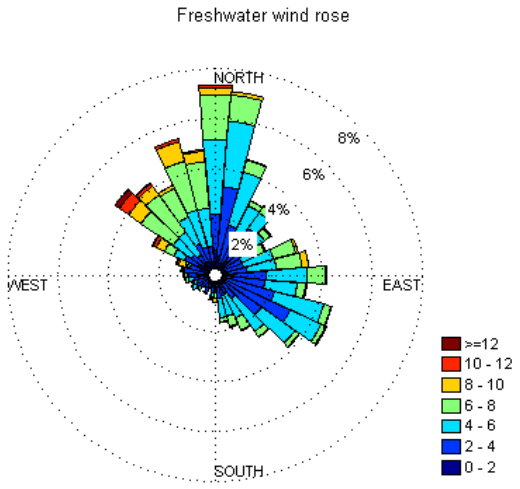

Figure 6.3 Wind rose compiled from site FRWL1 during 12/15/2012 and 1/20/ 2013.

Despite the seemingly complex synoptic weather patterns during this period, there were several general patterns that can be identified. First of all, according to the observed time of cold front passages (summarized in Table 6.1), we can easily find the return period of the cold front event for the study area to be 3 to 8 days (Fernandez-Partagas and Mooers, 1975; Angelovic, 1976; DiMego et al., 1976). By comparing the weather maps and wind data from the study area, each cold front event can be identified based on the wind pattern characterized by the abrupt change in wind direction, when the surface wind quickly shifts from the prefrontal southeast wind to the stronger postfrontal northwest wind (Figure 6.1). This direction persists until the next cold front approaches. For the study area, each cold front event lasted around 2 days except the fifth which lasted for almost 10 days. The wind intensity varies significantly by increasing from the non-event speed of about 6 m/s to around 15 m/s. Before the cold front arrives, the air pressure decreases steadily. While the front is passing, the value first reaches the locally lowest point and then followed by a rapid increase. After the front passes the area, the barometric pressure continues to increase slowly. The air temperature shows a similar pattern, where the air temperature at the frontal passage has a sharp decrease.

The FRWL1 wind magnitude is usually smaller than that from ocean stations such as WAVCIS CSI06 (Figure 6.5), where the phase shift (3-4 hours) is due to the distance (about 190 km) between the two stations. FRWL1 has a better agreement with CSI03 than CSI06 since CSI03 is located near the 5 m isobath on the inner shelf south of Vermilion Bay. Overall, NDBC FRWL1 wind data are more representative of the wind over the Wax Lake-Atchafalaya delta complex, and therefore is used in the modeling of the passage of each cold front.

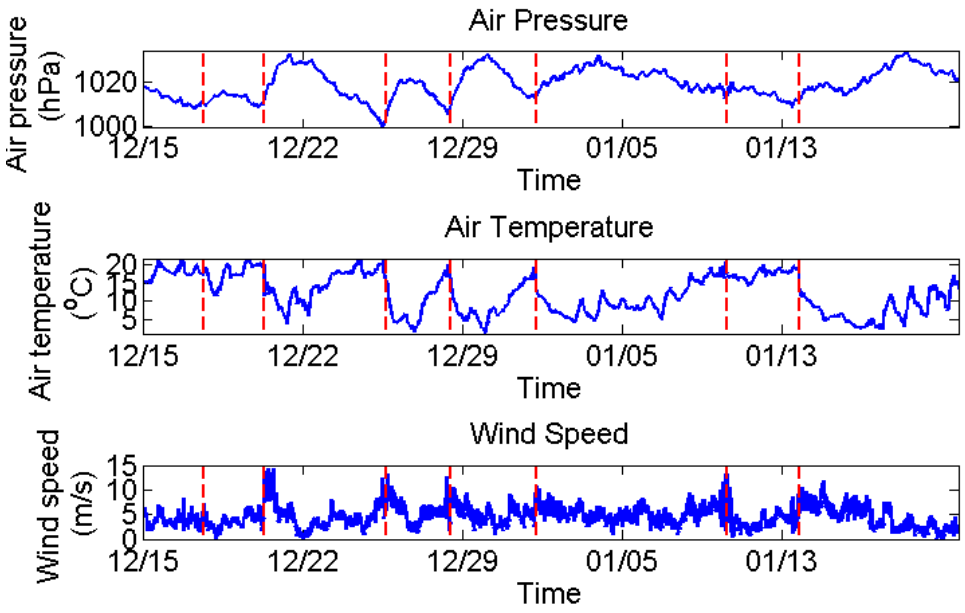

Figure 6.4 Observed cold front events (meteorological data from FRWL1) during December 12, 2012 and January 13, 2013. Upper panel: atmospheric pressure; middle panel: air temperature; lower panel: wind speed. Vertical dashed lines indicate time of cold front passages.

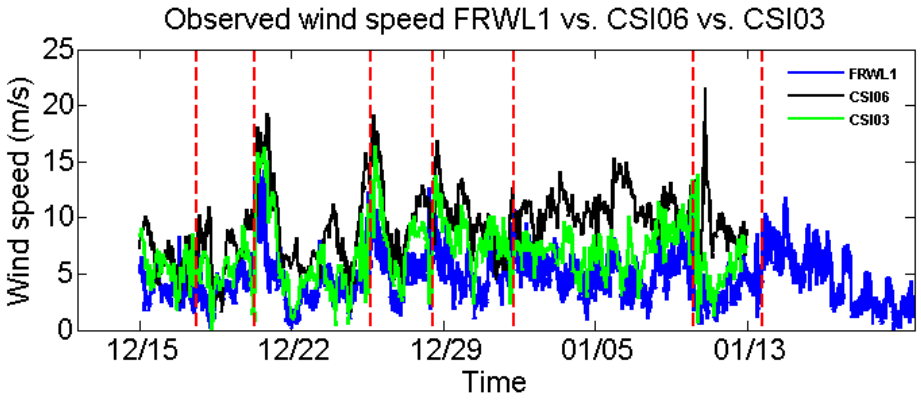

Figure 6.5 Comparison of observed wind speed at NDBC FRWL1, WAVCIS CSI06 and WAVCIS CSI03 during the cold front events between December 12, 2012 and January 13, 2013. Vertical dashed lines indicate time of cold front passages.

6.3 CIRCULATION FROM MODEL RESULTS

In this section, the model results for the response of water level and circulation are analyzed. The model setup and run is first discussed, followed by a discussion of results on the circulation within the domain outside of the bay. A discussion on the Wax Lake delta area is then focused on.

6.3.1 Offshore Circulation Patterns

In this section, the simulated near-surface velocity vectors are discussed when different cold fronts passed the Wax Lake-Atchafalaya delta region (Figure 6.6-6.9). Results showed that the surface currents over the water south of the delta complex followed the cold front winds. Both cyclonic (12/24/12, 12/25/12) and anti-cyclonic (12/21/12, 12/22/12) gyres were created under the cold fronts associated with wind direction change. Strong winds itself cannot necessarily generate gyres, it is however the wind direction that plays a more important role.

On December 21, 16:00 UTC, the strong postfrontal northwestern wind of 11 m/s dominated the whole domain, resulting in an eastward transport of water offshore of the Vermilion Bay and West Cote Blanche Bay. The postfrontal wind strongly affected the surface currents over the shallow Wax-Atchafalaya delta system with southwesterly and westerly currents reached 1 m/s. The response of the shelf south of the two deltas was an anti-cyclone gyre with southward currents in the east and northward currents in the west, exhibiting stronger currents at the north and eastern limb. As a result of persistent northerly to northwesterly winds, southward to southeastward currents were dominant over the shelf during the hours that cold front translated the outer and inner shelves. Another anti-cyclonic gyre was generated on the west of the Mississippi delta on December 21, 20 UTC, under the northwesterly wind, which had the similar pattern of stronger currents on the eastern and north limbs. This gyre lasted less than 8 hours. On December 22, 08 UTC, the first gyre on the shelf also disappeared, with a westward to southwesterly current. 4 hours later (December 22, 12 UTC) however, the gyre reappeared, as an anti-cyclone with stronger currents on the east limb. The wind at this time were northeasterly, creating a westerly transport of water flow pattern offshore of the Barataria and Terrebonne Bay.

The wind direction was toward the southwest, so the gyre moved in this direction as well. Until the wind became southeast, the gyre disappeared and the whole offshore domain was dominated by northwest currents.

A cyclonic gyre on the shelf south delta was observed from model results on December 24, UTC 08, with a northward currents in the east and southward currents in the west, which follows the strong prefrontal winds. In the next four hours, in spite of increased wind speed by 1 m/s, the gyre appeared a little bit weaker. But offshore south of the Wax Lake-Atchafalaya delta as well as Barataria and Terrebonne Bay seemed to have more energetic activities. When the wind is toward northeast, the gyre were almost invisible. Until December 24, 16 UTC, the surface current in the domain followed the wind direction, indicating the predominant effect of wind stress on near-surface currents.

On December 25 04 UTC, two visible cyclonic gyres were formed on the shelf south of the Atchafalaya Bay as well as Barataria and Terrebonne Bay, with stronger currents of 0.3 m/s on the north side. This gyre disappeared when the wind shifted from south became the prefrontal southeasterly. Since then, the surface currents offshore west of the Barataria Bay followed the winds while the currents offshore on the east side moved to northeast.

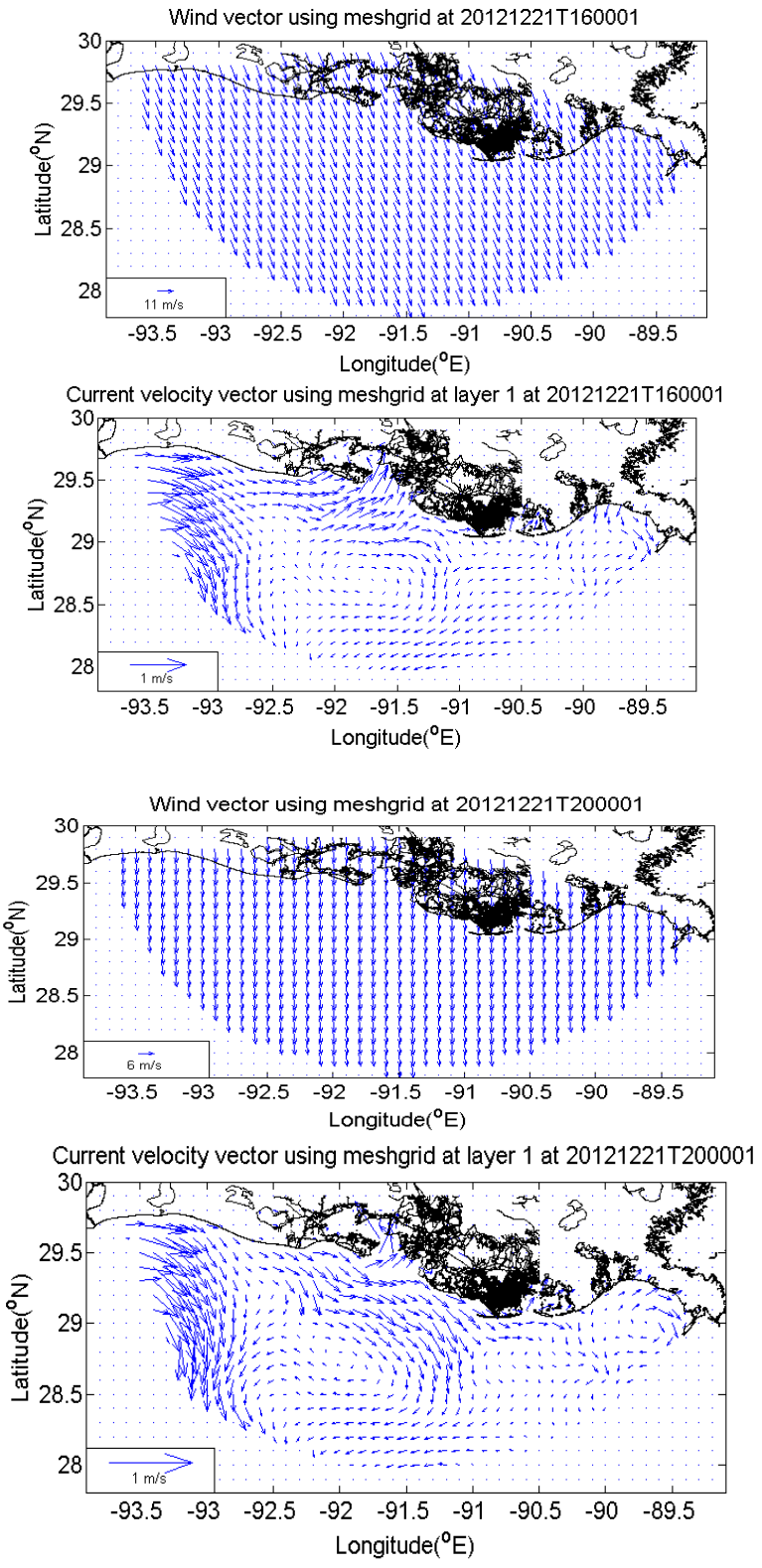

Figure 6.6 Simulated near-surface currents induced by cold fronts on December 22, 2012.

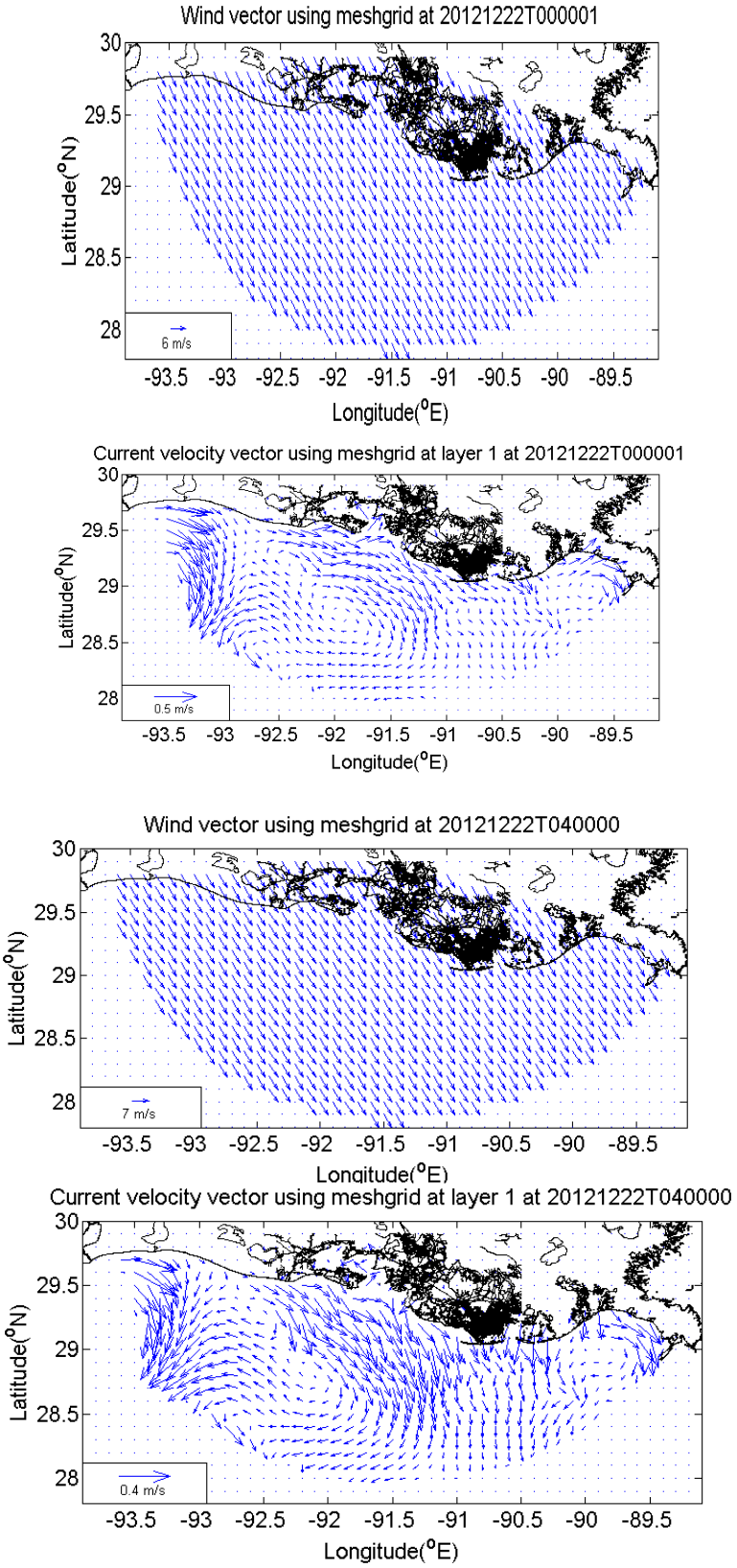

Figure 6.6 continued.

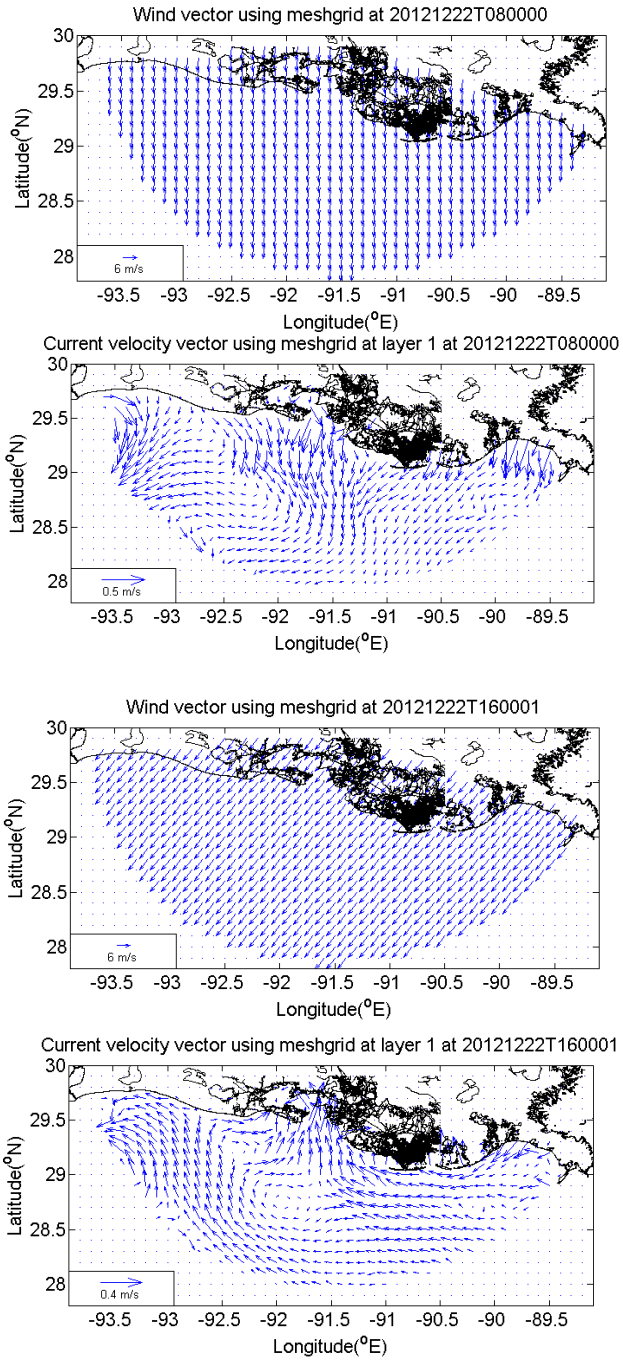

Figure 6.6 continued.

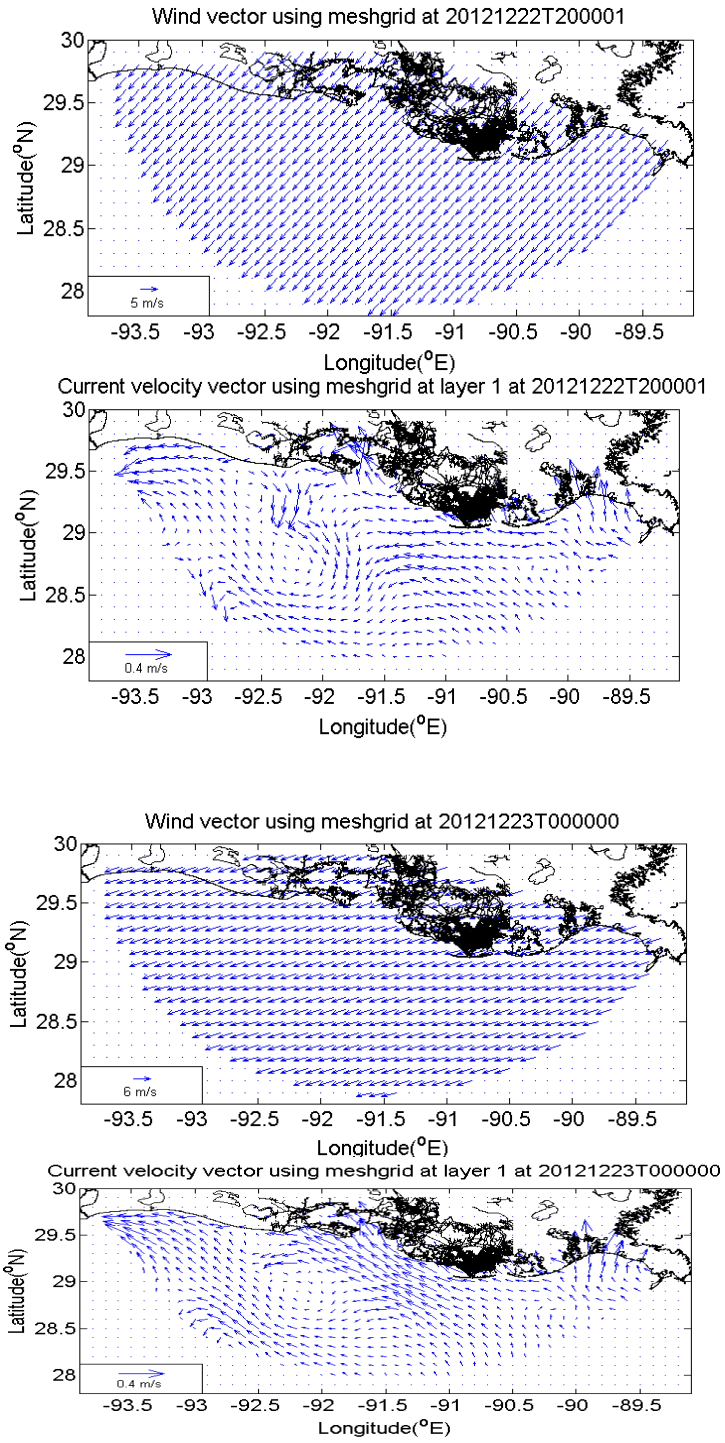

Figure 6. 7 Simulated near-surface currents induced by cold fronts on December 23, 2012.

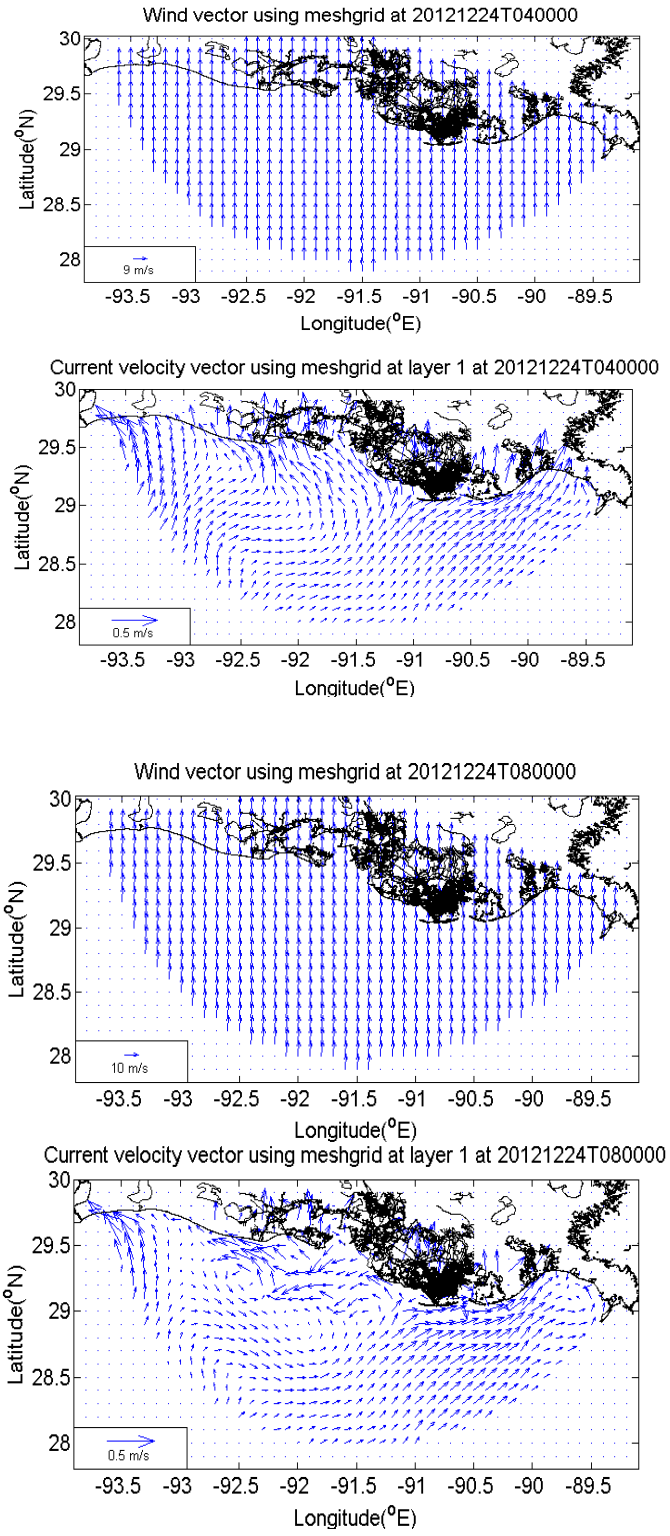

Figure 6. 8 Simulated near-surface currents induced by cold fronts on December 24, 2012.

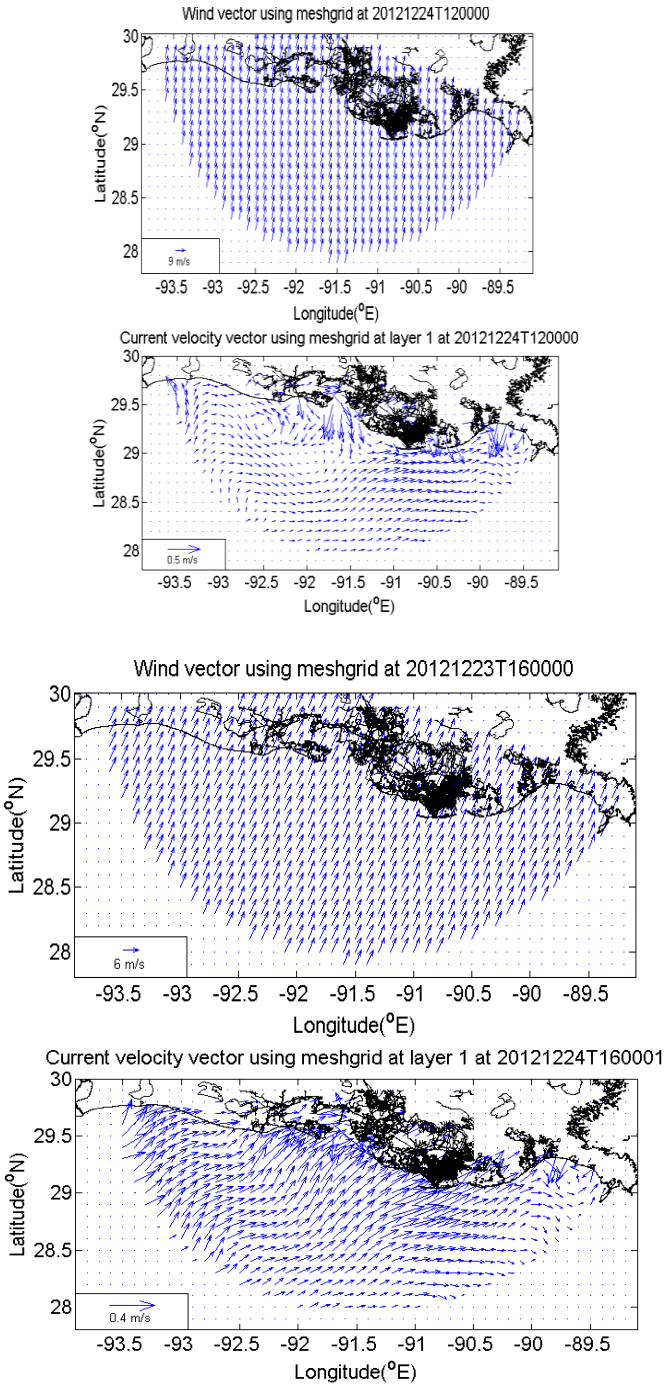

Figure 6. 8 continued.

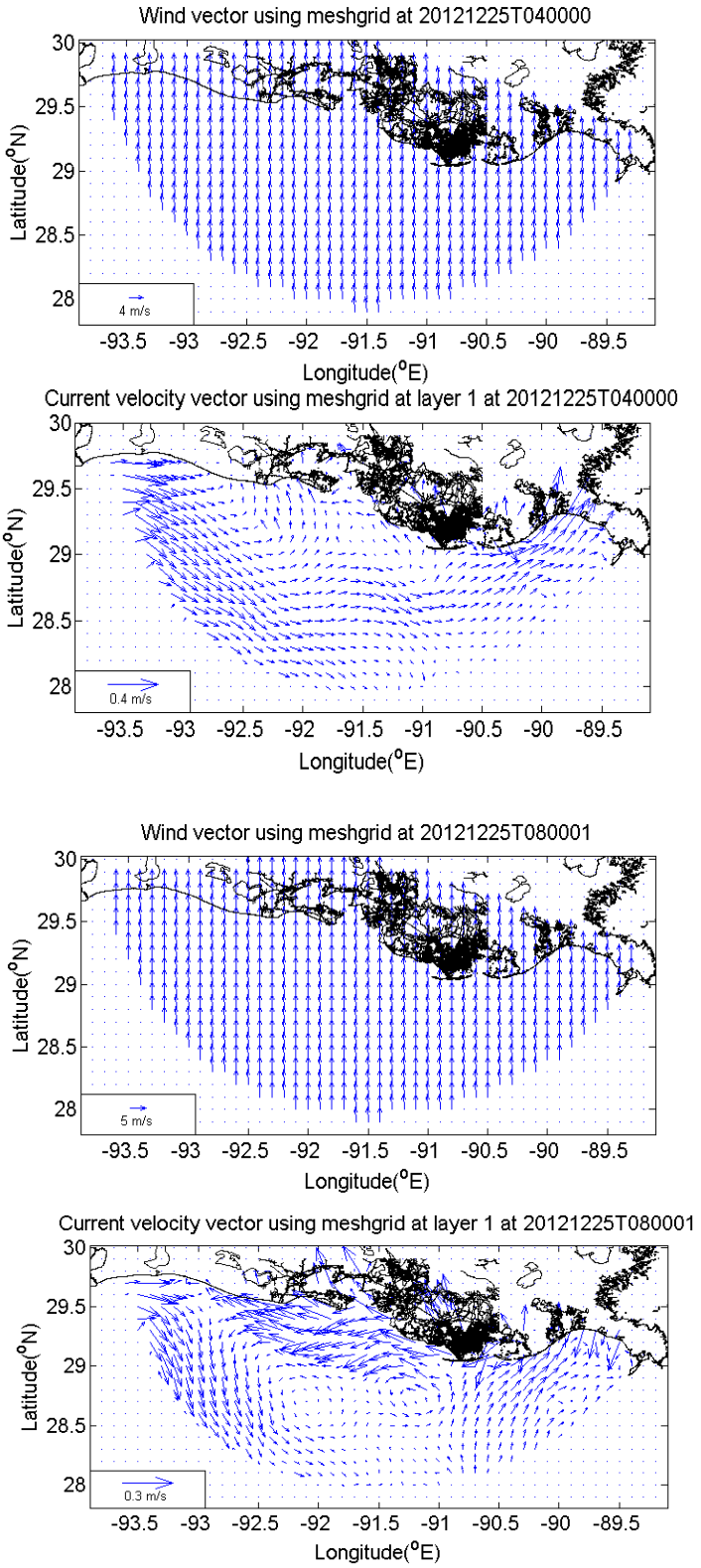

Figure 6. 9 Simulated near-surface currents induced by cold fronts on December 25, 2012.

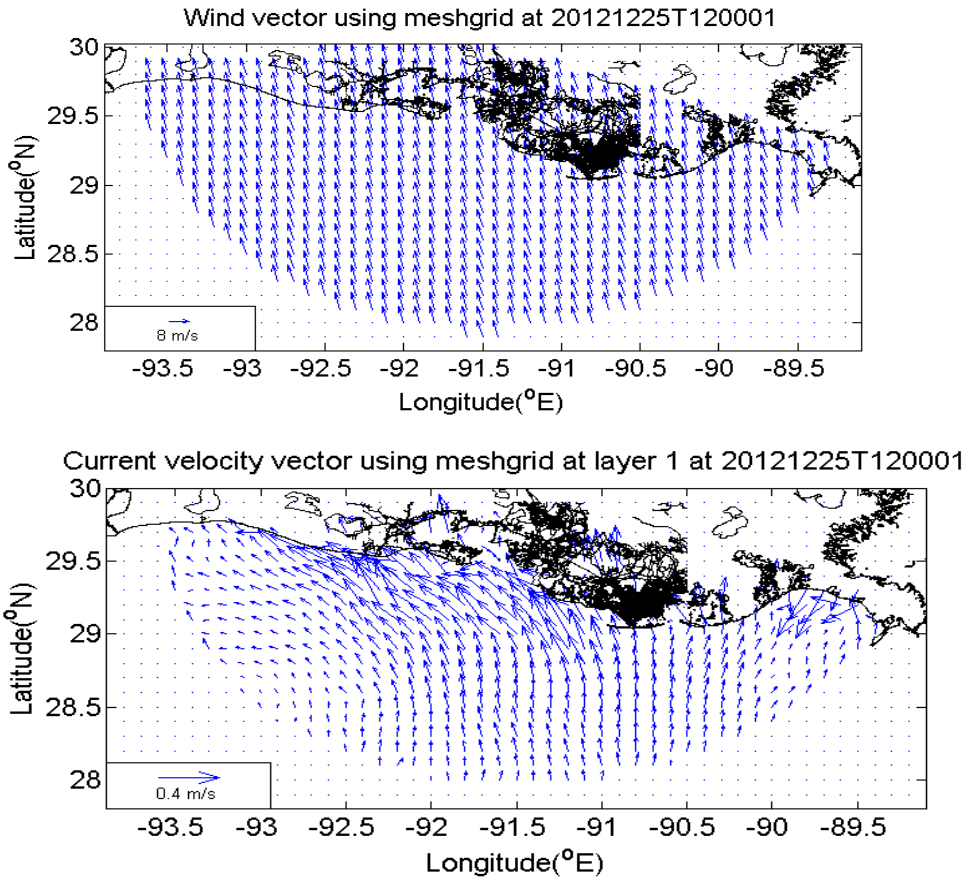

Figure 6. 9 continued.

6.3.2 Current Pattern in the Wax Lake Delta

The simulated near-surface velocity vectors, surface elevation, and spatially uniform wind fields are presented (Figure 6.10-6.16) for 7 cold front events from December 15, 2012 to January 13, 2013. The first cold front on December 17 was not very strong, where the magnitude of 4 m/s southeaster wind can be read from the wind field map. Basically the currents offshore the Wax Lake delta followed the prefrontal wind, moving southerly. Some of the flow might enter into the Wax Lake delta bifurcating channels, but would not shift the flow direction due to stronger (0.7 m/s) and persistent discharge input from the upper stream. Instead the channel outflow pushed the wind-induced currents offshore, resulting in a clockwise pattern, which could be clearly identified during the frontal passage phase (Figure 6.10 lower right). That was also a result of

wind shift by blowing easterly and an obvious water setdown would serve as a verification of offshore circulation. The second cold front (December 20, 2012) was a typical one due to clockwise shift in wind direction and stronger and persistent postfrontal offshore wind. The prefrontal moderate wind set up the water level and drove a westward surface field. It was observed from the model results that the current on the east side of the domain tended to deflect to the right, which believed to be the Coriolis effect. Strong northwest wind generated an offshore clockwise current pattern, especially in the inland area that was inundated during the prefrontal phase. The 3rd prefrtonal wind (December 25, 2012) induced a larger water level surge as well as stronger onshore currents than those of the first two events, due to the larger wind magnitude of 8 m/s. The current velocity was comparable to the outflow in the channel, resulting in a reverse flow and big water intrusion in the subaerial area adjacent to the distributaries in the Wax Lake delta. Again, a counterclockwise current pattern formed on the west of the delta while a clockwise circulation on the east side. Four hours later, the wind changed direction to blowing north to northeast. The flow field in the domain shifted accordingly too, with a weaker strength. When the wind changed to westerly, the water level was set down and strong southeast flow pattern were formed. The postfrontal wind lasted for another 16 hours until becoming persistent northwest on December 26, 20 UTC. On December 28, 2012, 20 UTC, the fourth cold front initiated a southeast wind of 6 m/s, where stronger offshore currents, return flow in the channel and water intrusion on inland areas inside the Wax Lake delta were clearly visible. Especially a anti-cyclonic gyre were formed on the east boundary. The winds were then weakened (3 m/s) by blowing northeast and persisted as a postfrtonal northwest wind with magnitude of 8 m/s in 8 hours, followed by the similar circulation pattern in current flow. The 5th cold front persisted about 7 days from January 1, 2013, where the westward currents were generated by southeast

wind. When the wind changed from southerly to northerly, a clockwise gyre was formed on the west of the delta. It was noticed that the flow direction diverted prior to the wind shift. Since the postfrontal offshore wind dominated for about 6 days, the inundation and reverse flow were weak compared to previous frontal passages. The 6^{th} event started with an easterly wind that induced a westward flow field. During the frontal passage, the current flow changed in advance by intruding the inland area of the delta. When the wind blew southerly, a stronger eastward current field was generated on the south of the delta. For the 7the cold front, it started with westward flow induced by prefrontal onshore wind. Since the wind shift from south to west a clockwise pattern on the offshore west of the Wax Lake delta was formed.

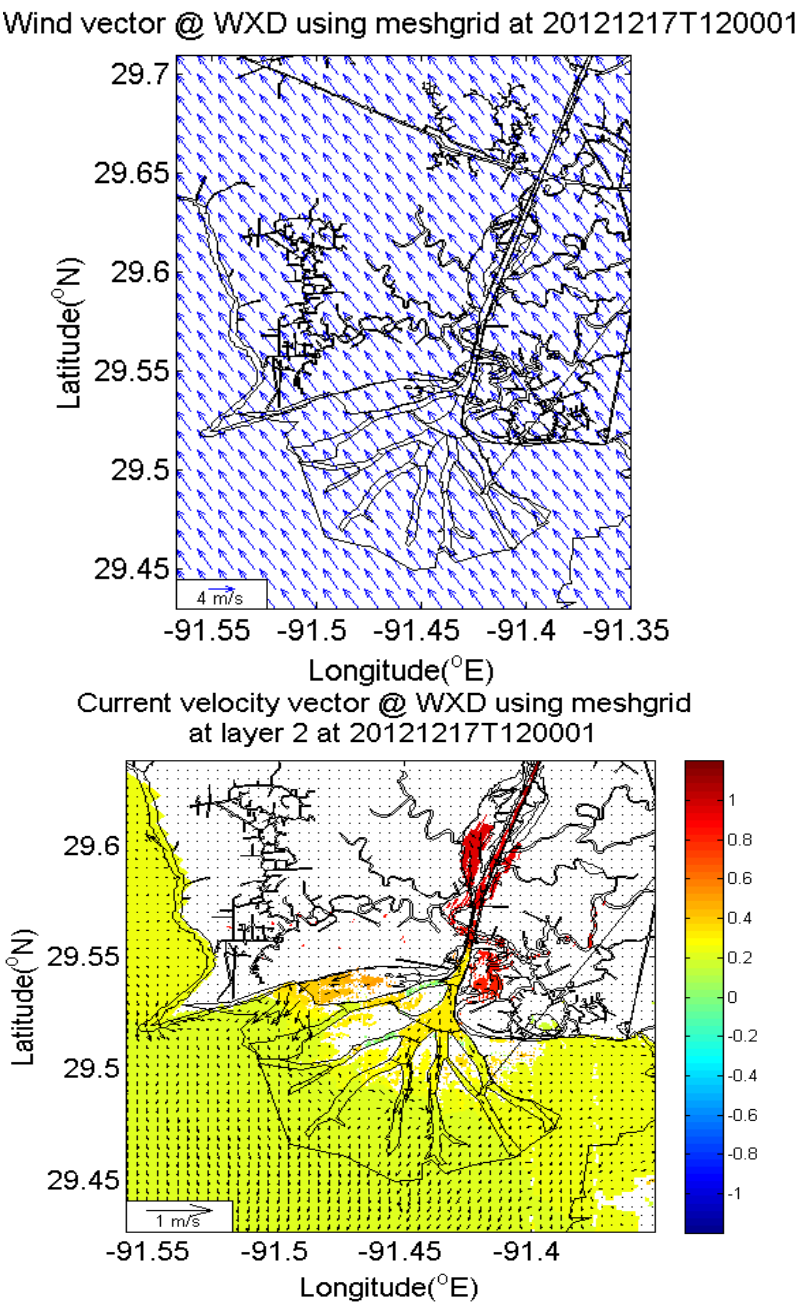

Figure 6.10 Plan views of the spatially uniform surface wind field, simulated surface elevation contours and near-surface velocity fields during the prefrontal, frontal, and postfrontal stages of cold front (cf1).

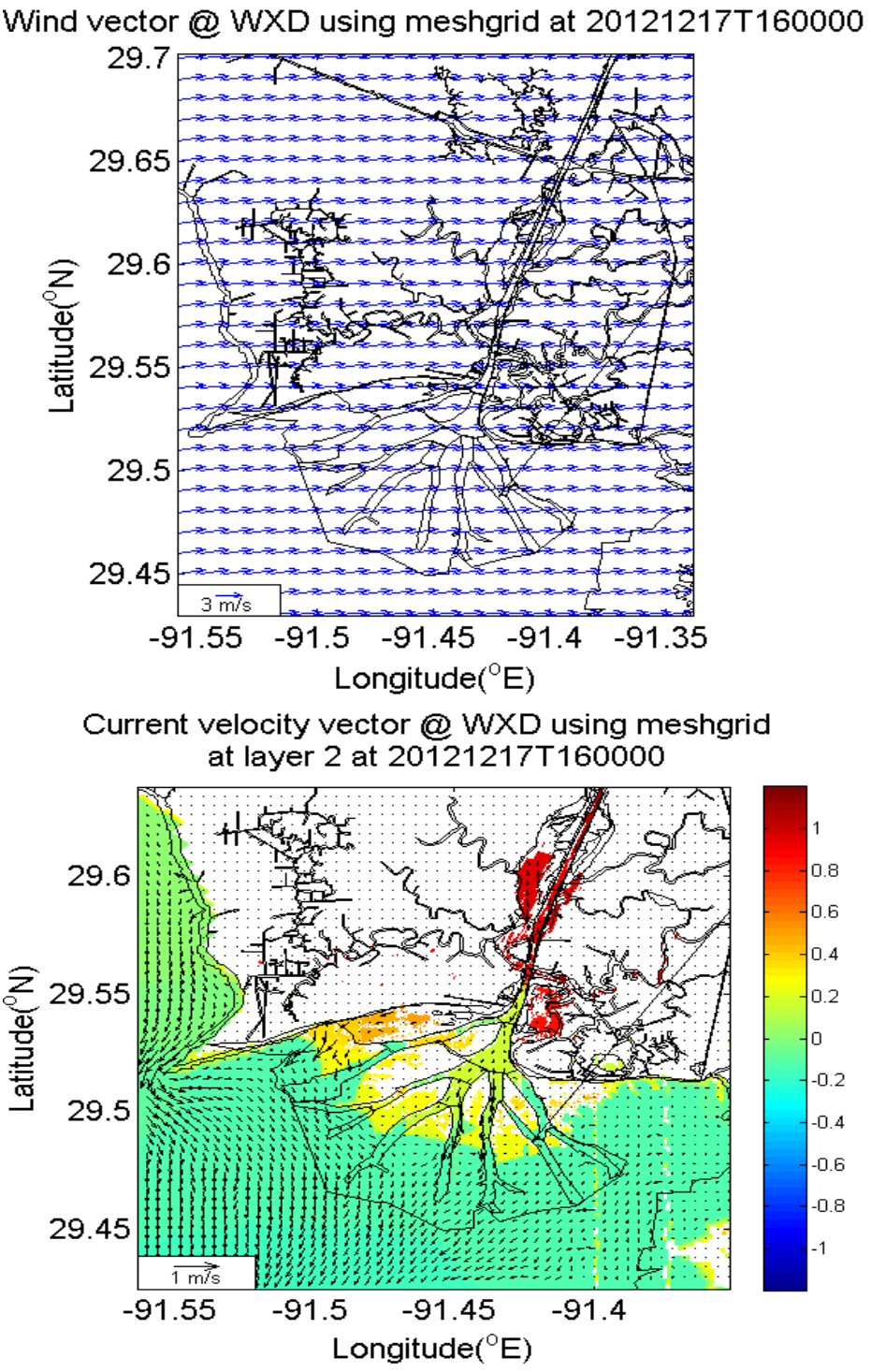

Figure 6.10 continued.

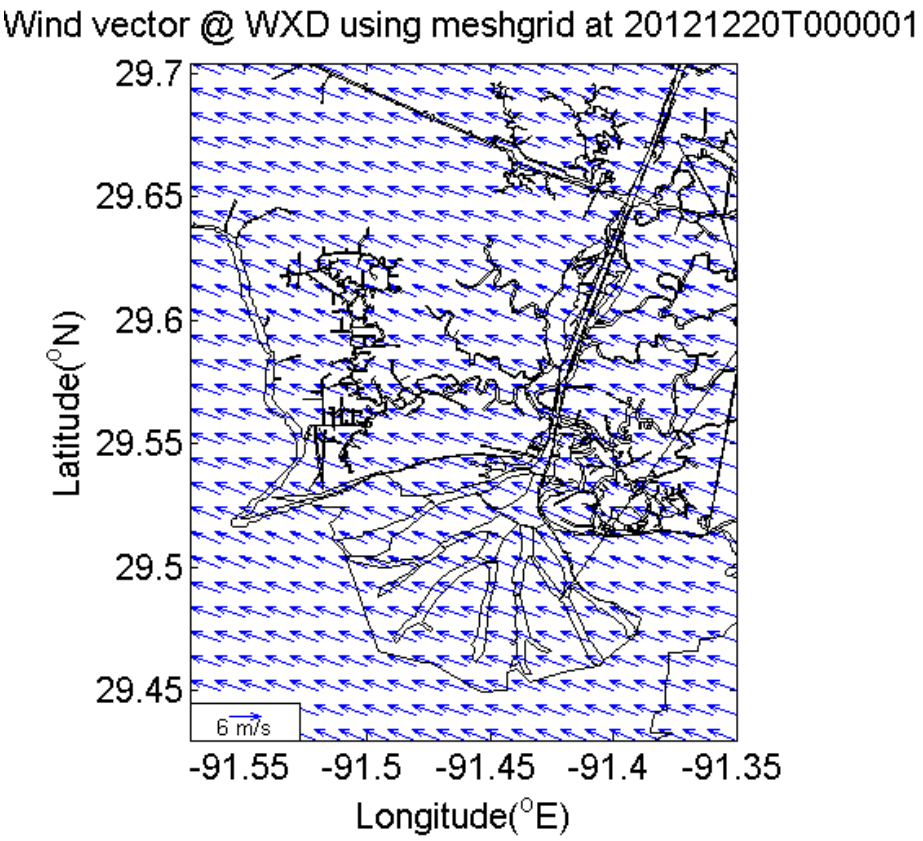
Wind vector @ WXD using meshgrid at 20121220T000001
29.7
29.65
29.6
29.55
29.5
29.45
Latitude(°N)
6 m/s
-91.55
-91.5
-91.45
-91.4
-91.35
Longitude(°E)

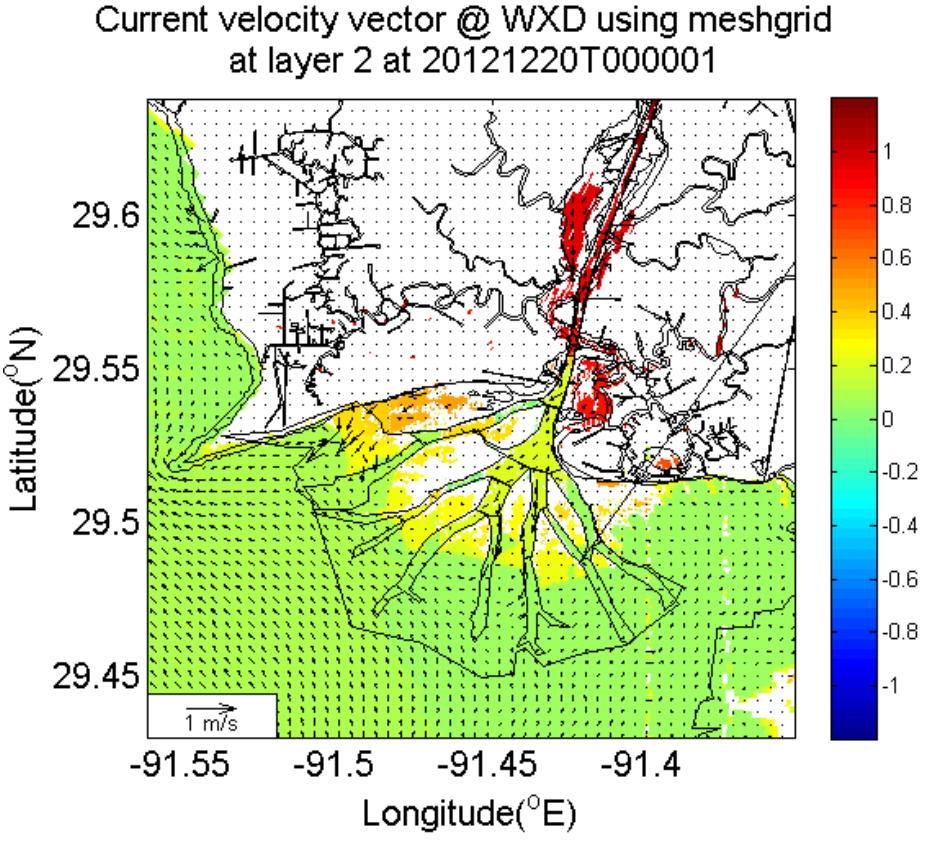
Current velocity vector @ WXD using meshgrid
at layer 2 at 20121220T000001
29.6
29.55
29.5
29.45
Latitude(°N)
1 m/s
-91.55
-91.5
-91.45
-91.4
Longitude(°E)
1
0.8
0.6
0.4
0.2
0
-0.2
-0.4
-0.6
-0.8
-1

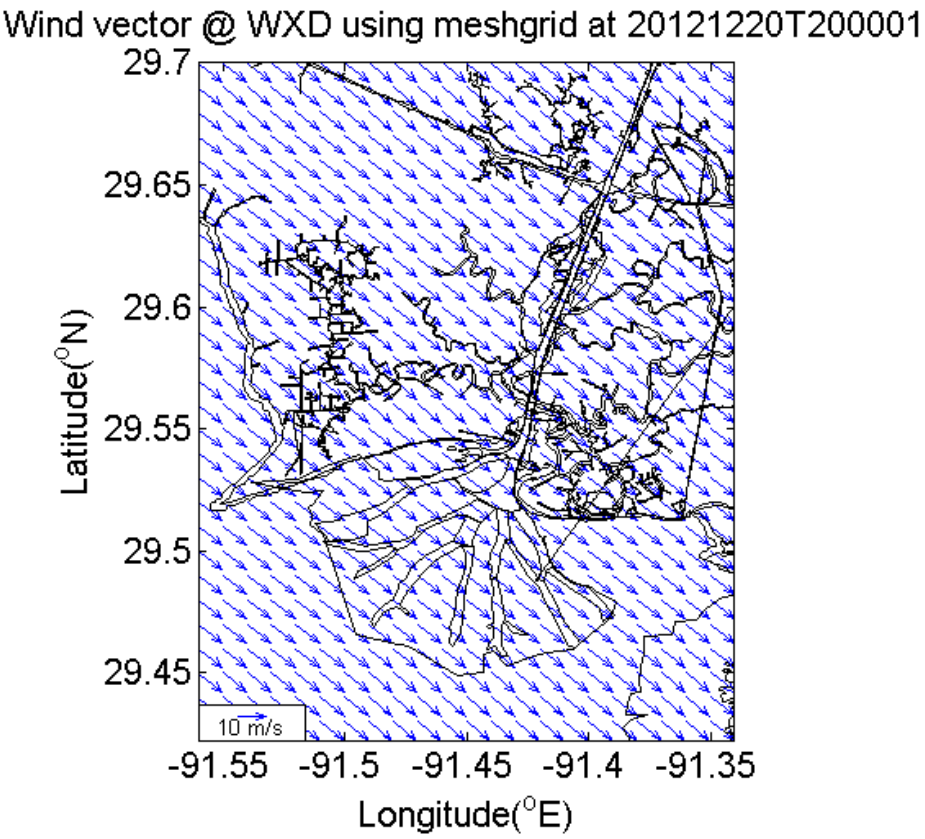
Wind vector @ WXD using meshgrid at 20121220T200001
29.7
29.65
29.6
29.55
29.5
29.45
Latitude(°N)
10 m/s
-91.55
-91.5
-91.45
-91.4
-91.35
Longitude(°E)

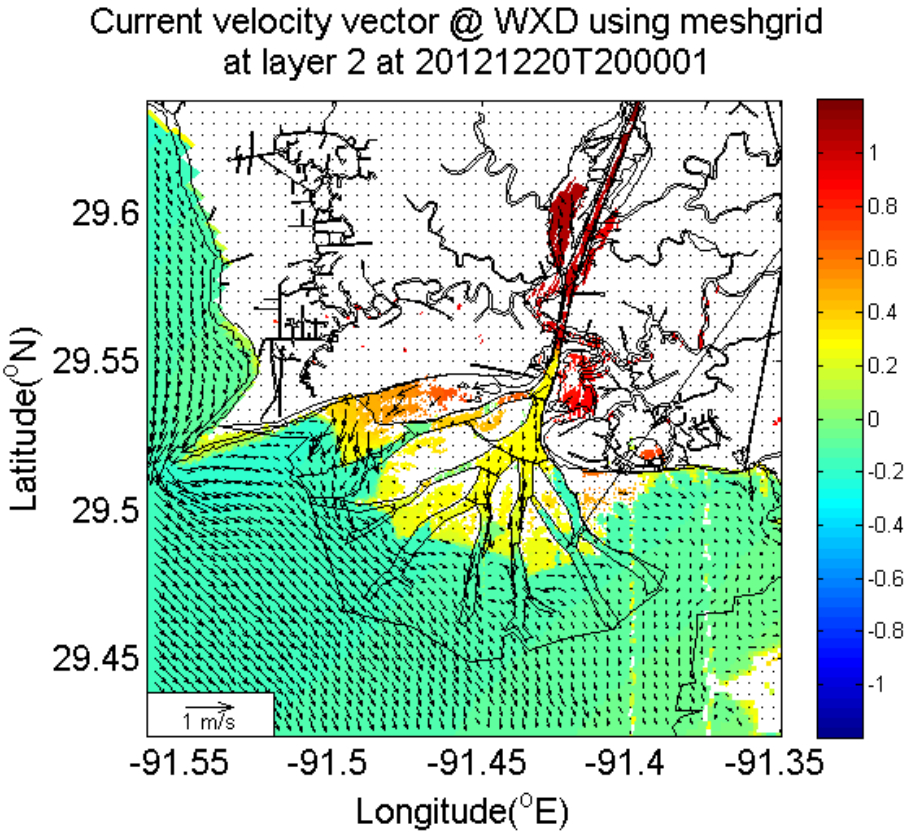
Current velocity vector @ WXD using meshgrid
at layer 2 at 20121220T200001
29.6
29.55
29.5
29.45
Latitude(°N)
1 m/s
1
0.8
0.6
0.4
0.2
0
-0.2
-0.4
-0.6
-0.8
-1
-91.55
-91.5
-91.45
-91.4
-91.35
Longitude(°E)

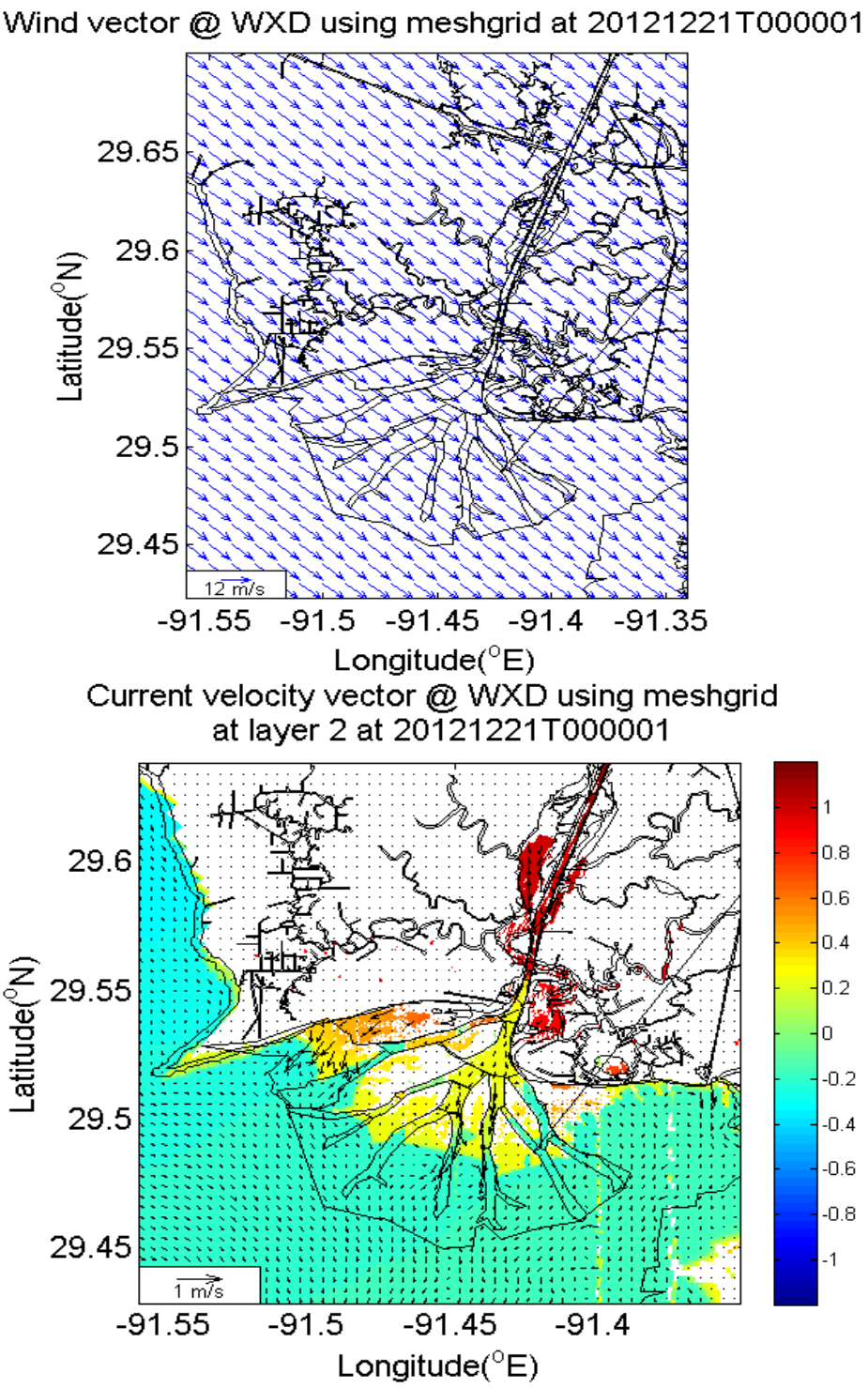

Figure 6.11 Plan views of the spatially uniform surface wind field, simulated surface elevation contours and near-surface velocity fields during the prefrontal, frontal, and postfrontal stages of cold front (cf2).

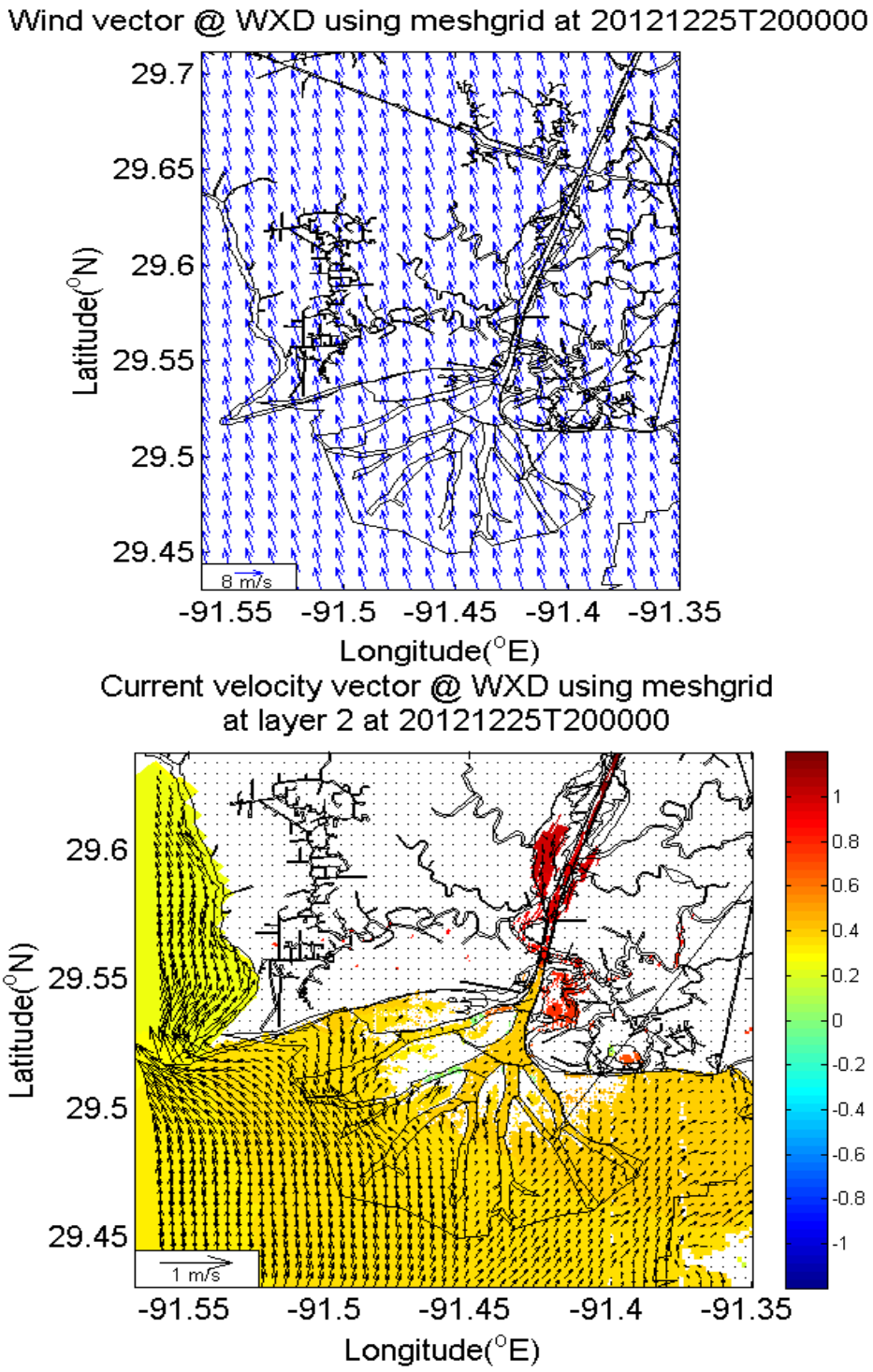

Figure 6.12 Plan views of the spatially uniform surface wind field, simulated surface elevation contours and near-surface velocity fields during the prefrontal, frontal, and postfrontal stages of cold front (cf3).

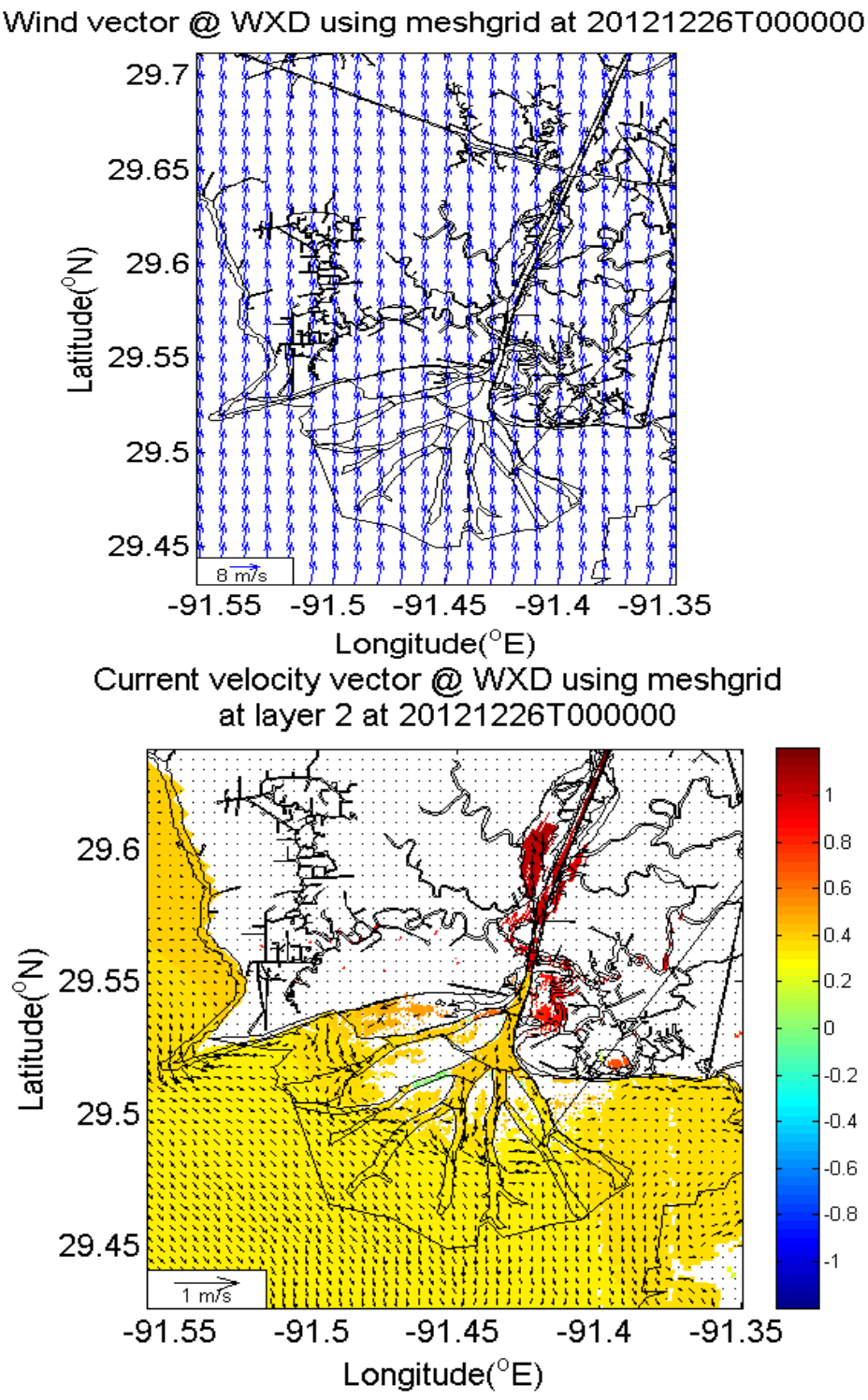

Figure 6.12 continued.

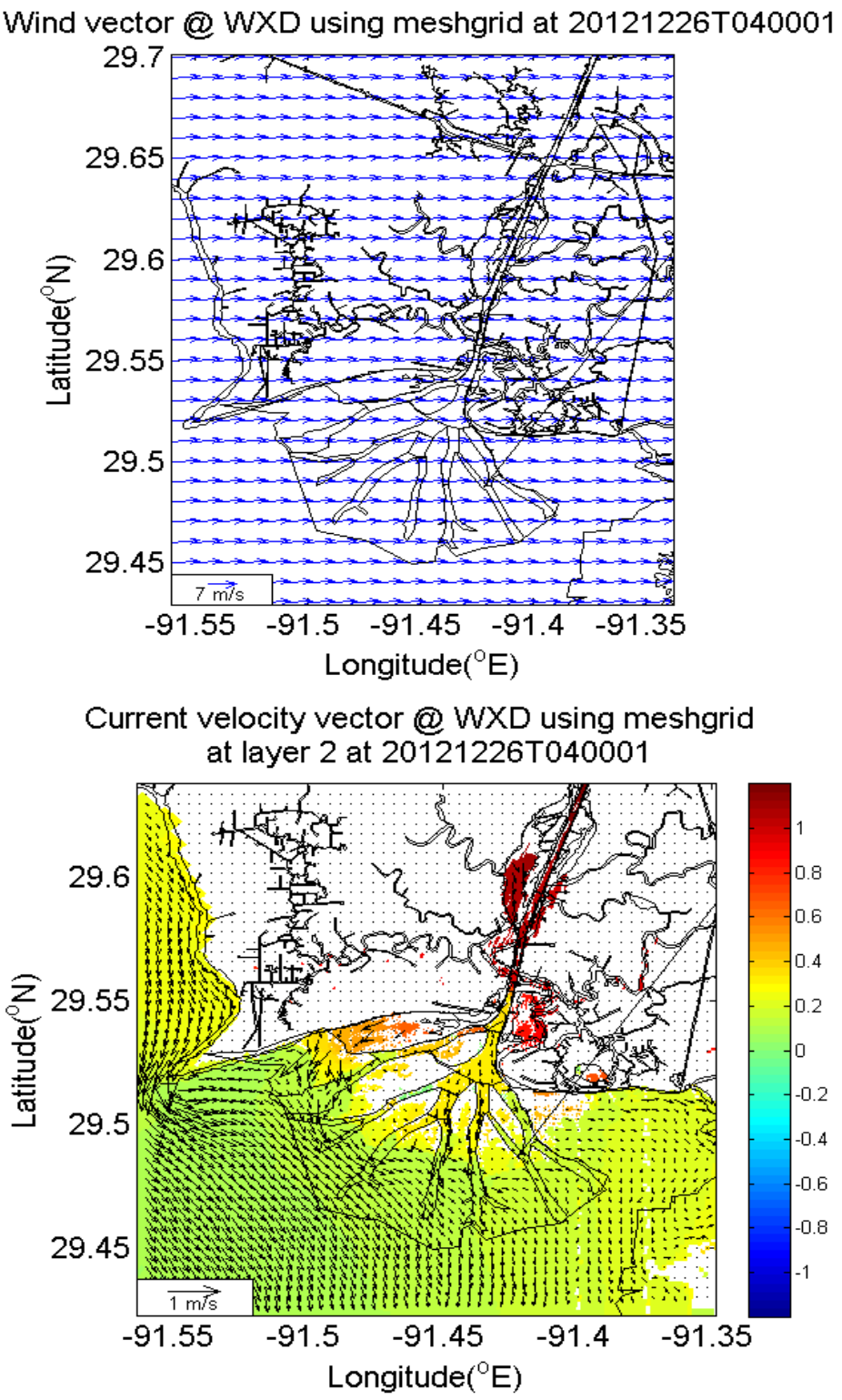

Figure 6.12 continued.

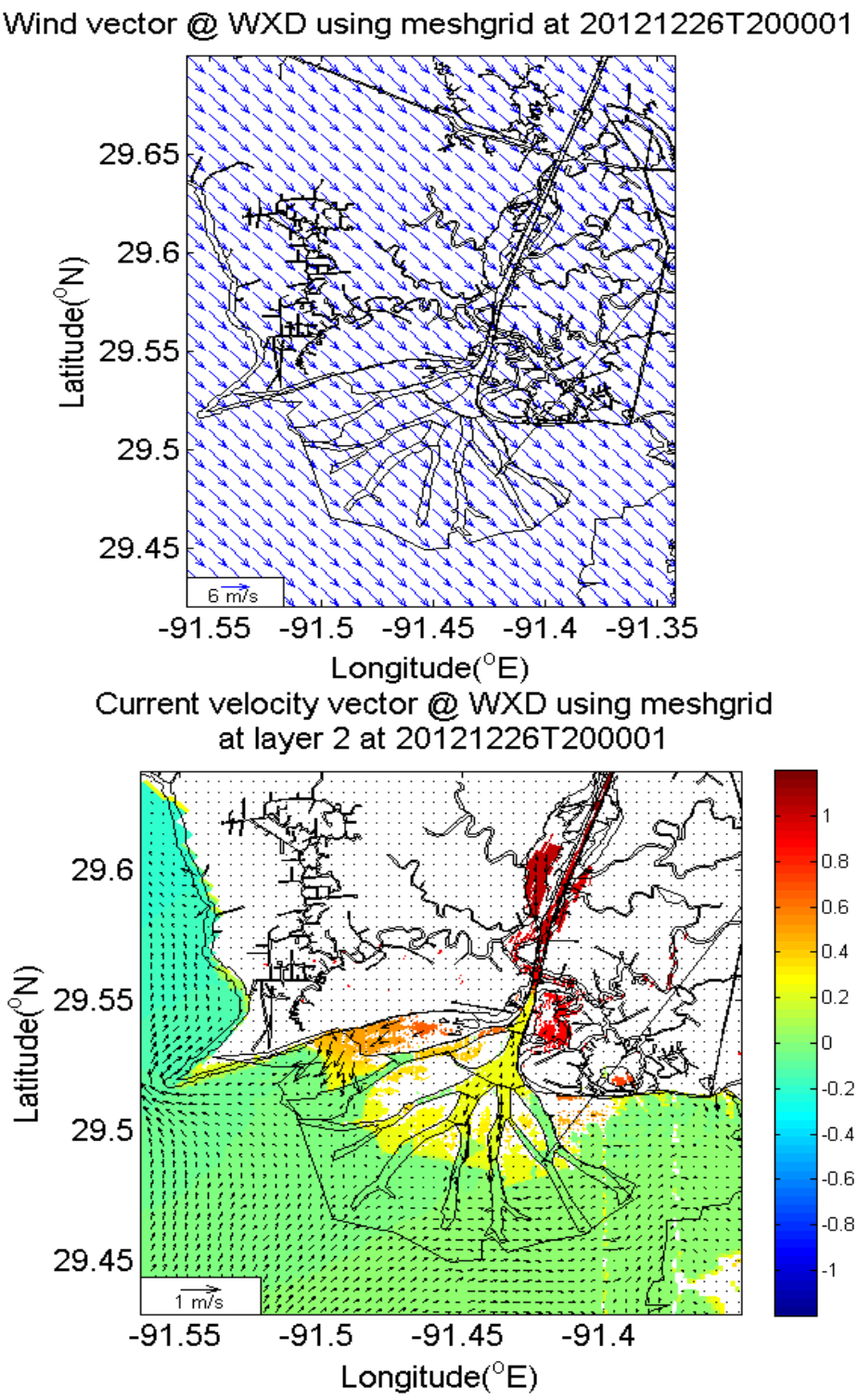

Figure 6.12 continued.

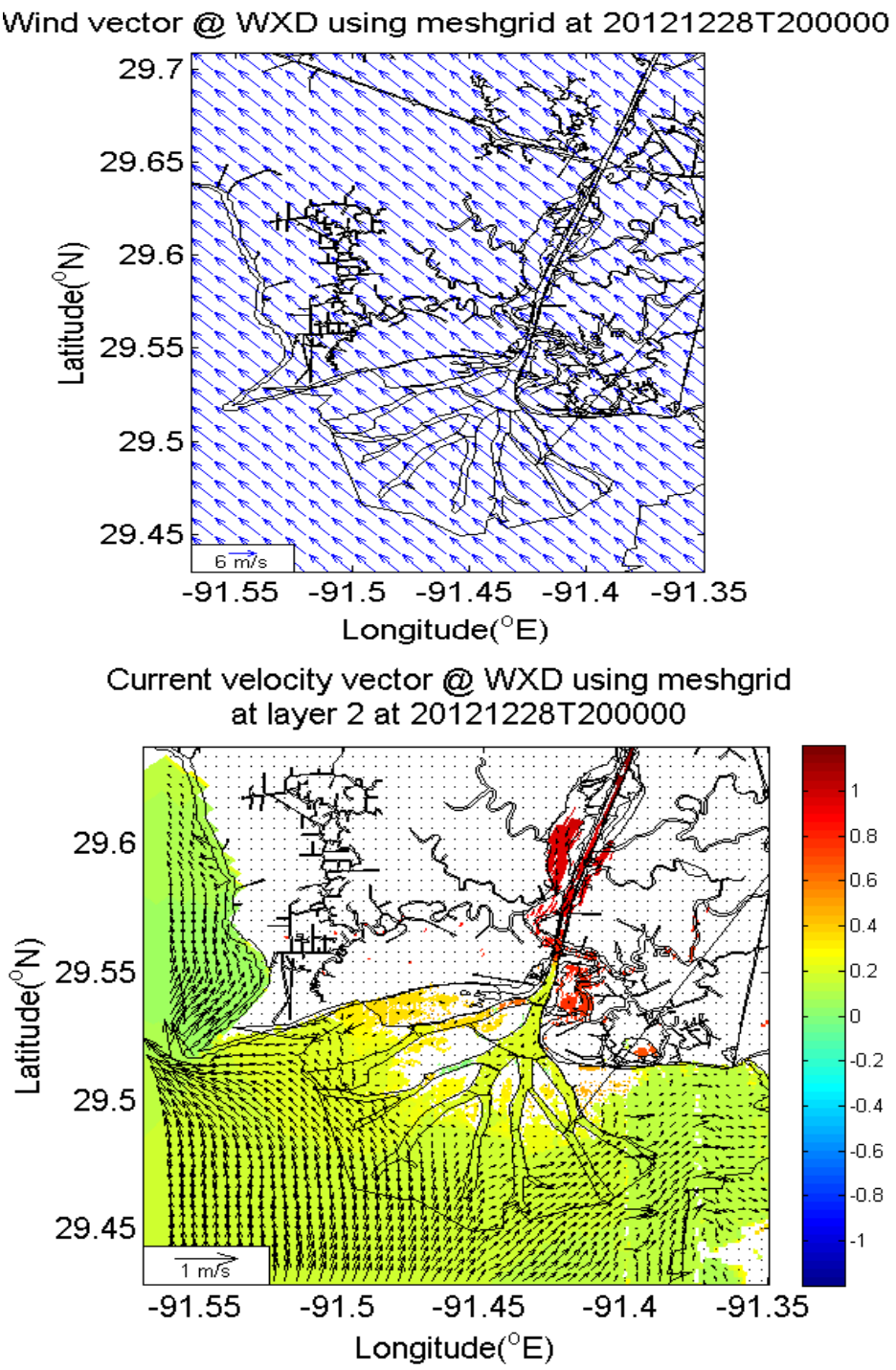

Figure 6.12 continued.

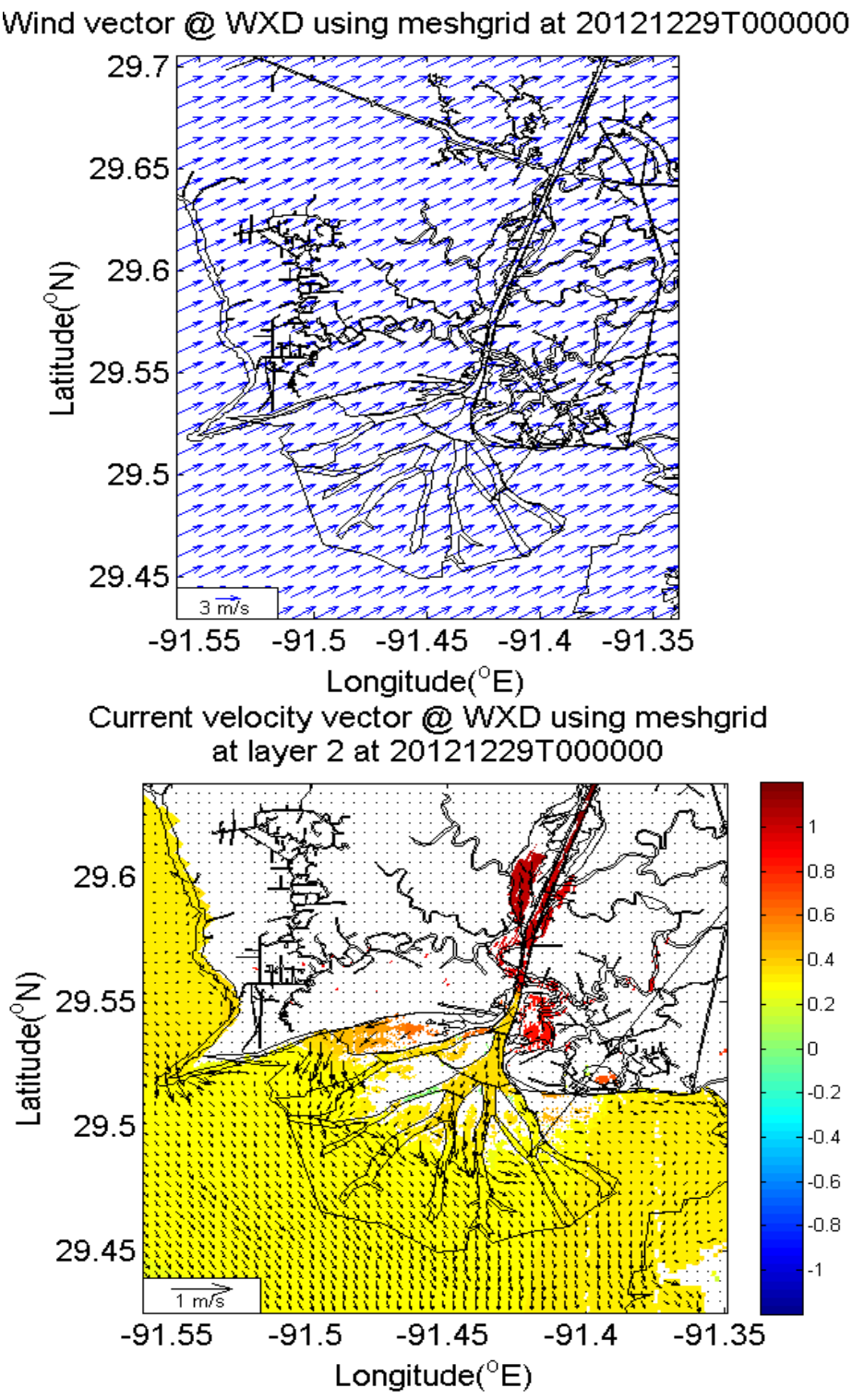

Figure 6.12 continued.

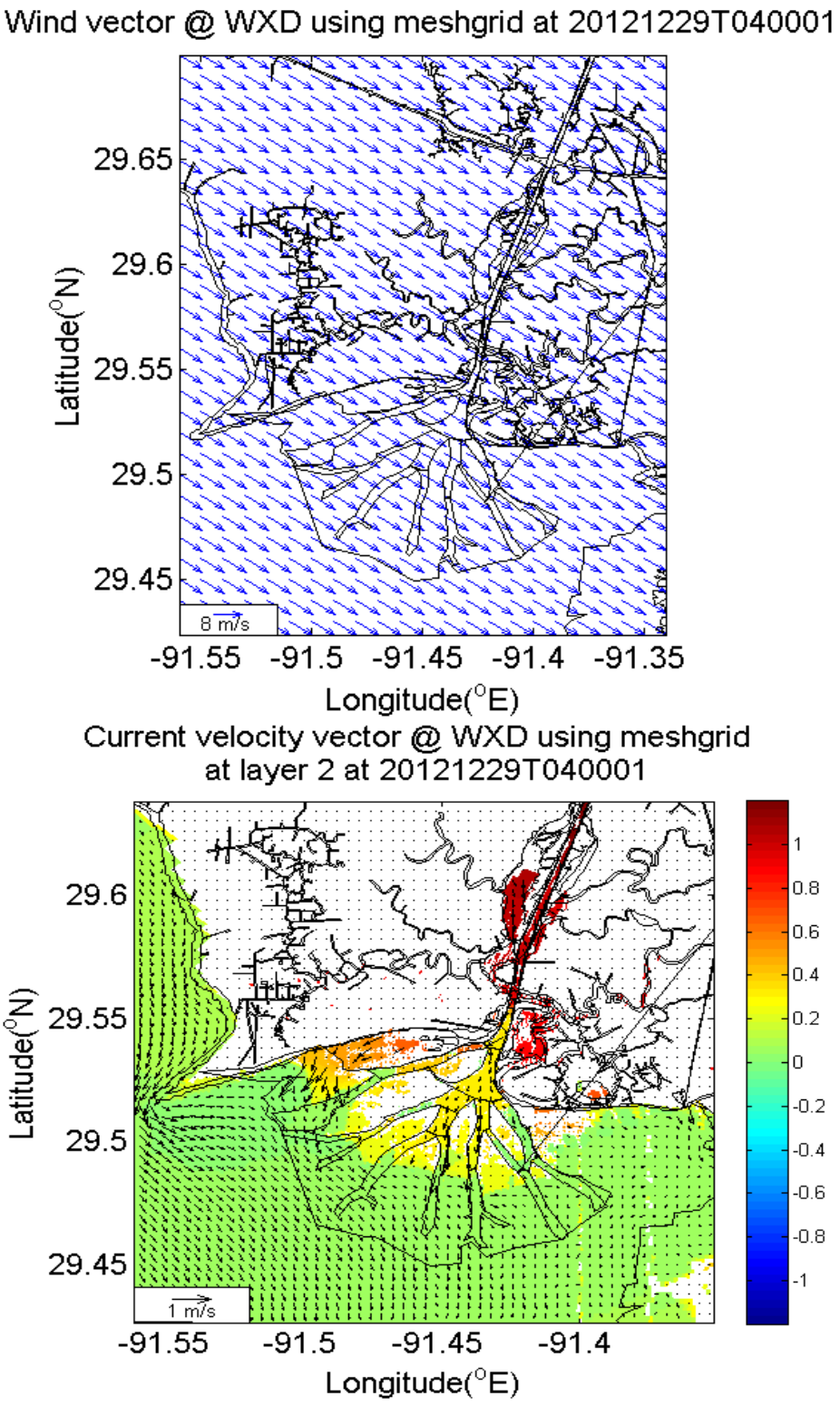

Figure 6.13 Plan views of the spatially uniform surface wind field, simulated surface elevation contours and near-surface velocity fields during the prefrontal, frontal, and postfrontal stages of cold front (cf4).

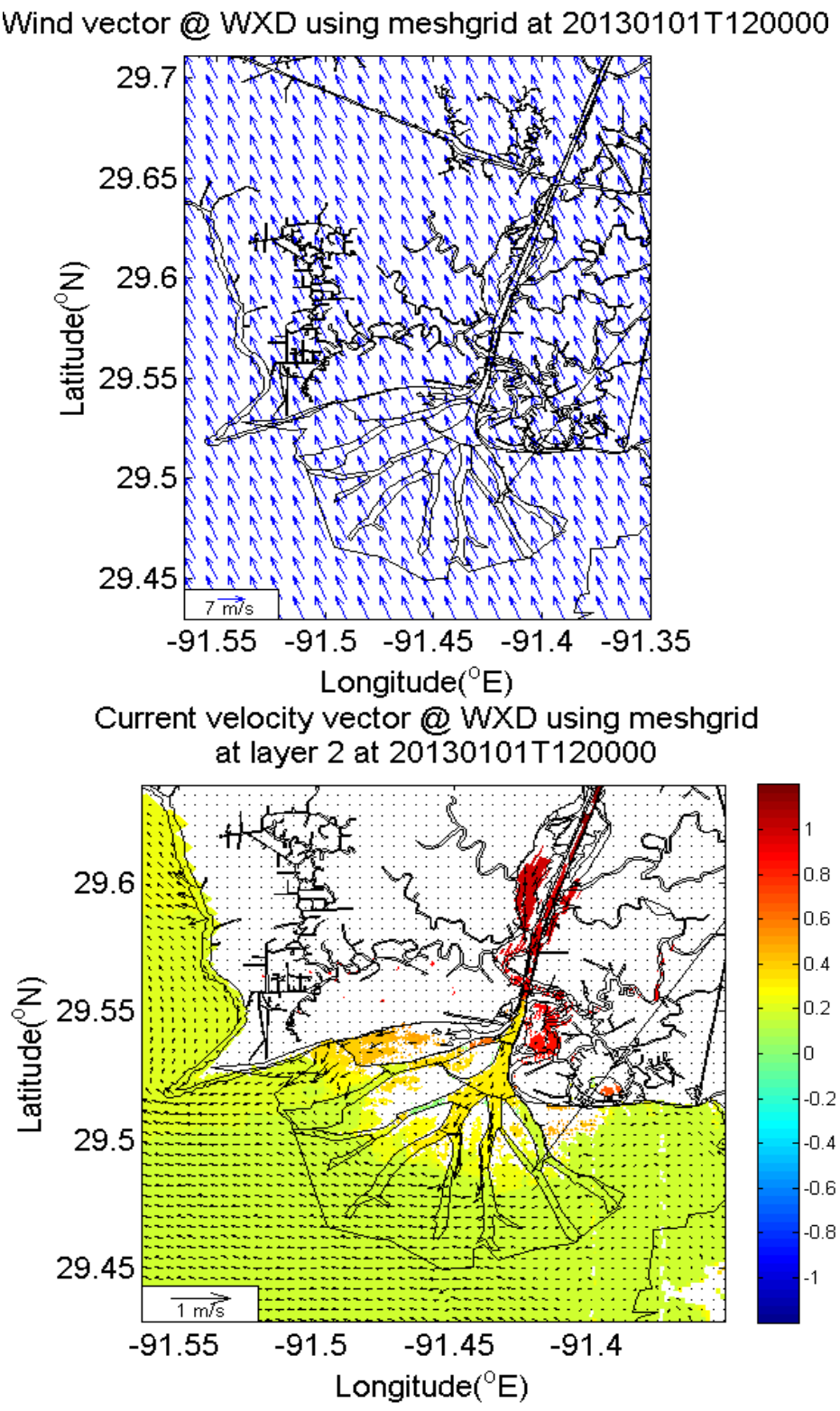

Figure 6.14 Plan views of the spatially uniform surface wind field, simulated surface elevation contours and near-surface velocity fields during the prefrontal, frontal, and postfrontal stages of cold front (cf5).

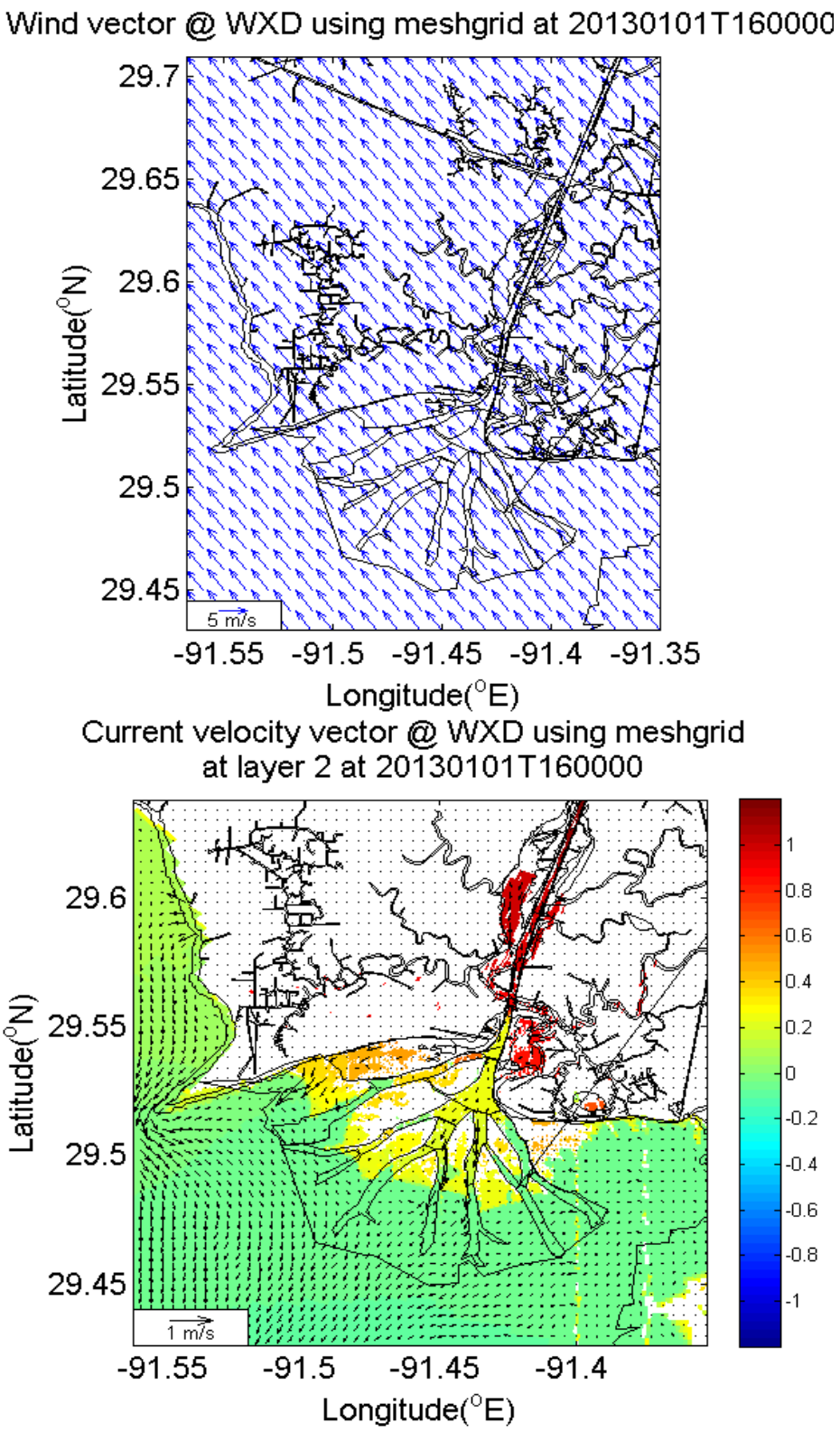

Figure 6.14 continued.

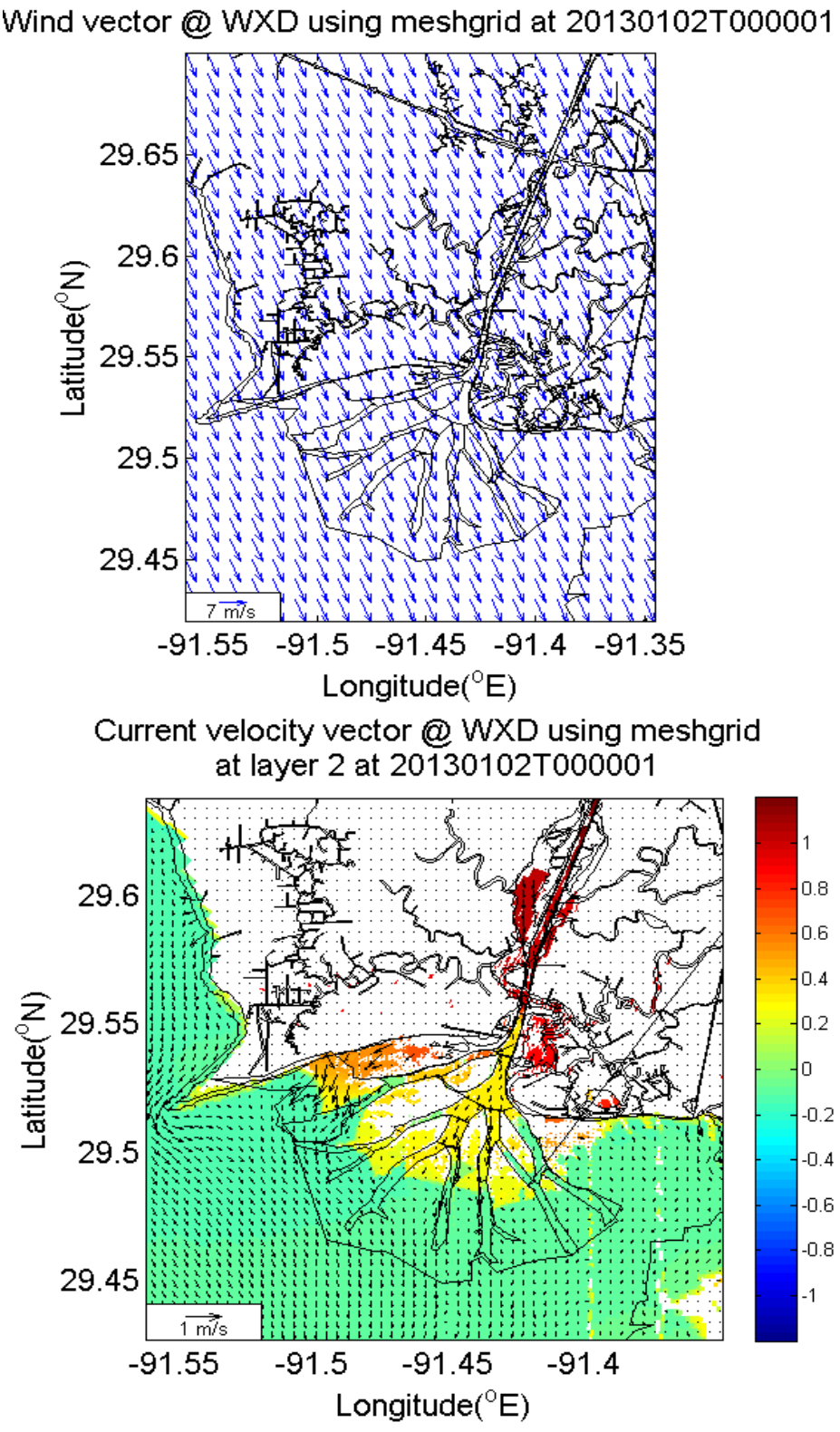

Figure 6.14 continued.

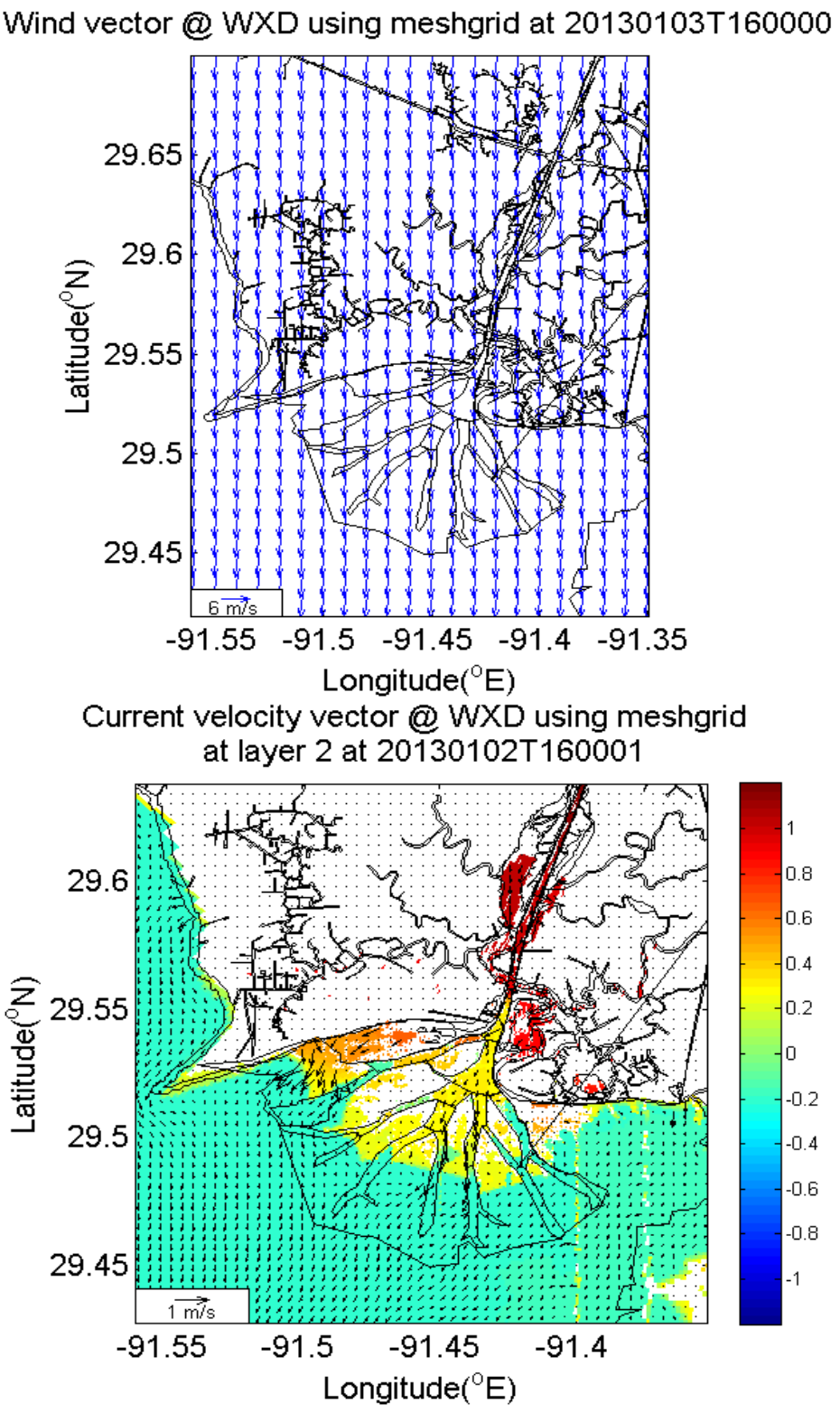

Figure 6.14 continued.

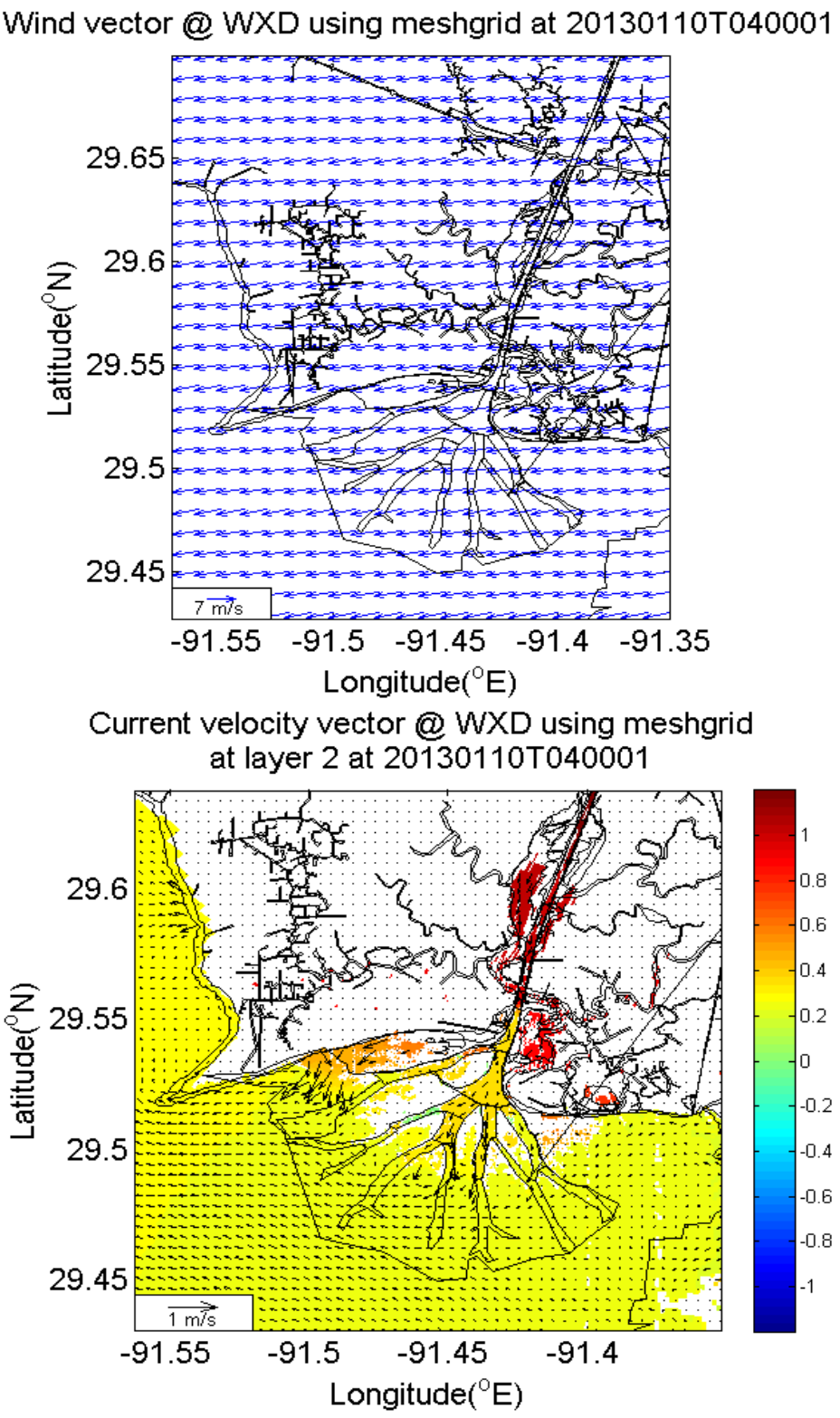

Figure 6.15 Plan views of the spatially uniform surface wind field, simulated surface elevation contours and near-surface velocity fields during the prefrontal, frontal, and postfrontal stages of cold front (cf6).

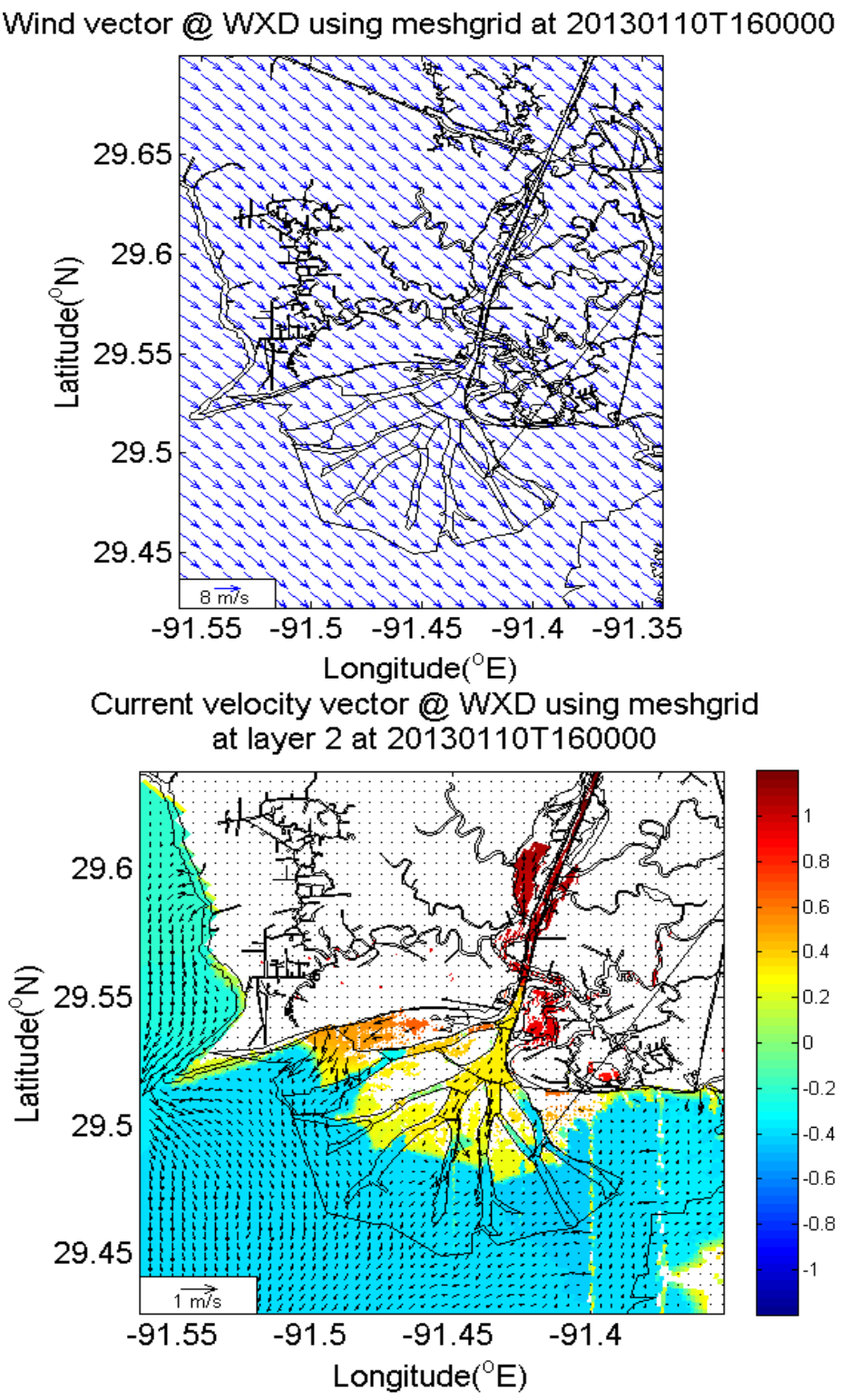

Figure 6.15 continued.

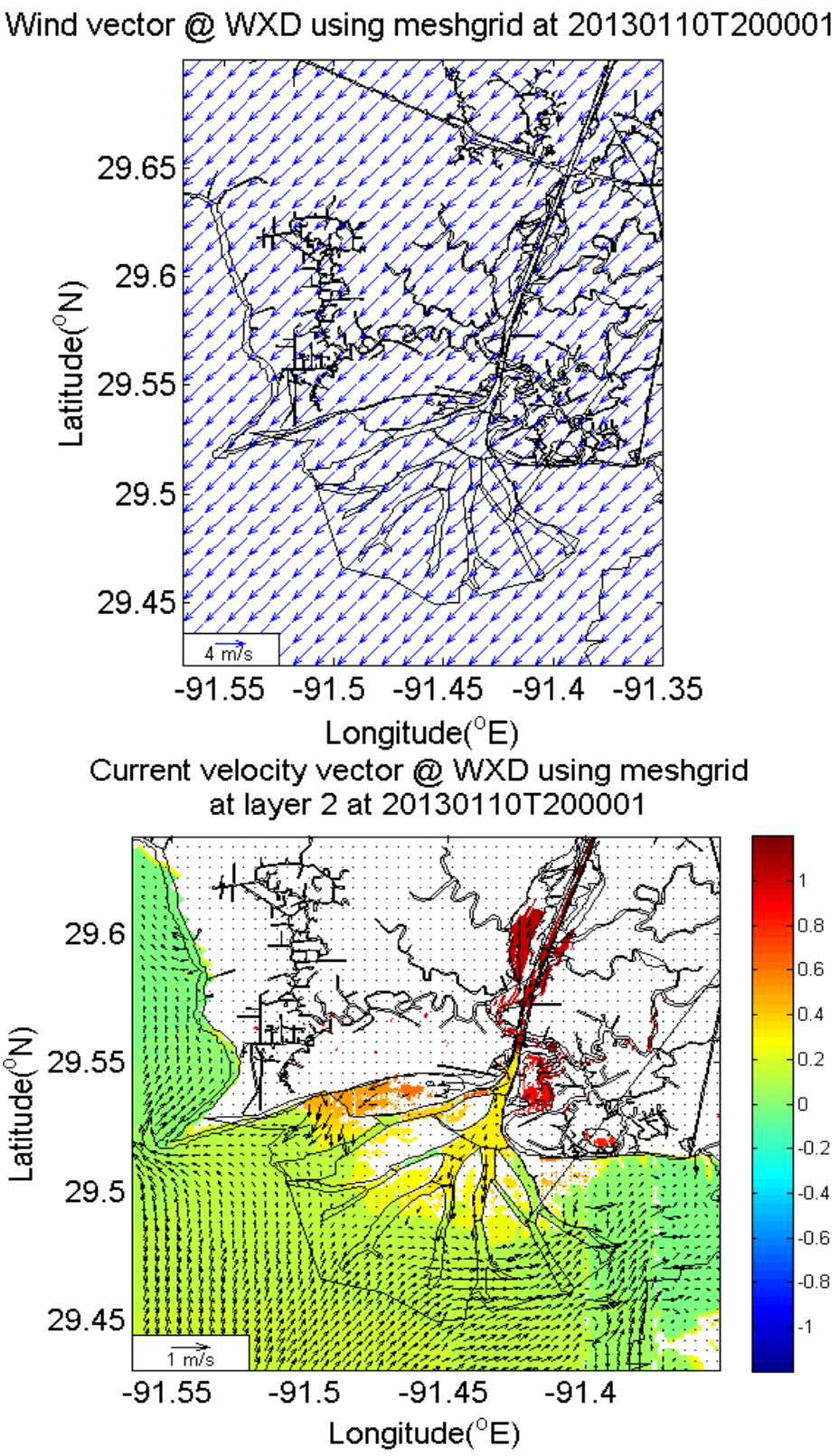

Figure 6.15 continued.

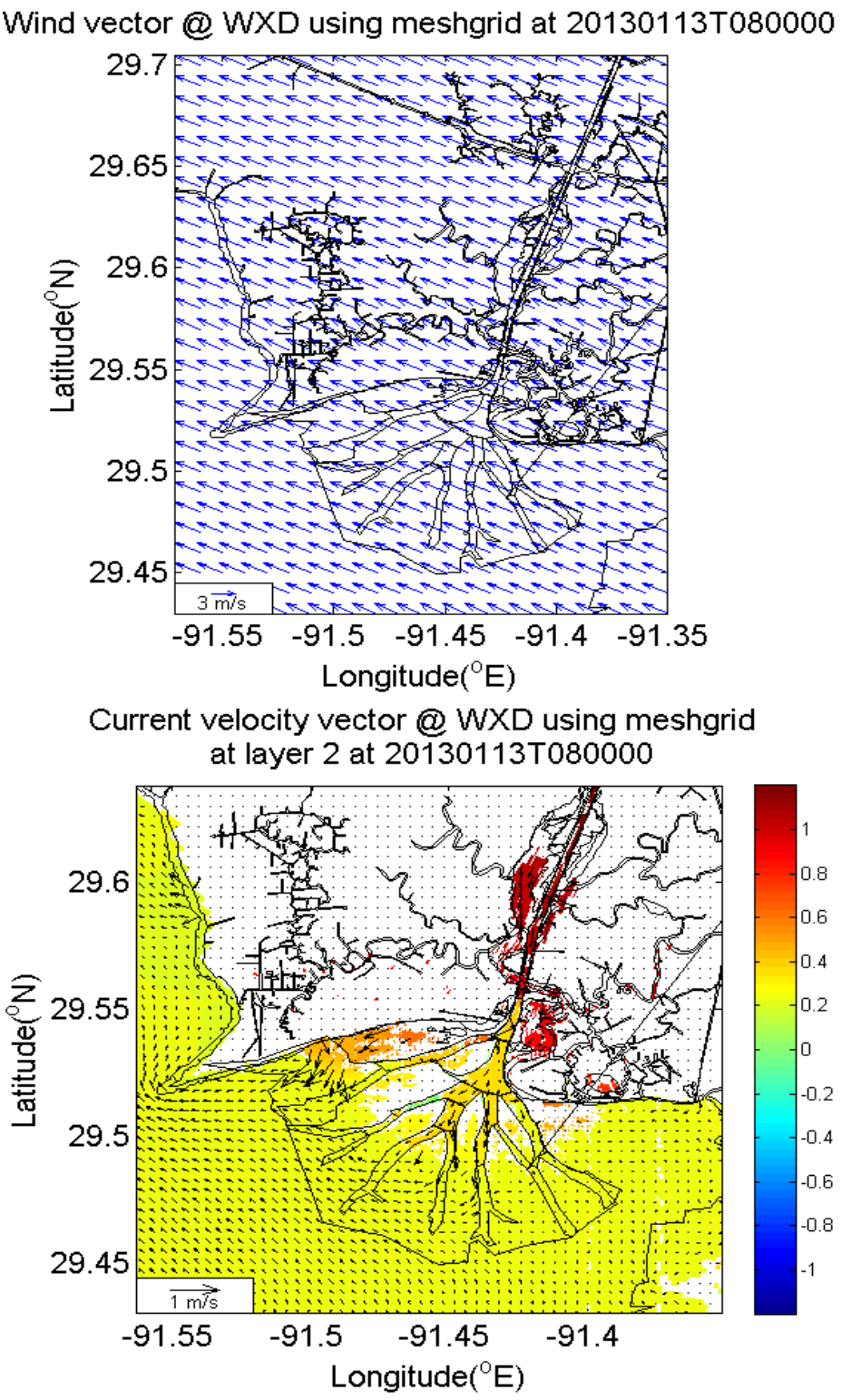

Figure 6.16 Plan views of the spatially uniform surface wind field, simulated surface elevation contours and near-surface velocity fields during the prefrontal, frontal, and postfrontal stages of cold front (cf7).

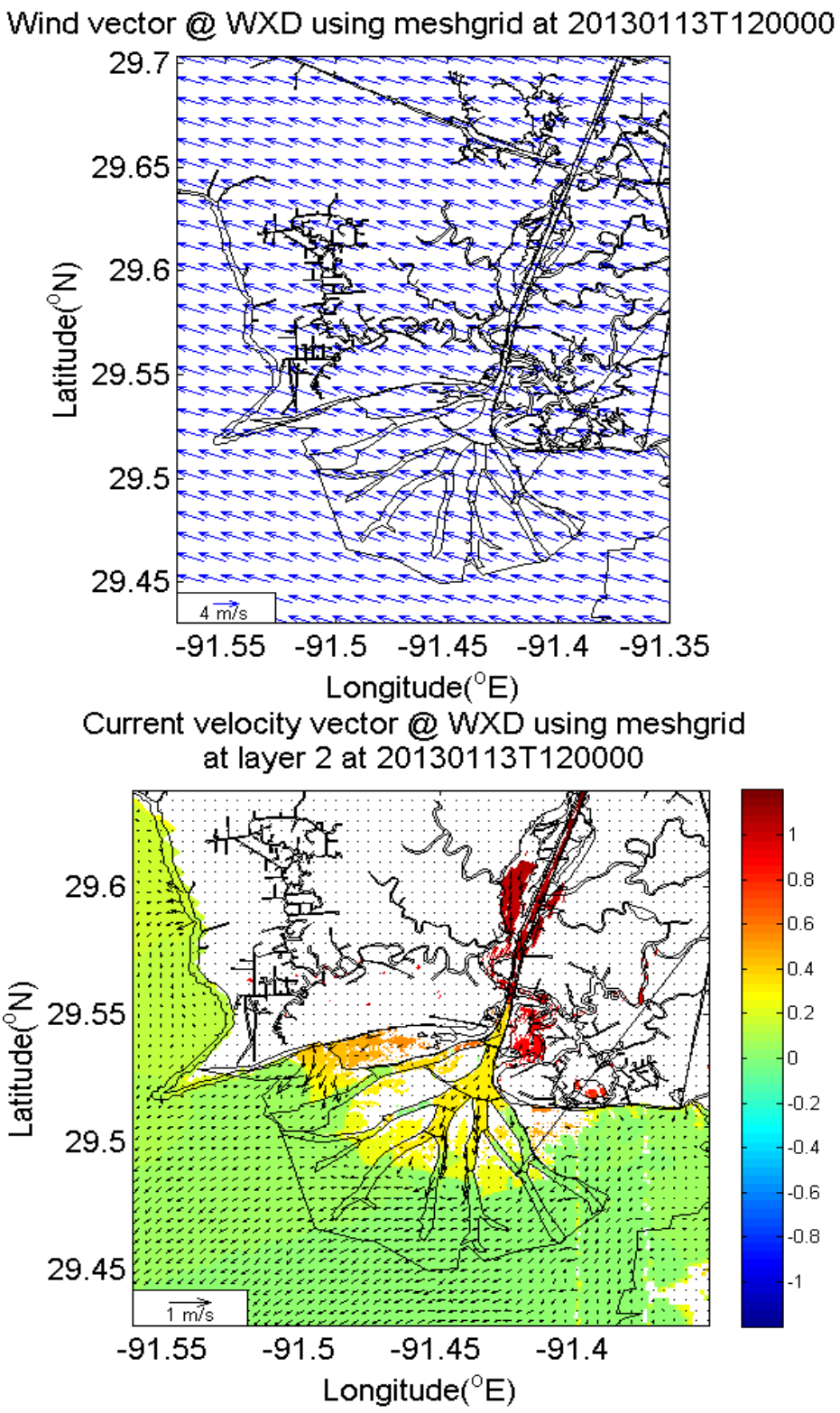

Figure 6.16 continued.

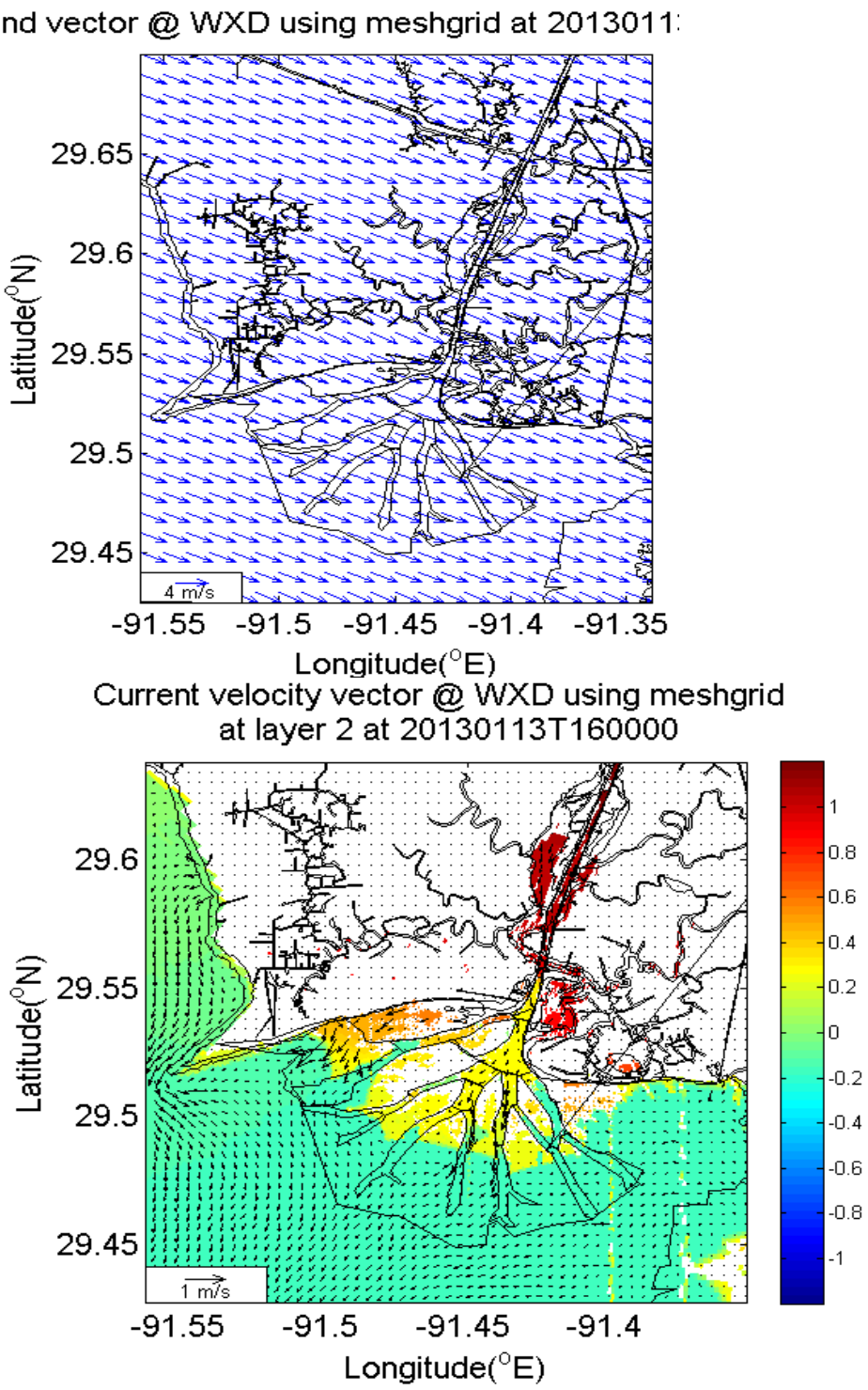

Figure 6.16 continued.

6.3.3 Cold Fronts and Current Flows

In this study, we used WAVCIS stations CSI03 and CSI06, as well as station Delta 1, to examine the relationship between winds and current fields. The reason we picked those three stations is because they are located at different geographic locations and surrounding environments, and have diverse bathymetry conditions. CSI03 and CSI06 are offshore stations with open waters constantly influenced by the combined effects of winds, tides and river flows from deeper water. While they are also different in that CSI03 is near the 5-m isobaths south of Vermilion Bay that is generally within the impacting area of the Atchafalaya River discharge. CSI06 however is deeper and further away on the inner shelf near the 20-m isobaths south of Terrebonne Bay, which is very unlikely less impacted by the Atchafalaya River than by the freshwater advected westward from Southwest Pass of the Mississippi River (Walker and Hammack, 2000). Delta 1, located in a much shallower and narrower channel (channel 6 in Figure 6.28), where the flow activities seem experiencing the total effects of winds, river discharge, tides, and especially topography.

The time series of surface current at CSI03 and CSI06 generally follows the winds shift (Figure 6.17 and 6.19). The contour of subtidal current (Figure 6.18 and 6.20) clearly demonstrates the close relationship between cold front event and the subtidal current in whole water column. The alongshore component contour color changes from light or dark blue to yellow or red during the frontal passage, indicating abrupt direction switch. But this shift lasts for only a short period of time of 1-3 days (except for the 5^{th} cold front with persistent northerly wind for about 8 days) by weakening itself and finally becomes the stable and persistent westward component (this is the so-called reestablish process) before the incoming of next storm. This westward component

agrees with alongshore downcoast flow pattern and is also called Louisiana Coastal Current (Wiseman and Kelly, 1994; Rouse et al., 2004; Rouse et al., 2005; Walker, 2005). During the study period, the cold front events were strong enough to completely hinder the westward movement was by the cold front events.

Note that during most winters storm in the study period, the current at all three stations reverses direction throughout almost the entire water column (Figure 6.18 and 6.20), which suggests strong vertical mixing by wind-induced shear. The north/south components also show similar response to cold front events although slightly weaker than alongshore current. The north current is weak in the pre-frontal phase, but abruptly reverses to southward and also intensifies after the passage. During the study period (December 15 2012 to January 20, 2013), due to more frequent (seven were captured in one month) and persist cold front passages, it is hard to summarize a general surface current pattern as a persistent and strong westward movement and cold fronts do take significant effects. Plus the westward reestablishment is quite obvious.

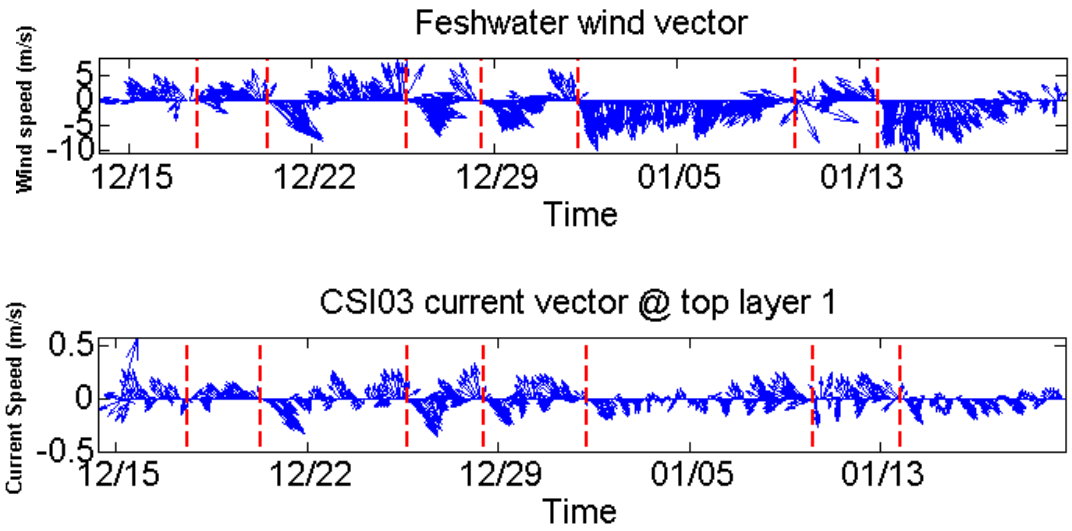

Figure 6.17 Winds and model predicted near-surface currents at CSI03 between December 15, 2012 and January 13, 2013.

It is also noticed that the subtidal current is generally uniform (Figure 6.18 and 6.20 upper panel) throughout the vertical column and only slightly decreases with depth, except at CSI06, where the near-surface north/south component (Figure 6.20 lower panel) is much stronger than the mid-layer and near-bottom current during most of the time. The strongest current is found within 0.5-1 m below the surface.

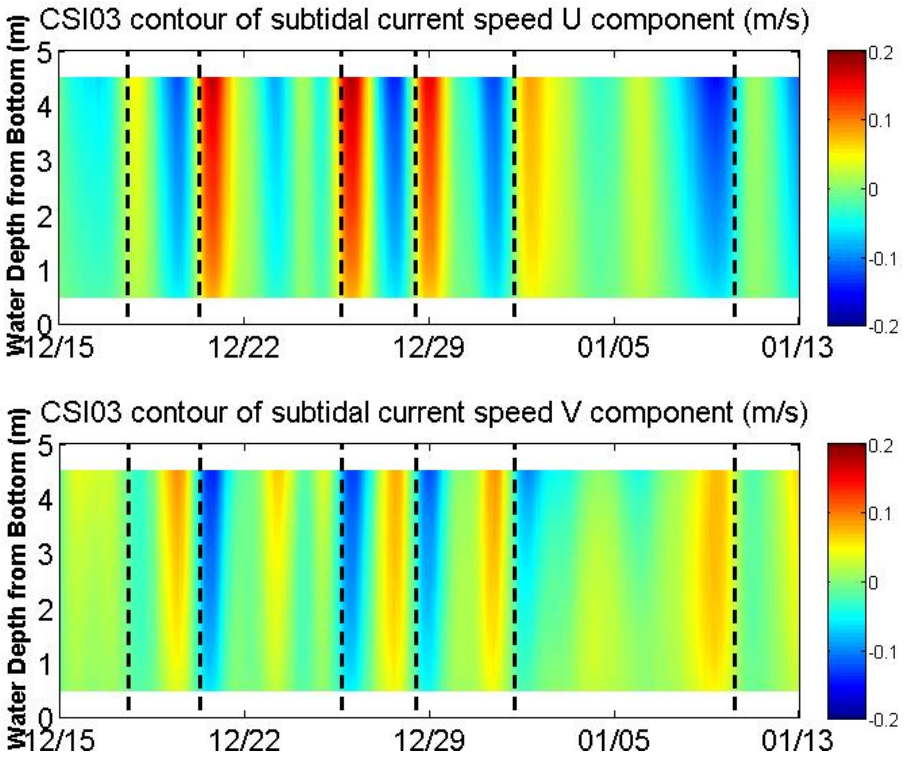

Figure 6.18 Contours of subtidal east/west (east positive) and north/south (north positive) components of model predicted current at CSI03 from December 15, 2012 and January 13, 2013. The black vertical lines indicate cold front passages.

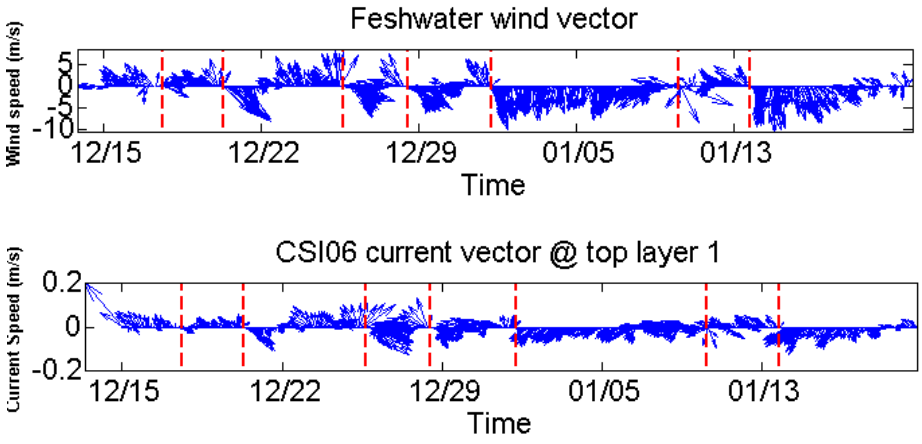

Figure 6.19 Winds and model predicted near-surface and near-bottom currents at CSI06 between December 15, 2012 and January 13, 2013.

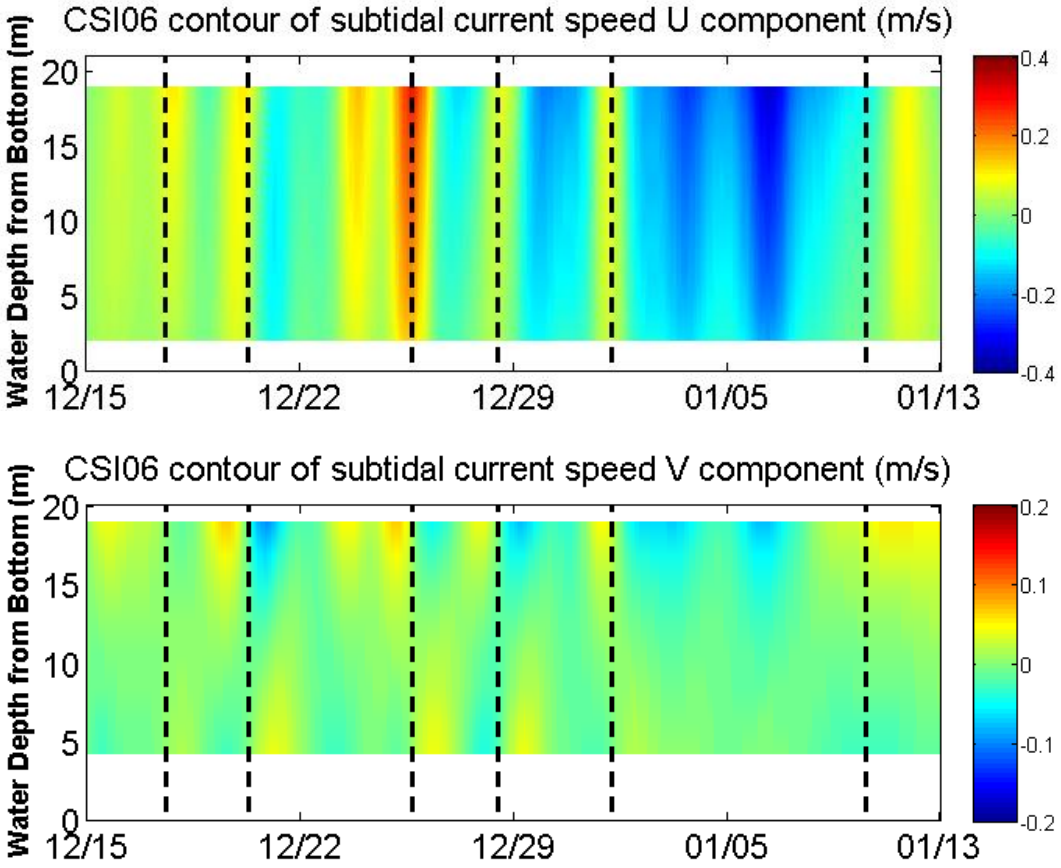

Figure 6.20 Contours of subtidal east/west (east positive) and north/south (north positive) components of model predicted current at CSI06 from December 15, 2012 and January 13, 2013. The black vertical lines indicate cold front passages.

Due to the shallow water depth (< 2m) at Detla1 and the residing inside the channel, we investigate this station by presenting the time series of current velocity (Figure 6.21 lower panel), subtidal along-channel current (Figure 6.22), as well as the subtidal along-channel current profile (Figure 6.23). Due to residing inside one channel of the Wax Lake delta, the cross-channel fetch is limited and not our interest in this study, so the profile is not shown here. Both three figures clearly demonstrates that the along-channel component dominates the whole study period. The along-channel current does show occurrence of return flow during the frontal passage, which however does not last long. The strongest current is observed within the depth 0.2-0.5 m below

the surface. The subtidal current is generally uniform (Figure 6.23) throughout the vertical column and only slightly decreases with depth. The flow structure is somewhat similar to the near-surface current of CSI03, but also demonstrates some distinct characteristics. Firstly, the prevailing subtidal along-channel flow is stronger than that of CSI03 and CSI06. Secondly, the subtidal current field at Delta1 seems more sensitive to the cold front events than at CSI03 and CSI06, which can be seen from the fact that the post-frontal along-channel current is usually stronger than that of those two stations.

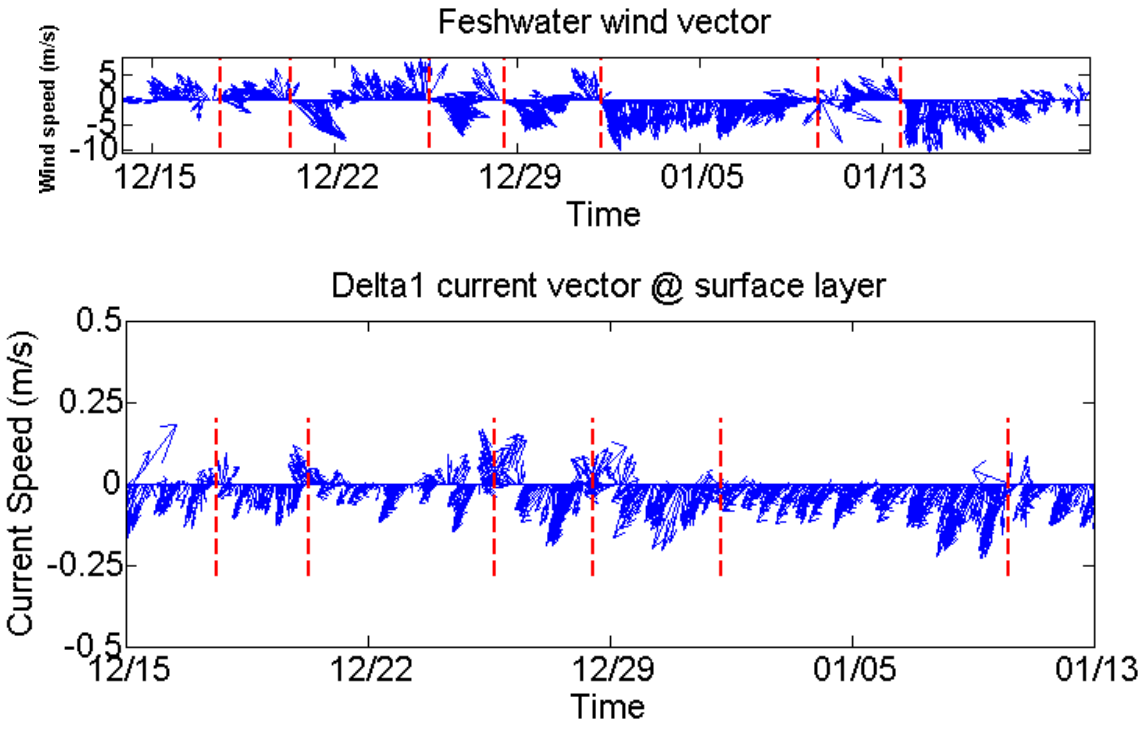

Figure 6.21 Winds and model predicted near-surface current at Delta1 between December 15, 2012 and January 13, 2013. North/south component indicates along-channel (positive = going out) while east/west indicates cross-channel (positive = northwest) direction.

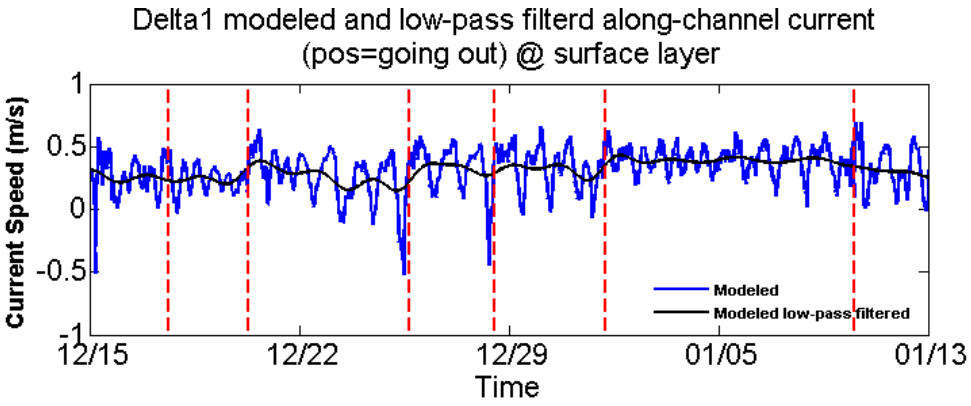

Figure 6.22 Modeled and subtidal along-channel (positive = going out) current at Delta1 between December 15, 2012 and January 13, 2013.

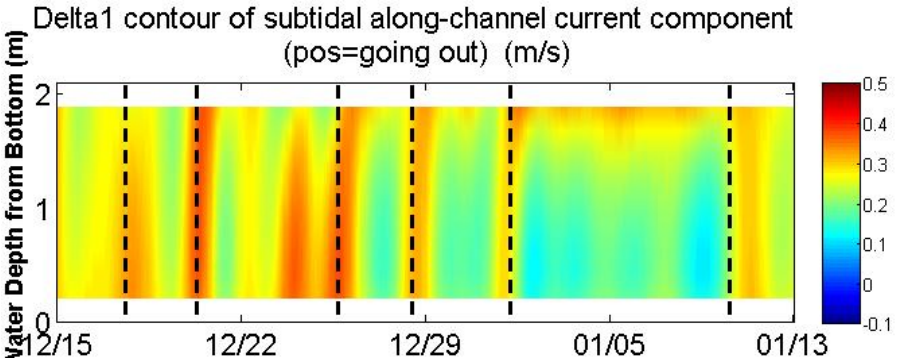

Figure 6.23 Contours of subtidal along-channel (positive indicates going out) components of model predicted current at Delta1 from December 15, 2012 and January 13, 2013. The black vertical lines indicate cold front passages.

6.4 AMPLITUDE SPECTRAL OF WATER LEVEL

In this section, we compute the amplitude-frequency spectra of one-month time series of model predicted water level data from 15 stations for December 2012 to January 2013, both inside and outside of the Wax Lake delta.

6.4.1 Diurnal and Semidiurnal Constituents

Figure 6.24 shows the amplitude spectrum, covering the frequency range of 0-2.5 cycles per day (CPD). All stations except Berwick show dominant diurnal tidal signals. Two highest peaks have

frequencies of 0.9418 and 1.0009 CPD, equivalent to periods of 25.48 and 23.79 hours, respectively. Note that O_1, M_1, K_1, S_1 and P_1 tides have frequencies of 0.9295, 0.9664, 1.0027, 1.0000, and 0.9973, which are very close to the peaks identified from the spectra.

Although semidiurnal tidal signals can be seen from the spectra of most stations, their energies are lower than diurnal tides. Three major peaks are identified with frequencies of 1.884, 1.951, and 2.018 CPD, or periods of 12.74, 12.30 and 11.89 hours, which are very close to N2 (1.8960), M2 (1.9323), and S2 (2.0000) tides. Within the semidiurnal frequency band, five stations, including Delta1, BigHogs1, SmallTripod, LargeTripod, Freshwater Canal Lock (FRWL1), Lawma, and CSI-3, have relatively higher semidiurnal signals than the others. The amplitudes of highest semidiurnal peaks account for 27% to 39% of those of diurnal peaks. Also note that all these stations are west of 91^0W, whether inside, offshore or west of Atchafalaya-Vermilion Bays. Lawma (LAP) is located at the mouth of Atchafalaya River. Stations CSI03 and FRWL1 have the largest semidiurnal tidal signals among all the stations. Delta1 and BigHogs1, and Lawma, which are inside Wax Lake delta, in the middle of Wax Lake and Atchafalaya deltas, and inside the Atchafalaya delta, respectively, have relatively lower semidiurnal tidal signals. These results are consistent with current meter records that the areas southwest of the Atchafalaya Bay have the largest M2 tidal current of the entire Louisiana-Texas shelf (DiMarco and Reid, 1998).

Station Berwick and BridgeADCP are located in the upper channel of the Atchafalaya River and Wax Lake Outlet, respectively. Both stations are more than 25 km upstream of the Wax Lake-Atchafalaya delta complex. That is why the two small peaks of diurnal constituents and semidiurnal

tidal signals are barely identifiable. In contrast, low-frequency fluctuations less than 0.5 CPD are dominant.

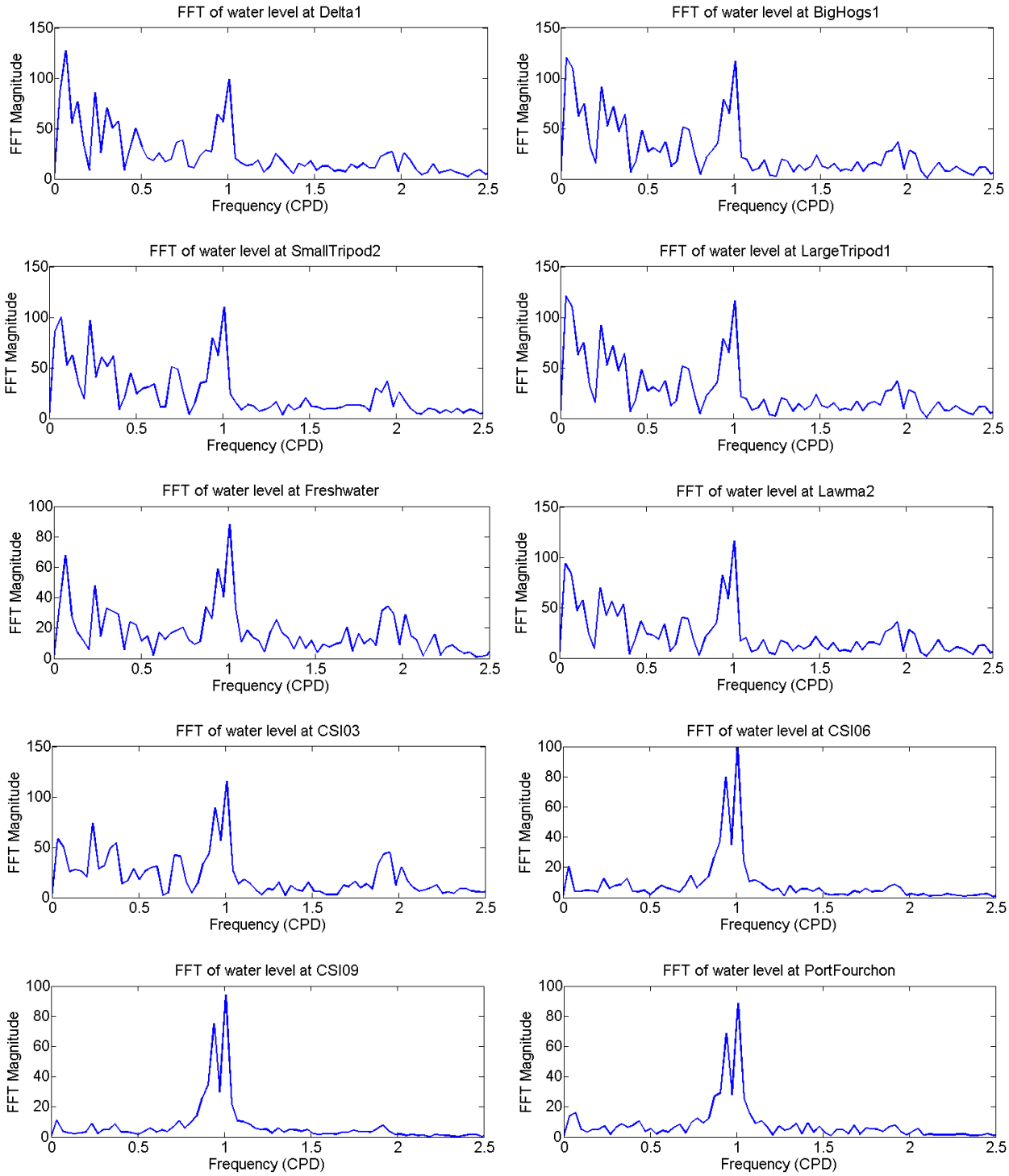

Figure 6.24 Amplitude spectra (0-2.5 CPD) of water levels at 15 stations.

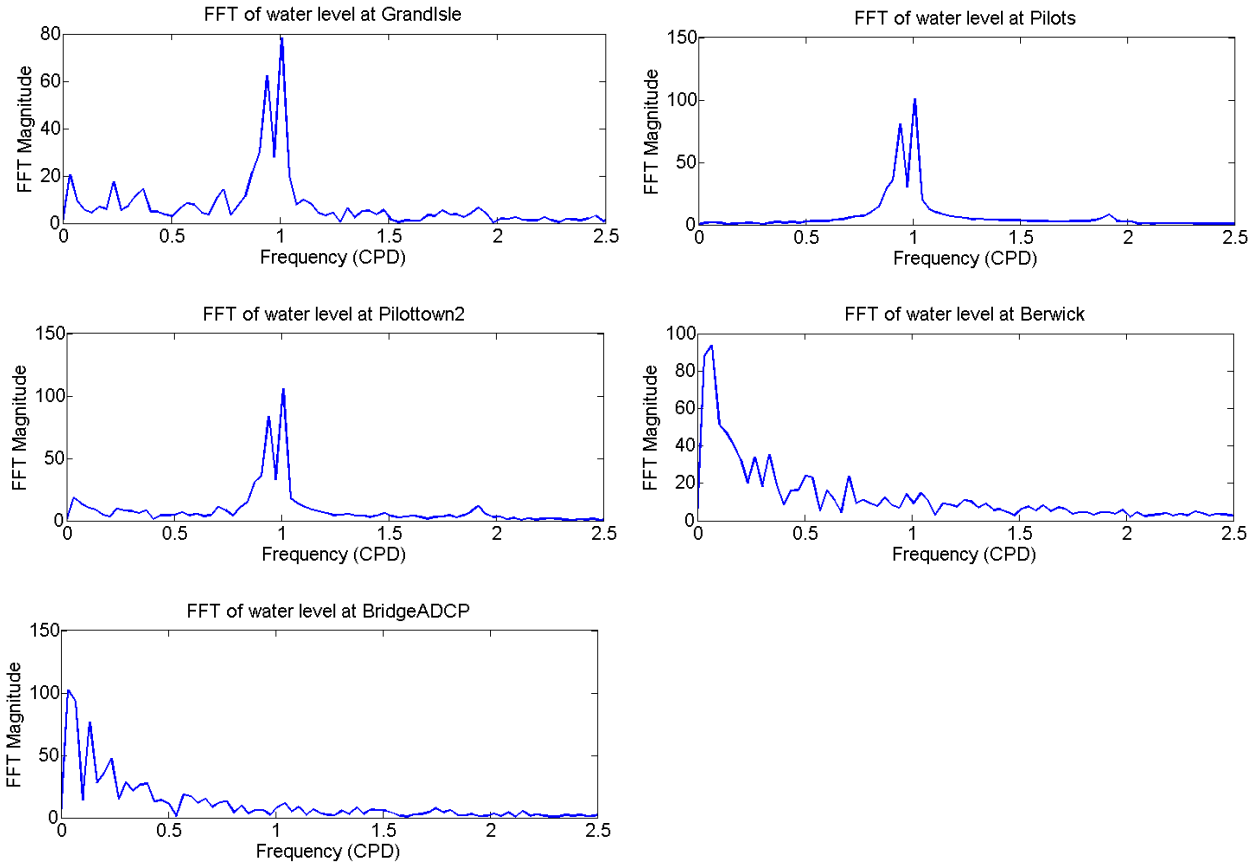

Figure 6.24 continued.

6.4.2 Subtidal Constituents

Figure 6.25 shows the amplitude spectra of water level, which are zoomed into the lower frequency range of 0-0.5 CPD, covering more than 2 days periodicities, which is intervals of frontal passages. This coincides with the frequencies of cold-front-induced oscillations that are usually less than 0.5 CPD (i.e., equivalent return period longer than 2 days). Unlike tidal oscillations, cold-front-induced oscillations do not have fixed frequencies. In general, the energy is distributed throughout the low frequency range.

Stations of FRWL1, Delta1, BridgeADCP, SmallTripod, LargeTripod, CSI03, BigHogs1, Lawma, and Berwick seem to respond strongly to the wind forcing, where the FFT magnitude of water level at these stations is high in this 3-7 day band. In comparison, stations CSI06, CSI09, GrandIsle,

PortForchon, Pilottown, and Pilots are barely influenced. The spectra of Delta1 and BigHogs1 seem to have similar amplitudes but slightly different patterns in the very low frequency range (0-0.1 CPD). BigHogs and LargeTripod also display very similar patterns in magnitude but with phase differences. The spectrum of BigHogs1 and Lawma appear to have similar patterns but different amplitudes, although both stations are in the Atchafalaya delta. All of these may suggest that subtidal water levels of the stations respond to wind forcing differently. It may be explained by the geographic differences: Delta1 is located in one of the main channels of the Wax Lake delta surrounded with shallow depth; BigHogs1, although shallow too, is impacted by both deltas; while Lawma is more open to the inner shelf and deeper.

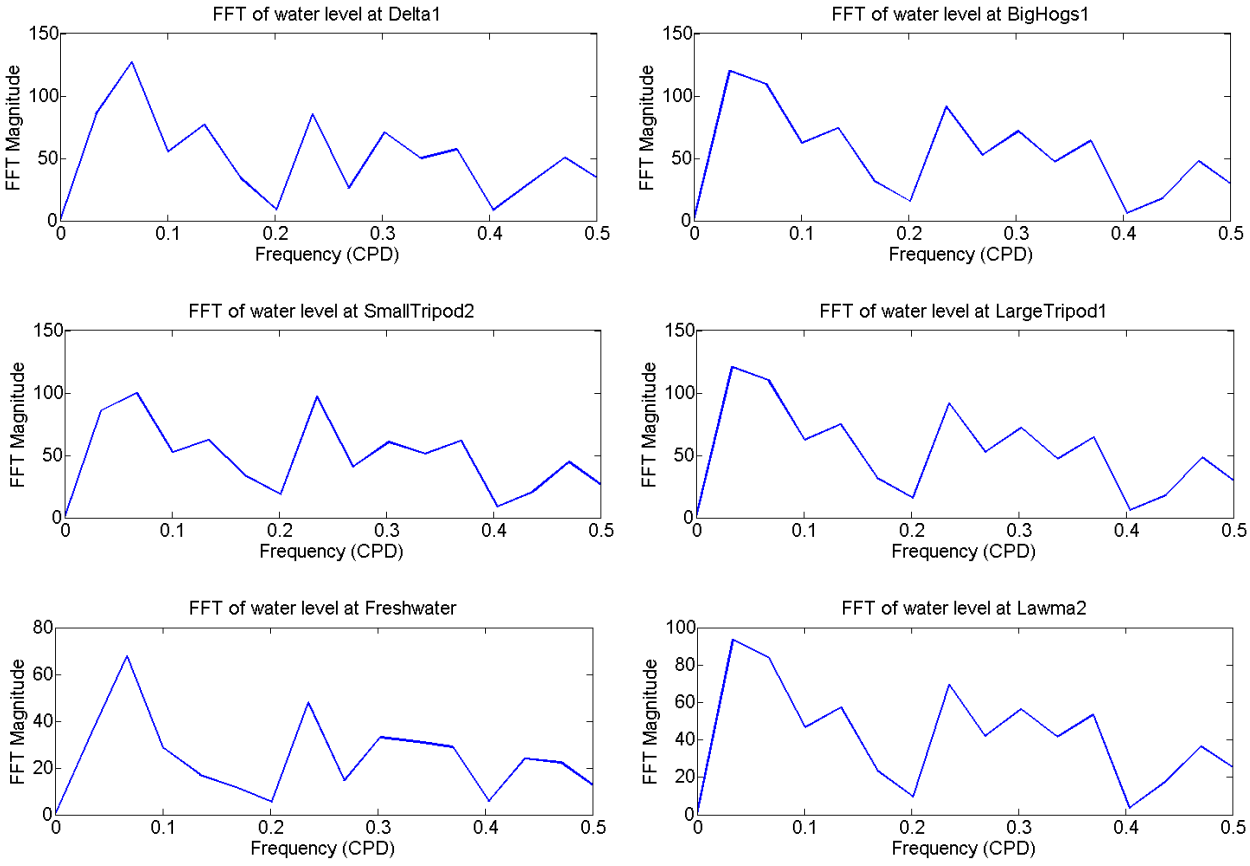

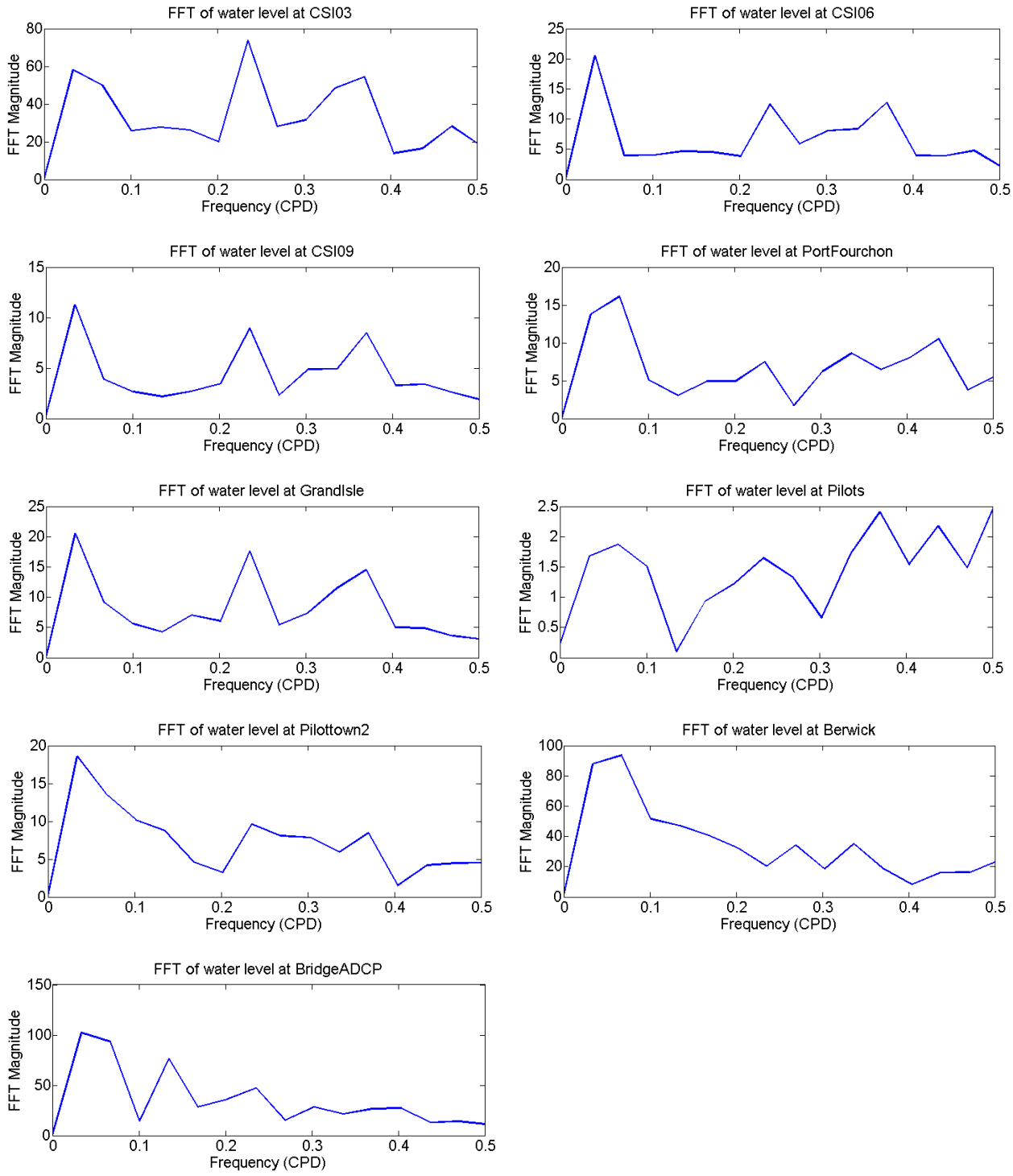

Figure 6.25Amplitude spectra (0-0.5 CPD) of water levels at 15 stations.

6.5 SUBTIDAL WATER LEVEL VARIATION

The general subtidal (low-frequency of 0-0.5 CPD) wind-induced oscillations can also be illustrated by low-pass filtered water level, with a 6^{th} order Butterworth filter with a cutoff frequency of 0.6 CPD (i.e., equivalently a 40-hr filter). This filter has the advantage of a close to ideal passing band of almost 100% energy beyond the cutoff frequency and a relatively narrow and monotonic transition band (Li et al., 2011). Figure 6.26 demonstrates the modeled (blue lines) and subtidal (black lines) water levels at Delta1, BigHogs, SmallTripod, LargeTripod, FRWL1, Lawma, CSI03, CSI06, CSI09, Port Fourchon, GrandIsle, Pilots, Pilottown, BridgeADCP and Berwick. First of all, it is noted that cold front events (dashed vertical lines) timing is consistent with the major set-up and set-down of subtidal water level. The pre-frontal winds from southern quadrant pile up the water masses. After cold fronts pass through the stations, northerly winds dominate and water level is pushed down by the reversed wind stress. The variability between different events is large, where the magnitude range varies from less than 0.1 m to close to 1 m, depending on the strength of the cold front events, approaching angle, wind stress, direction and duration. In addition, the impact of the same cold front event on different stations varies significantly. In general among 15 stations, Delta1, BigHogs, SmallTripod, LargeTripod, FRWL1, Lawma, and CSI03 seem to have the largest variability than others, which is mainly due to the relatively shallow water depths (1-5 m) at these stations. This also supports the idea that shallow water is more sensitive to wind forcing. The low-pass filtered water level curves of CSI06, CSI09, Port Fourchon (PF), Grand Isle (GISL1), Pilots (PSTL1), and Pilottown (PILL1) show similar patterns, indicating the dominant tidal oscillations overwhelm the minimal wind-induced subtidal oscillations at these locations. In contrast, the

tidal oscillations at Berwick and BridgeADCP are minimal while wind-induced subtidal oscillations dominate.

The model results show an obvious wind surge shown in the water level at the Atchafalaya Bay stations - Delta1, SmallTripod, LargeTripod, BigHogs, FRWL1, LAP, and CSI03, where the resulted water level setup was greater than 0.5 m (van Heerden, 1980). This highest water level is recorded on December 26th, 2012. The wind surge occurred between two successive cold front passages, caused by strong, persistent and long-fetch onshore winds (magnitude over 10 m/s) from south or southeast quadrants for 2-3 days (Figure 6.1).

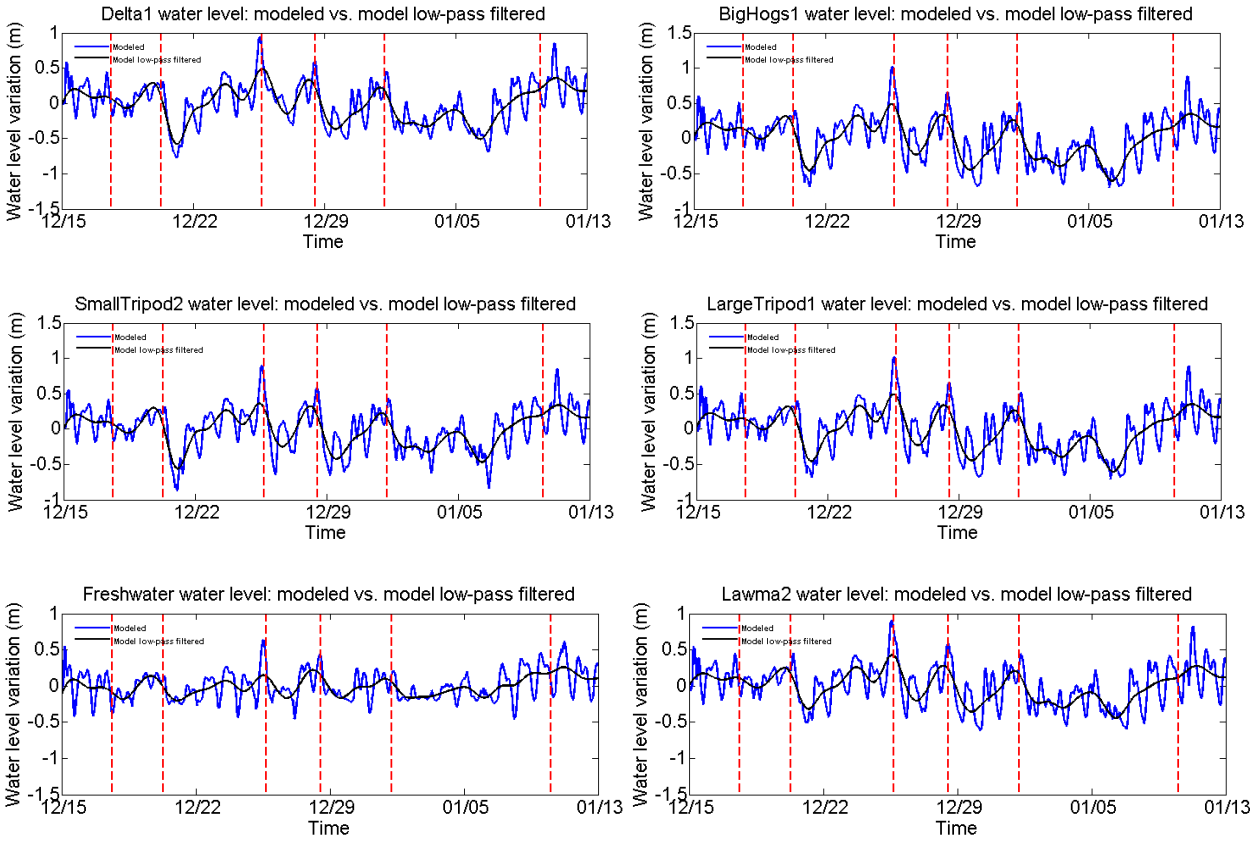

Figure 6.26 Modeled and modeled subtidal water levels at 15 stations.

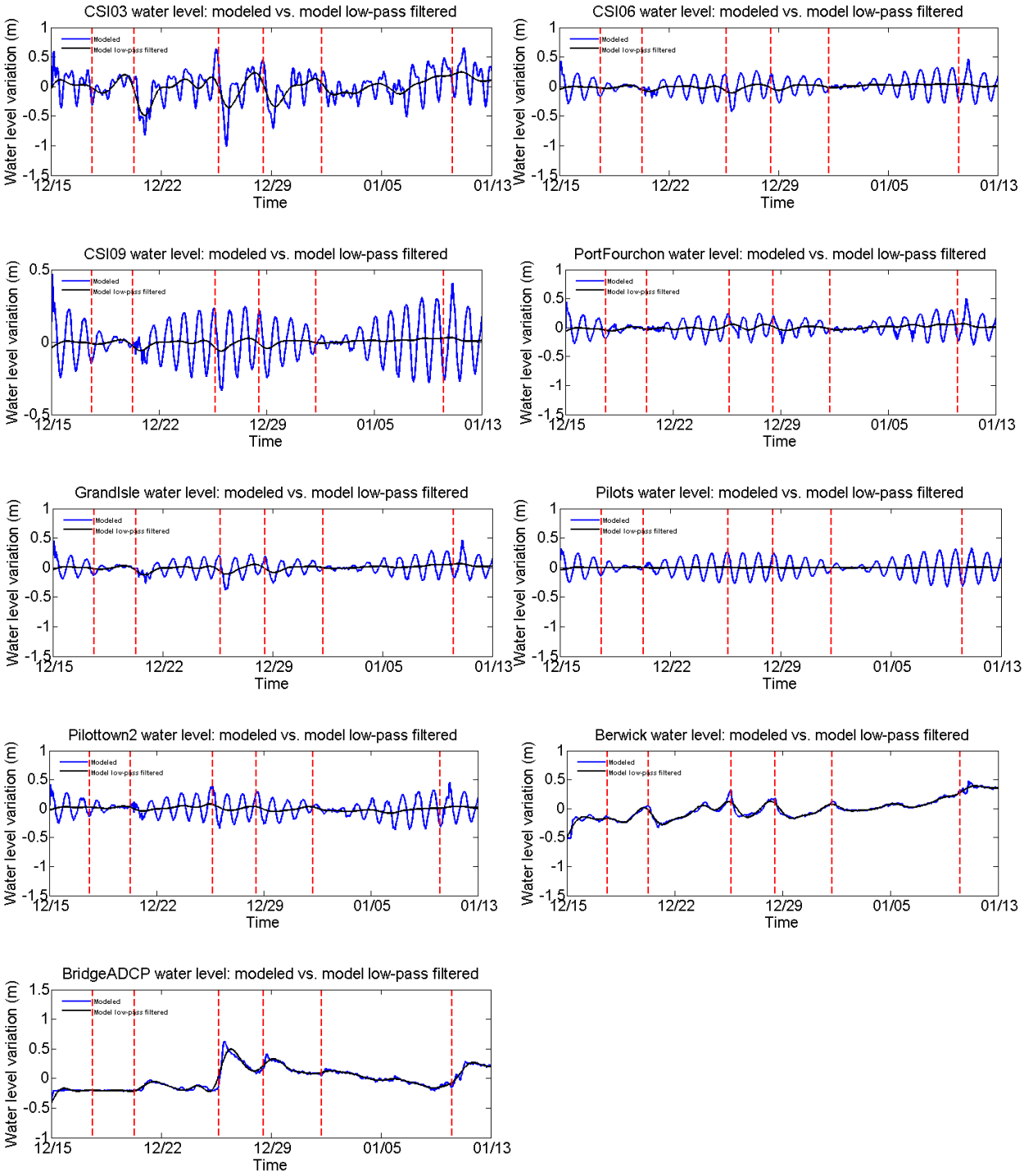

Figure 6.26 continued.

6.6 ENERGY DISTRIBUTION AND DOMINANT FORCING

Since the simulations involve tides, river discharge, and wind forcing, we are now interested in what processes are more important than the other and how the energy is distributed among different processes. The hydrodynamic energy regimes is determined for 15 stations and shown in In Figure 6.27. In general, the energy distribution presented a consistent pattern, which primarily consists of subtides, diurnal, and semidiurnal tides. However their individual contribution varies from station to station. For example diurnal tidal energy contribution ranges between 24%-68%; while subtial energy spans the range from 10% to 46%; and semidiurnal between 10% and 21%. we can see that the diurnal tide is dominating CSI06, CSI09, PF, GISL1, PSTL1 and PILL1, with subtidal forcing (i.e., winds) as the secondary driving force. It is also noticed that all those stations are located west of the Atchafalaya-Wax Lake complex. In contrast, CSI03 and FRWL1 that are located on the east side, have very similar pattern of energy distribution, with comparable contribution of diurnal, semidiurnal tide, and subtidal factors. Inside the Wax Lake delta, however, model results for stations Delta1 BigHogs, SmallTripod, and LargeTripod, show that the subtidal energy accounts for 46%-66% of total energy while diurnal tide contributes to only 13%-25%. This confirms that the weather impact due to atmospheric cold front passages is significant in this area (Li, et al., 2014).

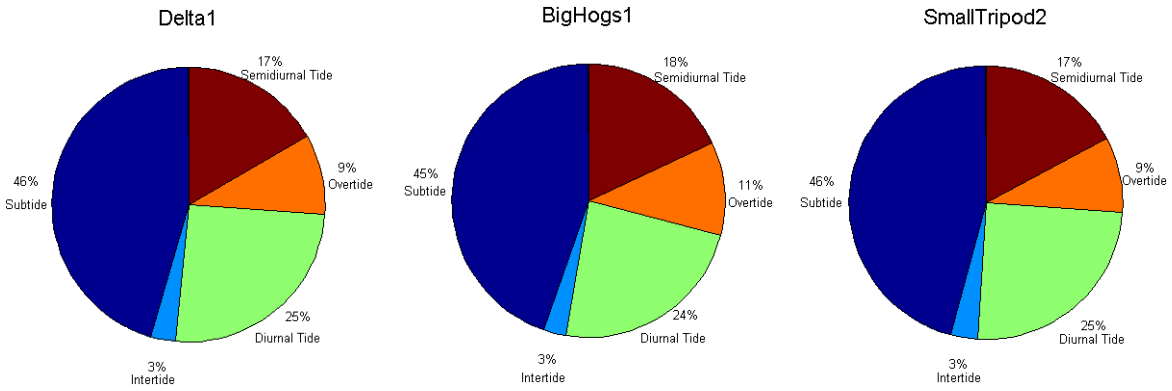

Figure 6.27 Energy distribution of 13 stations.

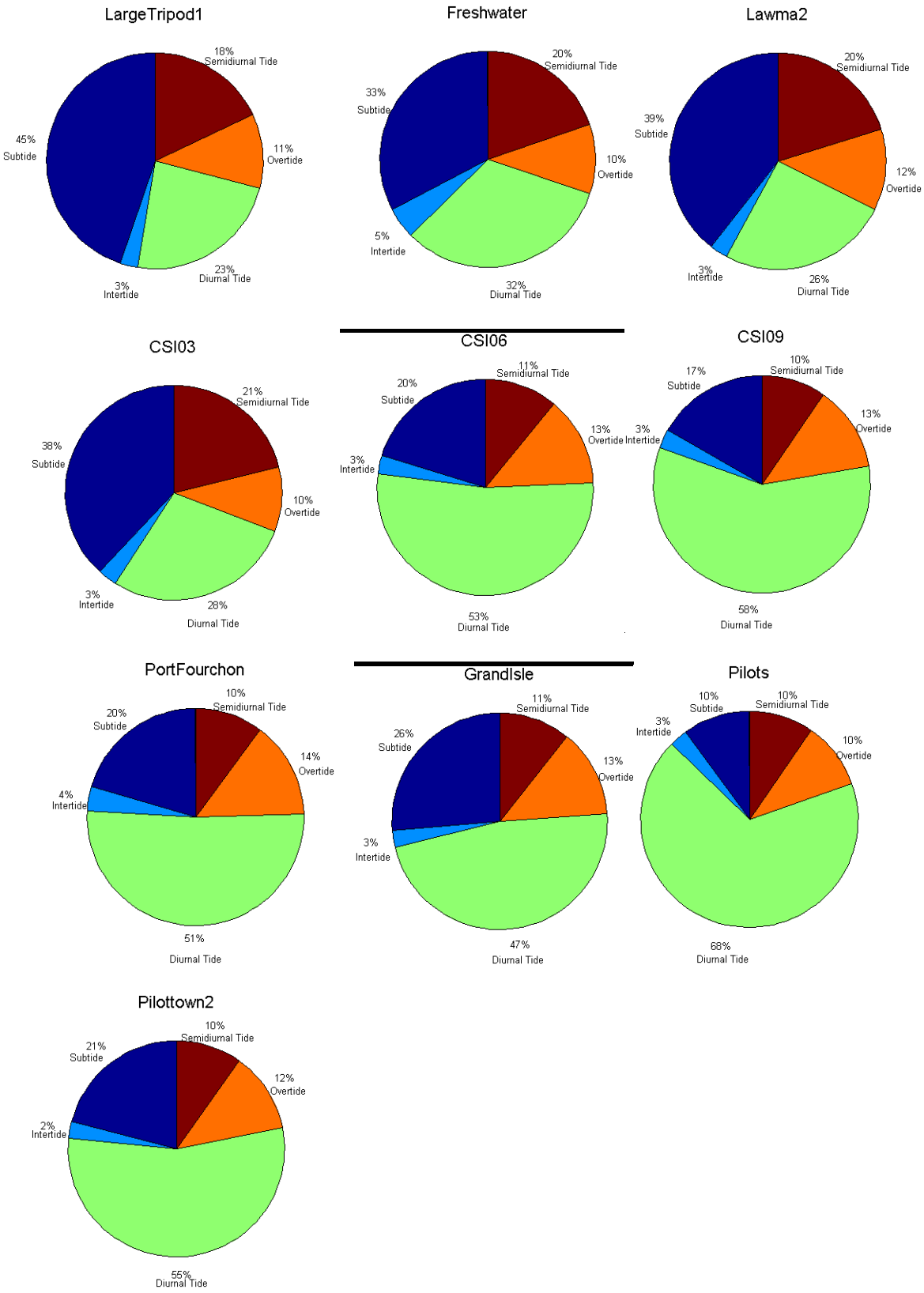

Figure 6.2 continued.

6.7 WATER TRANSPORT DURING COLD FRONT PASSAGE

6.7.1 The Geometry

The Wax Lake delta has seven major passes (Figure 6.28) and a number of secondary channels connecting the inundated wetland interiors. The structure of the channel network has a primary control on the dynamics and water flux in a distributary system. Both the subaerial (above the water surface; light green lobes in the figure) and subaqueous (under the water surface; blue regions; determined by bathymetry, Shaw, 2013) regions are demonstrated. It is noted, however, that the subaqueous portion of Wax Lake delta is relatively small and it is the subaqueous portion that have determined the network topography in the Wax Lake delta. Red lines indicate the transect locations of water flux rate to be analyzed from the model results among which the exterior outline is composed of 46 piecewise line segments used to accurately calculate the total water transport of the Wax Lake delta predicted by the model. It can be seen that generally the system is a number of channels radiating outward. By separating the wet and dry areas, characterization of global and local hydrodynamic behavior of the whole network, as well as the dynamic responses to winter cold fronts among channels, can be made. The distributary channels are bounded by naturally grown vegetation island that, depending on environmental conditions, may be dry (subaerial) or wet (subaqueous). Overtopping of the oasis may result in flow exchange between the channels and the surrounding areas. The exchange between the channels is thus an interaction among river discharge, tides, wind, and vegetation. Information about the water transport across the interdistributaries is based primarily on the bathymetry and thus important for the transport of sediment and nutrients (Hiatt, 2013). As to the flow direction, here in the case of Wax Lake delta, based on investigation and discussion of the circulation map in Section 6.4.2, the net flow/flux is usually out of the delta into the Gulf of Mexico. Waves, tides,

and winds may affect the flow. Topographic gradient can also contribute to the variations. Although the Wax Lake Outlet made contribution to diverting approximately 30% of the flow and sediment from the Atchafalaya River, in this study, we are more interested in the flow distribution and circulation inside the delta.

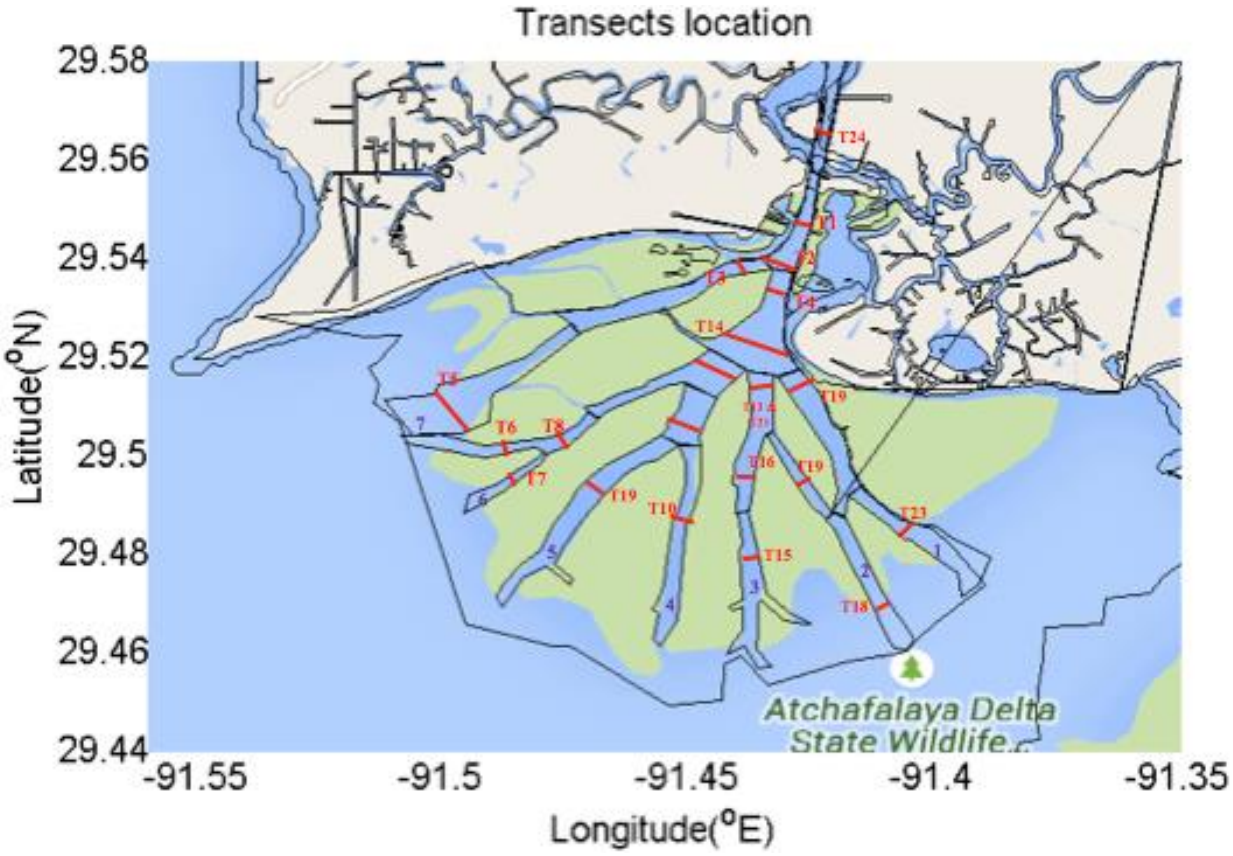

Figure 6.28 Transect locations for the modeling study in the Wax Lake delta. The light green lobes are subaerial region (above the water surface) by tracing channel centerlines from satellite imagery. Red lines indicate the transect locations of water flux to be analyzed. Purple numbers from 1-7 indicate the seven channels from east to west. Red numbers starting with 'T' indicate transect locations inside the delta selected for model result analysis.

6.7.2 Cold-front-induced Water Exchange

In this section, cold-front-induced bay-shelf water exchange from the model results is discussed for the study area.

6.7.2.1 Calculation of Flux and Accumulated Flux

Water flux, also called volume flux, is defined as the rate of water flow across a unit area. So by definition, we have the following equation,

$$F = \int_S \vec{v} \cdot \vec{n}\, dS \qquad (6-1)$$

where F is the volume flux (m^3/s); $\vec{v}$ is the current field, a time series of which can also be obtained from model output; S is a unit of area, and $\vec{n}$ is the normal vector of the surface. Since the water volume flux can be defined as the amount of water volume that passed through a transect in a unit time, the formula can be also written as:

$$F(x,y,t) = \int_{-H(x,y)}^{\zeta} \int_0^L v_n(x,y,z,t)\, dldz \qquad (6-2)$$

where $v_n(x,y,z,t)$ is the horizontal velocity component that is normal to the transect, such that the water volume flux is perpendicular to the given transect. The total water depth in z directon is the summation of the local undisturbed water depth ($H(x,y)$) and surface elevation (ζ) by model output. L is the width of the transect in l direction. And t is time (s) in UTC. Total flux, or accumulated flux, means how much flux has crossed the surface over a certain time, thus requiring an integration over time, and Equation (6-2) becomes

$$F(x,y,t) = \int_{t_0}^{t} \int_{-H(x,y)}^{\zeta} \int_0^L v_n(x,y,z,t)\, dldzd\tau \qquad (6-3)$$

where $\tau \in [t_o\ t]$, the unit of the total flux is m^3 instead of m^3/s. So basically the water flux is the flux calculation at an instant time, while accumulated flux is the summation, which is a standard calculus technique.

In specific, in order to calculate the water flux of the study area, I manually drew 46 points at the external boundary of the Wax Lake delta (Figure 6. 29) for time series of both water level and current velocity from model output. After the numerical simulation was completed, the water

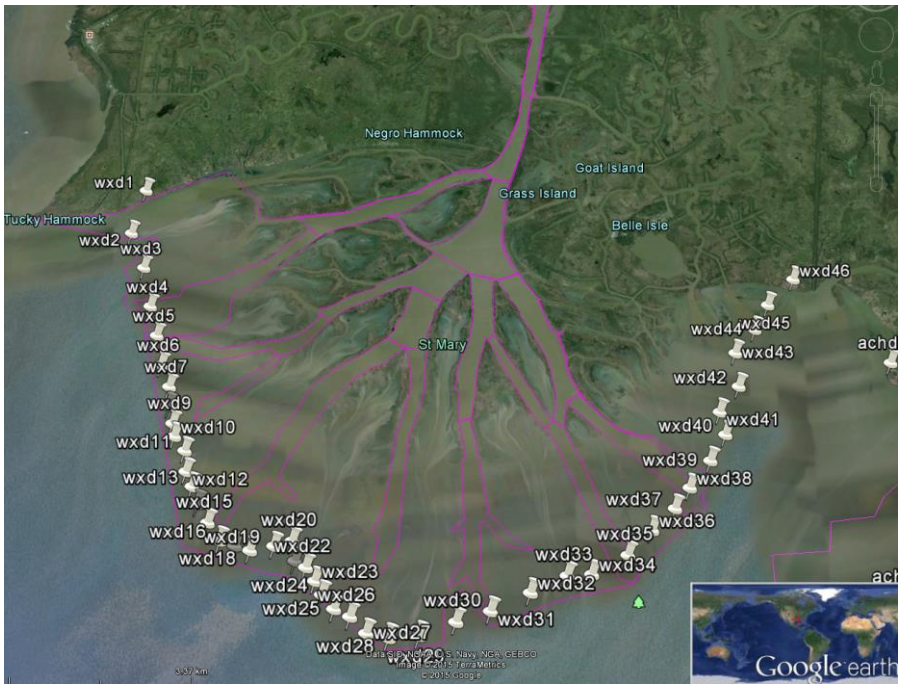

Figure 6. 29 Points at the boundary of the Wax Lake delta for water flux calculation.

level and current information could be directly available. Then I used linear interpolation to calculate the water depths at those points, after which the total water depth at all boundary points could be obtained by summation of water level and the local water depth. In order to implement Equation (6-2), we also need to know the distance or width of each transect between two adjacent points. Since the geographic location were available for all the points, we could easily calculate the width as well as the normal vector of transect surface. Plus, the current vector were saved in model. So the doc product of current vector and area surface will project the current onto the transect surface, producing the horizontal velocity component that is normal to the transect, i.e., v_n. The integration can then be implemented by trapezoidal numerical integration

technique. By this means, we can not only calculate the water flux at specific time but also over a period of time. In addition, the time series of water flux information is also very helpful for us to find out the cold front impacts on the hydrodynamics of the study area. In particular, the simulation data were low-pass filtered by a 6^{th}-order Butterworth filter with a cutoff frequency of 0.6 CPD to study the Wax Lake delta responses to the cold front event. More details will be given in the next section.

6.7.2.2 Water Flux Variation and Cold Front Passage

The time series of water flux and accumulated volume transport in Wax Lake delta, and the Atchafalaya Bay respectively are shown in Figure 6.30. First of all an obvious diurnal periodicity can be found from the water flux variation, which can also be supported by the spectra analysis of both regions in Figure 6.30. Each cold front induced a decrease in water flux quantity, when wind direction quickly shifts from south to north in the post-frontal passage. The total water flux at both regions also demonstrated the similar flux out pattern, but with different orders of magnitude. The Atchafalaya Bay encloses the Wax Lake delta, Atchafalaya delta, as well as the surrounding water bodies, thus it has the largest flux amplitude an order of magnitude higher than that of the Wax Lake delta. Such differences can be explained by two factors: water body area and basin geometry. The Atchafalaya Bay has the area of approximately $2410\ km^2$, which is roughly 17 times of that of Wax Lake delta (approximately $138\ km^2$). The basin geometry also impacts the magnitude of water exchange. The Atchafalaya Bay has an obvious much wider open boundary directly open to the Gulf of Mexico, and thus quite a large amount of water exchange between the bays and the inner shelf; while the Wax Lake delta, as described in the Geometry section, is a shallower system consisting of numbers of channels radiating outward,

with a series of bifurcated lobe extensions at the river mouth of the lower Wax Lake Outlet and more than 200 km away from the continental shelf, and thus very limited amount of water exchange between the bays and the inner shelf.

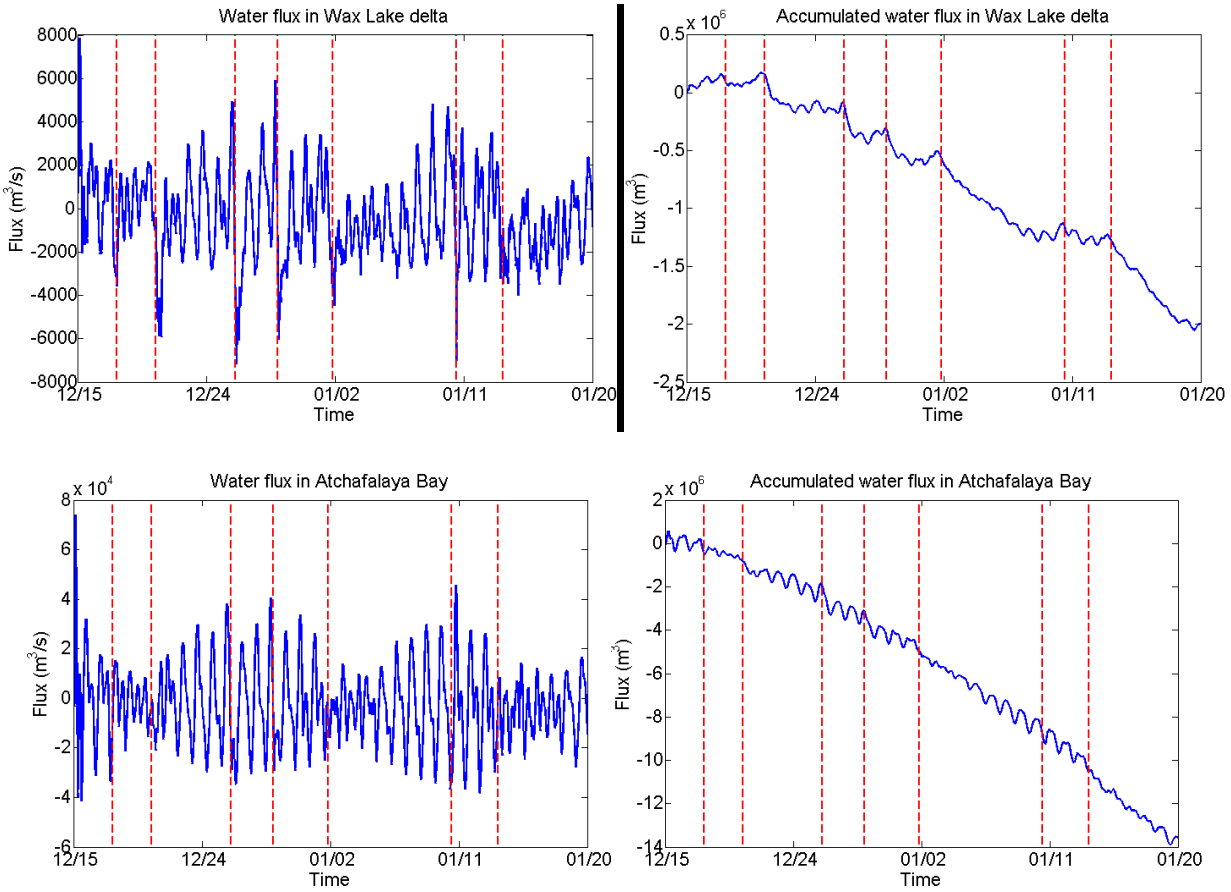

Figure 6. 30 Water flux (LHS) and accumulated water flux (RHS) in the Wax Lake delta (upper panel) and the Atchafalaya Bay (lower panel), respectively. The positive and negative values correspond to flux in and out, respectively. Vertical lines indicate time of cold fronts passing through the bays.

The amplitude spectra (0-2.5 CPD) of flux associated with the subtidal flux is also calculated using the time-series of velocities from the model output of sectional flux (Figure 6.31). Here a dominant diurnal pattern can be observed from both the Wax Lake delta and the Atchafalaya Bay. The subtidal effects is comparable to semidiurnal forcing in the Wax Lake delta; while in perspective of the whole Atchafalaya Bay, this subtidal wind forcing does not seem to

predominant as much as in the Wax Lake delta, due to the same reasons discussed earlier. Subtidal water flux variation for both regions, although on different orders of magnitude, perfectly coincided the timing of the outward flushing events of the bays (vertical lines in Figure 6.31) with each cold front event, indicating its importance of cold front in water transport.

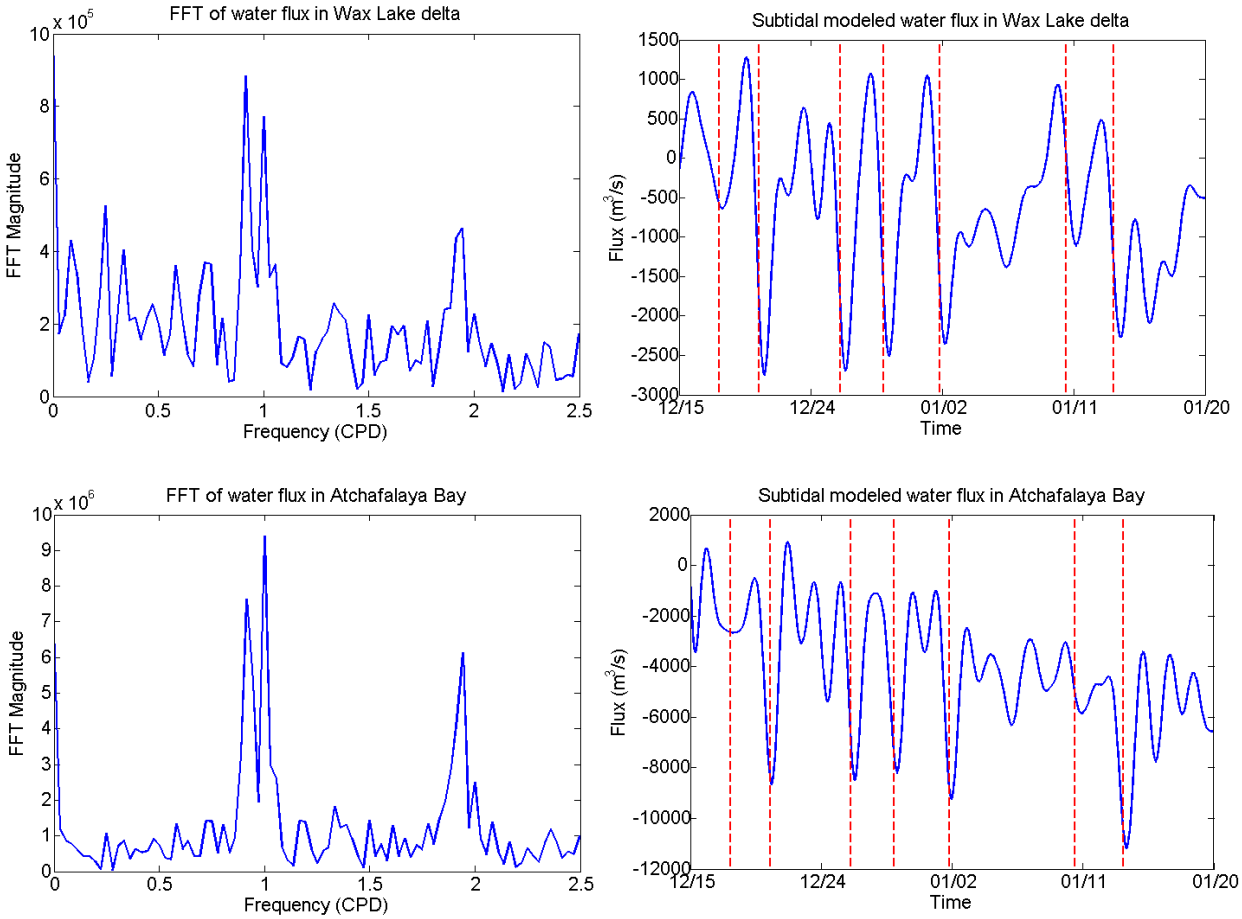

Figure 6.31 The amplitude spectrum (0-2.5 CPD) of water flux (LHS) and subtidal water flux (RHS) in the Wax Lake delta (upper panel) and the Atchafalaya Bay (lower panel), respectively, from December 15 2012 to January 20 2013. The positive and negative values correspond to flux in and out, respectively. Vertical lines indicate the times of cold fronts passing through the bays.

Subtidal water flux also showed that, in the Wax Lake delta, among the 7 captured cold fronts, the 2nd, 3rd, 4th and 5th are much stronger than the others, which corresponds to relatively stronger and persistent northerly wind during those events. So we would like to take a closer look at the relationship between winds, subtidal water level, and subtidal water flux during those cold front

processes (Figure 6.32). All those four events have a typical clockwise pattern in wind direction shifts. Subtidal water level was lifted during the prefrontal passage by onshore southerly wind, reaching the maximum and started to drop 6-9 hours prior to the frontal passage. Similarly, the subtidal influx reached the highest first and then changed into outflux. The subtidal outflux reached the maximum 5-11 hours after the frontal passage as a result of the persistent and strong northwest winds (>10 m/s), and then decreases with the weakening of wind speed and

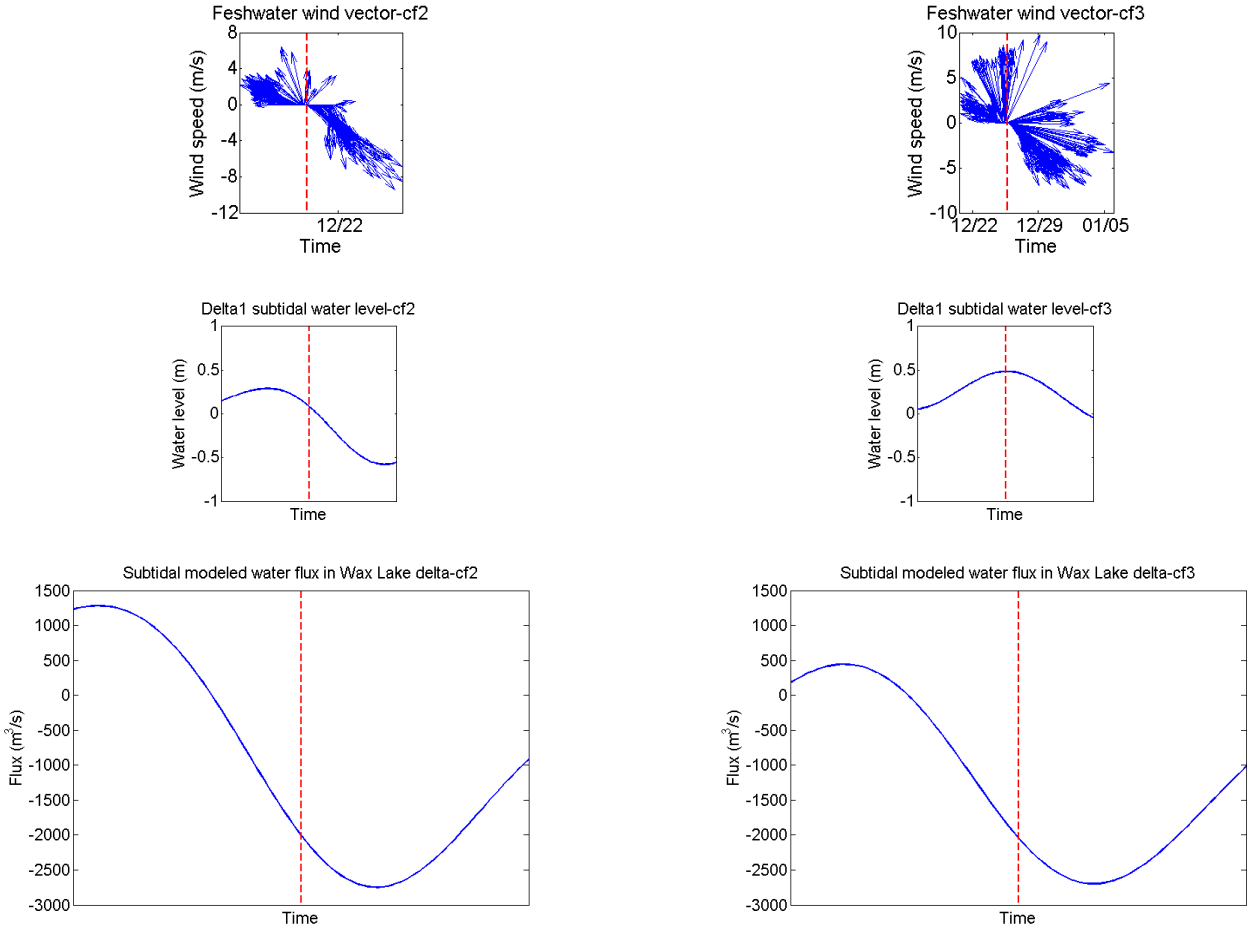

Figure 6.32 Wind vectors (upper panels), modeled subtidal water level (middle panels), and modeled subtidal water flux (lower panels) of the Wax Lake delta, associated with the four flushing events. The winds are plotted in the vector format.

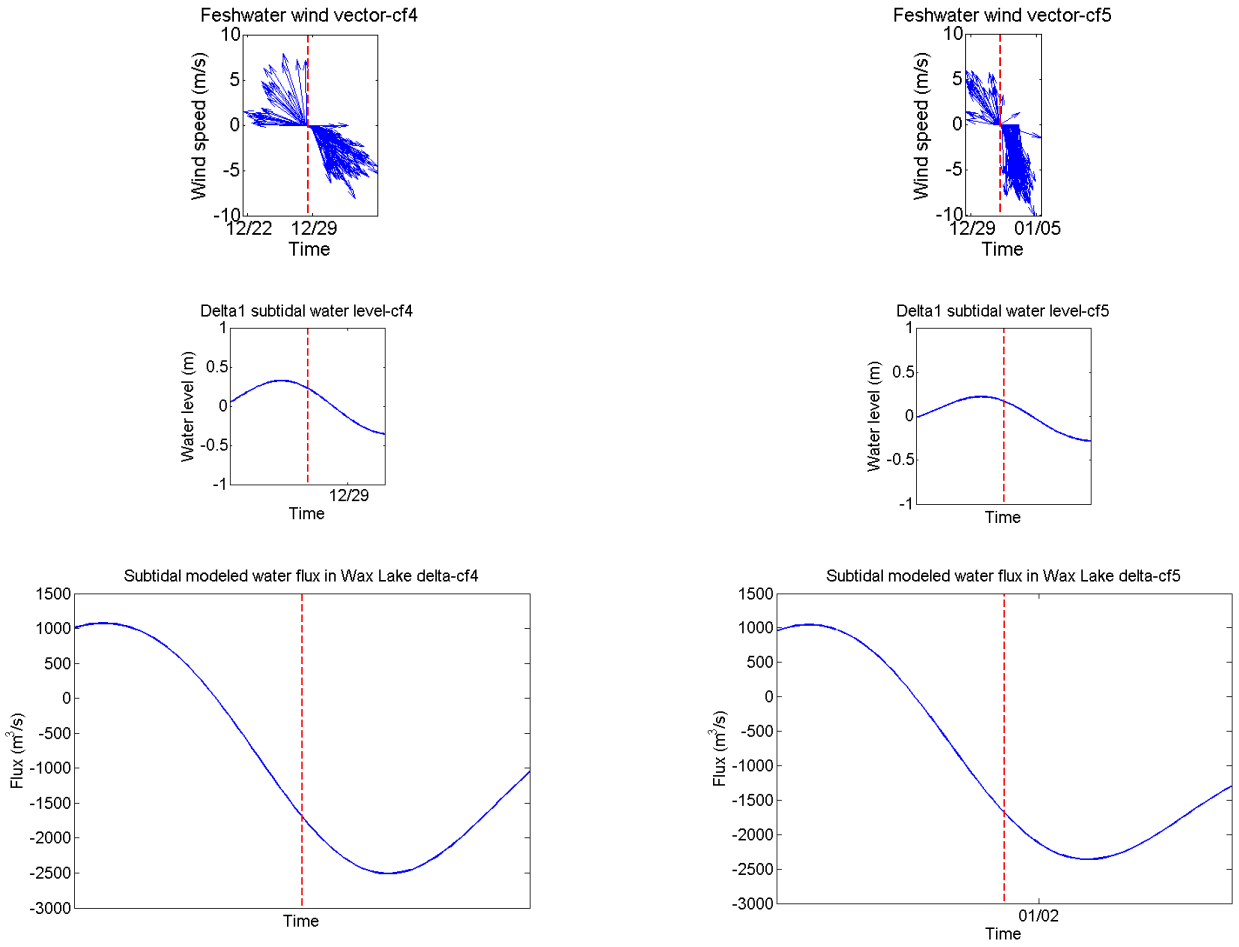

Figure 6.32 continued.

continuous clockwise rotation of wind direction. The northwest/north winds seem to be the most effective forcing in flushing water out of the bays, which agree with measurement analysis results that the northwest to north winds maximize bay flushing (Feng, 2009; Li et al., 2011).

6.7.2.3 River Flux vs. Cold Front-Induced Water Exchange

The amounts of subtidal water volume flushed out by cold fronts are compared with river flux of the delta (Table 6.2). The cold-front-induced flushing event lasts 41-185 hours in the Wax Lake delta. 32% to 76% of the total waters in the Wax Lake delta are flushed out by these seven

events. This also suggests that strong cold front events may flush more than 76% of the water outside onto the shelf within a less than 45-hour period.

The river discharge is included in the simulation implementation. But its contribution to water level variation and water transport is much weaker compared to the cold front induced transport. The impacts of other factors (e.g., rainfall, evaporation, and runoff) are usually even minor.

Table 6.2 The duration, total volume transport, and percentage of volume flushed out during seven cold fronts. MC: migrating cyclone. (The '+' sign means the cold front is still going on.)

Cold front event	Type	Wax Lake delta		
		Duration (hr)	Subtidal Volume (m^3)	Percentage (%)
1	MC	41.5	2.4734×10^6	32.66
2	MC	69	1.1266×10^7	68.61
3	MC	44.5	1.0226×10^7	76.64
4	MC	65	1.0148×10^6	55.18
5	MC	65	1.0148×10^6	55.18
6	MC	185	2.6714×10^6	39.00
7	MC	160.5+	2.9290×10^7+	36.18+

6.7.3 Flow Partitioning

Now we are interested in the questions of how discharge is partitioned among the distributary channels and how tidal and wind driven flow is affecting the dynamics between the channels and the surrounding areas. In order to capture the flow-partitioning among the major distributary channels, velocity, cross-sectional bathymetry, and flow direction were needed. Figure 6.33

shows the simulated time series of water volume flux and accumulated volume flux over a period of time at selected cross sectional locations inside the Wax Lake delta.

Circulation could also be examined by quantifying the water volume flux through the selected transects (Figure 6.28). Again all time series of water volume flux (Figure 6.33) at main 7 channels have shown diurnal pattern. The maximum water volume flux at transect T22 in channel 1, and then transects T18 and T20 in channel 2 and 3, respectively, followed by T10 in channel 4. The channel morphology seemed to have determined the flow partitioning for Wax Lake delta. However it is found that not all 100% of the flow is delivered to the Atchafalaya Bay via channelized discharge. Take T14 for instance, which diverts flow into channel 1-6 through transections T12, T13 (or T21), and T22. From accumulated water flux at these locations, only 50% of T14's flow goes into channel 4-6 through T12, 15% into channel 2-3 through T13 (or 21), and 10% into channel 1 via T22, respectively. The explanation about this 25% discharge loss from the upper channels is most likely that it is diverted into the surrounding island lobes occupying much of the delta's land surface towards the delta shoreline (A+B+C=25% in Figure 6.34).

Figure 6.35 (Hiatt, 2013) shows the flow allocation map in the Wax Lake delta based on a field measurement collected from 02/04/2012-02/07/2012, which quantified the water volume flow dissipation of approximately 30% total discharge from the distributary channels into the surrounding vegetation regions. Earlier than this, Buttles et al., (2007) found a fraction of 15% discharge loss at the Wax Lake delta. Both literatures believed that during the water flow proceeds from upper stream Wax Lake Outlet down to the delta, some portion of water is

transported into the adjacent islands through broken crevasse channels immersing the delta's subaerial dry surfaces. And the similar discharge loss can be captured in our numerical experiment, where the model predicted rate of 25% loss lies in the interval from the work of Buttles et al., (2007) and Hiatt (2013) who found 15% and 30% loss at the Wax Lake delta, respectively. This phenomenon can also be qualitatively identified from the surface elevation contour and surface current maps (Figure 6.10-6.16), where the inundation and/or water intrusion occurs to those dry areas next to the bifurcating channels.

With regard to the accumulated water volume flux, all seven channels have almost indicated an offshore transport, although channel 1 and 7 have only a limited short period of time for onshore transport. And those onshore transport did not seem to affect the upstream T2 (refer to Figure 5.2). So the net upstream river discharge from the Wax Lake Outlet transported through T2 to T3 into channel 7 and to T14 and T22 into channel 1. Figure 6.33 also showed that channel 3-6 among all the channels seem to have the largest flow partition, which also agrees to the flow-partitioning framework that is summarized in Figure 6.35 by Hiatt (2013).

Figure 6.28 and Figure 6.33 also shows that those channels 1-6 carrying larger volume of flow occur in the southern part of the delta, which also tend to be surrounded by larger subaerial vegetation and wetlands (the surrounding island area information can refer to Hiatt, 2013). That may also support the statement that the relatively high discharge channels are more likely to feed inland subaerial areas through overbank inundation flow (Hiatt, 2013). Further downstream, the region is more likely subject to significant overbank flow.

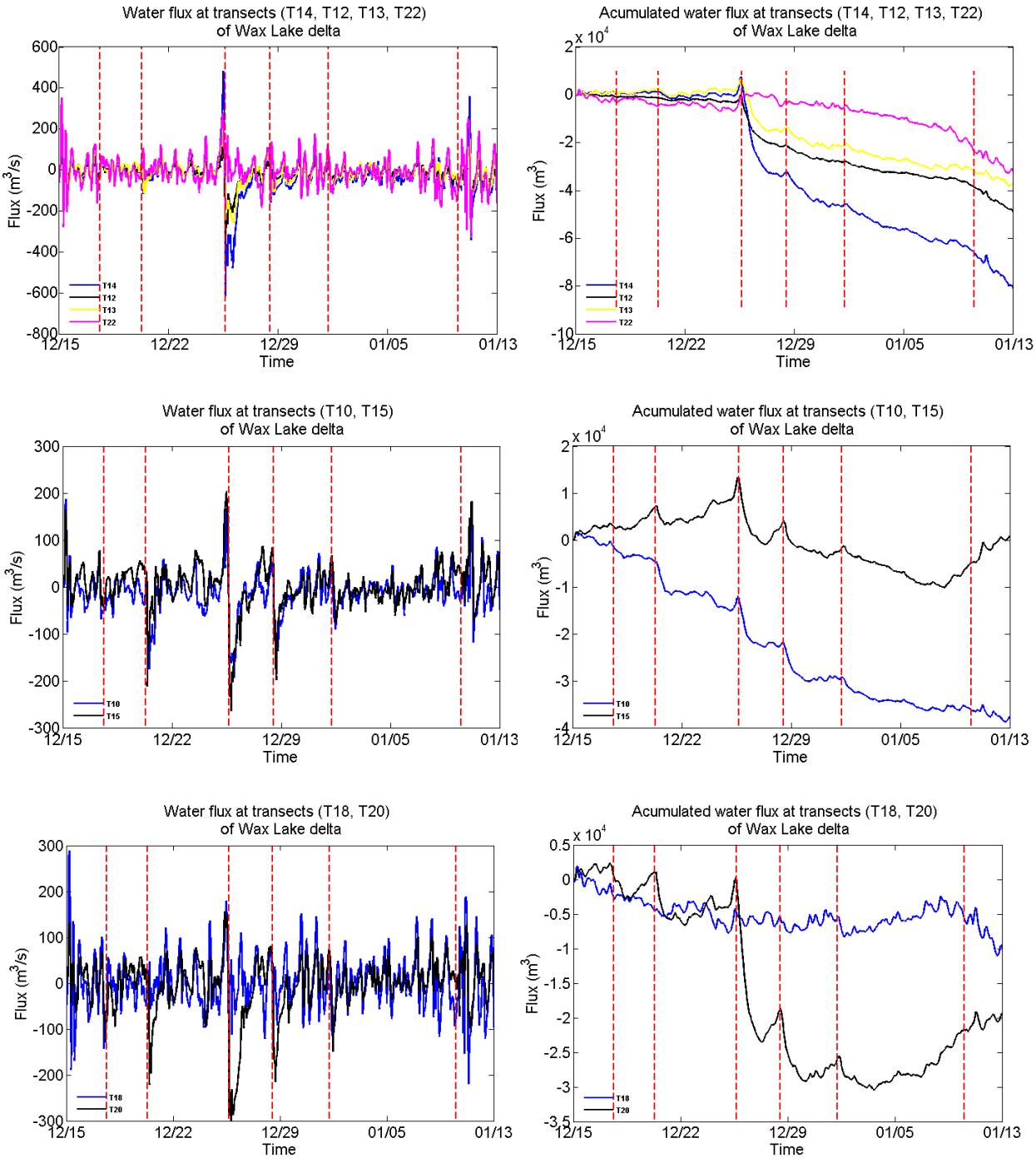

Figure 6.33 Simulated water volume flux and accumulated volume flux at different transects inside the Wax Lake delta. Vertical lines indicate time of cold front passage.

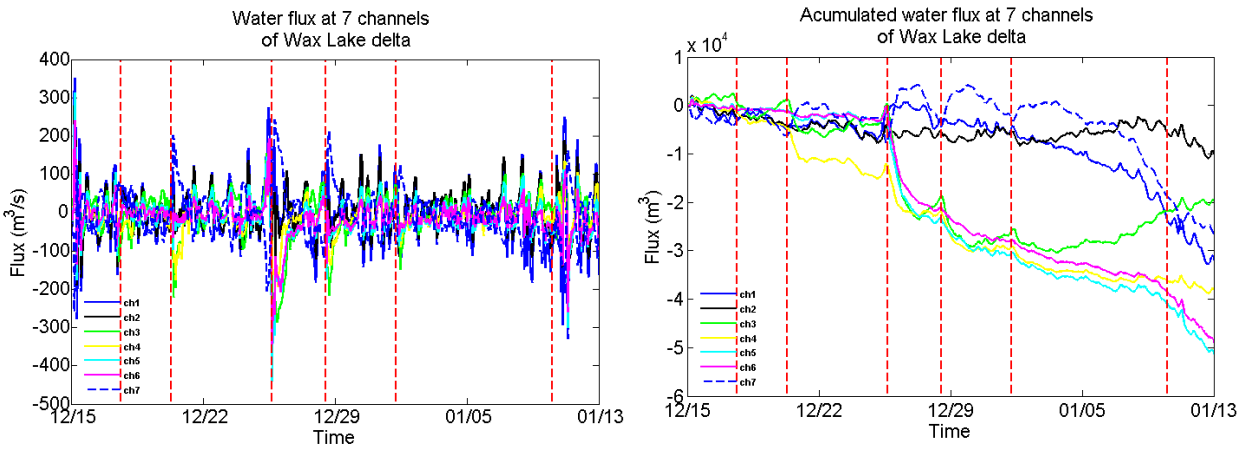

Figure 6.33 continued.

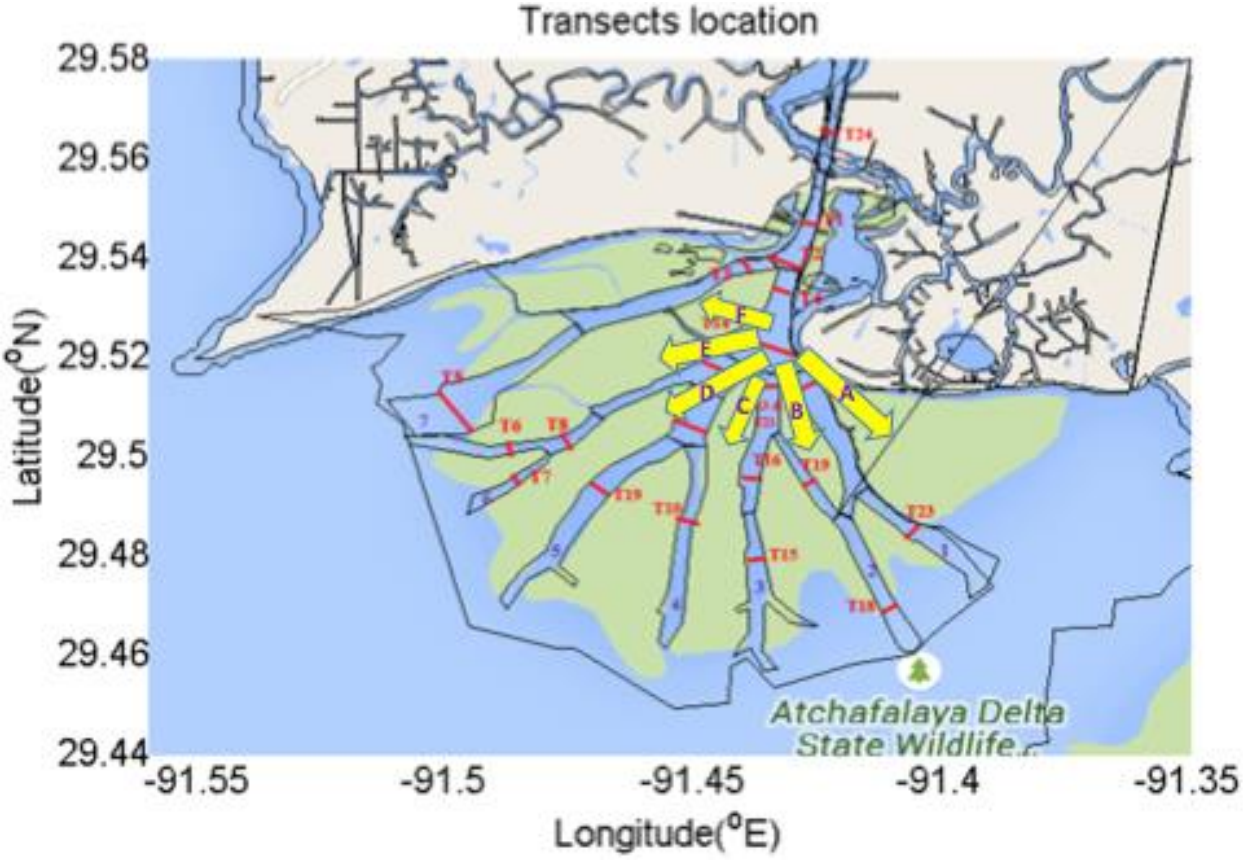

Figure 6.34 Flow partition at transect locations in the Wax Lake delta.

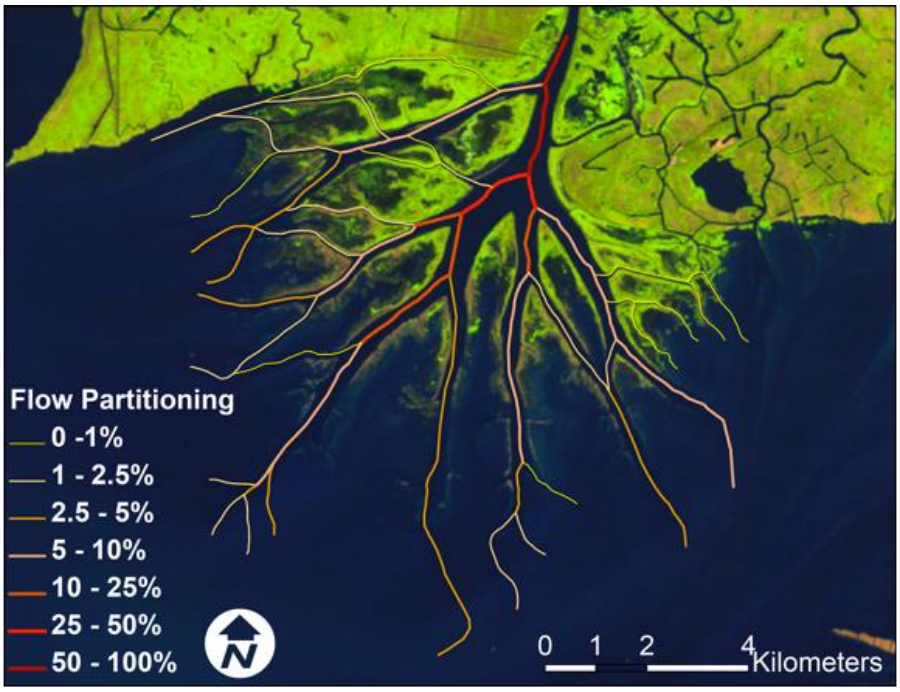

Figure 6.35 The flow-partitioning framework for Wax Lake Delta. The thickness and gradation of the link describes the associated calculated discharge (from measured velocity and cross-sectional area) as percentage of apex flow (from Hiatt, 2013).

CHAPTER 7 CONCLUSIONS AND DISCUSSION

7.1 CONCLUSION

In this study, a numerical model was applied for the Wax Lake delta area in the northern Gulf of Mexico (GOM) to simulate the circulation driven by the winter cold fronts from December 15, 2012 to January 20, 2013 in this region. The numerical model used here is the 3-D ECOM-si with tides, river discharge and wind stress as the forcing. Considering almost none numerical experiments have been done for cold-front-related hydrodynamics, the present work for the Wax Lake delta and the surrounding areas is a step forward: this work presents the first numerical experiments of the circulation under cold fronts in this area.

The numerical model used in this study was a modified version of the ECOM-si, which is a three-dimensional, primitive-equation, semi-implicit ocean circulation model.
The present model has 380×250 curvilinear orthogonal grids in the horizontal and 11 uniform levels in the vertical. In order to examine the influence of variable bathymetry and cold-front-driven flow in the study area, the present model utilized realistic bottom topography and coastline.

Our analysis shows that the modeled tidal and subtidal variations of flows and water levels in the Wax Lake delta and the surrounding areas during seven cold fronts were consistent with observations. Some discrepancy does exist between the modeled and measured currents which may be caused partially by the inaccuracy in bathymetry data.

The circulation analysis draws into two categories. The 1st part is to investigate the offshore circulation by plotting the near-surface currents on the whole computational domain. It can be summarized from those wind-gyre correspondences, that the northerly wind (including north, northwest, and northwest) tends to generate an anti-cyclonic (CW) gyre while the southerly wind (including south, southwest, and southeast) tends to generate a cyclonic (CCW) gyre on the continental shelf (covering latitude of $28.5^o - 29.5^o$) offshore south of the Atchafalaya Bay, Barataria and Terrebonne Bay and/or west of Mississippi Delta. It is also noted that not every cold front event can generate such gyres and the gyre extent and intensity vary from one to one. The 2nd part is to focus on the circulation pattern inside the Wax Lake delta alone by plotting the near-surface velocity and water level contour in one figure. Basically the current flows follow the wind direction change: the prefrontal onshore winds induce a counterclockwise (CCW) circulation where the current magnitude is not comparable to the postfrontal wind-induced current. Water intrusion is visible and a reverse flow in the delta channel tip can be easily identified but disappear very soon. And inundation occurs in the inland subaerial areas between distributary channels. In contrast, the postfrontal winds generate a much stronger clockwise (CW) circulation. Under typical northeasterly winds the current flow is blown downstream following the topography in each channel from upper stream discharge with southwestward direction when confluence with the deeper Gulf water. So does the surrounding subaerial inundated island area. Under southeasterly winds prior to the cold front passage, the seaward expansion of the current flow is considerably reduced and the onshore strong winds increase coastal water levels and result in a water setup, inducing a surge event. After the cold front passage, when the atmospheric pressure rises and wind abruptly shifts to an even stronger

northwesterly, the water level is reduced rapidly and water is flushed onto the surrounding island areas, leading to a seaward transport (Feng et al., 2010).

Three stations (CSI03, CSI06, and Delta1) were picked to examine the relationship between winds and currents. The time series of near-surface current at CSI03 and CSI06 generally follows the winds shift (Figure 6.20). It is noted that during winters storm in this study period, the current at all three stations reverses direction throughout almost the entire water column (Figure 6.18, 6.20 and 6.23), suggesting strong wind-induced vertical mixing. The model results also showed that the subtidal current is generally uniform (Figure 6.20 and 6.23 upper panel) throughout the vertical column and only slightly decreases with depth, except at CSI06. Model results of Detla1, which is shallow (depth < 2m) residing inside the channel, clearly demonstrates that the along-channel component dominates the whole study period. The along-channel current does show occurrence of return flow during the frontal passage, although it does not last long. The flow structure at Delta1 is similar to the near-surface current of CSI03, but also demonstrates some distinct characteristics. Firstly, the prevailing subtidal along-channel flow is stronger than that of CSI03 and CSI06. Secondly, the subtidal current field at Delta1 seems more sensitive to the cold front events than at CSI03 and CSI06, based on the fact that the post-frontal along-channel current is usually stronger than that of those two stations. The current flow is significantly altered from westward direction to eastward by the surface wind stress, which indicated that strong cold front events may disturb the initial downcoast flow system by inducing an up coast flow. During the study period between December 15 2012 and January 20, 2013, due to more frequent (seven were captured in one month) and persist cold front passages, it is hard to

summarize a general surface current pattern as a persistent and strong westward movement since cold fronts do take significant effects, although the westward reestablishment is quite obvious.

Through the power spectrum analysis, it is found that the subtidal energy accounts for over 45% of total energy while tidal energy contributes to less than 25%. River discharge has little impact on the water level and water exchange during the study period, compared to tides and wind effects. This confirms that the circulation within this shallower delta system is primarily dominated by the wind in winter.

The time series of water flux and accumulated water flux variation was calculated for every cell at each transect enclosing the Wax Lake delta. Cold-front-induced bay-shelf water exchange from the model results is also discussed for the study area. Subtidal water level was lifted during the prefrontal passage by onshore southerly wind, reaching the maximum and started to drop 6-9 hours prior to the frontal passage. Similarly, the subtidal influx reached the highest first and then changed into outflux. The subtidal outflux reached the maximum 5-11 hours after the frontal passage as a result of the persistent and strong northwest winds (>10 m/s), and then decreases with the weakening of wind speed and continuous clockwise rotation of wind direction. The northwest/north winds seem to be the most effective forcing in flushing water out of the bays, which agree with measurement analysis results that the northwest to north winds maximize bay flushing (Feng, 2009; Li et al., 2011). The amounts of subtidal water volume flushed out by cold fronts are compared with river flux of the delta (Table 6.2). The cold-front-induced flushing event lasts 41-185 hours in the Wax Lake delta. 32% to 76% of the total waters in the Wax Lake delta are flushed out by these seven events. This also suggests that strong cold front events may

flush more than 76% of the water outside onto the shelf within a less than 45-hour period. The model results showed that the cold front wind is the most important factor for the hydrodynamic processes of the Wax Lake delta in winter.

Analysis of the model results shows that water fluxes in the delta distributary network from the upper stream (Wax Lake Outlet at Calumet, LA or USGS 07381590) are not solely propagated within the distributary channels but also between the channels (Figure 6.34), where the inundated island interiors are surrounded by subaerial vegetation. This accounts for an approximately 25% of loss at the major channels of the Wax Lake delta.

7.2 DISCUSSION

The implication of this study lies in that the flow partition and inundation pattern onto the surrounding areas could also indicate the sediment transport pattern in the Wax Lake delta. Besides the along-channel water transport, the cross-channel water transport during post-frontal passage is much stronger, occurring at the southwestern lobe, with an approximate estimation of instantaneous water flux of $300 - 1000\ m^3/s$. If this southeastward water transport continues, with taking into account of sediment transport carried by the water flows, this will ultimately lead to the lobe movement in this area. In fact, an obvious lobe merge has been observed surrounding channel 6 from Google Earth image from 2014 to 2015 (Figure 7.1), which will indicate a long-term impact on the geomorphology change of the delta.

Figure 7.1 Wax Lake delta comparison between 2014 and 2015 from Google Earth.

One limitation of the current study is that the present modeling used spatially uniform wind as input driving force. One reason is the difficulty in obtaining the high resolution observations of wind, where the 2.5-degree NCEP global wind model result may be too sparse for interpolation. On the other hand, the cold front is such a large-scale weather system that the spatial variation in wind speed is negligible.

In evaluation of the numerical model robust capability, we picked several parameters to be adjusted for calculating current velocities, including bottom friction parameters, horizontal mixing and advection parameters, and vertical mixing parameters. The comparison between the model results and observation data did show significant differences. The final modified modeling parameters was then using a minimum bottom roughness value of 0.0025 m, horizontal diffusion calculated using the Smagorinsky's parameterization method with a constant Smagorinsky coefficient (HORCON) and horizontal Prandtl number (HPRNU) of 0.1 and 1.0, respectively. For vertical mixing, we chose the MY25 closure (Mellor Yamada Level 2.5 Closure with a parabolic wall proximity function) method for vertical eddy viscosity, with a background mixing

coefficient (UMOL) of $0.00001\ m^2/s$, a vertical eddy viscosity coefficient of 1.0. On the other hand, as we mentioned in Section 4.3.3, the wet/dry condition $D_{min} = 0.2\ m$ is also very important because it determines the inundation process (the flooding extent, area, as well as the flooding time, etc.) by this critical depth for separating water and land

In this study, we only focused on the hydrodynamics effects of cold front events on the Wax Lake delta, but the coastal environmental responses such as salinity, temperature, wave actions and river plume during the cold fronts were not discussed. Future modeling studies focusing on those processes will eventually provide us with additional and more comprehensive insights on the mechanisms relating meteorological forcing, hydrodynamic processes, and coastal environmental changes.

Although modeling efforts and network analyses in the Wax Lake delta were involved, a continuation in development of the flow-partitioning model that will more accurately reflect the flow allocation and interaction between distributary channels and adjacent subaerial island lobes regarding flux propagation in both water discharge and sediment plume should be planned. This exploration will be straightly related to the delta evolution and morphology, thus guiding the study work of other delta networks.

REFERENCES

Acoustic Doppler Current Profilers, Principles of Operation, A Practical Primer, RD Instruments, January, 2011.

Ahrens, D.C., 2007. Meteorology Today: an introduction to weather, climate, and the environment, Thomas Learning, Inc., 20067, 624pp.

Allison, M.A.; Kineke, G.C.; Gordon, E. S., and Goni, M.A., 2000. Development and reworking of a seasonal flood deposit on the inner continental shelf off the Atchafalaya River. *Continental Shelf Research*, 20, 2267–2294.

Allison, M.A., and Meselhe, E.A., 2010. The use of large water and sediment diversions in the lower Mississippi River (Louisiana) for coastal restoration: *Journal of Hydrology* (Amsterdam), v. 387, p. 346–360, doi:10.1016/j .jhydrol.2010.04.001.

Angelovic, J.W., Environmental Studies of the South Texas Outer Continental Shelf, 1975, 2, Physical Oceanography, U.S. Department of Commerce, NOAA, Washington, D.C., 1976.

Arakawa, A. 1966. Computational design for long-term numerical integration of the equation of fluid motion: two dimensional incompressible flow. *J. Comput. Phys*. 1:119–143.

Arakawa, A., and Lamb, V.R., 1977. Computational design of the basic dynamical processes of the UCLA general circulation model. Methods in Computational Physics, Vol. 17, Academic Press, New York, 174-265.

Blumberg, A. F. (1994), A primer for ECOM-si, technical report, 66 pp., HydroQual, Inc., Mahwah, N. J

Blumberg, A. F. and G. L. Mellor, 1987, A description of a three-dimensional coastal ocean circulation model, in Three-Dimensional Coastal Ocean Models, Coastal Estuarine Sci., vol. 4, edited by N. Heaps, 208 pp., American Geophysical Union (AGU), 1987, Washington, D. C.

Boehlert, G. W. & Mundy, B. C., 1988. Roles of behavioral and physical factors in larval and juvenile fish recruitment to estuarine nursery areas. American Fisheries Society Symposium 3: 51–67.

Boyd, R. and Penland, S., 1981. Washover of deltaic barriers on the Louisiana Coast, *Trans. Gulf Coast Assn. of Geol. Soc*. 31: 243-248.

Browning K.A. and Gurney R.J., 1999. Global Energy and Water Cycles, Cambridge University Press, Feb 1, 1999, 304 pages.

Buttles, J., Mohrig, D., Nittrouer, J., McElroy, B., Baitis, E., Allison, M., et al., 2007. Partitioning of Water Discharge by Distributary Channels in the Prograding Wax Lake

Delta, Coastal Louisiana, USA. *American Geophysical Union, Fall Meeting 2007,* American Geophysical Union.

Carlson, T. N., 1991. Mid-Latitude Weather Systems, HarperCollins Academic, 1991, 507 pp.

Carter, J., Keil S., Kirk W., Lindy B., Brian H., Rebecca M., and Jennifer H., 2012. Lidar 101: An Introduction to Lidar Technology, Data, and Applications, National Oceanic and Atmospheric Administration (NOAA) Coastal Services Center, 2012, p. 14.

Castellanos, D. L. & V.R. L. P. x 2001. Nekton use of submerged aquatic vegetation, marsh, and shallow unvegetated bottom in the Atchafalaya River Delta, a Louisiana tidal freshwater ecosystem. *Estuaries* 24: 184–197.

Casulli, V. 1990. Semi-implicit finite-difference methods for the two-dimensional shallow water equations. *J. Comput. Phys*. 86:56–74.

Casulli, V, and Cheng, RT, 1992. "Semi-implicit Finite Difference Methods for Three-Dimensional Shallow Water Flows," *Int J Numer Methods Fluids*, Vol 15, pp 15 629-15 648.

Cattrijsse, A. & H. Hampel, 2006. European intertidal marshes: a review of their habitat functioning and value for aquatic organisms. Marine Ecology Progress Series 324: 293–307.

Celoria, F., 1966, Delta as a geographical concept in Greek literature, Isis 57(3): 385-388, doi: 10.1086/350146.

Chapman, D.C. and Lentz, S.J., 1994. Trapping of a coastal density front by the bottom boundary layer. *Journal of Physical Oceanography*, 24, 1464–1479.

Chen, C. H., Huang, R. C., Beardsley, H. Liu, Q. Xu and Cowles, G. 2007. A finite-volume numerical approach for coastal ocean circulation studies: comparisons with finite difference models. *J. Geophys. Res*. 112. C03018, doi:10.1029/2006JC003485.

Chen, C., Liu, H., Beardsley, R., 2003. An unstructured, finite-volume, three-dimensional, primitive equation ocean model: application to coastal ocean and estuaries. *J. Atm. &Oceanic Tech.*, 20, 159-186.

Chen, C., Zhu, J., Ralph, E., Green, S.A., Budd, J.W., and Zhang, F.Y., 2001. Prognostic modeling studies of the Keweenaw Current in Lake Superior, part I: Formation and evolution, *J. Phys. Oceanogr.*, 31, 379–395, doi:10.1175/1520-0485(2001)031<0379:PMSOTK>2.0.CO;2.

Chen, C., Zhu, J., Zheng, L., Ralph, E., and Budd J. W. ,2004. A nonorthogonal primitive equation coastal ocean circulation model: Application to Lake Superior, *J. Great Lake Res*., 30, 41–54.

Chen, C., Beardsley R. C., and Cowles, C., 2006. An unstructured grid finite-volume coastal ocean model: FVCOM user manual, SMAST/UMASSD-06-0602, 324 p.

Chen, C., Xu, Q., Ralph, E., Budd, J.W. and Lin, H.,2004. Response of Lake Superior to mesoscale wind forcing: A comparison between currents driven by QuikSCAT and buoy winds. *Journal of Geophysical Research* 109: doi: 10.1029/2002JC001692. issn: 0148-0227.

Chen, C.S., Qi, J. H., Li, C. Y., Beardsley, R. C., Lin, H. C., Walker, R., and Gates, K., 2008, Complexity of the flooding/drying process in an estuarine tidal-creek salt-marsh system: An application of FVCOM, *J. Geophys. Res.*, 113, C07052, doi:10.1029/2007JC004328.

Childers, D. L., Day Jr. J. W. & Muller, R. A., 1990. Relating climatological forcing to coastal water levels in Louisiana estuaries and the potential importance of El Nino-Southern oscillation events. *Climate Research*, 1: 31–42.

Chu, P.C., Ivanov, L.M., and Melnichenko, O.M., 2005. Fall-winter current reversals on the Texas-Louisiana continental shelf (paper download). *Journal of Physical Oceanography*, American Meteorological Society, 35, 902-910.

Chuang, W.S. and Wiseman, W.J., Jr., 1983. Coastal sea level response to frontal passages on the Louisiana-Texas Shelf. *Journal of Geophysical Research*, 88, C4, 2615-2620.

Cochrane, J.D., Kelly, F.J, 1986. Low-frequency Circulation on the Texas- Louisiana Continental shelf, *J. Geophysics Research*., 91(C9), 10645-10659.

Co, D.S, Preller, R.H, and Martin, P.J., 2003b. An experimental Real-Time Intra- Americas sea ocean nowcast/forecast system for coastal prediction. AMS 5th conference on coastal Atmospheric and Oceanic prediction and processes, 5-8 August 2003, Seattle, WA, pp 97-100

Coasts & Habitats, Part 1 of 2, 2010. SU Ports, Sustainable management for European local ports.

Cobb, M.; Keen, T.R., and Walker, N.D., 2008a. Modeling the circulation of the Atchafalaya Bay system during winter cold front events. Part 1: model description and validation. *Journal of Coastal Research*, 24(4), 1036–1047. West Palm Beach (Florida), ISSN 0749-0208.

Cobb, M.; Keen, T.R., and Walker, N.D., 2008b. Modeling the circulation of the Atchafalaya Bay system, part 2: River plume dynamics during cold fronts. *Journal of Coastal Research*, 24(4), 1048–1062. West Palm Beach (Florida), ISSN 0749-0208.

Cochrane, J. D. and Kelley, F.J., 1986, Low-frequency circulation on the Chenier Plain coast on the Texas-Louisiana continental shelf, *Journal of Geophysical Research*, 91, 10,645-10,659.

Coleman, J.M., 1988, Dynamic changes and processes in the Mississippi River delta, *Geological Society of America Bulletin*, 100, 999-1015.

Coleman, J.M., Roberts, H.H., and Huh, O.K., 1986, Chapter 5, Deltaic landforms, In: Short NM, Blair RW, Jr (eds) Geomorphology from space: A global overview of regional landforms, NASA-SP-486, US Government Printing Office, Washington, DC, pp317-352.

Connor, W.H., DAY, J.W.;,Baumann, R.H., and Randall, J.M., 1989, Influence of hurricanes on coastal ecosystems along the northern Gulf of Mexico.Wetlands Ecology and Management, 1(1), 45-56.c.

Couvillion, B.R., Barras, J.A., Steyer, G.D., Sleavin, William, Fischer, Michelle, Beck, Holly, Trahan, Nadine, Griffin, Brad, and Heckman, David, 2011, Land area change in coastal Louisiana from 1932 to 2010: U.S. Geological Survey Scientific Investigations Map 3164, scale 1:265,000, 12 p. pamphlet.

Cragg, J., Mitchum G., and Sturges, W., 1983. Wind-induced sea-surface slopes on the West Florida Shelf. *Journal of Physical Oceanography*, 13, 2201-2212.

Cratsley, D.W., 1975, Recent deltaic sedimentation, Atchafalaya Bay, Louisiana: MS thesis, Department of Marine Sciences, Louisiana State University, Baton Rouge, LA, 142 p.

Crout, R. L. 1983. Wind-driven, near-bottom currents over the west Louisiana inner shelf. Ph.D. Dissertation, Louisiana State Univ., Baton Rouge, Louisiana. 117 p.

Cunningham, R.H.W., 1978, Atchafalaya-Vermilion estuarine complex studies: Contract report to US Army Corps of Engineers, New Orleans District, New Orleans, Louisiana. 206 p.

Current, C.L. 1996. Spectral model simulation of wind driven subinertial circulation on the inner Texas-Louisiana Shelf, Ph.D. Thesis, Tex. A&M University, College Station. 144 pp.

Day, J.W., Jr., Boech, D.F., Clairain, E.J., Kemp, G.P., Laska, S.B., Mitsch, W.J., Orth, K., Mashriqui, H., Reed, D.J., Shabman, L., Simenstad, C.A., Streever, B.J., Twilley, R.R., Watson, C.C., Wells, J.T., Whigham., D.F., 2007. Restoration of the Mississippi Delta: lessons from Hurricanes Katrina and Rita. *Science*, 115, 1679-1684.

DeLaune, R. D. & C. J. Smith, 1984. The carbon cycle and the rate of vertical accumulation of peat in the Mississippi River deltaic plain. Southeastern Geology 25: 61–69.

DeLaune, R. D., R. J. Buresh & W. H. Patrick Jr., 1978. Sedimentation rates determined by ^{137}Cs dating in a rapidly accreting salt marsh. *Nature*, 275: 532–533.

DeLaune, R. D., R. H. Baumann & J. G. Gosselink, 1983a. Relationships among vertical accretion, coastal submergence, and erosion in a Louisiana Gulf Coast marsh. *Journal of Sedimentary Petrology* 53(1): 147–157.

DeLaune, R. D., C. J. Smith & W. H. Patrick Jr., 1983b. Methane release from Gulf Coast wetlands. Tellus 35B: 8–15.

Delft3D-QUICKIN, 2013, Delft3D-QUICKIN User Manual, Generation and manipulation of grid-related parameters such as bathymetry, initial conditions and roughness, Hydro-Morphodynamics & Water Quality, Deltares, Version: 4.00.30932, November 22, 2013.

Delft3D-RGFGRID, 2013, Delft3D-RGFGRID User Manual, Generation and manipulation of curvilinear grids for Delft3D-FLOW and Delft3D-WAVE, Hydro-Morphodynamics, Deltares, Version: 4.00.30932, November 22, 2013.

Denes, T.A., Caffrey, J.M., 1988. Changes in seasonal water transport in a Louisiana Estuary, Fourleague Bay, Louisiana. *Estuaries*, 11(3), 184-191.

DiMarco, S.F., and R.O. Reid. 1998. Characterization of the Principal Tidal Current Constituents on the Texas-Louisiana Shelf. *J. Geo. Res. - Oceans*, 103 (2), 3093-3110.

Draut, A.E., Kineke, G.C., Huh, O.K., Grymes, J.M., III, Westphal, K.A., and Moeller, C.C., 2005a. Coastal mudflat accretion under energetic conditions, Louisiana Chenier-Plain coast, USA. *Marine Geology*, 214, 27–47.

E. Kalnay , M. Kanamitsu , R. Kistler , W. Collins , D. Deaven , L. Gandin , M. Iredell , S. Saha, G. White , J.Woollen , Y. Zhu , A. Leetmaa , and R. Reynolds, The NCEP/NCAR 40-year reanalysis project, *Bull. Amer. Meteor. Soc*., 77, 437-470, 1996.

Edmonds, Douglas A., The growth and evolution of river-dominated deltas and their distributary networks, Ph.D. Dissertation, The Pennsylvania State University, 2009, 156 pages.

Edmonds, D., and Slingerland, R., 2007, Mechanics of river mouth bar formation: Implications for the morphodynamics of delta distributary networks: *Journal of Geophysical Research*, v. 112, F02034, doi:10.1029/2006JF000574.

Edmonds, D.A., Paola, C., Hoyal, D.C.J.D., and Sheets, B.A., 2011, Quantitative metrics that describe river deltas and their channel networks, *Journal of Geophysical Research*, v. 116, F04022, doi:10.1029/2010JF001955.

Egbert, G.D. and Erofeeva, S.Y., 2002. Efficient inverse modeling of barotropic ocean tides. *Journal of Atmospheric and Oceanic Technology*, 19, 183–204.

Emery W.J., and Thomson, R.E., 200. Data Analysis methods in physical oceanography, 2nd edition. Oxford, UK, Elsevier, 638pp.

Esposito, C.R., Georgiou, I.Y., and Kolker, A.S., 2013, Hydrodynamic and geomorphic controls on mouth bar evolution: *Geophysical Research Letters*, v. 40, p. 1540–1545, doi:10.1002/grl.50333.

Falcini, F., and Jerolmack, D.J., 2010, A potential vorticity theory for the formation of elongate channels in river deltas and lakes: *Journal of Geophysical Research*, v. 115, F04038, doi:10.1029/2010JF001802.

Federico Falcini, Nicole S. Khan, Leonardo Macelloni, Benjamin P. Horton, Carol B. Lutken, Karen L. McKee, Rosalia Santoleri, Simone Colella, Chunyan Li, Gianluca Volpe, Marco D'Emidio, Alessandro Salusti, Douglas J. Jerolmack.Linking the historic 2011 Mississippi River flood to coastal wetland sedimentation. *Nature Geoscience*, 2012; 5 (11): 803 DOI: 10.1038/ngeo1615

Feng, Z, 2009, Hydrodynamic response to cold fronts along the Louisiana coast, MS Thesis, Department of Oceanography and Coastal Sciences, Louisiana State University, 120p.

Feng, Z and Li, C., 2010, Cold-front-induced flushing of the Louisiana Bays, *Journal of Marine Systems*, 82:252-264.

Fisk, H.N., 1944, Geological investigation of the alluvial valley of the Lower Mississippi River, U.S Army Corps of Engineers(1984), Mississippi river, Baton Rouge to the Gulf Louisiana Project, Final environmental Impact statement supplement II, appendix E, pp. E-10.

U.S. Army Corps of Engineers, Mississippi River Commission, Vicksburg, Ms., 78 p.

Fisk, H.N., 1952, Geologic investigation of the Atchafalaya Basin and the problem of Mississippi River diversion, U.S. Army Corps of Engineers, Mississippi River Commission, Vicksburg, Ms., 145 p.

Fisk, H.N., 1955, Sand facies of recent Mississippi delta deposits, Proceedings of 4th World Petroeum Congress (Rome, Italy), Section 1-3, p. 377-398.

Fisk, H.N. and Mcfarlan, E., JR., 1955, Late Quaternary deltaic deposits of the Mississippi River, Geological Society of America Special Paper, no. 62, p. 279-302.

FitzGerald, S. M., 1998, The development and sand body geometry of the Wax lake Outlet delta, Atchafalaya Bay, Louisiana: PhD dissertation. Department of Oceanography and Coastal Sciences, Louisiana State University, 130 p.

Flather, R. A. and N. S. Heaps. 1975. Tidal computations for Morecambe Bay. Geophys. *J. Roy. Astr. Soc*., 42:489-517.

Flocks, J.G., Kindinger, J.L., and Swarzenski, P.W., 2002, Sediment-hosted contaminants and distribution patterns in the Mississippi and Atchafalaya River Deltas: *Gulf Coast Association of Geological Societies Transactions*, v. 52, p. 277–290.

Folger, P. 2011. Geospatial Information and Geographic Information Systems (GIS): An Overview for Congress. Congressional Research Service. (Prepared for Members and Committees of the United States Congress).

Frazier, D.E., 1967, Recent deltaic deposits of the Mississippi River, their development and chronology, *Transactions Gulf Coast Association of Geological Societies*, 17, 287-315.

Gagliano, S.M., 1989, Controlled diversions in the Mississippi River deltaic plain, In: Kusles,

Gard, T., 2004, Wax Lake Delta Outlet St. Mary Parish, Louisiana, Lafayette Geological Society Field trip, 10 p.

Gagliano, S.M.; Meyer-arendt, K.J. and Wicker, K.M., 1981. Land loss in the Mississippi River deltaic plain. *Transactions of the Gulf Coast Association of Geological Societies*, 31, 295-300.

Gallucci, F. & S. A. Netto, 2004. Effects of the passage of cold fronts over a coastal site: an ecosystem approach. Marine Ecology Progress Series 281: 79–92.

Galperin, B., Kantha, L. H., Hassid, S., and Rosati, A., 1988, A quasi-equilibrium turbulent energy model for geophysical flows, *J. Atmospheric Sci*., 45, pp.55–62.

Garcia, S., 1983. The stock-recruitment relationship in penaeid shrimps: reality of artifacts and misinterpretations? Oceanographic Tropicale 18: 25–48.

Garwood, R.W., Fett, R.W., Rabe, K.M. and Brandli, H.W., 1981, Ocean frontal formation due to shallow water cooling effects as observed by satellite and simulated by a numerical model, *Journal of Geophysical Research* 86, doi: 10.1029/JC080i011p11000, issn: 0148-0227.

Geleynse, N., Storms, J., Stive, M., Jagers, H., and Walstra, D., 2010, Modeling of a mixed-load fluvio-deltaic system: *Geophysical Research Letters*, v. 37, L05402, doi:10.1029/2009GL042000.

Georgiou, I.Y., FitzGerald, D.M., and Stone, G.W., 2005, The impact of physical processes along the Louisiana coast, *Journal of Coastal Research*, Special Issue No. 44, p. 72–89.

Goree, B.B.; Lovelace, W.M.; Montgomery, P.A.; Resweber, J.C.; Sasser, D.C., JR., and Walters, D.J., 2001. Water Resources Data—Louisiana, Water Year 2000. U.S. Geological Survey Water- Data Report LA-00-1, 581p.

Gregory W. Stone, Zhang, X.P., Gibson, W., and Fredericks, R., A New Wave-Current Online Information System for Oil Spill Contingency Planning (WAVCIS), Proceedings of 24th Arctic and Marine Oilspill Program Technical Seminar 2001, Edmonton, Alberta, CANADA, 401-425.

Grenci, L.M., and Nese, J.M., 2006. A world of Weather: fundamentals of meteorology, Kendall/Hunt publishing Co., 780pp.

Grenci, L.M., and Nese, J.M., 2001. A world of Weather: fundamentals of meteorology: a Text/ Laboratory Manual, Kendall Hunt, 2001, 550pp.

Hiatt, M., 2013, A network-based analysis of river delta surface hydrology: An example from Wax Lake Delta, Master Thesis, 105pp.

Holton, J. R., 2004, An Introduction to Dynamic Meteorology, Academic Press, 277 pp.

Hsu, S.A., 1988. Coastal Meteorology. San Diego, California: Academic Press, Inc., 260pp.

Isacks, T.S., 1989, Geological evolution and sedimentary facies of the Timbalier Island, Louisiana, MS Thesis, Department of Geology, Louisiana State University, 191p.

Hsu, S.A., 1993. The Gulf of Mexico — a breeding ground for winter storms. *Mariners Weather Log*, 37 (2), 4-11.

Huh, O.K., Wiseman, W.J., Jr., and Rouse, L.J., Jr., 1978. Winter cycle of sea surface thermal patterns, northeastern Gulf of Mexico. *Journal of Geophysical Research*, 83(C9), 4523-4529.

Huh, O.K., and Rouse, L.J., Jr., 1984. Cold air outbreaks over the northwest Florida continental shelf: heat flux processes and hydrographic changes. *Journal of Geophysical Research*, 89(C1), 717-726.

Huh, O.K., Moeller, C.C., Menzel, W.P., Rouse, L.J., Jr., and Roberts, H.H., 1996. Remote sensing of turbid coastal and estuarine waters: a method of multispectral water-type analysis., *Journal of Coastal Research*, 12 (4), 984-995.

Huh, O.K.; Roberts, H.H., Rouse, L.J., and Rickman, D.A., 1991. Fine grain sediment transport and deposition in the Atchafalaya and Chenier Plain sedimentary system. Coastal Seiments ’91: Proceedings of Specialty Conference (June 25-27, 1991, Seattle, Washington), *American Society of Civil Engineers*, New York, PP. 817-830.

Huh, O.K., Walker, N.D., and Moeller, C., 2001. Sedimentation along the Eastern Chenier Plain coast: down drift impact of a delta complex shift. *Journal of Coastal Research*, 17, 72–81.

Ip, J. T. C., D. R. Lynch, and C. T. Friedrichs. 1998. Simulation of estuarine flooding and dewatering with application to Great Bay, New Hampshire. Estuarine, *Coastal and Shelf Science*, 47:119-141.

Jack L. Kindinger, Noreen A. Buster, James G. Flocks, Julie C. Bernier, and Mark A. Kulp, Louisiana Barrier Island Comprehensive Monitoring (BICM) Program Summary Report: Data and Analyses 2006 through 2010, Open-File Report 2013-1083, U.S. Department of the Interior, U.S. Geological Survey.

J.A. and Daly, S., (eds.), Proceedings of International Symposium (Wetlands and River Corridor Management, July 5-9, Charleston, South Carolina), Association of Westland Managers, pp. 257-268.

John B. Shaw and David Mohrig, 2013, The Importance of Erosion in Distributary Channel Network Growth, Wax Lake Delta, Louisiana, USA, Geology, Data Repository Item 2014008, dio:10.1130/G34751.1.

J.B. Shaw and D. Mohrig, Distributary Channel Evolution - GSA Data Repository 2014008.

Kahn, J.H. and Roberts, H.H., 1982. Variations in storm response along a microtidal transgressive barrier-island arc. *Sedimentary Geology*, 33, 129–146.

Kamphuis, J.W. (2000), "Introduction to Coastal Engineering and Management", World Scientific Press, 437 pp.

Kara, A.B.; Barron, C.N.; Martin, P.J.; Smedstad, L.F., and Rhodes, R.C., 2006. Validation of interannual simulations from the $1/8^o$ global Navy Coastal Ocean Model (NCOM). Ocean Modeling, 11, 376–398.

Kanh, J.H., 1980, The role of hurricanes in the long-term degradation of a barrier island chain, MS Thesis, Department of Marine Sciences, Louisiana State University, 120p.

Kemp, G.P., 1986, Mud deposition at the shorface: wave and sediment dynamics on the Chenier Plain of Louisiana, Ph. D. dissertation, 146 pp., Louisiana State University, Baton Rouge, LA.

Kemp, G.P., Wells, J.T. and van Heerden, I.LI., 1980, Frontal passages affect delta development in Louisiana, Coastal Oceanographic and Climatological News, v. 3, p. 4-5.

Kim, W., Mohrig, D., Twilley, R., Paola, C., and Parker, G., 2009, Is it feasible to build new land in the Mississippi River delta?, EOS Transactions, *American Geophysical Union*, Vol. 90, p. 373–374, doi:10.1029/2009EO420001.

Kineke, G.C.; Higgins, E.E.; Hart, K., and Velasco, D., 2006. Fine-sediment transport associated with cold-front passages on the shallow, Gulf of Mexico. *Continental Shelf Research*, 26, 2073–2091.

Kneib, R. T., 1997, The role of tidal marshes in the ecology of estuarine nekton, Oceanography and Marine Biology: An Annual Review 35: 163–220.

Kolb, C.R., and Van Lopik, J.R., 1958, Geology of the Mississippi deltaic plain-southeastern Louisiana, U.S. Army Corps of Engineers, Waterways Experiment Station, Technical Report 2, 482 p.

Kostic, S., and G. Parker (2003), Progradational sand-mud deltas in lakes and reservoirs: Part 1.

Theory and numerical modeling, *J. Hydraul. Res*., 41(2), 127–140.

Kourafalou, V.H.; Oey, L.-Y.; Wang, J.D., and Lee, T.N., 1996. The fate of river discharge on the continental shelf 1. Modeling the river plume and the inner shelf coastal current. *Journal of Geophysical Research*, 101(C2), 3415–3434.

Kusky, T., 2003, Geological hazards: a sourcebook, Greenwood Press, 297 pages.

Large, W. G. and Pond, S., 1981, Open ocean momentum flux measurements in moderate to strong winds, *J. Phys. Oceanogr*., 11, 324–336, 1981.

Latimer, R.A., and Schweitzer, C.W., 1951. The Atchafalaya River Study: A report based upon engineering and geological studies of the enlargement of Old and Atchafalaya rivers. US Army Corps of Engineers, Mississippi River Commission, Vicksburg, Mississippi, vols. 1 and 3.

Leblanc, R.J., 1973, Significant studies of modern and ancient deltaic sediments, In: M.L. Broussard, (ed.), Deltas. Houston, Texas: Houston Geological Society, pp. 13-85.

Lee, J.M., Wiseman, W.J. Jr., and Kelly, F.J., 1990. Barotropic, subtidal exchange between

Calcasieu Lake and the Gulf of Mexico. *Estuaries*, 13 (3), 258-264.

Leendertse, J.J., 1970, A water quality simulation model for well mixed estuaries and coastal seas, l, Memo RM-6230-RC, Rand Corporation, Santa Monica, California.

Lewis, J.K., and Hsu, S.A., 1992. Mesoscale air-sea interactions related to tropical and extratropical storms in the Gulf of Mexico, *Journal of Geophysical Research*, 97, 2215-2228.

Li, C., 2013, Subtidal Water Flux through a Multi-inlet System: Observations Before and During a Cold Front Event and Numerical Experiments, *JGR-Oceans*, VOL. 118, 1–16, doi:10.1029/2012JC008109, 2013.

Li, C., and C. Chen, 2014, Shelf Circulation Prior to and Post a Cold Front Event Measured from Vessel-based Acoustic Doppler Current Profiler, *Journal of Marine System*, 139 (2014): 38-50.

Li, C., Weeks, E., and Blanchard, B. W., 2010, Storm surge induced flux through multiple tidal passes of Lake Pontchartrain estuary during Hurricanes Gustav and Ike, Estuarine, Coastal and Shelf Science, 87 (2010) 517–525.

Li, C, Roberts, H.H., Weeks, E, Delaune, R, White, J, Sasser, C, Braud, D, and Khalil, S, Hydrodynamic energy regimes in the Wax Lake Delta, State of the Coast, 2014.

Li, C, Roberts, H.H., Stone, G.W., 2011, Wind surge and saltwater intrusion and Atchafalaya Bay during onshore winds prior to cold front passage, Hydrobiologia, v. 658, pp. 27-39.

List., J.H., Jaffe, B.E., Sallenger, A.H., Jr., and Hansen, M., 1997. Bathymetric comparisons adjacent to the Louisiana barrier islands: processes of large-scale change. *Journal of Coastal Research*, 13(3), 670-678.

Lovelace, J. K., 1992, Storm-tide Elevations Produced by Hurricane Andrew along the Louisiana Coast, August 25-27, 1992 (Open File Report 94-371, U.S. Geological Survey, Baton Rouge, LA, 1994).

Luettich, R.A., Jr., J.J. Westerink, and N.W. Scheffner, 1992, ADCIRC: an advanced three-dimensional circulation model for shelves coasts and estuaries, report 1: theory and methodology of ADCIRC-2DDI and ADCIRC-3DL, Dredging Research Program

Technical Report DRP-92-6, U.S. Army Engineers Waterways Experiment Station, Vicksburg, MS, 137p.

Lyczkowski-shultz, J., D. L. Ruple, S. L. Richardson & J. H. Cowan, 1990. Distribution of fish larvae relative to time and tide in a Gulf of Mexico barrier island pass. *Bulletin of Marine Science* 46(3): 563–577.

Markowski, P., and Richardson, Y., 2011, Mesoscale Meteorology in Midlatitudes John Wiley & Sons, Sep 20, 2011, 430 pp.

Marmorino, G.O., 1982. Wind-induced sea level variability along the West Florida Shelf (winter, 1978). *Journal of Physical Oceanography*, 12, 389-405.

Marmorino, G.O., 1983. Small-scale variations of wind-driven coastal sea-level response in the West Florida Bight. *Journal of Physical Oceanography*, 93, 93-102.

Majersky, S., H.H. Roberts, R. Cunningham, G.P. Kemp, and C.J. John, 1997, Facies development in the Wax Lake Outlet delta: Present and future trends: Basin Research Institute Bulletin 7, p. 50-66.

McManns, J., 2002, the history of sediment flux to Atchafalaya Bay, Louisiana: in S.J. Jones and L.E. Frostick (eds.) Sediment Flux to Basins: Causes, Controls, and Consequences: Geological Society of London, Special Publication 191, p. 209-226.

Mellor, G. L., and Yamada, T., 1982, Development of a turbulence closure model for geophysical fluid problem, Rev. *Geophys*., 20, 851 – 875.

Mesinger, F. and A. Arakawa (1976), Numerical Methods Used in Atmospheric Models, GARP Publ. Ser., vol. 1, WMO-ICSU Joint Organizing Comm., Univ. of Calif., Los Angeles.

Miller, J. M., 1988. Physical processes and the mechanisms of coastal migrations of immature marine fishes. American Fisheries Society Symposium 3: 68–76.

Miller, J. M., J. P. Reed & L. J. Pietrafesa, 1984. Patterns, mechanisms and approaches to the study of migrations of estuarine-dependent fish larvae and juveniles. In McCleave, J. D., G. P. Arnold, J. J. Dodson & W. H. Neill (eds), Mechanisms of Migration in Fishes. Plenum Publishing Corporation, New York: 209–225.

Miller, J. M., L. B. Crowder, & M. L. Moser. 1985. Migration and utilization of estuarine nurseries by juvenile fishes: an evolutionary perspective. In M. A. Rankin (ed.), Migration: Mechanisms and Adaptive Significance. Contributions in Marine Science 27(Suppl):338–352.

Milliman, J.D and Meade, R.H 1983, worldwide delivery of river sediment to the ocean. *Journal of Geology*, 91, 1-21.

Moeller, C.C.; Huh, O.K.; Roberts, H.H.; Gumley, L.E., and Menzel, P.W., 1993. Response of Louisiana coastal environments to a cold front passage. *Journal of Coastal Research*, 9, 434–447.

Morgan, J.P., J.R. Van Lopik, and J.G. Nichols, 1953, Occurrence and development of mudflats along the western Louisiana coast. Louisiana State University, Coastal Studies Institute Technical Report 2, 34 p.

Morgan, J.P. and P.B. Larimore, 1957, Change in the Louisiana shoreline: *Transactions Gulf Coast Association Geological Societies,* v. 7, p. 303-310.

Morrison, D., 1984. Seasonality of Batophora oerstedi (Chlorophyta), a tropical macroalga. *Marine ecology progress series*, Oldendorf 14: 235–244.

Mossa,J. , 1990, Discharge-Suspended Sediment Relationship in the Mississippi-Atchafalaya River System, Louisiana, Ph.D. Thesis, Louisiana State University, Baton Rouge, Louisiana, 180 p.

Mossa, J., and H.H. Roberts, 1990, Synergism of riverine and winter storm-related sediment transport processes in Louisiana's coastal wetlands. *Transactions Gulf Coast Association of Geological Societies*, v. 40, p. 635-642.

Mukai, A.Y., Westerink, J. J., and Luettich, R. A., 2001, Guidelines for using Eastcoast 2001 database of tidal constituents within Western North Atlantic Ocean, Gulf of Mexico and Caribbean, Coastal and Hydraulics Engineering Technical Note CHETN-IV-40, U.S. Army Engineer Research and Development Center, Vicksburg, MS.

Mukai A.Y., J.J. Westerink, R.A. Luettich Jr., and D. Mark, 2002a, Eastcoast 2001: a tidal constituent database for the western North Atlantic, Gulf of Mexico and Caribbean Sea, US Army Engineer Research and Development Center, Coastal and Hydraulics Laboratory, Technical Report, ERDC/CHL TR-02-24, September 2002, 201p.

Mukai, A.Y., J.J. Westerink, and R.A. Luettich Jr., 2002b, Guidelines for Using the Eastcoast 2001 Database of Tidal Constituents within the Western North Atlantic Ocean, Gulf of Mexico and Caribbean Sea, Coastal and Hydraulic Engineering Technical Note (IV-XX), 24p.

Murray, S.P., 1975, Trajectories and speeds of wind-driven currents near the coast, *Journal of Physical Oceanography*, 5, 347-360.

Narayanan, C. and Garvine, R.W., 2002. Large scale buoyancy driven circulation on the continental shelf. *Dynamics of Atmospheres and Oceans*, 36, 125–152.

National Center for Earth-surface Dynamics (NCED), 2007, 2007 Annual report, An NSF science and technology center.

National Geophysical Data Center (NGDC), 2001. U.S. Coastal Relief Model - Central Gulf of Mexico. National Geophysical Data Center, NOAA. doi:10.7289/V54Q7RW0

National Research Council. Landscapes on the Edge: New Horizons for Research on Earth's Surface. Washington, DC: The National Academies Press, 2010.

Neill, C.F., and Allison, M.A., 2005, Subaqueous deltaic formation on the Atchafalaya shelf, Louisiana: *Marine Geology*, v. 214, p. 411–430.

Nickles, C.R. and T.J. Pokrefke, Jr., 1988, Wax Lake outlet control structure Atchafalaya River, Final Report, U.S. Army Corps of Engineers, Waterways Experiment Station, Vicksburg, MS., 54 p.

NOAA, 2005. U.S. Estuarine Bathymetric Data Sets. http://estuarinebathymetry.noaa.gov/ (accessed November 1, 2005).

NOAA, 2013, LIDAR – Light Detection and Ranging – is a remote sensing method used to examine the surface of the Earth, June 4, 2013.

Noble, M.A., Schroeder, W.W., Wiseman, W.J., Jr., Ryan, H.F., and Gelfenbaum, G., 1996, Subtidal circulation patterns in a shallow, highly stratified estuary: Mobile Bay, Alabama., *Journal of Geophysical Research*, 101(11), 25689-25703.

Norcross3-L- and Shaw.R.F. (1984) Oceanic and estuarine transport of fish eggs and larvae, a review. *Trans. Am. Fish. Soc*, 113,153-165.

Nowlin, W. D., Jr., A. E. Jochens, R. O. Reid, and S. F. DiMarco, 1998, Texas–Louisiana shelf circulation and transport processes study. Synthesis Report, Vol. 1, Texas A&M University, 1–5.

Nowlin, W.D. Jr, Paker, C.A., 1974. Effects of a cold-air outbreak on shelf waters of the Gulf of Mexico. *Journal of Physical Oceanography*, 4, 467-486.

Nyman, S. A., R. D. Dlaune, S. R. Pezeshki & W. H. Patrick Jr., 1995. Organic matter fluxes and marsh stability in a rapidly subsiding estuarine marsh. *Estuarine* 113(18): 207–218.

Oey, L., 1995: Eddy- and wind-forced shelf circulation. *J. Geophys. Res*., 100, 8621–8637.

OEY, L.-Y. and MELLOR, G.L., 1993, Subtidal variability of estuarine outflow, plume, and coastal current: a model study. *Journal of Physical Oceanography*, 23, 164–171.

Paola, C., Twilley, R.R., Edmonds, D.A., Kim, W., Mohrig, D., Parker, G., Viparelli, E., and Voller, V.R., 2011, Natural processes in delta restoration: Application to the Mississippi Delta: Annual Review of Marine Science, v. 3, p. 67–91, doi:10.1146/annurev-marine-120709-142856.

Parker, G., et al. (1998), Alluvial fans formed by channelized fl uvial and sheet fl ow: I. Theory, *J. Hydraul. Eng*., 124(10), 985–995.

Penland, S. and Boyd, R., 1981, Shoreline changes on the Louisiana barrier coast, *IEEE Oceans*, 81, 209-219.

Parker, G., et al. (2006), Large scale river morphodynamics: Application to the Mississippi delta, in River Flow 2006: Proceedings of the International Conference on Fluvial Hydraulics, Lisbon, Portugal, 6–8 September 2006, edited by R. M. L. Ferreira et al., pp. 3–11, Taylor and Francis, London.

Parker, G., T. Muto, Y. Akamatsu, W. E. Dietrich, and J. W. Lauer (2008), Unravelling the conundrum of river response to rising sea- level from laboratory to fi eld: Part I. Laboratory experiments, *Sedimentology*, 55(6), 1643–1655.

Penland, S., Boyd, R., Nummedal, D., and ROBERTS, H.H., 1981, Deltaic barrier development on the Louisiana coast, *Transactions Gulf Coast Association of Geological Societies*, 31, 471-476.

PENLAND, S.; CONNOR, P.F.; BEALL, A.; FEARNLEY, S., and WILLIAMS, S.J., 2005. Changes in Louisiana's shoreline: 1855–2002. *Journal of Coastal Research*, Special Issue No. 44, 7–39.

Penland, S., and Ramsey, K.E., 1990. Relative sea level rise in Louisiana and the Gulf of Mexico: 1908-1988. *Journal of Coastal Research*, 6(2), 323-342.

Penland, S.P., Suter, J.R., and Boyd, R., 1985, Barrier island areas along abandoned Mississippi River deltas, *Marine Geology*, 63, 197-233.

Penland, S.P., Boyd, R., and Suter, J.R., 1988, The transgressive depositional systems of the Mississippi River delta plain: A model for barrier shoreline and shelf sand development, *J. Sedimentary Petrology*, 58(6), 932-949.

Pepper. D.A., and Stone, G.W., 2004. Hydrodynamics and sedimentary responses to two contrasting winter storms on the inner shelf of the northern Gulf of Mexico. *Marine Geology*, 210, 43-62.

Perez, B.C.; DAY, J.W., JR.; ROUSE, L.J.; SHAW, R.F., and WANG, M., 2000. Influence of Atchafalaya River discharge and winter frontal passage on suspended sediment concentration and flux in Fourleague Bay, Louisiana. *Estuarine, Coastal, and Shelf Science*, 50, 271–290.

Pettigrew, N. R., R. C. Beardsley and J. D. Irish (1986) Field evaluations of a bottom mounted Acoustic Doppler Profiler and conventional current meter moorings, Proceedings of the IEEE Third Working Conference on Current Measurement, January 22-24, 1986, Airlie, Virginia, 153-162.

Roberts, H.H., 1997. Dynamic changes of the Holocene Mississippi River delta plain: The delta cycle, *Journal of Coastal Research*, 13(3), 605-627.

Roberts, H.H., 1998, Delta switching: Early responses to the Atchafalaya River diversion: *Journal of Coastal Research*, v. 14, 882-899.

Roberts, H.H., 1999, Atchafalaya Basin and Atchafalaya-Wax Lake deltas: Guidebook, AAPG Modern Deltas field Seminar, 68 p.

Roberts, H.H., Adams, R.D., and Cunningham, R.H.W., 1980, Evolution of sand-dominant subaerial phase, Atchafalaya Delta, Louisiana, American Association of Petroleum Geologists Bulletin, 64, 264-279.

Roberts, H.H., Bailey, A., and Kuecher, G.J., 1994, Subsidence in the Mississippi River delta: Important influences of valley filling by cyclic deposition, primary consolidation phenomena, and early diagenesis, *Transactions Gulf Coast Association of Geological Societies*, 44, 619-629.

Roberts, H.H., Beaubouef, R.T., Walker, N.D., Stone, G.W., Bentley, S., Shermet, A., and van Heerden, I.I., 2003b, San-rich bayhead deltas in Atchafalaya Bay (Louisiana): Winnowing by cold front forcing: Proceedings Coastal Sediments '03, Clearwater, Florida, p. 1-15.

Roberts, H.H., Coleman, J.M., Bentley, S.J., and Walker, N., 2003a, An embryonic major delta lobe: a new generation of delta studies in the Atchafalaya-Wax Lake delta systems, *GCAGS/GCSSEPM Transactions*, volume 53, 690-703.

Roberts, H.H.; Huh, O.K.; Hsu, S.A.; Rouse, L.J., and Rickman, D.A., 1987. Impact of cold-front passages on geomorphic evolution and sediment dynamics of the complex Louisiana coast. In: American Society of Civil Engineers Proceedings of Coastal Sediments '87, pp. 1950–1963.

Roberts, H. H., Huh, O.K., Hsu, S.A., Rouse, R. J. Jr., and Rickman, D.A., 1989, Winter Storm impacts on the Chenier plain coast of Southwestern Louisiana: *Gulf Coast Association of Geological Societies Transactions*, v.39, p. 515-522.

Roberts, H.H., Sneider J., 2003, Atchafalaya-Wax Lake Deltas the new regressive phase of the Mississippi River delta complex: Guidebook, A Field Seminar for the GCAGS Convention, 71 p.

Roberts, H.H., Suhada, J.N., and Coleman, J.M., 1980, Sediment deformation and transport on low-angle slopes: Mississippi River delta, In: Coates, D.R. and Vitek, J.D., (eds.), Thresholds in Geomorphology, London: Allen and Unwin, pp. 131-167.

Roberts, H.H., Walker, N., Cunningham, R., Kemp, G.P., and Majersky, S., 1997, Evolution of sedimentary architecture and surface morphology: Atchafalaya and Wax Lake deltas, Louisiana: *Transactions Gulf Coast Association of Geologic Societies*, v. 47, 477-484.

Roberts, H.H., Walker, N., Sheremet, A., Stone, G.W. 2005, Effects of Cold Fronts on Bayhead Delta Development: Atchafalaya Bay, Louisiana, USA, High Resolution Morphodynamics and Sedimentary Evolution of Estuaries, Coastal Systems and Continental Margins, pp 269-298, Volume 8, Springer.

Roberts, H.H., Weimer, P., and Slatt, R, 2012, Chapter 17 River deltas, In: Regional Geology and Tectonics: Principles of Geologic Analysis, Elsevier Science (1 edition), 2012, pp 490-511.

Rogers, B. D., R. F. Shaw, W. H. Herke & R. H. Blanchet, 1993. Recruitment of postlarval and juvenile brown shrimp (Penaeus aztecus Ives) from offshore to estuarine waters of the northwestern Gulf of Mexico. *Estuarine, Coastal and Shelf Science* 36: 377–394.

Rouse, L.J., Jr., H.H. Roberts, and R.H.W. Cunningham, 1978, Satellite observation of the subaerial growth of the Atchafalaya delta, Louisiana: Geology, v. 6, p. 405-408.

Rouse, L.J., W.J. Wiseman, Jr., L.C. Bender, N.L. Guinasso, Jr., F.J. Kelly, D.A. Brooks, Y-T.

Lo, J. She, and A. Valle-Levinson. 2004. Observational and predictive study of inner shelf currents over the Louisiana-Texas shelf. U.S. Dept. of the Interior, Minerals Management Service, Gulf of Mexico OCS Region, New Orleans, LA. OCS Study MMS 2004-036. 207 pp.

Rowe, F. and J. Young, 1979, An ocean current profiler using Doppler sonar, Oceans ‘79 Proceedings.

Russell, R.J., 1936, Physiography of lower Mississippi River delta: Lower Mississippi River Delta, *Geological Bulletin* 8, Louisiana Geological Survey, 199 p.

Russell, R.J., 1939, Louisiana stream patterns, *American Association of Petroleum Geologists Bulletin*, 23, 1199-1227.

Russell, R.J., 1940, Quaternary history of Louisiana, *Geological Society of America Bulletin*, 51, 1199-1234.

Schlemon, R.J., 1975. Subaqueous delta formation-Atchafalaya Bay, Louisiana, In: M.L. Broussard (ed.), Deltas: models for exploration, Houston Geological Society, Houston, Texas, p. 209-221.

Schumann, S., Johnson, G.A., Moser, J., Walker, N.D., and Hsu, S.A., 1995. An overview of a strong winter low in the Gulf of Mexico, March 12-13, 1993. National Weather Digest, 20 (1), 11-25.

Shaw, R. F., W. J. Wiseman Jr., R. E. Turner, L. J. Rouse Jr., R. E. Condrey & F. J. Kelly Jr., 1985. Transport of larval gulf menhaden Brevoortia patronus in continental shelf waters of western Louisiana: a hypothesis. *Transactions of the American Fisheries Society* 114(4): 452–460.

Shaw, R. F., B. D. Rogers, J. H. Cowan Jr. & W. H. Herke, 1988. Ocean-estuary coupling of ichthyoplankton and nekton in the Northern Gulf of Mexico. American Fisheries Society Symposium 3: 77–89.

Shlemon, R.J., 1975, Subaqueous delta formation-Atchafalaya Bay, Louisiana. In: Broussard, M.L. (Ed.), Deltas: Models for Exploration, Houston Geological Society, pp. 209-221.

Trowbridge, A.C., 1930, Building of the Mississippi Delta, *American Association of Peroleum Geologists Bulletin*, 14, 867-901.

Signell R.P., Jenter H. L. and Blumberg A. F. 1996. Circulation and effluent dilution modeling in Massachusetts Bay: model implementation, verification and results. USGS Open File Report 96-015, U.S. Geological Survey, Woods Hole.

Smagorinsky, J. (1963), General circulation experiments with the primitive equations. I. The basic experiments, Mon. Weather Rev., 91, 99–164.

Smolarkiewicz, P. K. (1984), A fully multidimensional positive definite advection transport algorithm with small implicit diffusion, *J. Comput. Phys*., 54, 325–362.

Smolarkiewicz, P. K., and T. L. Clark (1986), The multidimensional positive definite advection transport algorithm: Further development and applications, *J. Comput. Phys*., 86, 355–375.

Snedden, G.A., Cable, J.E., and Wiseman, W.J., Jr., 2007. Subtidal sea level variability in a shallow Mississippi River deltaic estuary, Louisiana. *Estuaries and Coasts*, 30(5), 802-812.

Stone, G.W., Williams, S.J., Burruss, A.E., 1997. Louisiana's barrier islands: an evaluation of their geological evolution, morphodynamics and rapid deterioration. *Journal of Coastal Research* 13 (3), 591–592.

Strong, B, BH Brumley, EA Terray and GW Stone, 2000: Performance of ADCP-Derived Directional Wave Spectra and Comparison with Other Independent Measurements, Proc. Oceans 00, IEEE, New York.

Swarzenski, C.M., 2003. Surface-Water Hydrology of the Gulf Intracoastal Waterway in South-central Louisiana, 1996–99. U.S. Geological Survey Professional Paper 1672, 51p.

Swenson, E.M., Chuang, W.-S., 1983. Tidal and subtidal water volume exchange in an estuarine system. *Estuarine, Coastal and Shelf Science* 16, 229–240.

Tao, JF (2006). "Research on Three Dimension Baroclinic Flow Numerical Model in Estuarine and Coastal Waters", Ph.D. dissertation, Hohai University, 236pp (in Chinese).

Talke, S. A. & M. T. Stacey, 2008. Suspended sediment fluxes at an intertidal flat: the shifting influence of wave, wind, tidal, and freshwater forcing. *Continental Shelf Research* 28: 710–725.

Terray, EA, BH Brumley and B Strong, 1999: Measuring Waves and Currents with an Upward-Looking ADCP, Proc. IEEE 6th Working Conference on Current Measurement, IEEE, New York, 66-71.

Turner, R. E. 2006. Will lowering estuarine salinity increase Gulf of Mexico oyster landings? *Estuar. Coasts* 29:345–352.

USGS, 2008, The Mississippi River & Tributaries Project: Designing the Project Flood, United States Army Corps of Engineers, April 2008.

USGS-NWRC, 100+ Years of Land Change for Southeast Coastal Louisiana, Map ID: USGS-NWRC 2003-03-085.

U.S. GEOLOGICAL SURVEY, 2001. National Water Information System (NWISWeb) data. http://waterdata.usgs.gov/nwis/ (accessed December 1, 2005).

Unified Surface Analysis Manual, 2013, Weather Prediction Center, Ocean Prediction Center, National Hurricane Center, and Honolulu Forecast Office, November 21, 2013, http://www.wpc.ncep.noaa.gov/sfc/UASfcManualVersion1.pdf .

Van de Voorde, N.E., and Dinnel S.P., 1998. Observed directional wave spectra during a frontal passage. *Journal of Coastal Research*, 14 (1), 337-346.

Van Heerden, I.LI., 1980, Sedimentary responses during flood and non-flood conditions, new Atchafalaya delta, Louisiana: MS thesis, Department of Marine Sciences, Louisiana state University, 76 p.

Van Heerden, I.LI., 1983, Deltaic sedimentation in eastern Atchafalaya Bay, Louisiana. PhD dissertation, Department of Marine Sciences, Louisiana State University, Baton Rouge, La., 151 p.

Van Heerden, I.LI., and Roberts, H.H., 1980a, The Atchafalaya Delta: Rapid progradation along a traditionally retreating coast (south central Louisiana), Zeitschrift Fur Geomorphologie, 34, 188-201.

Van Heerden, I.LI. and Roberts, H.H., 1980b, the Atchafalaya Delta- Louisiana's new prograding coast, Transactions, *Gulf Coast Association of Geological Societies*, v. 30, p. 497-506.

Van Heerden, I.LI., 1983, Deltaic sedimentation in eastern Atchafalaya Bay, Louisiana. PhD dissertation, Department of Marine Sciences, Louisiana State University, Baton Rouge, La., 151 p.

Van Heerden, I.LI. and Roberts, H.H., 1988, Facies development of Atchafalaya Delta, Louisiana: a modern bayhead delta, *AAPG Bulletin*, v. 72, p. 439-453.

Van Heerden, I.LI.; Wells, J.T., and Roberts, H.H., 1983. Riverdominated suspended-sediment deposition in a new Mississippi delta. *Canadian Journal of Fisheries and Aquatic Sciences*, 40, 60–71.

Walker, N.D., and Hammack, A.B., 1999, Impacts of river discharge and wind forcing on circulation, sediment distribution, sediment flux and salinity changes: Vermilion/Cote

Blanche Bay System, Louisiana, Final Report, U.S. Army Corps of Engineers, Waterways Experiment Station, Vicksburg, MS., 157 p.

Walker, N.D. and Hammack, A.B., 2000, Impacts of winter storms on circulation and sediment transport: Atchafalaya-Vermilion Bay Region, Louisiana, *Journal of Coastal Research*, v. 16, no. 4, p. 996-1010.

Walker, N.D., Rouse L.J., and Huh, O.K., 1987. Response of subtropical shallow-water environments to cold-air outbreak events, Satellite radiometry and heath flux modeling., *Continental Shelf Research*, 7, 735-757.

Walker, N.D., 1993. A preliminary look at cyclogenesis in the Gulf of Mexico during the March 1993 blizzard. Marine Weather Log, 37 (2), 8-9.

Walker, N.D., 2001a. Tropical storm and hurricane wind effects on water level, salinity, and sediment transport in the river-influenced Atchafalaya-Vermilion Bay system, Louisiana, USA., *Estuaries*, 24 (4), 498-508.

Wang, D.P., 1979. Subtidal sea level variations in the Chesapeake Bay and relations to atmospheric forcing. *Journal of Physical Oceanography* 9, 413–421.

Wang, J., and Ikeda. M. 1995. Stability analysis of finite difference schemes for inertial oscillations in ocean general circulation model. In Computer Modeling of Seas and Coastal Regions, ed. C.A. Brebbia et al., pp. 19–27. *Computational Mechanics Publications*, Southampton.

Wang, J, and Ikeda, M (1997). "Inertial Stability and Phase Error of Time Integration Schemes in Ocean General Circulation Models," Monthly Weather Review, Vol 125, pp 2316-2327.

Wells, J.T., S.J. Chinburg, and J.M. Coleman, 1982, Development of the Atchafalaya River Deltas: Generic analysis: U.S. Army Corps of Engineers, waterways Experiment Station, Vicksburg, MS, 96 p.

Wang, J, Mysak, LA, and Ingram, RG, (1994). "A Three-Dimensional Numerical Simulation of Hudson Bay Summer Ocean Circulation: Topographic Gyres, Separations, and Coastal Jets," *Journal of Physical Oceanography*, Vol 24, pp 2496-2514.

Wang, W., W.D. Nowlin, Jr., and R.O. Reid. 1996. Analyzed surface meteorological fields over the northwestern Gulf of Mexico for 1992-1994: Mean, seasonal, and monthly patterns., Mon. Wea. Rev. 126:2864-2883.

Wu, H., and Zhu, J., 2010, Advection scheme with 3rd high-order spatial interpolation at the middle temporal level and its application to saltwater intrusion in the Changjiang estuary, *Ocean Modell*., 33, 33–51, doi:10.1016/j.ocemod.2009.12.001.

Walker, N.D., Rouse L.J., and Huh, O.K., 1987. Response of subtropical shallow-water environments to cold-air outbreak events: Satellite radiometry and heath flux modeling. *Continental Shelf Research*, 7, 735-757.

Walker, N.D., 1993. A preliminary look at cyclogenesis in the Gulf of Mexico during the March 1993 blizzard. *Marine Weather Log*, 37 (2), 8-9.

Walker, N.D., 1996. Satellite assessment of Mississippi River plume variability: causes and predictability. *Remote Sens. Environ*., 58, 21-35.

Walker, N.D., Huh, O.K., Rouse, L.J. Jr., and Murray, S.P., 1996. Evolution and structure of a coastal squirt off the Mississippi River delta: Northern Gulf of Mexico. *Journal of Geophysical Research*, 101 (C9), 20643-20655.

Walker, N.D., and Hammack, A.B., 2000. Impact of winter storms on circulation and sediment transport: Atchafalaya-Vermilion bay Region, Louisiana, U.S.A. *Journal of Coastal Research*, 16(4), 996-1010.

Walker, N.D., Jarosz, E., Murray, S.P., 2001. An investigation of pressure and pressure gradients along the Louisiana/Texas inner shelf and their relationships to wind forcing and current variability. OCS Study MMS 2001-057. U.S. Dept. of the Interior Minerals Mamt. Service, Gulf of Mexico OCS region, New Orleans, LA. 40pp.

Walker, N.D., 2001b. Wind and eddy related circulation on the Louisiana/Texas shelf and slope determined from satellite and in-situ measurements: October 1993-August 1994, OCS Study

MMS 2001-025. U.S. Dept. of the Interior Minerals Mamt. Service, Gulf of Mexico OCD region, New Orleans, LA. 58pp.

Walker, N.D., Huh, O.K., Babin, A., Haag, A., Cable, J., Snedden, G., Braud, D., Wilensky, D., and Prasad, K., 2003. A Role for Remote Sensing in Managing Mississippi River Diversions., Backscatter, Vol. 1, 25-28, *AMRS Association*, 2003.

Walker, N.D., 2005. Wind and Eddy-Related Shelf/Slope Circulation Processes and Coastal Upwelling in the Northwestern Gulf of Mexico. Circulation in the Gulf of Mexico: Observations and Models, Wilton Sturges III and Alexis Lugo-Fernandex, Eds. *American Geophysical Union Monograph*, 295-314.

Walker, N.D.; Roberts, H.; Stone, G.; Bentley, S.; Huh, O.; Sheremet, A.; Rouse, L.; Inoue, M.; Welsh, S.; Hsu, S.A., and Myint, S., 2002. Satellite-based assessment of sediment transport, distribution and resuspension associated with the Atchafalaya River discharge plume. *Gulf Coast Association of Geological Societies Transactions*, 52, 967–973.

Walker, N.D., Wiseman, W.J. Jr., Rouse L.J. Jr. and Babin A., 2005a. Effects of river discharge, wind stress, and slope eddies on circulation and the satellite-observed structure of the Mississippi River plume. *Journal of Coastal Research*, 21 (6), 1228-1244.

Walker N.D., Leben, R.R., and Balasubramanian, S., 2005b. Hurricane-forced upwelling and chlorophyll a enhancement within cold-core cyclones in the Gulf of Mexico., *Geophysical Research Letters*, 32, L18610, doi:10.1029/2005GL023716.

Walker N.D., and Rabalais, N.N., 2006. Relationships among satellite chlorophyll a, river inputs, and hypoxia on the Louisiana continental shelf, Gulf of Mexico. *Estuaries and Coasts*, 29 (6B), 1081-1093.

Wave User's Guide, RD Instruments, April 2001, 74 pages.

Wells, J.T. and Kemp, P.W., 1981. Atchafalaya mud stream and recent mudflat progradation: Louisiana Chenier Plain. In: *Gulfs Coast Association of Geological Societies Transactions*, 31st Annual Meeting (21–23 October, Corpus Christi, Texas), pp. 409–416.

Wellner, R., Beaubouef, R., Van Wagoner, J., Roberts, H.H., and Sun, T., 2005, Jet-plume depositional bodies: The primary building blocks of Wax Lake Delta: *Transactions of the Gulf Coast Association of Geological Societies*, v. 55, p. 867–909.

Westerink, J.J., 1993, Tidal prediction in the Gulf of Mexico/Galveston Bay using model ADCIRC-2DDI, Contractors Report to the US Army Engineer Waterways Experiment Station, Vicksburg, MS, January 1993.

Westerink, J.J., Blain, C.A., Luettich, Jr. R.A., and N.W. Scheffner, 1994, ADCIRC: an advanced three-dimensional circulation model for shelves coasts and estuaries, report 2: users manual for ADCIRC-2DDI, Dredging Research Program Technical Report DRP-92-6, U.S. Army Engineers Waterways Experiment Station, Vicksburg, MS., 156p.

Westerink, J.J., Luettich, Jr. R.A., and Scheffner, N.W., 1993, ADCIRC: an advancedthree-dimensional circulation model for shelves coasts and estuaries, report 3: development of a tidal constituent data base for the Western North Atlantic and Gulf of Mexico, Dredging Research Program Technical Report DRP-92-6, U.S. Army Engineers Waterways Experiment Station, Vicksburg, MS, 154p.

Wu, H., Zhu J.R., Shen, J., Wang, H., 2011. Tidal modulation on the Changjiang River plume in summer. *Journal of Geophysical Research*, 116, C08017, doi:10.1029/2011JC007209, 2011.

Xing, J. and Davies, A.M., 1999. The effect of wind direction and mixing upon the spreading of a buoyant plume in a non-tidal regime. Continental Shelf Research, 19, 1437–1483.

Xu, K.H., Harris, C.K., Hetland, R.D., Kaihatu, J. M., 2011. Dispersal of Mississippi and Atchafalaya Sediment on the Texas-Louisiana Shelf: Model Estimates for the Year 1993, *Continental Shelf Research*, 31, 1558-1575. doi:10.1016/j.csr.2011.05.008.

Zetler, B. D., and D. V. Hansen, Tides in the Gulf of Mexico. In Contributions on the Physical Oceanography of the Gulf of Mexico, Texas A&M Oceanogr. Stud., 2,265-275, 1972.

Zhang, X, 2003, Design and implementation of an ocean observing system: WAVCIS (Wave-Current-Surge Information System) and its application to the Louisiana coast, Ph.D. Dissertation, Louisiana State Univ., Baton Rouge, Louisiana. 182 p.

Zheng, L.Y., Chen, C.S., and Liu, H.D., 2003a, A modeling study of the Satilla River estuary, Georgia, part I: Flooding/drying process and water exchanges over the salt marsh-estuary-shelf, *Estuaries*, 26: 651-669.

Zheng, L.Y., Chen, C.S., Alber, M., and Liu, H.D., 2003b, A modeling study of the Satilla River estuary, Georgia, part II: Suspended sediment, *Estuaries*, 26: 670-679.

Zhu, J., Chen, C., Ralph, E., and Green, S. A., 2001, Prognostic modeling studies of the Keweenaw current in Lake Superior. part II: Simulation, *J. Phys. Oceanogr.*, 31, 396–410.

Zimmerman, R. J. & T. J. Minello, 1984. Densities of Penaeus aztecus, Penaeus setiferus and other natant macrofauna in a Texas salt marsh. *Estuaries* 7(4A): 421–433.

VITA

Qian Zhang attended the Harbin Engineering University, China in September, 2002, and received her Bachelor of Science degree in Automation in June, 2006. She continued with her graduate study in Harbin Institute of Technology, China from September 2006 to July 2008, with a degree of Master of Science in Control Science & Mechatronics Engineering.

Since fall 2008, Qian was enrolled in the Engineering Science program at Louisiana State University, and earned her second Master of Science degree in August 2011, major in Coastal Engineering and minor in Computer Science, focusing on numerical modeling and simulation of nearshore hydrodynamics and wave-current-wind interactions. Afterwards she studied with Dr. Chunyan Li in the Department of Oceanography and Coastal Sciences, working on quantitative simulation of ocean-atmosphere dynamics. She expects to earn her Doctor of Philosophy degree in August 2015, with a major in Oceanography and Coastal Sciences and minor in Electrical and Computer Engineering. She also plans her postdoctoral research at the National Center for Atmospheric Research starting from summer 2015.